

ICHTHOLOGY, MINERALOGY, AND PALEOENVIRONMENTAL
IMPLICATIONS OF THE VERDINE AND GLAUCONY
FACIES IN SEDIMENTARY ROCKS

by

Sherie C. Harding

A dissertation submitted to the faculty of
The University of Utah
in partial fulfillment of the requirements for the degree of

Doctor of Philosophy

in

Geology

Department of Geology and Geophysics

The University of Utah

December 2014

Copyright © Sherie C. Harding 2014

All Rights Reserved

The University of Utah Graduate School

STATEMENT OF DISSERTATION APPROVAL

The dissertation of **Sherie C. Harding** has been approved by the following supervisory committee members:

Allan A. Ekdale, Chair

May 5, 2014

Date Approved

Marjorie A. Chan, Member

May 5, 2014

Date Approved

Erich U. Petersen, Member

May 5, 2014

Date Approved

Genevieve Atwood, Member

May 12, 2014

Date Approved

Daniel Horns, Member

May 11, 2014

Date Approved

and by John Bartley, Chair of the Department of Geology and Geophysics

and by David B. Kieda, Dean of The Graduate School.

ABSTRACT

The ichnology and mineralogy of selected occurrences of trace fossils and green minerals in verdine and glaucony facies were investigated, and the nature and significance of their association were evaluated. Trace fossils and green marine clays commonly occur together and are genetically related. At each site fecal pellets in marine shelf sediments were determined to be the most likely precursor of the green minerals. Fecal pellets, which are common on shelf sea floor, are organic rich, and they provide microenvironments of reduction for green mineral authigenesis, which promotes the formation of glauconitic pellets or odinite-rich pellets depending upon the paleoenvironmental conditions. Fecal pellets in intensely burrowed sediment represent a direct link between ichnology and green mineral authigenesis.

Five Phanerozoic sites representing terrigenous marine shelf deposits were examined: the Middle Eocene Crockett Formation in eastern Texas; two Cambrian sites including the Reno Member, Lone Rock Formation in southern Wisconsin and the Lion Mountain Member, Upper Riley Formation in central Texas; and two Mesozoic sites including the Jurassic Curtis Formation in central Utah and the Cretaceous Shannon Sandstone in central Wyoming. All sites represent times during the geologic past when global temperature was abnormally high.

The verdine facies, dominated by odinite-rich pellets, was identified in the “Main Glauconite Bed” (MGB) of the Crockett Formation. Odinite in the modern sea floor is

confined to tropical latitudes, and its association with trace fossils made by shallow marine animals suggests a shallower and more tropical paleoenvironment during the Middle Eocene than was previously recognized. Glauconitic pellets were found at all the other sites, where sedimentologic characteristics, stratigraphic occurrence, ichnofabric, and trace fossil assemblages indicate a multistage, reworked depositional history. The story of sea level dynamics unfolds where glauconitic minerals indicate elevated sea level during a marine transgression. Subsequently, quartz grains and shallow-marine burrows indicate an interval of regression. Finally, shallow shifting-sand substrate occupied by burrowing organisms indicates adaptation for life in water too shallow for glauconitic mineral authigenesis. These findings document the paleoenvironment of the marine shelf during times of fluctuating sea level and warm paleoclimate.

TABLE OF CONTENTS

ABSTRACT	iii
ACKNOWLEDGMENTS	ix
CHAPTERS	
1. INTRODUCTION	1
Objectives	1
Green Minerals	3
Ichnology	5
Applications	6
Summary of Chapters	8
References	17
2. ICHNOLOGY AND MINERALOGY OF THE MAIN GLAUCONITE BED, CLAIBORNE GROUP, MIDDLE EOCENE, TEXAS: PALEOENVIRONMENTAL IMPLICATIONS	20
Extended Abstract	21
Ichnology of the MGB	21
Clay Mineralogy of the MGB	21
Paleoenvironmental Implications	24
Acknowledgments	25
References Cited	25
3. ICHNOLOGY AND SEDIMENTOLOGY OF AN EOCENE GREENSAND IN TEXAS: BEHAVIORAL RESPONSE TO THE MIDDLE EOCENE CLIMATIC OPTIMUM (MECO)	27
Abstract	27
Introduction	28
Study Locality	29
Trace Fossils and Ichnofabrics	30
Pellets	32
Sediment Chemistry and Clay Mineralogy	34
Discussion	36

	Ichnology	36
	Paleoclimate	40
	Conclusion	41
	Acknowledgments	43
	References	60
4.	MINERALOGY AND GEOCHEMISTRY OF THE MAIN GLAUCONITE BED IN THE MIDDLE EOCENE OF TEXAS: PALEOENVIRONMENTAL IMPLICATIONS FOR THE VERDINE FACIES	63
	Abstract	64
	Introduction	64
	Previous Work on the MGB	65
	Background on Green Clay Minerals	65
	Green clay minerals	65
	Authigenesis	67
	Diagenesis and weathering	69
	Methods	71
	Sampling	71
	Mineral Identification	71
	X-ray diffraction analysis	72
	Electron microprobe analysis	72
	Mössbauer spectroscopy	72
	QEMSCAN analysis	72
	Results	72
	Petrography	72
	Sediment	72
	Pellets	73
	Color	73
	Mineral Composition	73
	Clay	73
	Siderite and apatite	77
	Discussion	82
	Pelleted Component	83
	Sequence Stratigraphy	86
	Paleoenvironment	86
	Conclusion	87
	Supporting Information	87
	Acknowledgments	87
	Author Contributions	88
	References	88
5.	TRACE FOSSILS AND ICHNOFABRICS ASSOCIATED WITH GLAUCONITIC MINERALS AT TWO CAMBRIAN SITES, WISCONSIN AND TEXAS	90

Upper Cambrian Reno Member, Lone Rock Formation, Tunnel City Group, Southwestern Wisconsin	90
Introduction	90
Previous Work	92
Regional geology	92
Local geology	94
Glauconitic minerals	94
Methods	96
Sampling	96
Mineral Identification	96
Thin section microscopy	97
X-ray diffraction analysis	98
Electron microprobe analysis	98
QEMSCAN analysis	99
Results	100
Characterization of glauconitic minerals	101
Sedimentology	104
Stratigraphy	107
Ichnology	108
Palaeophycus	108
Skolithos	109
Diplocraterion	110
Ichnofabric	112
Ichnofacies	112
Discussion	113
Ichnological implications	114
Mineralogical implications	115
Implications for paleoenvironment	116
Cambrian Lion Mountain Member, Upper Riley Formation in Central Texas ..	118
Introduction	118
Previous Work	119
Methods	121
Sampling	121
Mineral identification	121
Thin section microscopy	121
X-ray diffraction analysis	122
Electron microprobe analysis	122
QEMSCAN analysis	123
Results	124
Characterization of glauconitic minerals	124
Sedimentology	127
Stratigraphy	128
Ichnology	129
Skolithos	130
Planolites	131
Discussion	132

Compare and Contrast the Two Cambrian Sites.....	133
Ichnological Comparison.....	134
Mineralogical Comparison.....	135
Implications for Paleoenvironment.....	137
References.....	189
6. TRACE FOSSILS AND ICHNOFABRICS ASSOCIATED WITH GLAUCONITIC MINERALS IN TWO MESOZOIC SEAWAYS, UTAH AND WYOMING.....	193
Cretaceous Shannon Sandstone.....	193
Introduction.....	193
Previous Work.....	194
Methods.....	195
Results.....	195
Discussion.....	197
Jurassic Stump Formation.....	198
Introduction.....	198
Previous Work.....	199
Methods.....	200
Results.....	201
Discussion.....	202
References.....	210
7. CONCLUSION.....	212
Summary.....	212
Discussion.....	213
Paleoclimatic Implications.....	216
Conclusions.....	219
Future.....	222
References.....	224
APPENDIX: CAMBRIAN OF WISCONSIN DETAILED PETROGRAPHY.....	226

ACKNOWLEDGMENTS

I wish to acknowledge M.D. Dyar, C.J. Flis, J.E. Flis, J.M. de Gibert, B.P. Nash, T. Olszewski, W.T. Parry, E.U. Petersen, J.E. Warne, and T.E. Yancey for access to critical samples and for comments about sedimentological, mineralogical, and paleoecological implications. J.L. Allen, C.D. Bradbury, M. Crocker, D.L. Brandau, N.F. Dahdah, T.R. Gadek, M.A. Gorenc, P.D. Pahnke, W.T. Parry, S.L. Potter, and W.D. Mace provided valuable and much appreciated technical assistance. My advisor and mentor, A.A. Ekdale, provided continuous invaluable support throughout the process.

Portions of this project were funded by research grants to A.A.E. from the ACS Petroleum Research Fund (PRF Grant 47560-AC-8) and Division of Earth Sciences of the National Science Foundation (NSF Grant DES-1052661) and by student grants to S.C.H. from the Gulf Coast Association of Geological Societies and the Department of Geology and Geophysics of the University of Utah. Microprobe, XRD, and QEMSCAN analyses were accomplished in the Department of Geology and Geophysics at the University of Utah. QEMSCAN Model EVO 50, SERIAL # E430 located at Energy and Geoscience Institute (EGI), was used for additional QEMSCAN analyses.

I especially want to thank my very supportive friends and family for offering understanding and helpful advice: M.A. Cone, W.M. Cryan, C.T. Elliott, T.R. Gadek, T.R. Good, M.A. Gorenc, J.R. Lehane, T.M. Richards, L.A. Sherbeck, B.M. Walters, C.D. Walters, C.J. Walters, J.A. Walters, and T.H. Walters.

CHAPTER 1

INTRODUCTION

Trace fossil-bearing green marine clays are common throughout the geologic record and throughout the world. The fact that trace fossils and green marine clay minerals often occur together suggests a genetic relationship. This dissertation investigates the ichnology and mineralogy of selected occurrences of trace fossils and green minerals in verdine and glaucony facies and considers the nature and significance of their association. The findings reflect the paleoenvironment of the marine shelf, which has implications about benthic paleoecology, sea floor geochemistry, mineral authigenesis, paleoclimate, paleoceanography, sea level dynamics, and sequence stratigraphy.

Objectives

This study documents the green clay mineralogy and trace fossils at five selected sites. Crucial scientific questions are 1) whether the green minerals were autochthonous (formed in place) or allochthonous (reworked or transported from the site of origin) and 2) whether the trace fossils were syndepositional or postdepositional. To answer these questions requires knowledge of the sedimentological characteristics, stratigraphic occurrence, ichnofabric, and trace fossil assemblage at each site. When these questions

are answered and all the characteristics are assessed in combination, the most probable paleoenvironmental interpretation can be made for each site.

The study locations (Figure 1.1) include the Middle Eocene Crockett Formation in eastern Texas (Chapters 2, 3, and 4), two Cambrian sites including the Reno Member of the Lone Rock Formation in southern Wisconsin and the Lion Mountain Member of the Upper Riley Formation in central Texas (Chapter 5), and two Mesozoic sites including the Jurassic Curtis Formation in central Utah and the Cretaceous Shannon Formation in central Wyoming (Chapter 6). The Eocene Lisbon Formation in southern Alabama and the Miocene Tarragona Basin northeastern Spain were researched for background information, but are not reported in detail here.

Each of the seven occurrences represents a time in the geologic past when the climatic state was extreme greenhouse Earth, and global sea level was relatively high (Figure 1.2); thus, this study documents sea floor mineralogy and benthic faunal activity on paleo continental shelves during warm paleoclimates. Each selected site would likely be characterized by favorable nutrient supply and high biological productivity, as is common on continental shelves especially during a warm climate. This poses interesting questions: Do most occurrences of green marine clays correlate with warm paleoclimate? Can this study of benthic paleoenvironment and behavioral response to ambient climatic conditions have implications for modern shelf environments and the impact of today's climate warming on benthic shelf fauna? Indeed, this research does imply so, and it opens the door for future enquiry.

Green Minerals

The mention of green marine clay minerals brings to mind the most common type: glauconitic minerals. However, not all that is green marine sediment contains glauconitic minerals. Table 1.1 lists the variety of green clay minerals that represent shallow marine environments. Odin, in his treatise on *Green Marine Clays*, inventoried green minerals in the modern marine environment and classified them into four facies (Odin, 1988). Each facies was distinguished on the basis of substantially different seafloor environments of origin, as well as substantially different clay mineralogy (Table 1.1).

Two of those mineral facies were encountered in this research: the verdine facies, dominated by odinite-rich pellets, was found in the Middle Eocene site and is described in Chapter 4, and the glaucony facies, comprised of glauconitic pellets, was found at the two Cambrian and the two Mesozoic sites and is described in Chapters 5 and 6. The glaucony facies is fairly common in modern and ancient environments with a wide geographical occurrence, while the verdine facies (predominantly odinite) is rare in ancient environments with a geographical occurrence limited to tropical latitudes (Bailey, 1988; Odin, 1988). A schematic diagram (Figure 1.3 A and B) depicts the continental shelf depositional environments for the glaucony and verdine facies.

Glauconitization and verdinization processes are fundamentally tied to the marine seafloor substrate (Odin, 1988). The most common substrate for glauconitization or verdinization is granular, generally occurring as pelleted spheroids or ovoids, which typically originated as fecal pellets and mud fillings of foraminiferal tests (Triplehorn, 1966). Workers have noted a close relationship between glauconitic minerals and fecal

pellets (Ekdale et al., 1984; Pryor, 1975). The dominant substrate component at each study site described in this dissertation was originally comprised of fecal pellets. Fecal pellet authigenesis in shallow marine environments leads to glauconitic pellets or odinite rich pellets depending upon the paleoenvironmental conditions. The microreducing environments associated with fecal pellets provide favorable sites for authigenic processes. The fecal pellet maturation process is depicted in the schematic diagram in Figure 1.4 (Bailey, 1988; Carozzi, 1993; Moore and Reynolds, 1997; Odin, 1988).

The environmental conditions favorable for glauconitization in modern oceans requires seafloor water temperatures below 15°C, water depths of more than 50 meters, seawater of normal salinity with pH around 8, Eh between oxidizing bottom water and less oxidizing interstitial water, where the pelleted substrate offers microenvironments of reduction. Persistence of these conditions for 10^3 to 10^6 years with minimal sediment influx allows for glauconitic mineral authigenesis (Carozzi, 1993; Odin, 1988).

The level of maturity of glauconitic minerals is reflected in the amount of K_2O present, which occurs along a continuum from K-poor, disordered glauconitic smectite to K-rich, ordered glauconitic mica. Stages of development are defined by increasing potassium oxide content where 2–4 wt. % K_2O is nascent stage, 4–6 wt. % K_2O is slightly evolved (slightly mature), 6–8 wt. % K_2O is evolved (mature), and greater than 8 wt. % K_2O is highly evolved (highly mature) glauconitic minerals. The level of maturity is a reflection of residence time on the sea floor and the low rate of sedimentation. Evolution to the highly mature stage takes 10^5 to 10^6 years in recent material that is situated far from continental detrital input (Odin, 1988).

Once formed, glauconitic minerals are highly resistant and persist in the marine

environment. They are crystalline, chemically stable, and surprisingly compact, with a smooth, rounded, glossy surface, which are factors that all contribute to resistance to dissolution, weathering, and erosion. Glauconitic minerals are found in all oceans except in the extreme coldest areas of the globe, and they are found throughout the geologic record. It is assumed that the present environment of glauconitization reflects the past processes. In many instances, however, mature glauconitic grains are found outside of their environment of genesis, where they occur as relicts after surviving other geological processes.

The environmental conditions favorable for verdinization are found in the tropics. Verdine facies minerals (dominated by odinite) follow a different authigenic path and commonly originate from fecal pellets (Figure 1.4). They form rather quickly, probably in thousands of years, partly because of increased seafloor temperature ($\sim 25^{\circ}\text{C}$). They tend to occur in shallower water under normal salinity and basic pH (7.5–8.5). Observed water depth where verdine minerals are forming today is between 15 and 60 m and locally in 5 m depths. Circulating currents are required in proximity to continental water input and abundant Si, Mg, and Fe in warm water environments (Bailey, 1988; Ku and Walter, 2003; Odin, 1988).

Ichnology

Fecal pellets are trace fossils, and they are intimately associated with the green minerals because the organics associated with fecal pellets provide the sites for mineral authigenesis. The common clay fecal pellet size (200 to 500 μm) seems to exhibit an optimum dimension for mineral authigenesis. Smaller and larger sizes generally produce

less mature glauconitic minerals, as if some specific distance is optimal from the outside of a grain in the substrate (Odin, 1988). The pellets are converted to glauconitic minerals or to verdine minerals depending on the geochemical environment.

Abundant fecal pellets were produced in the original substrate at each study site. Referred to as the biogenic pelletization of clay (Pryor, 1975), the process involves suspension feeding benthic fauna as well as deposit feeding annelids and bivalves, with possible contribution from pelagic animals. It is the ingestion-digestion-egestion process that can significantly change substrate texture from seafloor clays and suspension clays to sand sized fecal pellets (Ekdale et al., 1984). Deposit feeding polychaetes have the capacity to completely turn over the substrate and deposit vast numbers of fecal pellets.

Substrate characterized by abundant fecal pellets reflects a thriving seafloor community. This confirms that oxygen was available in the bottom water to support life. The numerous burrowing organisms introduce oxygenated water into the substrate, which further promotes mineral authigenesis. Thus, both fecal pellets and burrows are evidence to the intimate link between ichnology and green mineral authigenesis (Ekdale et al., 1984; Needham et al., 2004; Pryor, 1975).

Applications

The occurrence of green minerals and trace fossils are key in the interpretation of stratigraphic components and depositional history in paleoenvironments. Numerous studies link green mineralogy and sequence stratigraphy (Amorosi, 1995; Amorosi and Centineo, 2000; Harris and Whiting, 2000; Hesselbo and Huggett, 2001; Kitamura, 1998; Kronen and Glenn, 2000; McCracken et al., 1996; Odin, 1988; Savrda, 1991; Urash,

2005; Walker and Bergman, 1993). A similarly large number of studies link ichnology and sequence stratigraphic interpretation (Ekdale et al., 1984; Frey and Pemberton, 1990; Ghibaudo et al., 1996; James and Dalrymple, 2010; MacEachern et al., 2007; MacEachern et al., 1992; Pemberton and MacEachern, 1995; Pemberton et al., 1992; Savrda, 1991, 1995; Taylor and Gawthorpe, 1993; Urash, 2005). When evaluated together, green minerals and trace fossils provide exceptional insight to paleoenvironmental interpretation.

For example, a layer of glauconitic pellets may indicate transgression (Figure 1.5). In this case, pelleted substrate forms on the inner continental shelf, as is common in modern oceans where fecal pellets are prevalent from the shoreline to about 30 m depth. Glauconitization occurs on the middle to outer continental shelf at depths greater than 50 to 1000 m (Figure 1.5 A) (Odin, 1988). In order for the glauconitization zone to move shoreward over the fecal pelleted substrate, sea level rise and transgression must have occurred (Figure 1.5 B). Initial shoreline transgression followed by regression is a fitting interpretation at each site in this dissertation.

An informative example showing a transgression over a burrowed firmground is illustrated in Figure 1.6 (Savrda, 1991; Savrda et al., 2001). It shows a firmground horizon burrowed by crustaceans (Figure 1.6 A). A firmground is a stiff but unlithified marine substrate that indicates compaction in a near shore environment (Ekdale et al., 1984). Subsequently, the open burrows are filled by lag deposits, including green minerals, during transgression (Figure 1.6 B). Ultimately, in the geologic record, this sequence could appear as a coplanar sequence boundary-transgressive surface (SB/TS) (Figure 1.6 C). This schematic diagram provides an explanation for the burrowed

firmground at the Middle Eocene Texas site (described in Chapter 3). The paleoenvironment was a marine, trace fossiliferous, siliciclastic interval in a regressive-transgressive parasequence. The sequence illustrates the association of ichnology and green minerals with application to transgressive systems tract interpretation.

Summary of Chapters

Chapters 2, 3, and 4 are a study of the Main Glauconite Bed, Crockett Formation, Claiborne Group, Middle Eocene, Texas. Chapter 2 is an extended abstract that defines both the ichnology and mineralogy. Chapter 3 describes the ichnology, sedimentology, and behavioral response to the Middle Eocene Climatic Optimum (MECO). Chapter 4 details the identification of verdine facies minerals dominated by odinite in the Main “Glauconite” Bed (MGB). Occurrences of odinite in the geological record have not been published until recently (Harding et al., 2014). This finding of verdine facies minerals, rather than glaucony facies minerals, in the MGB of the Crockett Formation indicates a shallow and more tropical paleoenvironment during the Middle Eocene than was previously thought. In that context, the trace fossils and ichnofabric (discussed in Chapters 2 and 3) reflect a response to warm tropical climate associated with the Middle Eocene Climatic Optimum (MECO). Since the MECO was a severe, short-term global climate warming event, documentation of the behavioral response of benthos in the shelf environment can provide an ancient analog to warming of shelf seafloor today.

Chapter 5, entitled “Trace Fossils and Ichnofabrics Associated with Glauconitic Minerals at Two Cambrian Sites,” details the sedimentological occurrence of glauconitic pellets and associated quartz grains at the two sites. Findings indicate that the glauconitic

pellets were probably reworked in place. The stratigraphic and ichnological evidence clarifies a transgressive-regressive history at each site. The final event was occupation of the shallow shifting-sand substrate by burrowing organisms that were adapted for life in shallower water than that where the glauconitic minerals had formed previously.

Chapter 6, entitled “Trace Fossils and Ichnofabrics Associated with Glauconitic Minerals in Two Mesozoic Seaways, Utah and Wyoming,” presents data from another part of the geological column. These two epicontinental seaways, which occurred during the prolonged “greenhouse” climate interval of the Mesozoic (Figure 1.2), display glauconitic pellets in siliciclastic environments. The glauconitic grains were reworked and/or transported, thus indicating an allochthonous origin. The ichnological signature supports the interpretation of shifting-sand and dynamic depositional environment.

Chapter 7, the conclusion, provides the unifying thread in this dissertation. Each selected site is a siliciclastic marine paleo shelf deposit with known occurrence of green minerals and associated trace fossils. The fact that each era of the Phanerozoic is represented was intended. Each site also represents a time of high sea level and exceedingly warm climate. The findings, enumerated in the conclusion, reflect marine shelf paleoenvironmental conditions, with implications about the benthic paleoecology, seafloor geochemistry, mineral authigenesis, paleoclimate, paleoceanography, and sea-level dynamics during warm paleo climate.



Figure 1.1 Map of the United States showing study locations. Five sites (in bold) are reported here. One sites (not bold) was examined and slated for future work.

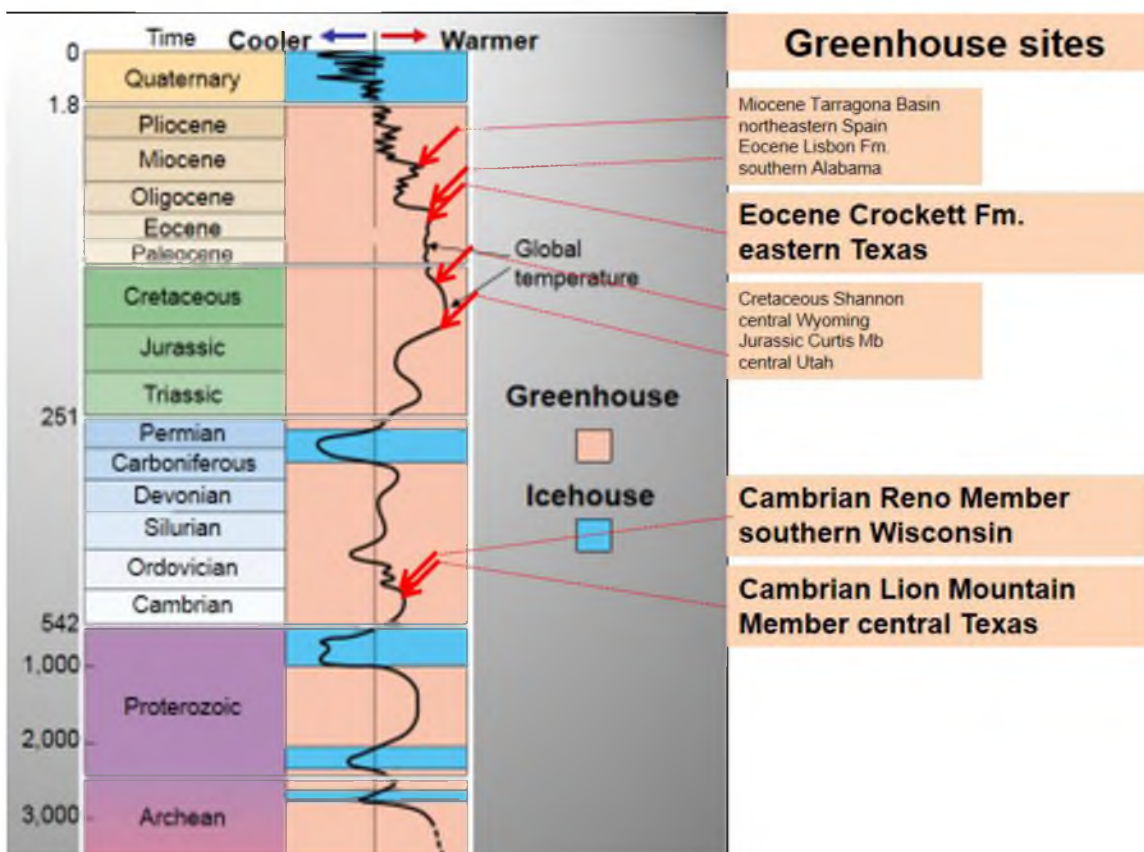


Figure 1.2 Global temperature curve showing greenhouse-icehouse conditions through Earth history (Marshak, 2004). Red arrows indicate temperature during deposition at study locations.

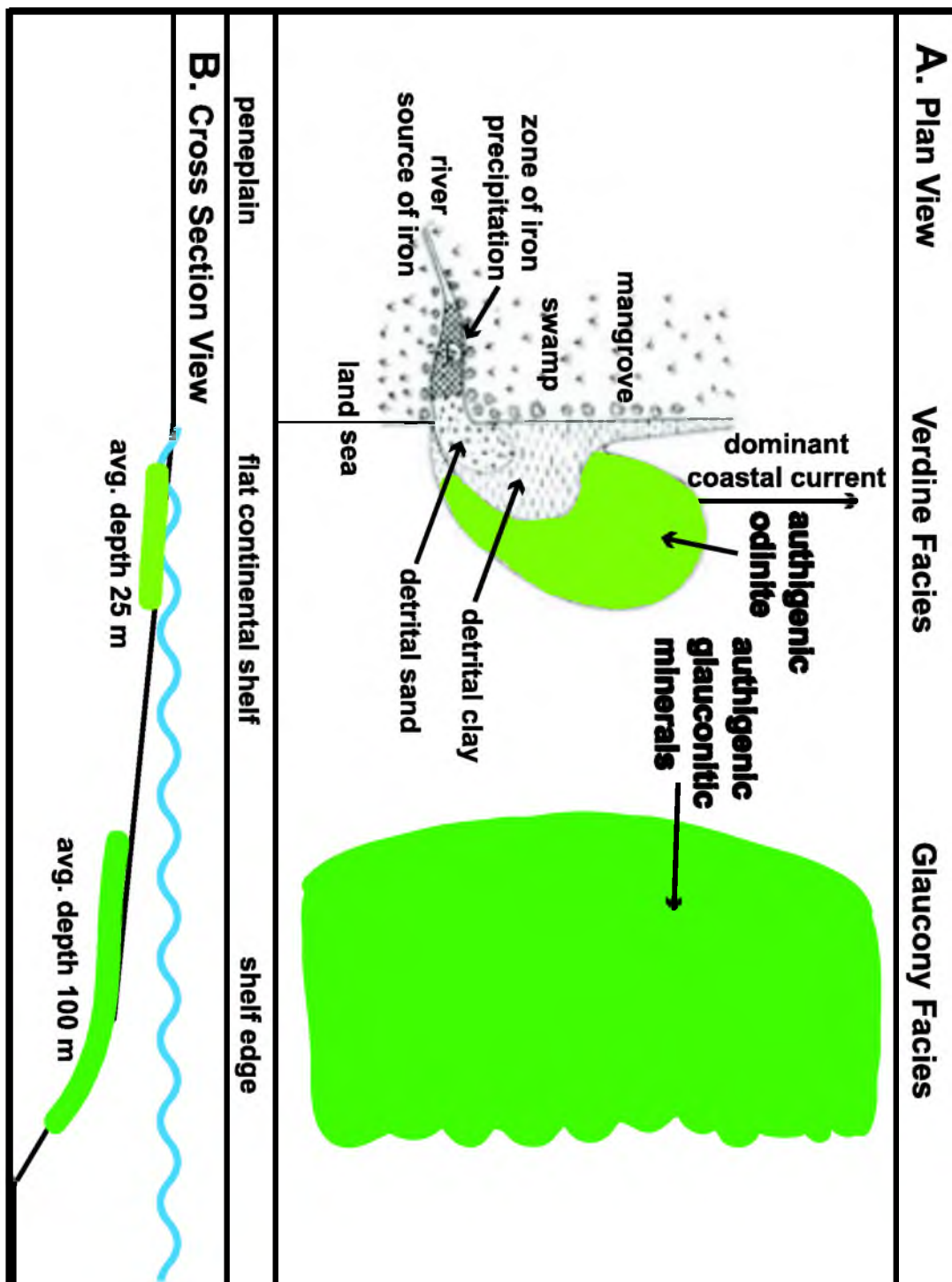


Figure 1.3 Schematic diagram showing the paleoenvironment of verdine and glaucony facies minerals where they form on the continental shelf. Green is the location of seafloor authigenesis. A) Plan view; B) Cross section view (modified after Odin, 1988)

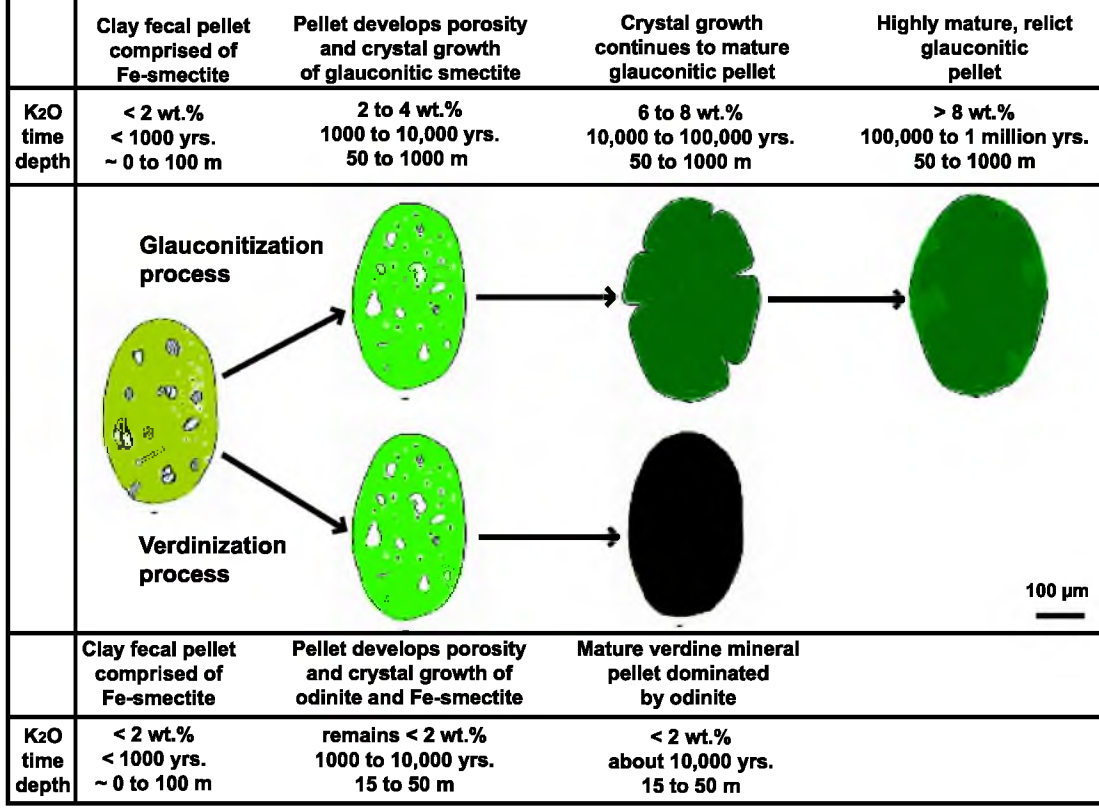


Figure 1.4 Fecal pellet maturity by glauconitization or, alternatively, by verdinization. The K₂O content, residence time on the sea floor, and depth of authigenesis vary between the two processes resulting in substantially different mineralogy (modified after Odin, 1988).

Glauconitic Pellets Formed During Transgression

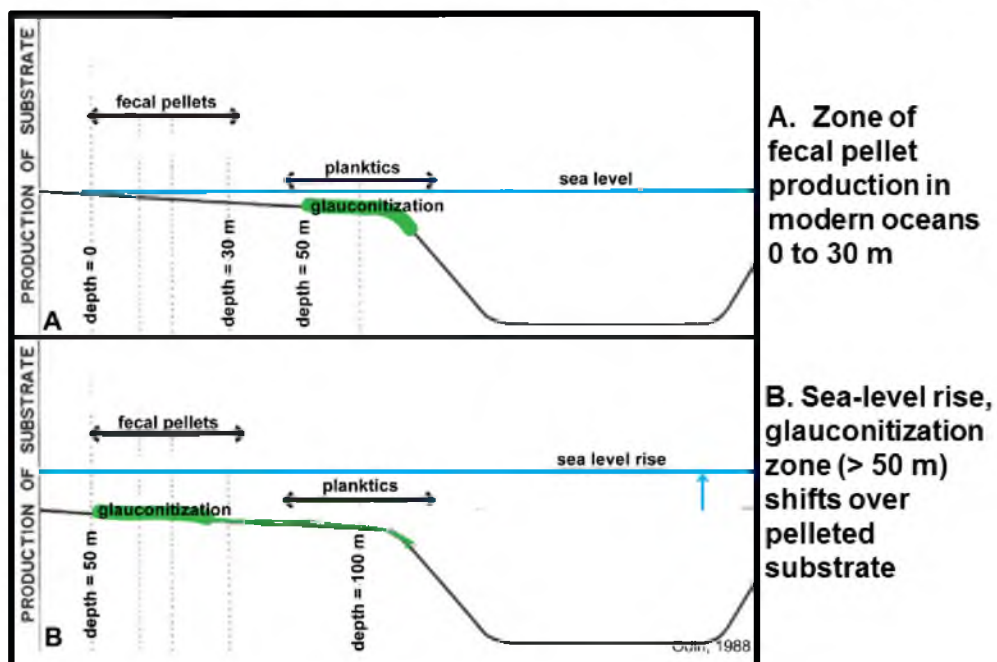


Figure 1.5 Model depicting pelleted substrate and the zone of glauconitization (modified after Odin, 1988). A) Shows fecal pellet production from 0 to 30 m depth and glauconitization > 50 m depth; B) shows sea level rise and migration of the glauconitization zone over the fecal pelleted substrate.

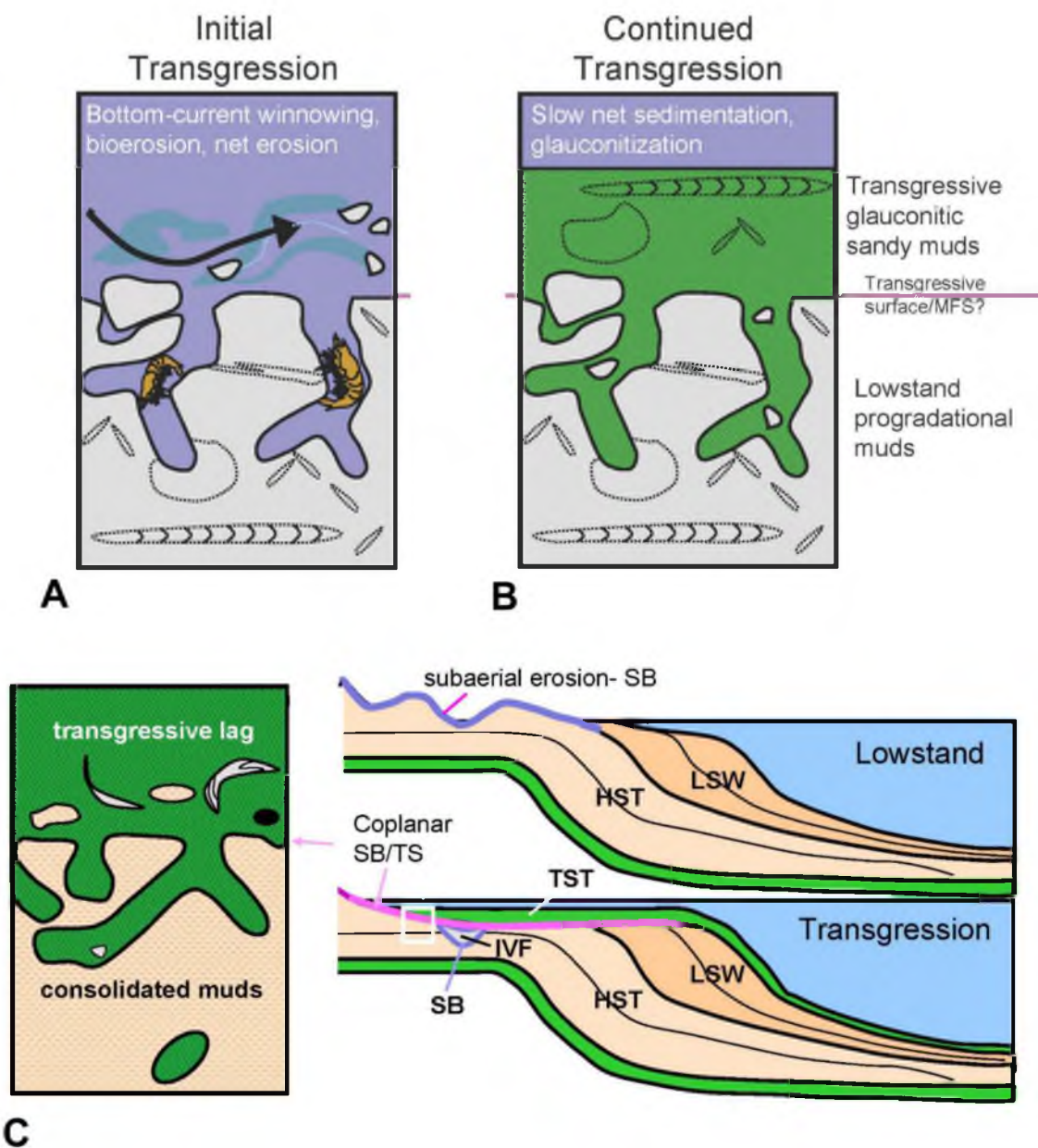


Figure 1.6 Schematic diagram depicting: A) active burrowing into consolidated muds by crustaceans during initial transgression; B) continued transgression, water deepening, and burrow fill form transgressive lag including green grains; C) development of a coplanar SB/TS (modified after Savrda, 1991)

Table 1.1 Characteristics of green clay minerals that form on the sea floor in shallow marine environments as identified and grouped into the mineral facies: oolitic ironstone, verdine, glaucony and celadonite-bearing facies (Odin, 1988). The clay minerals encountered in this study are highlighted in green.

Green clay mineral	Clay Group	Clay mineral structure	Iron content	Mineral facies	Paleoenvironment
Berthierine	Serpentine	1:1 (trioctahedral)	Fe ²⁺ rich	Oolitic ironstone	Forms on marine sea floors at the boundary between continent and coastal ocean, where there is low terrestrial runoff and available iron. Coastlines generally are flat with restricted, sheltered areas, such as seawater lagoons, embayments and delta fringe. Seawater circulation promotes oxidizing conditions and iron influx. Climate is tropical to subtropical.
Chamosite	Chlorite	2:1:1 (trioctahedral)	Fe ²⁺ rich	Oolitic ironstone	
Swelling chlorite	Chlorite	2:1:1 (trioctahedral)	Fe ²⁺ rich	Oolitic ironstone & Verdine	
Odinite	Serpentine	1:1 (di-trioctahedral)	75% Fe ³⁺ 25% Fe ²⁺	Verdine	Sediment starved inner shelf, fully marine, 5 to 50 m depth, with nearby river influx of iron rich sediment. Oxygenated, granular, often pelleted, substrate with <u>micro environments</u> of reduction. Climate is tropical, 25°C at the sea floor.
Fe-Smectite	Smectite	2:1 (trioctahedral)	Fe ³⁺ rich <u>low</u> Fe ²⁺	Verdine & Glaucony	
Glauconite	Mica	2:1 (dioctahedral)	Fe ³⁺ rich	Glaucony	Sediment starved outer shelf, upper slope, 50 to ~1000 m depth, oxygenated, granular, often pelleted, substrate, with <u>micro environments</u> of reduction. Climate, tropical to temperate, 10 to 15°C at the sea floor.
Celadonite	Mica	2:1 (dioctahedral)	Fe ³⁺ rich	Celadonite-bearing	Marine sea-floor lava flows where semi-confined void spaces are filled with altered clay minerals. Saponite forms as alteration of basaltic detritus in alkaline water.
Nontronite	Smectite	2:1 (dioctahedral)	Initially Fe ²⁺ rich	Celadonite-bearing	
Saponite	Smectite	2:1 (trioctahedral)		Celadonite-bearing	

References

- Amorosi, A., 1995, Glaucony and sequence stratigraphy: a conceptual framework of distribution in siliciclastic sequences: *Journal of Sedimentary Research, Section B: Stratigraphy and Global Studies*, v. 65, no. 4, p. 419–425.
- Amorosi, A., and Centineo, M.C., 2000, Anatomy of a condensed section: The lower Cenomanian glaucony-rich deposits of Cap Blanc-Nez (Boulonnais, northern France): *Special Publication - Society for Sedimentary Geology*, v. 66, no. 1060-071X, p. 405–413.
- Bailey, S.W., 1988, Odinite: A new dioctahedral-trioctahedral Fe (super 3+)-rich 1:1 clay mineral: *Clay Minerals*, v. 23, no. 3, p. 237–247.
- Carozzi, A.V., 1993, *Sedimentary Petrography: Sedimentary Geology Series: Englewood Cliffs, NJ, PTR Prentice Hall, 263 p.*
- Ekdale, A.A., Bromley, R.G., and Pemberton, S.G., 1984, *Ichnology: Trace fossils in sedimentology and stratigraphy. Tulsa, Oklahoma, Society of Economic Paleontologists and Mineralogists, SEPM short course, no. 15, 317 p.*
- Frey, R.W., and Pemberton, S.G., 1990, Ichnofacies and bathymetry: A passive relationship: *Journal of Paleontology*, v. 64, no. 1, p. 155–158.
- Ghibaudo, G., Grandesso, P., Massari, F., and Uchman, A., 1996, Use of trace fossils in delineating sequence stratigraphic surfaces (Tertiary Venetian Basin, northeastern Italy): *Palaeogeography, Palaeoclimatology, Palaeoecology*, v. 120, no. 3, p. 261–279.
- Harding, S.C., Nash, B.P., Petersen, E.U., Ekdale, A.A., Bradbury, C.D., and Dyar, M.D., 2014, Mineralogy and Geochemistry of the Main Glauconite Bed in the Middle Eocene of Texas: Paleoenvironmental Implications for the Verdine Facies: *PloS One*, v. 9, no. 2, p. e87656.
- Harris, L., and Whiting, B., 2000, Sequence-stratigraphic significance of Miocene to Pliocene glauconite-rich layers, on-and offshore of the US Mid-Atlantic margin: *Sedimentary Geology*, v. 134, no. 1-2, p. 129–147.
- Hesselbo, S.P., and Huggett, J.M., 2001, Glaucony in ocean-margin sequence stratigraphy (Oligocene-Pliocene, offshore New Jersey, USA; ODP Leg 174A): *Journal of Sedimentary Research*, v. 71, no. 4, p. 599–607.
- James, N.P., and Dalrymple, R.W., 2010, *Facies Models 4: St. John's, Newfoundland, Geological Association of Canada, GEOText 6, 575 p.*
- Kitamura, A., 1998, Glaucony and carbonate grains as indicators of the condensed section:

- Omama Formation, Japan: *Sedimentary Geology*, v. 122, no. 1-4, p. 151–163.
- Kronen, J., and Glenn, C.R., 2000, Pristine to reworked verdine: Keys to sequence stratigraphy in mixed carbonate-siliciclastic forereef sediments (Great Barrier Reef): *Society of Economic Paleontologists and Mineralogists, Special Publication*, v. 66, p. 387–404.
- Ku, T.C.W., and Walter, L.M., 2003, Syndepositional formation of Fe-rich clays in tropical shelf sediments, San Blas Archipelago, Panama: *Chemical Geology*, v. 197, no. 1-4, p. 197–213.
- MacEachern, J.A., Pemberton, S.G., Gingras, M.K., Bann, K.L., and Dafoe, L.T., 2007, Uses of trace fossils in genetic stratigraphy, *in* Miller III, Trace Fossils: Concepts, Problems, Prospects: Oxford, Elsevier B.V, 611 p.
- MacEachern, J.A., Raychaudhuri, I., and Pemberton, S.G., 1992, Stratigraphic applications of the Glossifungites ichnofacies: Delineating discontinuities in the rock record, *in* Proceedings, Applications of Ichnology to Petroleum Exploration—A Core Workshop. Society of Economic Paleontologists and Mineralogists, Core Workshop 1992, Volume 17, SEPM, p. 169–198.
- McCracken, S.R., Compton, J., and Hicks, K., 1996, 10. Sequence-stratigraphic significance of glaucony-rich lithofacies at site 903, *in* Mountain, G.S., Miller, K.G., Blum, P., Poag, C.W., and Twichell, D.C., eds., Proceedings of the Ocean Drilling Program, Scientific Results, College Station, Texas, 1996, v. 150, p. 171–187.
- Moore, D.M., and Reynolds, R.C., Jr., 1997, X-Ray Diffraction and the Identification and Analysis of Clay Minerals: Oxford, Oxford University Press, 378 p.
- Needham, S.J., Worden, R.H., and McIlroy, D., 2004, Animal-sediment interactions: The effect of ingestion and excretion by worms on mineralogy: *Biogeosciences*, v. 1, no. 2, p. 113–121.
- Odin, G.S., 1988, Green Marine Clays: Oolitic Ironstone Facies, Verdine Facies, Glaucony Facies and Celadonite-Bearing Facies—A Comparative Study: Amsterdam, Elsevier, Developments in Sedimentology, 445 p.
- Pemberton, S.G., and MacEachern, J.A., 1995, The sequence stratigraphic significance of trace fossils: Examples from the Cretaceous foreland basin of Alberta, Canada, *in* Sequence Stratigraphy of Foreland Basin Deposits—Outcrop and Subsurface Examples from the Cretaceous of North America: Tulsa, Oklahoma, AAPG, v. Memoir 64, p. 429–475.
- Pemberton, S.G., MacEachern, J.A., and Frey, R.W., 1992, Trace fossil facies models: Environmental and allostratigraphic significance, *in* Walker, R.G., and James, N.P., eds., Facies models: Response to Sea Level Change: St. John's, Newfoundland,

- Geological Association of Canada, p. 47–72.
- Pryor, W.A., 1975, Biogenic sedimentation and alteration of argillaceous sediments in shallow marine environments: *Geological Society of America Bulletin*, v. 86, no. 9, p. 1244–1254.
- Savrda, C.E., 1991, Ichnology in sequence stratigraphic studies: An example from the Lower Paleocene of Alabama: *Palaios*, v. 6, p. 39–53.
- Savrda, C.E., 1995, Ichnologic applications in paleoceanographic, paleoclimatic, and sea-level studies: *Palaios*, v. 10, p. 565–577.
- Savrda, C.E., Browning, J.V., Krawinkel, H., and Hesselbo, S.P., 2001, Firmground ichnofabrics in deep-water sequence stratigraphy, Tertiary clinoform-toe deposits, New Jersey slope: *Palaios*, v. 16, no. 3, p. 294–305.
- Taylor, A.M., and Gawthorpe, R.L., 1993, Application of sequence stratigraphy and trace fossil analysis to reservoir description: Examples from the Jurassic of the North Sea, *in* *Proceedings, Geological Society, London, Petroleum Geology Conference series*, Geological Society of London, v. 4, p. 317–335.
- Triplehorn, D.M., 1966, Morphology, internal structure, and origin of glauconite pellets: *Sedimentology*, v. 6, no. 4, p. 247–266.
- Urash, R.G., 2005, Sedimentology and ichnology of a passive-margin condensed section, Eocene Lisbon Formation, Southern Alabama [MS thesis]: Auburn, Auburn University, 114 p.
- Walker, R.G., and Bergman, K.M., 1993, Shannon sandstone in Wyoming: A shelf-ridge complex reinterpreted as lowstand shoreface deposits: *Journal of Sedimentary Research*, v. 63, no. 5, p. 839–851.

CHAPTER 2

ICHTHOLOGY AND MINERALOGY OF THE MAIN GLAUCONITE BED, CLAIBORNE GROUP, MIDDLE EOCENE, TEXAS: PALEOENVIRONMENTAL IMPLICATIONS

This article, "Harding, S.C., A.A. Ekdale, E.U. Petersen, B.P. Nash, and M.D. Dyar, 2013, Ichnology and mineralogy of the Main Glauconite Bed, Claiborne Group, Middle Eocene, Texas: Paleoenvironmental implications: GCAGS Transactions, v. 63, p. 549-554," is reproduced with permission of the Gulf Coast Association of Geological Societies, Kate Kipper, GCAGS Executive Director for use in the Ph.D dissertation of Sherie C. Harding. Permission is required for further publication use.

Ichnology and Mineralogy of the Main Glauconite Bed, Claiborne Group, Middle Eocene, Texas: Paleoenvironmental Implications

Sherie C. Harding¹, A. A. Ekdale¹, Erich U. Petersen¹, Barbara P. Nash¹, and M. Darby Dyar²

¹Department of Geology and Geophysics, University of Utah, 383 FASB,
115 South 1460 East, Salt Lake City, Utah 84112-0102

²Department of Astronomy, Mount Holyoke College, 217 Kendade Hall,
50 College St., South Hadley, Massachusetts 01075

EXTENDED ABSTRACT

The “Main Glauconite Bed” (MGB) of the Stone City Member, Crockett Formation, Claiborne Group, middle Eocene, a prominent 5.5 ft (1.7 m) thick green fossiliferous clay bed, crops out on the south bank of the Brazos River on the Texas Gulf Coastal Plain (Fig. 1). The MGB and the associated stratigraphic section have been studied extensively by paleontologists and stratigraphers. Thus, the general paleoenvironmental setting is well understood (Stanton and Nelson, 1980; Stenzel et al., 1957; Yancey, 1995). The present study combines ichnology and mineralogy to provide an innovative approach and new insight into the biological and sedimentary processes that occurred during accumulation of the MGB. Characterization of the composite ichnofabric, implications of the pelleted sedimentary fraction, ichnologic nature of the bed boundaries, and the clay mineralogy are brought together to provide an integrated approach to understanding this complex depositional environment.

Ichnology of the MGB

The central MGB is intensely bioturbated. The sediment was completely reworked by infauna during slow sedimentation. Petrographic analyses show that pellets are consistently oval in shape, although of various sizes, and the pellet surface is smooth and glossy. Pellets appear to be fecal in origin rather than foraminiferal infilling. In contrast, the top part of the MGB is lined with concretions of filled burrows that extend down into the central MGB. Individual trace fossils include *Gyrolithes*, *Thalassinoides*, and *Spongiomorpha*. Scratch traces are evident on the perimeter of the burrow fill, indicating burrowing in a firm ground substrate (Fig. 2). These are recognizable even after concretionary diagenetic processes. It is likely that some of the trace fossils previously reported as *Thalassinoides* may in fact be *Spongiomorpha*. The top of the bed with different ichnogenera than the central bed reflects a *Glossifungites* ichnofacies, where shallow water trace fossils colonized a substrate that was deposited originally in deeper water (Harding and Ekdale, 2009). This suggests that the top of the MGB may have been exposed during intertidal environment.

Clay Mineralogy of the MGB

A variety of analytical techniques were employed to ascertain mineral composition and textural distribution of clays in the MGB. X-ray diffraction (XRD) was carried out

Harding, S. C., A. A. Ekdale, E. U. Petersen, B. P. Nash, and M. D. Dyar, 2013, Ichnology and mineralogy of the Main Glauconite Bed, Claiborne Group, Middle Eocene, Texas: Paleoenvironmental implications: Gulf Coast Association of Geological Societies Transactions, v. 63, p. 549–554.

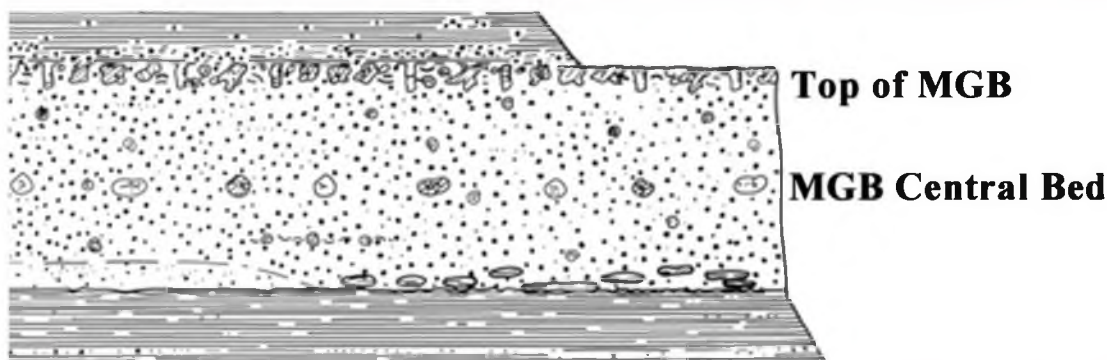


Figure 1. The Main Glaucinite Bed with near vertical exposure topped by a resistant ledge of concretionary burrow fill. Black dots represent clay pellets (modified after Stenzel, 1957).

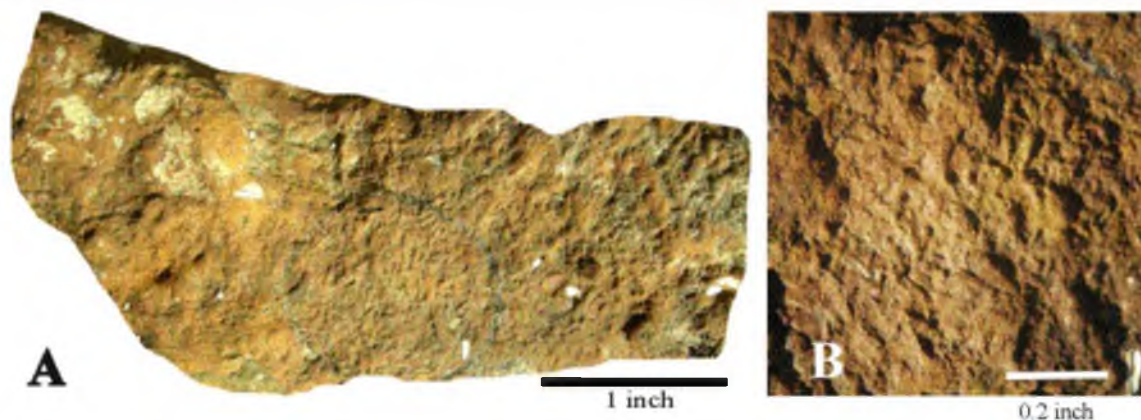


Figure 2. Scratch traces on perimeter of concretionary burrow fill, trace fossil *Spongiomorpha*. (A) Top of MGB concretion. (B) Bioglyphs on concretion wall.

on oriented and un-oriented clay samples. Strong diffraction peaks at 7.1 Å and 3.5 Å are consistent with odinite. The presence of minor amounts of smectite, illite and possibly chlorite cannot be excluded. Chemical analyses of selected clay pellets and matrix confirms that odinite is the predominant clay species. Odinite is described as an Fe³⁺-rich 1:1 layer clay (Bailey, 1988; Odin, 1988). Odinite is classified with the kaolin-serpentine group and the dioctahedral kaolin sub-group of phyllosilicates. Mössbauer spectroscopy on clay pellets and matrix demonstrate that the oxidation state of iron is consistent with that of odinite at approximately 3:1 Fe³⁺/Fe²⁺ ratio (Bailey, 1988; Odin, 1988). QEMSCAN (Quantitative Evaluation of Minerals by Scanning Electron Microscopy) data provide false color digital images that enhance the textural view, complement petrographic observation, and provide area percent measurements. The QEMSCAN images and photomicrographs, as shown in Figure 3, were used to select pellets and grains for EMPA (Electron Microprobe Analysis).

The compositional field of MGB clay is displayed in a triangular diagram of ferric iron, ferrous iron and magnesium oxide in wt.%. Chemical results overlie that of ideal odinite as published from its type locality (Bailey, 1988; Odin, 1988) (Fig. 4). Other Fe-rich clays, including odinite, berthierine, chlorite, glauconite and nontronite are plotted on the triangular diagram of Ku and Walter (2003) (Fig. 5). The following average mineral formula was calculated for MGB odinite pellets: (Fe³⁺_{0.89} Mg_{0.45} Al_{0.67} Fe²⁺_{0.30} Ti_{0.01} Mn_{0.01})_{Σ=2.33} (Si_{1.77} Al_{0.23}) O_{5.00} (OH)_{4.00} which is slightly more Mg-poor and Fe, Al-rich than the Bailey (1988) structural formula for the type odinite. Few glauconitic grains

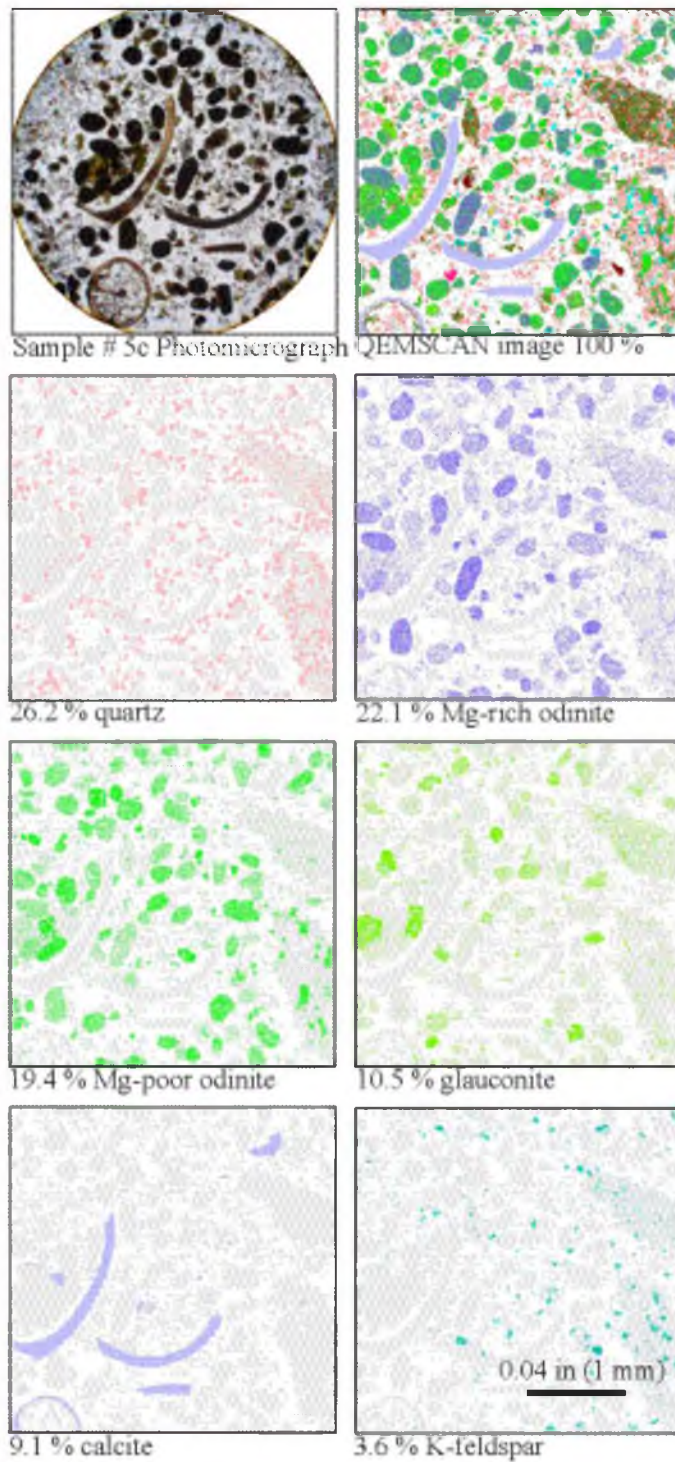


Figure 3. QEMSCAN image (in false color) of the MGB central bed showing compositional distribution of clay pellets in area % (sample #5c).

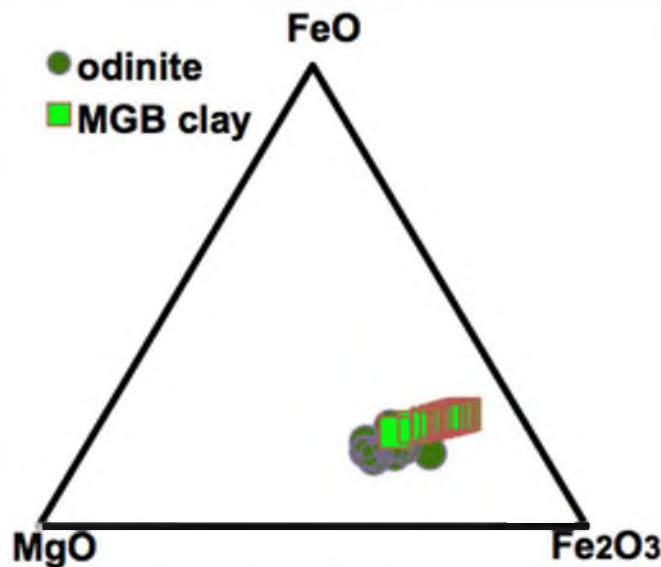


Figure 4. Triangle diagram (oxide weight) showing composition (electron microprobe analyses) of MGB clay minerals and odinite (wet chemical analyses) from its type locality (Bailey, 1988; Odin, 1988).

were detected in the olive to gray pelleted sediments of the MGB, and those are interpreted as allochthonous in origin. The concretionary burrow fill at top of the MGB is made up of siderite and apatite formed as cementing agents. The burrow fill incorporates some clay pellets, phosphate-rich pellets, quartz grains, and shell material.

Paleoenvironmental Implications

The clay mineral, odinite, is a dominant constituent of the verdine facies. The verdine facies is a clay mineral facies associated with shelf sediments in a proximal marine environment at tropical latitude with iron influx from nearby runoff. It is commonly identified in modern nearshore environments where its authigenesis is well documented (Bailey, 1988; Odin, 1988). The MGB consists of authigenic clays of the verdine facies rather than the glaucony facies which reflects substantially different clay types and implies different paleoenvironmental conditions. Recognition of odinite as the dominant constituent in an ancient green marine clay is not common. The MGB represents a well characterized locality of verdine facies clays in the geologic record. This contributes to understanding the physical and biological processes that occurred during its deposition.

The combined findings in ichnology and mineralogy indicate a contrast between the central and top part of the MGB. This demonstrates an environmental change through time. The central MGB reflects a subaqueous depositional environment that was somewhat sheltered with clay dominant low energy, slow sedimentation, gentle winnowing currents, and sufficient oxygenation to support intense biogenic activity and characteristic verdine minerals. The top of the MGB was subaerially exposed for at least part of the time in an intertidal environment. This interpretation is supported by characteristic burrowing patterns at top of the MGB. It represents an interval of non-deposition, dewatering, compaction and burrowing. Ultimately, the crustacean burrows were filled with detrital sediment indicating a return to the subaqueous environment and moderate energy. The MGB at Stone City Bluff accumulated during regional transgression and reflects coastal dynamics during a time of relative sea level high.

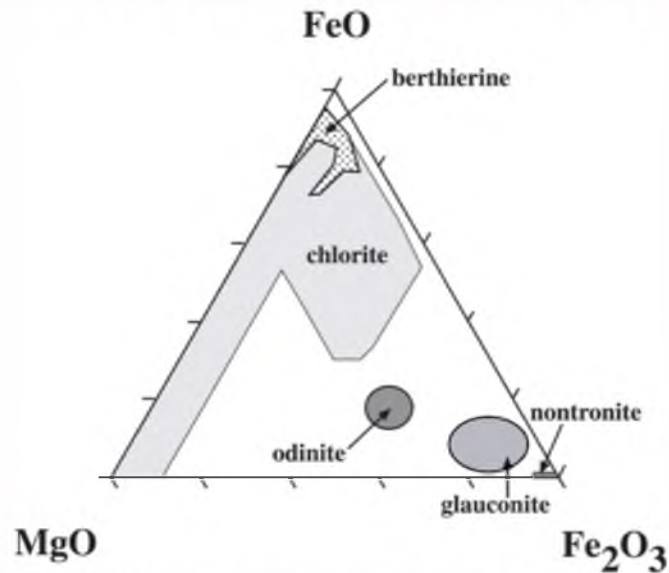


Figure 5. Triangle diagram (oxide weight) showing compositions of Fe-rich clays, including odinite, berthierine, chlorite, glauconite, and nontronite (Ku and Walter, 2003).

ACKNOWLEDGMENTS

The authors thank C. J. Flis, J. E. Flis, J. E. Warme, and T. E. Yancey for access to critical samples and for comments about sedimentological and paleoecological implications. J. Allen, C. D. Bradbury, N. Dahdah, T. Olszewski, and W. T. Parry provided analytical work and valuable assistance with XRD, EMPA and QEMSCAN. QEMSCAN Model EVO 50, SERIAL # E430 located at the Energy and Geoscience Institute (EGI) was used for the QEMSCAN analyses, and the EMPA and XRD analyses were accomplished in the Department of Geology and Geophysics at the University of Utah. This project was funded by research grants to A. A. Ekdale, PI from the ACS Petroleum Research Fund (PRF Grant 47560-AC-8) and Division of Earth Sciences of the National Science Foundation (NSF Grant EAR-1052661) and by student grants to S. C. Harding from the Gulf Coast Association of Geological Societies and the Department of Geology and Geophysics of the University of Utah.

REFERENCES CITED

- Bailey, S. W., 1988, Odinite; a new dioctahedral-trioctahedral Fe (super 3+)-rich 1: 1 clay mineral: *Clay minerals*, v. 23, no. 3, p. 237-247.
- Harding, S. C., and A. A. Ekdale, 2009, Trace fossils in the green zone: Ichnologic, sedimentologic and sequence stratigraphic implications of glaucony-rich greensands (Eocene, Texas): *Geological Society of America Abstracts with Programs*, v. 41, no. 7, p. 121.
- Ku, T. C. W., and L. M. Walter, 2003, Syndepositional formation of Fe-rich clays in tropical shelf sediments, San Blas Archipelago, Panama: *Chemical Geology*, v. 197, p. 197-213.
- Odin, G. S., 1988, Green marine clays: Oolitic ironstone facies, verdine facies, glaucony facies, and celadonite-bearing facies, a comparative study: *Developments in Sedimentology*, v. 45, 445 p.
- Stanton, R. J., Jr., and P. C. Nelson, 1980, Reconstruction of the trophic web in paleontology; community structure in the Stone City Formation (middle Eocene, Texas): *Journal of Paleontology*, v. 54, p. 118-135.

Stenzel, H. B., E. K. Krause, and J. T. Twining, 1957, Pelecypoda from the type locality of the Stone City beds (middle Eocene) of Texas: University of Texas Publication 5704, Austin, 237 p.

Yancey, T. E., 1995, Depositional trends in siliciclastic deposits of the Stone City transgressive systems tract, middle Eocene, Texas: Gulf Coast Association of Geological Societies Field Guide, Austin, Texas, p. 581–586.

CHAPTER 3

ICHTHOLOGY AND SEDIMENTOLOGY OF AN EOCENE GREENSAND IN TEXAS: BEHAVIORAL RESPONSE TO THE MIDDLE EOCENE CLIMATIC OPTIMUM (MECO)

Abstract

Although rarely employed in paleoclimate studies, ichnologic information may offer some useful insights about climatic conditions during a global warm interval. The Main Glauconite Bed (MGB) of the Middle Eocene Stone City Member, Crockett Formation, in eastern Texas displays multiple ichnocoenoses and demonstrates a sea level change during the Middle Eocene Climatic Optimum (MECO). The intensely bioturbated, pelleted, central MGB represents an environment probably dominated by infaunal annelid worms. The MGB top, marked by prominent concretionary burrows, represents a shallower environment associated with a firmground omission suite of trace fossils. *Spongeliomorpha* (showing scratch traces on burrow walls) along with *Thalassinoides* and *Gyrolithes* were produced by burrowing decapod crustaceans. A postomission ichnocoenosis is evident where open burrows at the MGB top were filled with sediment and then reoccupied by burrowers. The top of the MGB exhibits a composite ichnofabric including pre-omission, omission, and postomission suites of trace fossils. This bed contains abundant odinite, a green clay mineral that is indicative

of the tropical verdine facies. The MGB represents the response of a diverse benthic community to changing seafloor conditions and climatic warming during shoreline regression and expansion of the tropics in the Middle Eocene Climatic Optimum.

Introduction

Climate is well known as a major factor influencing the biogeographic distribution of organisms on land and in the sea. Climate also influences crucial physical aspects of depositional environments, such as temperature and substrate character, which likewise control not only the distribution but also the behaviour (including burrowing behaviour) of organisms. Few previous studies use ichnologic evidence to demonstrate or illuminate the biological response to warm climate dynamics in the shallow marine environment, which is the focal point of this study.

One informative example of an ichnological response during warm paleoclimate can be found in the Eocene Crockett Formation (Claiborne Group) in the Gulf of Mexico Coastal Plain in eastern Texas (Figures 3.1 and 3.2), where a sequence of heavily burrowed greensand deposits records the response of marine ichnocoenoses to changing seafloor conditions during a major climatic warming interval. The MECO (Middle Eocene Climatic Optimum) has been recognized worldwide, and the time frame has been dated as *ca.* 41.5–42.0 Ma (Bohaty and Zachos, 2003; Huggett, 2010; Zachos et al., 2008).

Study Locality

Siliciclastic marine strata of the Stone City Member of the Crockett Formation are exposed at Stone City Bluff along the south bank of the Brazos River in Burleson County, Texas. These strata were deposited during the MECO (Huggett et al., 2010). In the Middle Eocene this locality was characterized by relatively high and variable sedimentation rates during a transgressive systems tract, which resulted in a complex history of environmental and shoreline change, characterized by the upward-deepening transition zone of the Stone City Member (Davidoff and Yancey, 1993; Yancey, 1995; Yancey and Davidoff, 1994).

The greensands at Stone City Bluff have been referred to by many previous workers as “glaucanitic or pelleted sandstone” or by other similar terms (Stanton, 1979; Stenzel, 1934; Stenzel et al., 1957; Yancey, 1995) because of its green color and pellet content. True glauconite, however, is only a very minor component of the sediment, while odinite clay is the major component of the fecal pellets (Harding et al., 2014). The deposits are intensely burrowed, and they contain a very rich diversity of benthic invertebrate fossils, including more than 200 species of marine mollusks, as well as less common fossils of crustaceans, echinoderms, and a few other taxa (Emerson and Emerson, 2001; Stanton and Nelson, 1980; Stenzel et al., 1957).

The upper part of the section at Stone City Bluff contains a prominent marker bed, known locally as the Main Glauconite Bed (MGB), which is a 1.7 m-thick, pelleted, trace fossiliferous, shelly, and sandy mudstone (Figure 3.3). The MGB has been studied extensively by paleontologists and stratigraphers for more than 150 years (Davidoff and Yancey, 1993; Stanton and Nelson, 1980; Stanton and Warne, 1971; Stenzel, 1934;

Stenzel et al., 1957; Yancey, 1995; Zuschin and Stanton, 2002). Ichnologic features, however, have received only limited treatment (Stanton and Warne, 1971). The focus of this report is to describe and interpret the ichnology of the MGB at Stone City Bluff in the contexts of its original depositional environment, paleoecology, sequence stratigraphy, and a major paleoclimatic warm interval.

The ichnology and sedimentary mineralogy of the MGB are evaluated in two parts—central and top—because each is unique (Figure 3.4). The central part of the MGB is a shelly and sandy mudstone that is intensely bioturbated and contains a significant fraction of fecal pellets. The top of the MGB contains abundant concretions of filled burrows that extend down into the central MGB. These concretions are composed of siderite and apatite that form as cementing agents (B.P. Nash, written communication, 2013). The contrast in mineralogy and ichnology between the central and top parts of the MGB reflects a change in depositional environment through time.

Trace Fossils and Ichnofabrics

The ichnocoenoses of the central and top parts of the MGB are different. Sediment in the central MGB is intensely bioturbated and pelleted, and it represents an environment that apparently was dominated by infaunal annelid worms. The MGB top is marked by concretionary burrows that represent a shallower water environment in association with a firmground omission suite of trace fossils. A postomission ichnocoenosis is evident where sediment filled burrows at the top of the MGB were re-occupied by subsequent burrowers. The top part of the MGB thus represents a composite ichnofabric consisting of pre-omission, omission and postomission suites of trace fossils.

The central MGB is intensely bioturbated, but individual burrows are indistinguishable. Although the sediment is mottled heterogeneously in terms of texture and color hues, it is difficult to differentiate burrow filling from surrounding sediment. Except where minor storm layers occur, there is little evidence of primary laminae. The ichnofabric index is five (*ii5*) throughout this interval, which indicates that the sediment was completely reworked by infauna during slow sedimentation (Figure 3.5).

The top of the MGB is a prominent ledge reinforced by concretions. Most of the concretions are easily identifiable as mineralized burrow-fill sediment. *Thalassinoides* and *Gyrolithes* are the most common ichnogenera present (Figures 3.6 and 3.7), as observed by previous workers (Stanton and Warne, 1971). On close inspection, some burrow walls contain well defined bioglyphs (scratch traces) indicating that at least some of these trace fossils are *Spongiomorpha* (Figure 3.8 A), which has not been reported from this locality before now. All three ichnogenera probably were made by decapod crustacean burrowers. Diagenetic processes did not destroy the bioglyphs that remain evident in sparse patches on the margins of the concretionary burrow fill here where the margin of the concretion coincides precisely with the original margin of the burrow, and these bioglyphs are diagnostic of *Spongiomorpha*. The specimens in the MGB also commonly exhibit short, tapering, blind tunnels or alcoves (Figure 3.8 B), which are especially characteristic of *Spongiomorpha* as well (Gibert and Ekdale, 2010).

This occurrence of *Spongiomorpha* at the top of the MGB indicates burrowing in a firmground substrate that reflects an omission surface, sometimes referred to as a “*Glossifungites* Ichnofacies” (Ekdale et al., 1984; Knaust and Bromley, 2012; Pemberton and Frey, 1985). It is likely that at least some of the other trace fossils here previously

reported as *Thalassinoides* in fact may be *Spongeliomorpha*. The concretionary burrows extend downward into the central MGB as much as 25 cm. The burrow tunnels are circular to elliptical in cross section with distinctive spiraling (*e.g.*, *Gyrolithes*) and branching (*e.g.*, *Thalassinoides*) patterns. Sparse decapod crustacean body fossils have been reported in sediments of the central MGB, where loose dactyli of the crab *Calappilia* were found in washed residues (Stenzel, 1934).

The trace fossil *Piscichmus* isp., a feeding pit made by fish (in this case probably by rays), was observed in the section at SCB (Figure 3.9). This is the first published report of vertebrate trace fossils at this site. Abundant body fossils (teeth, bones, and otoliths) of marine vertebrates, including at least 50 species of sharks, rays, teleosts, and reptiles, have been collected from the Stone City Member (Breard and Stringer, 1999). *Piscichmus* made by rays is common in intertidal sediments (Howard et al., 1977; Martinell et al., 2001), which supports sea level dynamics in a transitional environment.

Pellets

Clay pellets are abundant throughout the MGB in varying concentrations. Sedimentologic characteristics indicate *in situ* fecal origin by a variety of producers. Pellets in the MGB are categorized on the basis of composition and size. Smaller clay pellets and larger heterogeneous pellets occur together (Figure 3.10). Readily observable are the small, green to black, ovoid clay pellets that are abundant in the central MGB and that also occur inside concretionary burrows at the top of the MGB. Less abundant are the larger pellets that are observed both in the central MGB and in concretionary burrow fills at the top of the MGB.

Clay pellets comprise as much as 50% in a clay matrix. These pellets vary in size but are consistent in shape, described as ovoid, ellipsoid, or elongate ovoid (Figure 3.11). Size ranges from 0.2 to 0.6 mm long and from 0.09 to 0.3 mm wide. Clay pellets show sharp margins and glossy surfaces, as if rubbed smooth and polished, and their surfaces are smoother than might be expected from normal abrasion. These characteristics suggest a fecal origin and possibly a variety of producers. Stenzel et al. (1957) suggested that the pellet producers probably were polychaete annelids and deposit-feeding pelecypods. A very few pellets may be fills of the chambers of foraminiferal tests. Angular quartz fragments occur in the clay matrix but are not found in the clay pellets. The clay pellets exhibit no evidence of internal canals, as might be expected in decapod crustacean fecal pellets, such as *Palaxius* or *Favreina*.

The larger pellets of heterogeneous composition are not obvious in outcrop or in hand samples, but they are clearly evident in thin sections. Pellet shape in two-dimensional view is oval to circular, depending on thin section orientation. Size is consistently larger (average length 1 mm and average width 0.6 mm) than the clay pellets described above. The larger heterogeneous pellets in the central bed are composed of a loosely packed mixture of clays and tiny clasts. These pellets were not found intact in disaggregated hand samples from the central MGB, so it is assumed that they were friable and fell apart. These pellets are evident in thin sections from the central bed and in the concretionary burrow fill at the top of the MGB. Their friable nature suggests that they were less likely than the clay pellets to withstand reworking and appreciable transport. It is more likely that these larger pellets were produced in place by the burrowing occupants of both the central bed and top of the MGB. These pellets probably were produced by

worms and/or pelecypods because their ovoid shape is not characteristic of fecal pellets produced by decapod crustaceans, which are generally cylindrical, and like the small clay pellets, they do not exhibit an internal canal pattern that is characteristic of decapod fecal pellets. Crustacean pellets may have existed but were not preserved.

Sediment Chemistry and Clay Mineralogy

Sediment ingestion, digestion and recycling by deposit-feeding and suspension-feeding organisms can be prevalent in shallow seafloor environments and may have an appreciable effect on the weathering of silicate minerals. Biogenic activity can induce mineral authigenesis and clay mineral precipitation (Needham et al., 2004). The effects of burrowing and sediment-feeding activity on sediment chemistry and clay mineralogy were investigated in this study. Intense biogenic activity is evident in the MGB. Every clay particle in the central MGB may have been cycled through an organism's digestive tract multiple times (Stenzel et al., 1957). The postburial effects of diagenesis and weathering in outcrop could have altered the green clay minerals in the MGB. In a case study of glauconitic minerals in Egypt, workers found that fresh samples were colored dark green, whereas weathered samples were colored olive green to yellowish brownish green (Pestitschek et al., 2012). The mineralogical findings in the MGB reflect animal-sediment interaction during authigenesis as well as diagenesis and weathering in outcrop.

The green pelleted sediments in the central MGB and the cemented concretionary burrow fill at the top of the MGB were analyzed by employing a variety of techniques. Thin sections were described petrographically, and X-ray diffraction (XRD) was carried out on the 2 μm clay fraction to determine clay mineralogy. Electron microprobe

(EMPA) analyses were done on selected pellets and matrix to determine chemical composition and to assist clay mineral identification. Mössbauer analyses were done on clay matrix and pellets to determine iron oxidation state (Dyar et al. 2006), which has bearing on EMPA data interpretation and significance for paleoenvironmental interpretation. QEMSCAN (Quantitative Evaluation of Minerals by Scanning Electron Microscopy) data were obtained to provide a textural view that complements and validates the petrographic and EMPA observations.

XRD results reveal that a clay mixture is present in the pellets and matrix of the central MGB. Even though the MGB traditionally has been termed a “glauconite” bed, the clay component actually is dominated by odinite with small amounts of smectite and illite (Figure 3.12), and there are very few glauconitic pellets. QEMSCAN analyses reveal mineral area percent and texture. The false color images in the QEMSCAN results represent the textural configuration of matrix and pellets in the central MGB (Figure 3.13). Similar clay pellets also were incorporated into the concretions of burrow fill that line the top of the MGB. Concretionary burrow fill is composed of siderite and apatite cementing agents with varying types and amounts of clasts in the burrow fill (Figure 3.14). The larger pellets can be seen in the QEMSCAN images. At the top of the MGB, these pellets were altered diagenetically to apatite and siderite, so they closely match the cemented concretionary burrow fill matrix. Their visibility is accentuated due to higher P_2O_5 in the pellets when compared to matrix.

The clay mineral, odinite, is found in modern seafloor environments and is diagnostic of the verdine facies. It is confined to tropical latitudes, between about 20° N and 20° S, in proximity to terrigenous clastic sources with iron influx. Present day

occurrences include the Senegal, Niger, Congo, and Koukoure River mouths and the lagoon of New Caledonia (Odin, 1988). Observed water depth where odinite and associated clay minerals are forming today is between 15 and 60 m, and locally in 5 m depths, in common association with fecal pellets. Water at the seafloor characteristically is normal to nearly normal salinity, elevated seafloor temperature ($\sim 25^{\circ}\text{C}$), basic pH (7.5–8.5), with abundant oxygen, and positive Eh (Bailey, 1988; Odin, 1988). The identification of odinite in the MGB samples is a significant finding because it provides important information for interpreting the paleoclimatic regime of the deposits in that unit.

Discussion

Ichnology

The ichnology of the MGB is characterized as varying from a softground ichnocoenosis to a firmground ichnocoenosis from the central MGB to the top of the MGB. The MGB progressed from an intensely bioturbated softground with abundant fecal pellets to a burrowed omission surface, to a postomission occupation of the burrow fill. An omission surface is a short term discontinuity that represents an interval of no sedimentation and may or may not reflect an erosional interval. Here it is interpreted as an association of shallow water trace fossils that colonized a deeper marine substrate.

The MGB displays a composite ichnofabric (Bromley and Ekdale, 1986). It represents a transient phase of benthic community succession. Each phase reflects an entirely different ichnocoenosis. For instance, the surface passes from softground through firmground and possibly to a hardground consistency. The resulting composite

ichnofabric reflects a sedimentologic response to environmental change through time. These characteristics indicate a *Glossifungites* Ichnofacies, which is defined as firm but unlithified substrate, probably occurring during an absence of sedimentation and possible exhumation (Ekdale et al., 1984).

The composite ichnofabric in the MGB reflects a cessation of sedimentation for an undetermined length of time. Such firmground substrates may develop subaerially as dewatered, compacted but unlithified mud in intertidal to supratidal environments. The majority of firmgrounds occur in shallow marine settings where exhumation may allow for subsequent exploitation by burrowing organisms. Although there is no bathymetric restriction on firmground conditions, they commonly are thought to occur mainly in shallow-marine settings where the sedimentologic effects of fluctuating sea level may be most apparent. Burrowing organisms inhabiting a firmground do not need to reinforce their burrow margins to prevent collapse, and so the burrow walls may show scratch traces. Characteristic ichnotaxa found at the top of the MGB include *Spongeliomorpha* isp. and firmground *Thalassinoides* and *Gyrolithes*. Here the upright spiral *Gyrolithes* may lead into the other ichnotaxa to form a compound trace fossil.

The *Thalassinoides* at top of the MGB is characterized by Y-shaped or T-shaped branch junctions that are somewhat enlarged (3 to 5 cm across) at the points of bifurcation. They were open burrows systems here through which oxygenated water flowed freely, and they were maintained as domichnial (dwelling) or fodinichnial (deposit feeding) structures. The trace-making organisms probably were decapod crustaceans, as indicated by the scratch traces characteristic of *Spongeliomorpha*. Once vacated by the occupants, open burrows are susceptible to passive infilling in a shallow

marine environment. As a result, such burrows commonly are preserved as concretionary burrow fills, such as is seen at the top of the MGB.

Clay pellets are abundant in the central MGB, and they are interpreted as fecal pellets based on their consistent shape and variable size. Fecal pellets originally contained organic matter, and thus they indicate more reducing conditions than the surrounding environment. Pellets provide localized environments for clay mineral authigenesis since odinite tends to form within sheltered, reducing, granular microenvironments (Bailey, 1988; Odin, 1988). Mössbauer spectral analyses show elevated amounts of reduced (ferrous) iron in the clay pellets, suggesting that these pellets in the MGB are more chemically reduced than the surrounding clay matrix (Figure 3.15). Since the clay pellets are more reducing, it is reasonable to assume that they were fecal pellets.

Clay pellets are not evenly distributed throughout the central bed, suggesting to some workers that they may have been reworked by gentle winnowing and episodic storms (Yancey, 1995; Zuschin and Stanton, 2002). The variation in pellet size is attributed to multiple producers, which may reflect the high faunal diversity of the benthic community. Clay pellets also occur in the concretionary burrow fill at the top of the MGB. It is possible that they were introduced into this environment along with the detritus that filled the burrow, or else they could have been left behind by the occupants of the postomission burrows. In any case, the clay pellets are not attributed to the decapod crustacean that produced the omission suite burrows (*Thalassinoides*, *Gyrolithes* and *Spongeliomorpha*). Apparently, the crustacean fecal material was not preserved, which may be due to subaerial exposure in an intertidal environment.

The abundant and varied fecal pellets and the intense bioturbation along with the high molluscan diversity are evidence for a highly productive shallow marine environment. Trophic web reconstruction of the central MGB reveals that the primary producers and primary consumers are underrepresented as body fossils (Stanton and Nelson, 1980). It is the burrows, fecal pellets and totally bioturbated ichnofabrics that represent the unpreserved soft-bodied members of the benthic community in the MGB. Such a prolific ecosystem suggests a favorable habitat that was characterized by warm shallow water, stable salinity, low hydrodynamic energy, and gentle currents providing winnowing and oxygenation.

A zone of scattered concretions exists within the central MGB. These concretions are roughly spherical and do not have distinctive trace fossil shapes, so their origin is uncertain. Odin (1988) refers to a zero Eh plane within the sediment; in other words, a redox boundary where the concretionary process takes place. Huggett et al. (2010) suggested a zone of methanogenesis located below horizons that indicate a break in sedimentation as the explanation for the site of concretion formation within beds in the Claiborne Group. This hypothesis probably indicates an oxidizing environment at the water-sediment interface overlying a redox boundary at depth within the substrate.

The clay pellets in the concretionary burrow fill may have been produced *in situ* by the burrow occupants or else transported into the open burrows as detritus. Clay pellets observed in the crustacean burrow fill show no abrasion and little fracturing. There are a very few glauconitic pellets (<3%), and they commonly are fractured. The firm, well indurated clay pellets would be resistant to abrasion and fracture. They probably could withstand reworking and redeposition during tidal action or a storm event.

They could be reworked from the central MGB and redeposited in the open burrows at the omission surface at the top of the MGB. Alternatively, pellets may have originated *in situ* from postomission burrow occupants. The larger friable pellets likely formed *in situ*.

Paleoclimate

The climatic warm interval at 41.5–42.0 Ma, known as the MECO (Bohaty and Zachos, 2003; Zachos et al., 2008), coincides with deposition of the upper part of the Stone City Member, which includes the MGB. Paleotemperature data are based on stable oxygen isotopes from benthic foraminifera in deep sea cores. The MECO reflects a major peak in deep ocean temperature, which is thought to have reached 10 °C (Huggett et al., 2010), and the effects apparently were global.

Climatic control of trace fossils and their latitudinal distribution in shallow marine environments have been examined in general terms (Cadée, 2001; Goldring et al., 2007; Goldring et al., 2004). A decrease in benthic diversity of coastal life from low to high latitudes is observed in modern marine fauna. Generally, low latitudes and warm water sustain a higher faunal diversity, especially of burrowing shrimps and crabs (Cadée, 2001; Goldring et al., 2004). The diversity of modern fauna and the diversity of body fossils, however, are distinct from ichnodiversity. Climatic influence on trace fossil distribution is most apparent in shallow water facies because of the greater lateral and temporal variability in such environments. Cenozoic occurrences of crustacean burrows were recognized as primarily tropical and subtropical in modern coastal and shoreface settings. *Thalassinoides* producers are most prominent in the tropics, although they also extend into the subtropical and temperate zones. Concretionary burrows at the top of the

MGB reflect habitation by abundant decapods during the warm MECO paleoclimate, and the well displayed ichnocoenosis of *Thalassinoides*, *Gyrolithes* and *Spongeliomorpha* in the MGB therefore is consistent with an expanded tropical zone during the MECO, as demonstrated clearly by the presence of odinite.

In studies of latitudinal variation in bioturbation in modern coastal zones, it was found that sediment reworking is greater along warmer coastlines because of the high diversity and abundance of the infauna (Cadée, 2001; Goldring et al., 2007; Goldring et al., 2004). The overall degree of sediment reworking between colder (arctic) coasts and warmer (temperate and tropical) coasts increases more than five fold at the warmer end of the spectrum. Such climatically influenced latitudinal changes should be recognizable in the fossil record. Sedimentation rate and event stratigraphy, however, also may be significant influences on the degree of bioturbation. The central MGB exhibits a high degree of bioturbation in a marginal marine environment during the warm MECO paleoclimate. Thus, the composite ichnofabric of the MGB coincides with a major climatic warm interval and may represent a tropical ichnofabric.

Conclusion

The MGB displays a composite ichnofabric that includes pre-omission, omission, and postomission suites of trace fossils. The intensely bioturbated, pelleted, central MGB was occupied by polychaete worms and deposit-feeding pelecypods. The MGB top was occupied by decapod crustaceans, represented by the concretionary burrows that line the MGB top and extend downward into the central bed. The MGB top was a firmground, as evidenced by scratch traces on sharp walls of *Spongeliomorpha* burrows. The

concretionary burrow fill shows evidence of reburrowing by postomission suite occupants. The MGB contains three ichnocoenoses and shows sequential occupation of a changing substrate consistency from softground to firmground. There was a concomitant change from the *Cruziana* Ichnofacies (probably subtidal) to the *Glossifungites* Ichnofacies (possibly intertidal), which indicates an upward-shallowing of the water depth.

This ichnologic study confirms shallowing to a firmground omission surface at the top of the MGB. At this locality the omission surface can be interpreted as a parasequence boundary. Passive-margin shelf sequences such as this one commonly exhibit condensed sections and biogenic reworking. We hypothesize that these conditions should be reflected by condensed-section ichnofabrics. Parasequence boundaries and condensed sections can be delineated by vertical changes in ichnofabric that reflect variations in sedimentation rate.

The ichnologic signature of the MGB adds significant new information to the numerous previous studies relating to this section. The MGB represents a parasequence in a complex transition zone within the overall upward deepening SCB section (Huggett et al., 2010; Yancey, 1995). The environmental change reflected in the MGB is an upward shallowing interval that remained mostly marine in an inner neritic setting. Paleoecologic and stratigraphic findings by other authors also suggest a nearshore setting with indications of shallow neritic to estuarine conditions (Stanton & Warne 1971; Stanton & Nelson, 1980; Yancey et al., 1993; Zuschin & Stanton 2002).

This mineralogic study suggests the likelihood of a nearby river mouth and iron influx, and the occurrence of authigenic odinite points to a tropical paleoclimate. Since

the paleolatitude of the MGB at Stone City Bluff in the Middle Eocene was about 29° N (outside the present day tropics) documentation of odinite clay, representing the verdine facies, suggests that the latitudinal limits of the tropics were expanded appreciably during the MECO. Ichnology and mineralogy are direct evidence of expanded tropics by at least 6° latitude during the warm MECO.

The top of the MGB is a surface that represents a temporary omission surface during the warm MECO. For this reason, the paleoclimatic implications revealed in the MGB are an important aspect of this study. The MGB represents dynamic seafloor conditions and high benthic biodiversity in a nearshore environment during the MECO climatic interval. As such, infaunal animal behaviour, as reflected in the trace fossils of the MGB, may provide an ancient analogue for animal behaviour today in the neritic seafloor environment. The MGB provides a reliable ancient analogue for tropical benthic community response to warm climate.

Acknowledgements

We dedicate this paper to the memory and legacy of our respected colleague and dear friend, Jordi Maria de Gibert. Portions of this project were funded by research grants to A.A.E. from the ACS Petroleum Research Fund (PRF Grant 47560-AC-8) and Division of Earth Sciences of the National Science Foundation (NSF Grant DES-1052661) and by student grants to S.C.H. from the Gulf Coast Association of Geological Societies and the Department of Geology and Geophysics of the University of Utah. We especially thank the following individuals for valuable assistance in the lab and in the field, as well as for providing useful samples and offering helpful advice: J.L. Allen, C.D.

Bradbury, N.F. Dahdah, M.D. Dyar, C.J. Flis, J.E. Flis, J.M. de Gibert, T.R. Good, M.A. Gorenc, J.R. Lehane, B.P. Nash, T. Olszewski, W.T. Parry, E.U. Petersen, J.E. Warne, and T.E. Yancey.



Figure 3.1 Location of study site at Stone City Bluff, Burleson County, Texas.

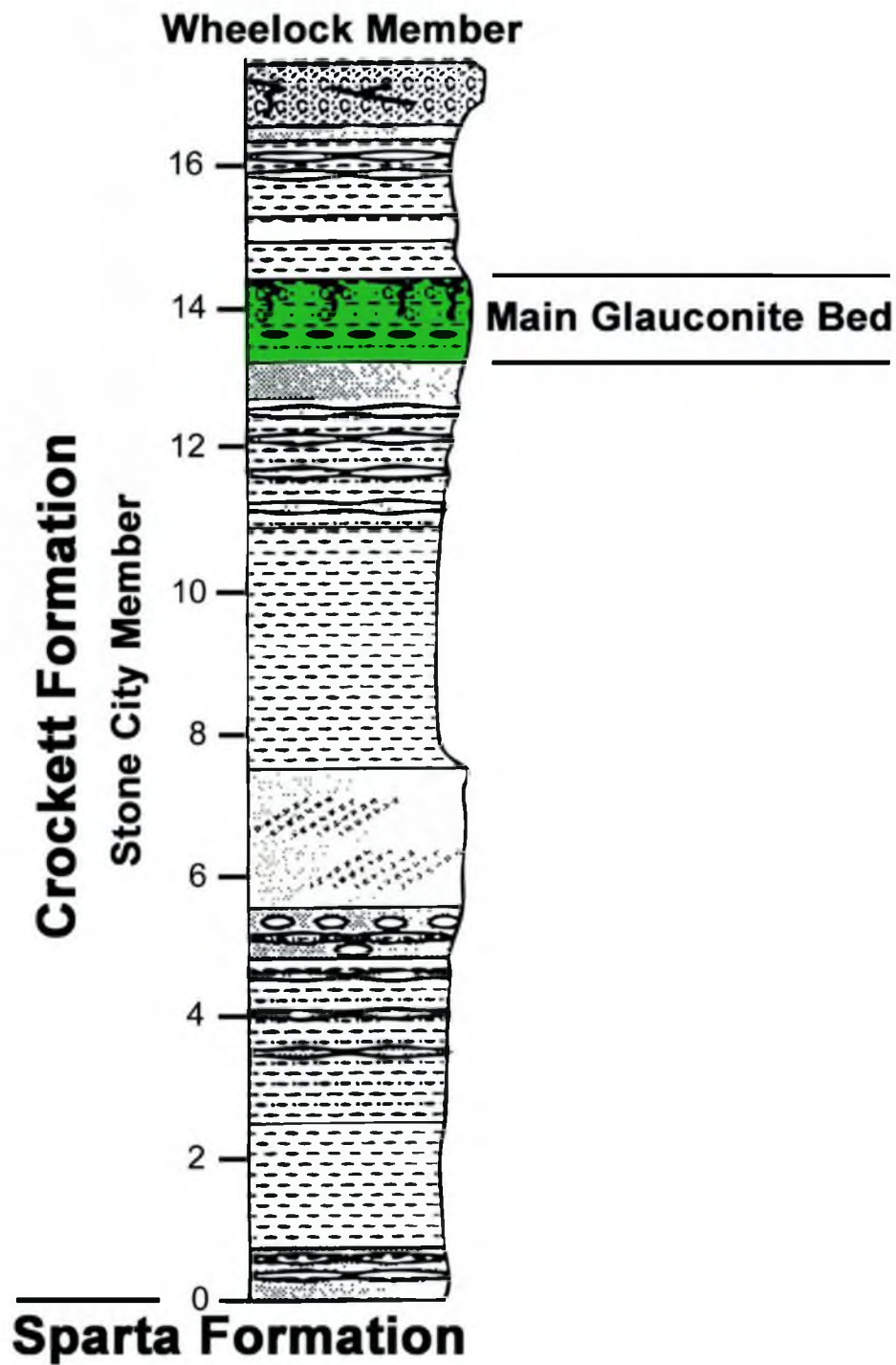


Figure 3.2 Stratigraphic section at Stone City Bluff, including Stone City Member, Crockett Formation, Claiborne Group. Main Glaucanite Bed (MGB) occurs within the “Transition Zone” of Huggett et al., (2010).



Figure 3.3 Stone City Bluff outcrop showing the Main Glaucanite Bed (MGB) on the south bank of the Brazos River, Burleson County, Texas.

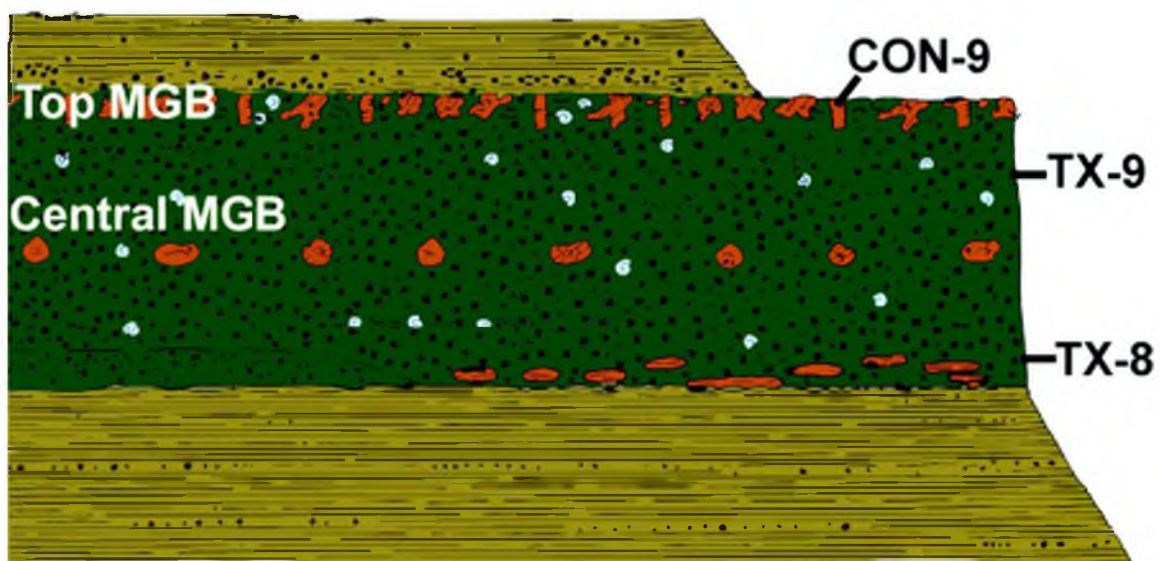


Figure 3.4 Main Glauconite Bed (MGB) at Stone City Bluff (modified after Stenzel et al., 1957, Figure 4). Locations of Samples TX-8, TX-9 and CON-9 are indicated.

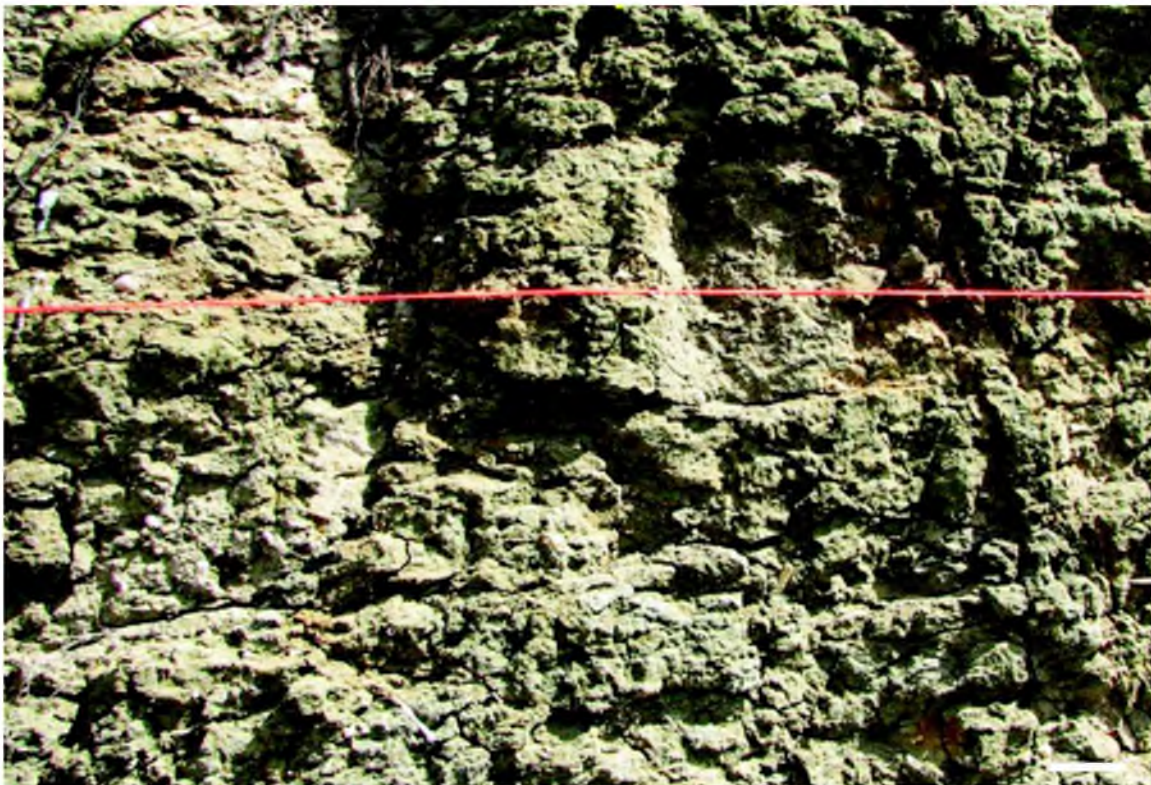


Figure 3.5 Intensely bioturbated (*ii5*) sediment in central part of MGB. Scale bar 2 cm. (Ignore red cord.)



Figure 3.6 Concretionary burrow fill of *Thalassinoides* isp. at the top of the MGB. Scale bar 5 cm.

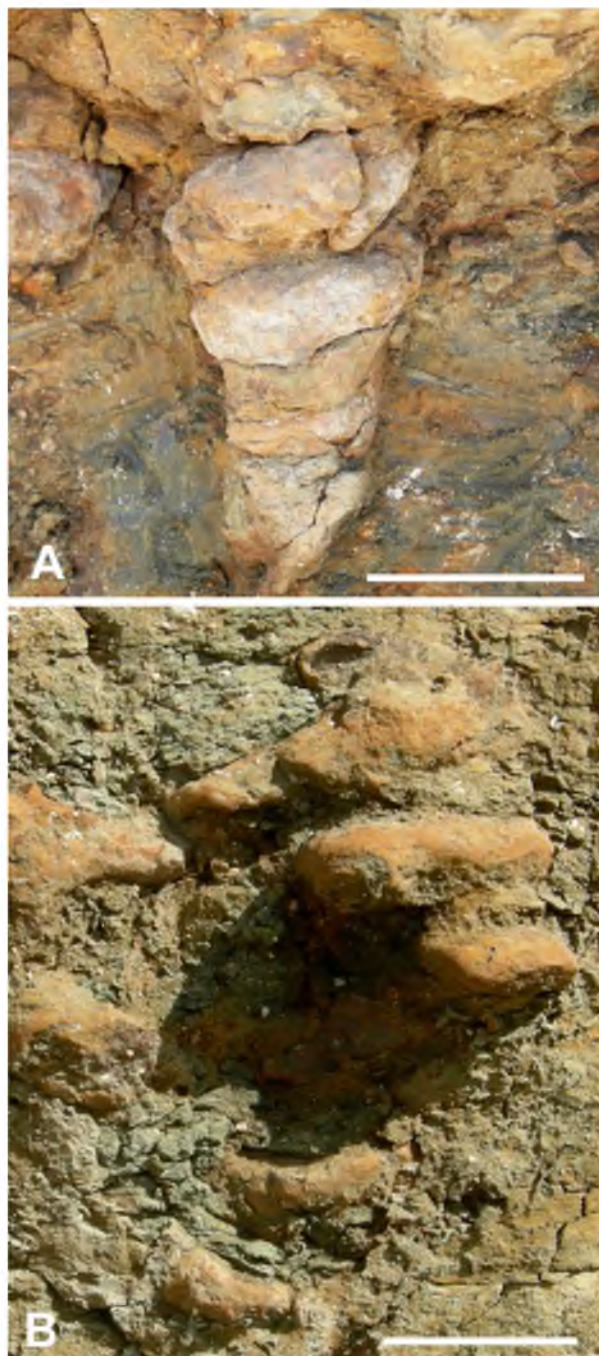


Figure 3.7 Concretionary burrow fill. A and B *Gyrolithes* isp. at the top of the MGB. Scale bars 5 cm.



Figure 3.8 Concretionary burrow fill. A) *Spongiomorpha* isp. showing bioglyphs (white arrow) on burrow wall. Scale bar 2 cm.; B) concretionary burrow fill of *Spongiomorpha* isp. showing the tapering blind alcoves (black arrows) that typify the ichnogenus. Scale bar 3 cm.



Figure 3.9 *Piscichnus* isp., a ray feeding trace, at Stone City Bluff. Scale bar 5 cm.

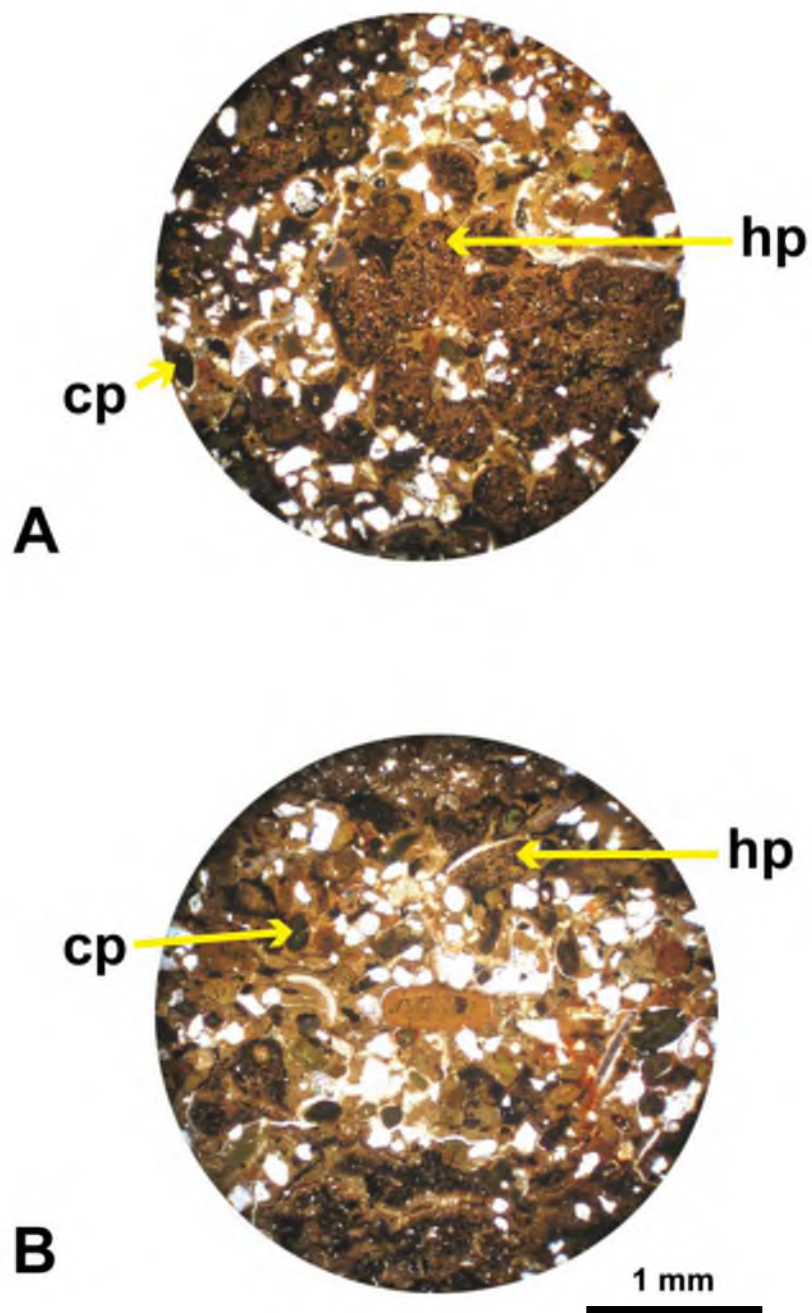


Figure 3.10 Photomicrographs of small clay pellets (**cp**) and larger pellets (**hp**) of heterogeneous composition. A) sample TX-8; B) TX-9 (see Figure 3.4).

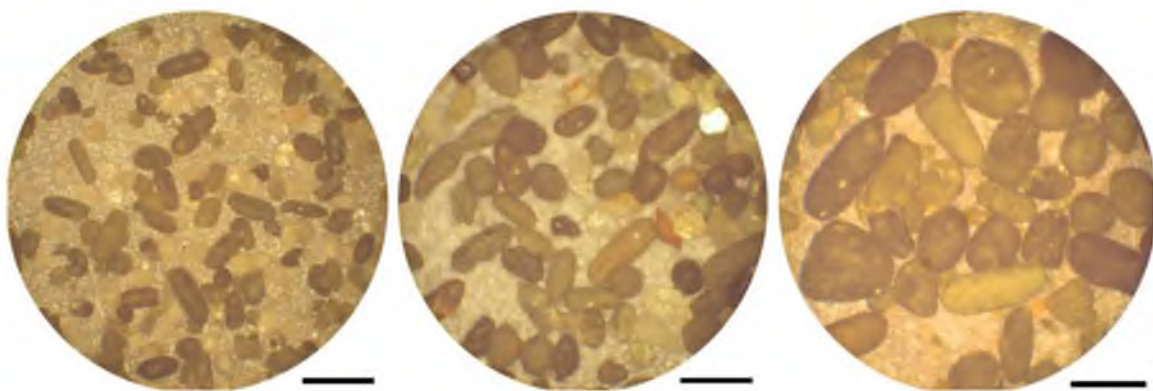


Figure 3.11 Clay pellets (separated via Franz magnetic separator) from central bed of MGB from three successive sieve fractions representing pellet size range. Scale bars 0.5 mm.

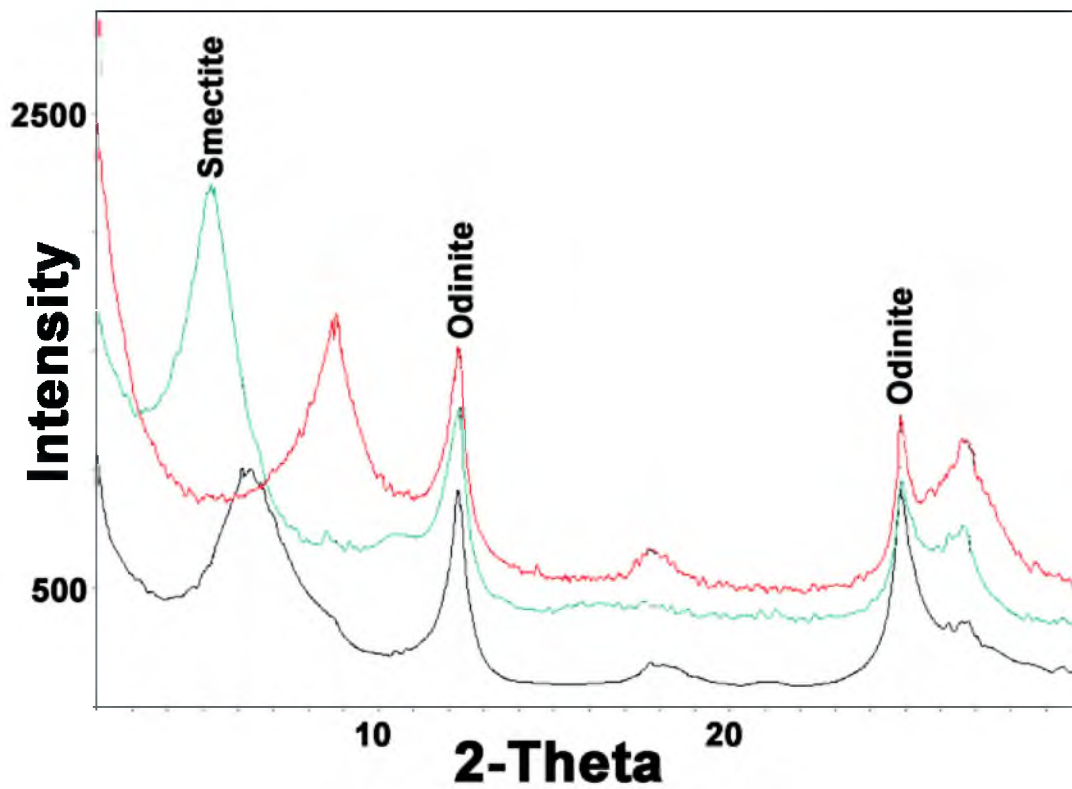


Figure 3.12 X-ray diffractogram of 2-micron clay fraction in sample TX-8 (see Figure 3.4). Black line, air-dried; green line, glycolated; red line, heated to 375°C.

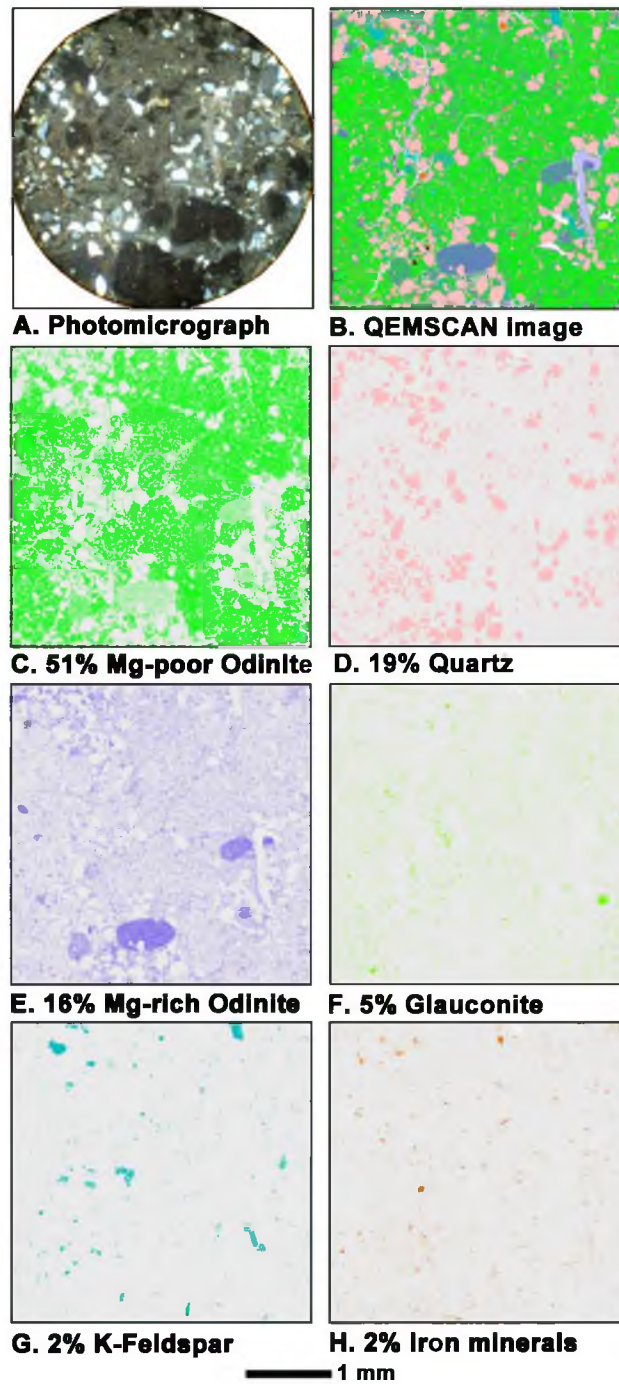


Figure 3.13 QEMSCAN images of sample TX-8 (see Figure 3.4). A) Thin section view (plane light) of scanned region; B) QEMSCAN view (false colors) showing constituent minerals in same scanned region; C-H) textural distribution of key constituent minerals (in false colors).

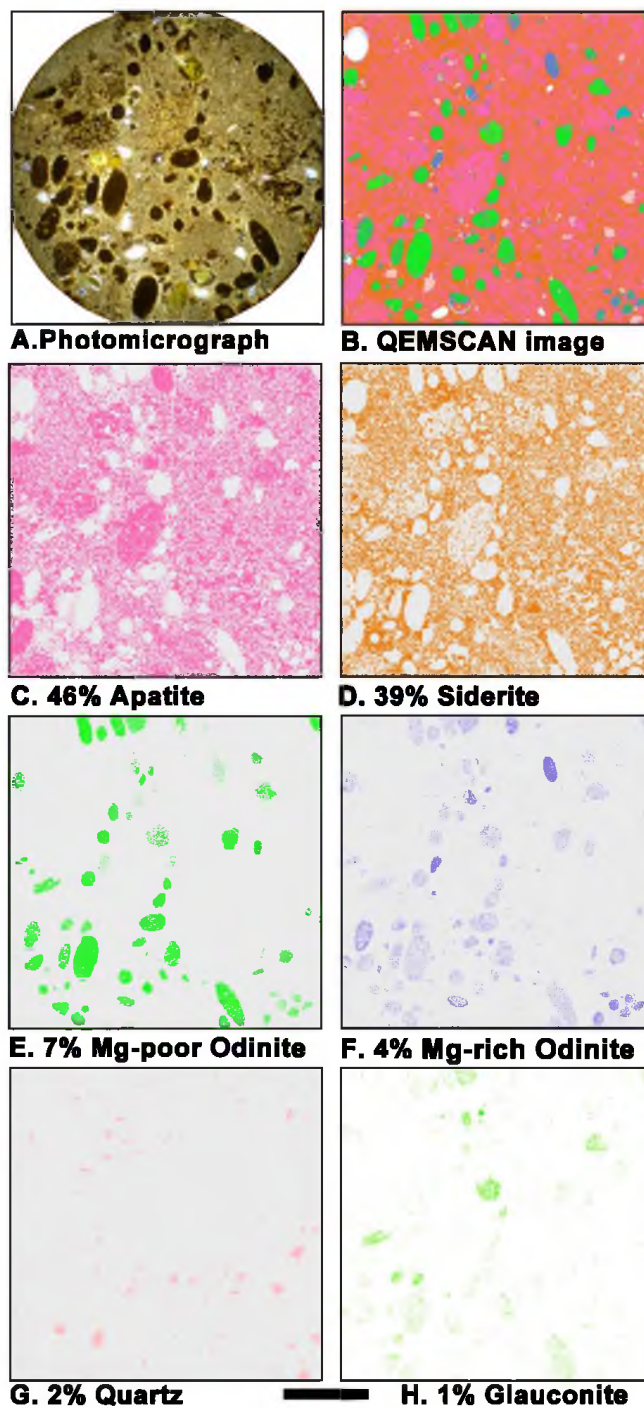


Figure 3.14 QEMSCAN images of sample CON-9 (see Figure 3.4). A) Thin section view (plane light) of scanned region; B) QEMSCAN view (false colors) showing constituent minerals in same scanned region; C-H) textural distribution of key constituent minerals (in false colors). Scale bar 1 mm.

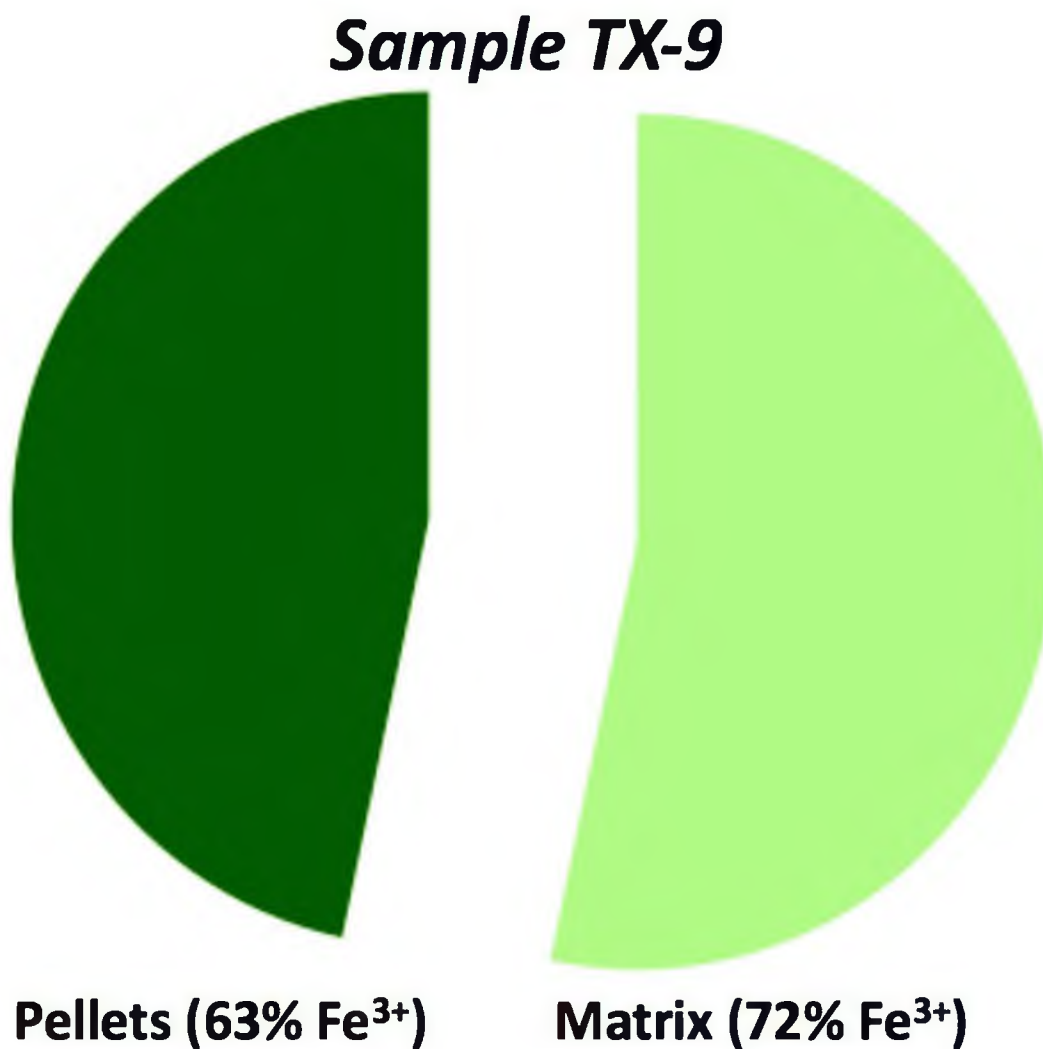


Figure 3.15 Mössbauer analysis of sample TX-9 (see Figure 3.4) showing Fe³⁺ percent of matrix and pellets. Lower Fe³⁺ content in pellets suggests that the pellets provide a reducing microenvironment, as would be expected for fecal pellets.

References

- Bailey, S.W., 1988, Odinite: A new dioctahedral-trioctahedral Fe (super 3+)-rich 1: 1 clay mineral: *Clay Minerals*, v. 23, no. 3, p. 237–247.
- Bohaty, S.M., and Zachos, J.C., 2003, Significant Southern Ocean warming event in the late middle Eocene: *Geology*, v. 31, no. 11, p. 1017–1020.
- Breard, S.Q., and Stringer, G.L., 1999, Integrated paleoecology and marine vertebrate fauna of the Stone City Formation (middle Eocene), Brazos River section, Texas: *Transactions of the Gulf Coast Association of Geological Societies*, v. 49, p. 132–143.
- Bromley, R.G., and Ekdale, A.A., 1986, Composite ichnofabrics and tiering of burrows: *Geological Magazine*, v. 123, no. 1, p. 59–65.
- Cadée, G.C., 2001, Sediment dynamics by bioturbating organisms: Ecological comparisons of sedimentary shores: *Ecological Studies*, v. 151, p. 127–148.
- Davidoff, A.J., and Yancey, T.E., 1993, Eustatic cyclicity in the Paleocene and Eocene: data from the Brazos River Valley, Texas: *Tectonophysics*, v. 222, no. 3-4, p. 371–395.
- Dyar, M.D., Agresti, D.G., Schaefer, M.W., Grant, C.A., and Sklute, E.C., 2006, Mössbauer spectroscopy of Earth and planetary materials: *Annual Review of Earth and Planetary Science*, v. 34, p. 83–125.
- Ekdale, A.A., Bromley, R.G., and Pemberton, S.G., 1984, Ichnology: the use of trace fossils in sedimentology and stratigraphy, *Society of Economic Paleontologists and Mineralogists, SEPM short course*, no. 15, 317 p.
- Emerson, J.H., and Emerson, B., 2001, Middle Eocene Claiborne Group invertebrate fossils from Stone City Bluff, Burleson County, Texas, *North Texas Paleogene References*, John H. Emerson, publisher, Houston, 136 p.
- Gibert, J.M.D., and Ekdale, A.A., 2010, Paleobiology of the crustacean trace fossil *Spongeliomorpha iberica* in the Miocene of southeastern Spain: *Acta Palaeontologica Polonica*, v. 55, no. 4, p. 733–740.
- Goldring, R., Cadée, G.C., and Pollard, J., 2007, Climatic control of marine trace fossil distribution: *Trace Fossils: Concepts, Problems, Prospects*, Amsterdam, Elsevier, p. 159–171.
- Goldring, R., Cadée, G.C., D'Alessandro, A., De Gibert, J.M., Jenkins, R., and Pollard, J.E., 2004, Climatic control of trace fossil distribution in the marine realm: *Geological Society, London, Special Publications*, v. 228, no. 1, p. 77–92.

- Harding, S.C., Nash, B.P., Petersen, E.U., Ekdale, A.A., Bradbury, C.D., and Dyar, M.D., 2014, Mineralogy and Geochemistry of the Main Glauconite Bed in the Middle Eocene of Texas: Paleoenvironmental Implications for the Verdine Facies: *PloS One*, v. 9, no. 2, p. e87656.
- Howard, J.D., Mayou, T.V., and Heard, R.W., 1977, Biogenic sedimentary structures formed by rays: *Journal of Sedimentary Research*, v. 47, no. 1, 339–346.
- Huggett, J.M., Gale, A.S., and McCarty, D., 2010, Petrology and palaeoenvironmental significance of authigenic iron-rich clays, carbonates and apatite in the Claiborne Group, Middle Eocene, NE Texas: *Sedimentary Geology*, v. 228, no. 3-4, p. 119–139.
- Knaust, D., and Bromley, R.G., 2012, Trace Fossils as Indicators of Sedimentary Environments: Amsterdam, Elsevier, *Developments in Sedimentology*, v. 64, 901 p.
- Martinell, J., De Gibert, J.M., Domènech, R., Ekdale, A.A., and Steen, P.P., 2001, Cretaceous ray traces?: An alternative interpretation for the alleged dinosaur tracks of La Posa, Isona, NE Spain: *Palaios*, v. 16, no. 4, p. 409–416.
- Needham, S.J., Worden, R.H., and McIlroy, D., 2004, Animal-sediment interactions: the effect of ingestion and excretion by worms on mineralogy: *Biogeosciences*, v. 1, no. 2, p. 113–121.
- Odin, G.S., 1988, Green Marine Clays: Oolitic Ironstone Facies, Verdine Facies, Glaucony Facies and Celadonite-Bearing Facies—A Comparative Study, Amsterdam, Elsevier, *Developments in Sedimentology*, 445 p.
- Pemberton, S.G., and Frey, R.W., 1985, The Glossifungites ichnofacies: modern examples from the Georgia coast, USA: *Biogenic Structures: Their Use in Interpreting Depositional Environments (SP35): The Society of Economic Paleontologists and Mineralogists (SEPM)*, no. 35, 237–259.
- Pestitschek, B., Gier, S., Essa, M., and Kurzweil, H., 2012, Effects of weathering on glauconite: Evidence from the Abu Tartur Plateau, Egypt: *Clays and Clay Minerals*, v. 60, no. 1, p. 76–88.
- Stanton Jr, R.J., 1979, The Stone City Formation, *in* Claiborne Sediments of the Brazos Valley, Southeast Texas: Field Trip Guidebook, Houston, published by The Houston Geological Society, p. 73–77.
- Stanton Jr, R.J., and Nelson, P.C., 1980, Reconstruction of the trophic web in paleontology: community structure in the Stone City Formation (Middle Eocene, Texas): *Journal of Paleontology*, v. 54, no. 1, p. 118–135.
- Stanton Jr, R.J., and Warme, J.E., 1971, Stop 1: Stone City Bluff: Trace fossils. A field guide to selected localities in Pennsylvanian, Permian, Cretaceous and Tertiary rocks

of Texas and related papers, *in* Perkins, B.F., ed., The Society of Economic Paleontologists and Mineralogists (SEPM), v. 71, p. 2–10.

Stenzel, H.B., 1934, Decapod crustaceans from the Middle Eocene of Texas: *Journal of Paleontology*, v. 8, no. 1, p. 38–56.

Stenzel, H.B., Krause, E.K., and Twining, J.T., 1957, Pelecypoda from the Type Locality of the Stone City Beds (Middle Eocene) of Texas: Austin, Texas, Bureau of Economic Geology, University of Texas, The University of Texas publication, no 5704: February 15, 1957, 237 p.

Yancey, T.E., 1995, Depositional trends in siliciclastic deposits of the Stone City transgressive systems tract, Middle Eocene, Texas: *Gulf Coast Association of Geological Societies Field Guide*, p. 581–586.

Yancey, T.E., and Davidoff, A.J., 1994, Paleogene sequence stratigraphy of the Brazos River section, Texas: *Gulf Coast Association of Geological Societies Field Trip Guide*, p. 104.

Zachos, J.C., Dickens, G.R., and Zeebe, R.E., 2008, An early Cenozoic perspective on greenhouse warming and carbon-cycle dynamics: *Nature*, v. 451, no. 7176, p. 279–283.

Zuschin, M., and Stanton Jr, R.J., 2002, Paleocommunity reconstruction from shell beds: a case study from the Main Glauconite Bed, Eocene, Texas: *Palaios*, v. 17, no. 6, p. 602–614.

CHAPTER 4

MINERALOGY AND GEOCHEMISTRY OF THE MAIN GLAUCONITE BED IN THE MIDDLE EOCENE OF TEXAS: PALEOENVIRONMENTAL IMPLICATIONS FOR THE VERDINE FACIES

This article is reproduced under the broad Creative Commons Attribution (CC BY) license developed and applied by PLOS. This license was developed to facilitate Open Access (OA), which is free immediate access to, and unrestricted reuse of, original works of all types. Under this license, authors retain ownership of the copyright for their content, but allow anyone to download, reuse, reprint, modify, distribute and/or copy the content as long as the original authors and source are cited. No permission is required from the authors or the publishers.

Mineralogy and Geochemistry of the Main Glauconite Bed in the Middle Eocene of Texas: Paleoenvironmental Implications for the Verdine Facies

Sherie C. Harding^{1*}, Barbara P. Nash¹, Erich U. Petersen¹, A. A. Ekdale¹, Christopher D. Bradbury¹, M. Darby Dyar²

1 Department of Geology and Geophysics, University of Utah, Salt Lake City, Utah, United States of America, **2** Department of Astronomy, Mount Holyoke College, South Hadley, Massachusetts, United States of America

Abstract

The Main Glauconite Bed (MGB) is a pelleted greensand located at Stone City Bluff on the south bank of the Brazos River in Burleson County, Texas. It was deposited during the Middle Eocene regional transgression on the Texas Gulf Coastal Plain. Stratigraphically it lies in the upper Stone City Member, Crockett Formation, Claiborne Group. Its mineralogy and geochemistry were examined in detail, and verdine facies minerals, predominantly odinite, were identified. Few glauconitic minerals were found in the green pelleted sediments of the MGB. Without detailed mineralogical work, glaucony facies minerals and verdine facies minerals are easily mistaken for one another. Their distinction has value in assessing paleoenvironments. In this study, several analytical techniques were employed to assess the mineralogy. X-ray diffraction of oriented and un-oriented clay samples indicated a clay mixture dominated by 7 and 14Å diffraction peaks. Unit cell calculations from XRD data for MGB pellets match the odinite-1M data base. Electron microprobe analyses (EMPA) from the average of 31 data points from clay pellets accompanied with Mössbauer analyses were used to calculate the structural formula which is that of odinite: $\text{Fe}^{3+}_{0.89} \text{Mg}_{0.45} \text{Al}_{0.67} \text{Fe}^{2+}_{0.30} \text{Ti}_{0.01} \text{Mn}_{0.01} \Sigma = 2.33 (\text{Si}_{1.77} \text{Al}_{0.23}) \text{O}_{5.00} (\text{OH})_{4.00}$. QEMSCAN (Quantitative Evaluation of Minerals by Scanning Electron Microscopy) data provided mineral maps of quantitative proportions of the constituent clays. The verdine facies is a clay mineral facies associated with shallow marine shelf and lagoonal environments at tropical latitudes with iron influx from nearby runoff. Its depositional environment is well documented in modern nearshore locations. Recognition of verdine facies clays as the dominant constituent of the MGB clay pellets, rather than glaucony facies clays, allows for a more precise assessment of paleoenvironmental conditions.

Citation: Harding SC, Nash BP, Petersen EU, Ekdale AA, Bradbury CD, et al. (2014) Mineralogy and Geochemistry of the Main Glauconite Bed in the Middle Eocene of Texas: Paleoenvironmental Implications for the Verdine Facies. PLOS ONE 9(2): e87656. doi:10.1371/journal.pone.0087656

Editor: Lee A. Newsom, The Pennsylvania State University, United States of America

Received: May 6, 2013; **Accepted:** December 31, 2013; **Published:** February 4, 2014

Copyright: © 2014 Harding et al. This is an open-access article distributed under the terms of the Creative Commons Attribution License, which permits unrestricted use, distribution, and reproduction in any medium, provided the original author and source are credited.

Funding: This project was funded by research grants to AA Ekdale, PI, from the ACS Petroleum Research Fund (PRF grant 47560-AC-8) and Division of Earth Sciences of the National Science Foundation (NSF grant EAR-1052661) and by student grants to SC Harding from the Gulf Coast Association of Geological Societies and the Department of Geology and Geophysics of the University of Utah. The funders had no role in study design, data collection and analysis, decision to publish, or preparation of the manuscript.

Competing Interests: The authors have declared that no competing interests exist.

* E-mail: sherie.harding@utah.edu

Introduction

Green clay-rich sediment is recognized throughout the geologic record, and the paleoenvironmental implications of green clay facies are not always understood clearly. This study reports the clay mineralogy and geochemistry of the Main Glauconite Bed (MGB), a shelly and sandy mudstone that has an olive-gray hue and is bioturbated, pelleted, and trace fossiliferous, with diverse body fossils. These characteristics, especially the abundant ovoidal, small clay pellets, probably led to its being named the Main Glauconite Bed. However, very few glauconitic minerals are present in the MGB.

The study area, Stone City Bluff, is located on the Gulf of Mexico Coastal Plain in east-central Texas (Figure 1). A detailed geologic map (Figure 2) shows the underlying Wilcox Group, formations of the Claiborne Group, and overlying formations of the Jackson Group. The Crockett Formation is also known as Cook Mountain Formation. The Middle Eocene, stratigraphic section (Figure 3) includes the Stone City Member, Crockett

Formation. The upper part of the section outcrops along the south bank of the Brazos River in Burleson County, where the MGB is a prominent 1.7 m thick greensand unit. The MGB in outcrop at Stone City Bluff is pictured in Figure 4. Sample locations in the central zone and concretionary burrows at the top of the MGB are shown (Figure 5).

The mineralogy and geochemistry of the central zone and top layer of the MGB are different. The central part of the MGB contains heterogeneous green marine clay that is intensely bioturbated with a significant fraction of fecal pellets. The top part of the MGB is lined with concretions of filled burrows that extend down into the central MGB. These concretions are composed of siderite and apatite that formed as cementing agents. The green minerals in the central zone of the MGB warrant close examination, as do the contrasting minerals at the top of the MGB, because they reflect a change in the depositional environment.

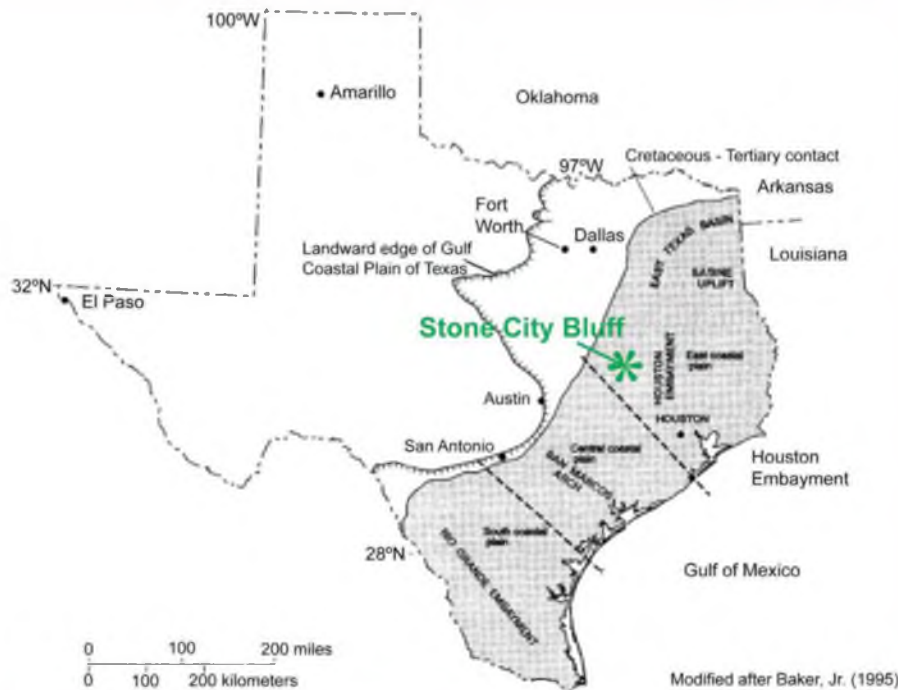


Figure 1. Location of the Stone City Bluff study area on the Texas Gulf Coastal Plain [59].
doi:10.1371/journal.pone.0087656.g001

Previous Work on the MGB

The MGB and associated stratigraphy have been studied extensively by other workers who have offered various mineralogical and paleoenvironmental interpretations [1–9]. Thornton [10] reported, in a master's thesis, that the green marine clay of the MGB had the characteristics of odinite. Huggert et al. [11] described the geochemistry of authigenic minerals in the Claiborne Group, including samples from Stone City Bluff, and concluded that the composition was dark green serpentine-rich mixed layer clay. This characterization of the clay mineralogy and geochemistry of the MGB clay pellets, as well as its ichnology (evidence from trace fossils), have not received detailed treatment until now. It contributes to a coordinated approach to understanding the complex processes during accumulation of the MGB.

Previous interpretations of the depositional environment of the Stone City Member suggest that it was dynamic and complex. Davidoff and Yancey [12] documented eustatic sea-level changes and identified major sequence boundaries and maximum flooding surfaces in the Middle Eocene and some parasequences that may be capped by an exposure surface. The regional sequence stratigraphy testifies to numerous sea-level fluctuations during the early Tertiary (Figure 6). Stanton and Nelson [13] and Zuschin and Stanton [9] reconstructed the paleocommunity of the MGB, and they identified a time-averaged, parautochthonous, highly diverse fossil assemblage in the central bed along with a complex sedimentologic and taphonomic history due to reworking by winnowing and bioturbation. Stanton and Warme [3] examined the trace fossils at Stone City Bluff, and they suggested an interfingering of off-delta transgression of the sea into interdeltic bays and sounds, marked by a gradual change from restricted and perhaps brackish delta-margin environments and biota to a

normal marine environment and biota. Berg [14] interpreted the Stone City section as restricted marine or lagoonal environment. Yancey [6] reported on depositional trends of the Stone City transgressive-systems-tract, and he suggested that it is a transgressive depositional system in an area characterized by high sedimentation rate during progressive marine deepening. He proposed that the Stone City Bluff section is capped by a maximum flooding surface of regional extent. Previous interpretations of paleoenvironment are varied. The mineralogical and geochemical findings in this study offer further information and complement findings in previous studies.

Background on Green Clay Minerals

Green clay minerals. Published research on green minerals in sedimentary rocks reveals a lack of consistency in use of mineralogical terms. Terms such as "glaucinite," "greensands," "glaucony," or "glaucinitic minerals," are used frequently in the literature, and confusion persists. Glaucinite, strictly speaking, is a series name for dioctahedral, interlayer-deficient micas with compositions of $K_{0.8}R^{3+}_{1.33}R^{2+}_{0.67}Al_{0.13}(Si_{3.87})O_{10}(OH)_2$ [15]. The term also has been employed as a common field term for small, rounded, green to black pellets and grains. Field identification often was confined to morphological appearance and color. In this report, as suggested by Odin [16], the term "glaucinitic minerals" is used for the minerals that are rich in Fe^{3+} with a potassium content greater than 2 wt.% K_2O in the interlayer. In the case of the MGB, the few glaucinitic minerals detected were usually confined to sparse, isolated grains.

Numerous studies have attempted to characterize clay mineralogy in marine sedimentary environments [11,16–24]. Odin's treatise on *Green Marine Clays* inventories green minerals in the

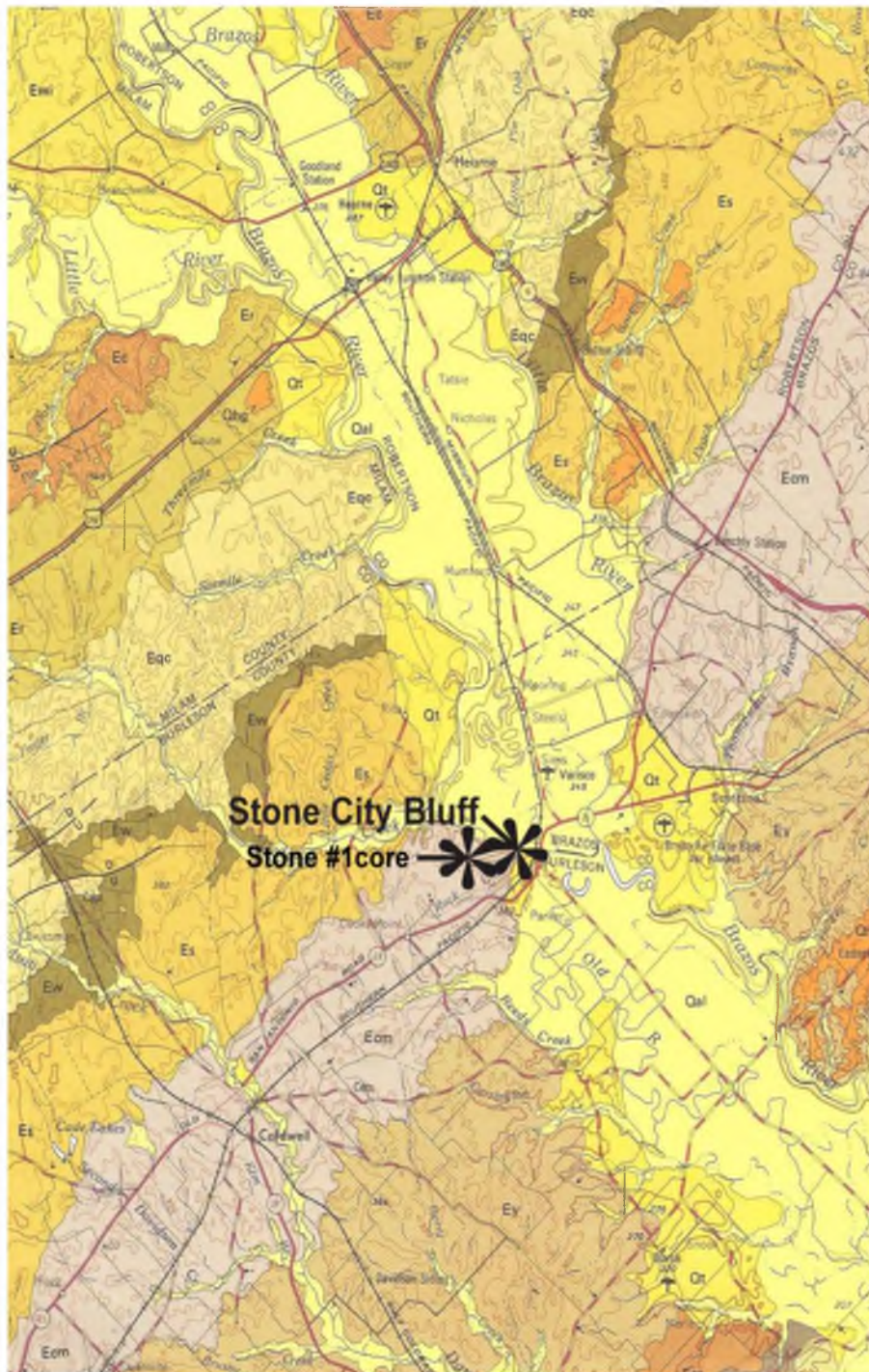


Figure 2. Geologic Atlas of Texas, Austin Sheet, Burleson and Brazos Counties [60]. Stone City Bluff and Stone #1 core located. Wilcox Group (Ewi); Crockett Fm., also known as the Cook Mountain Fm. (Ecm); and Caddell Fm. of the Jackson Group (Eca).
doi:10.1371/journal.pone.0087656.g002

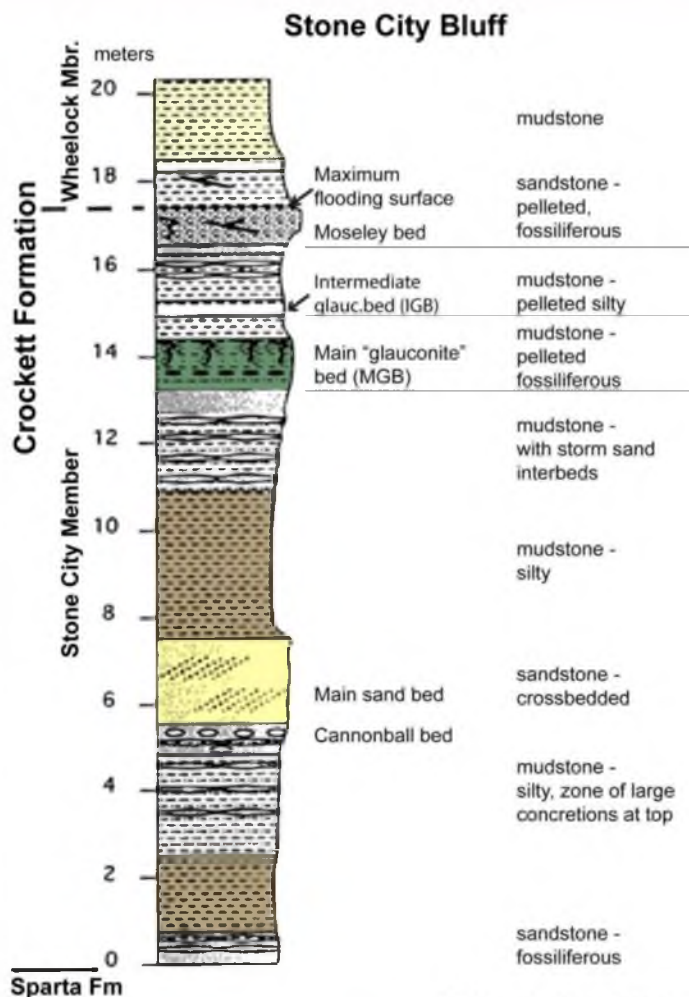


Figure 3. Middle Eocene stratigraphic section includes Stone City Member, Crockett Formation, Claiborne Group (modified after Yancey [6]).

doi:10.1371/journal.pone.0087656.g003

modern marine environment and separates green marine clays into four facies: oolitic ironstone facies, verdine facies, glaucony facies and celadonite-bearing facies, based on examples on today's ocean floors. Odin [16] demonstrated that clay minerals on the sea floor progressively transform by slow cation exchange. The term "glaucony" is introduced to designate the fully marine facies characterized by a green pigment made of 2:1 type clay minerals that include glauconitic minerals, which form today at water depths around 50 m to as much as 1000 m on the sea floor.

The verdine facies is represented by a variety of chlorite-like clays, with an alternative mineralogy and geological significance. The verdine facies is identified in modern, shallow, tropical environments, in proximity to a terrigenous clastic source with iron influx. It is characteristic of bottom sediments of nearly normal salinity, but at a shallower depth range of 15 to 60 m. Mineralogically, verdine facies clays are uniquely different from those in the glaucony facies. Glauconitic minerals are absent from

the verdine facies, while 7 and 14Å clays are present. Odin identified new clay minerals for the verdine facies, initially termed phyllite-V and phyllite-C clays, and later named odinite and iron smectite [16,24].

Authigenesis. Mineral authigenesis in sea-floor sediments can occur as glauconitization or verdinization, processes by which a sea-floor substrate is progressively modified to glauconitic minerals or to verdine minerals, respectively [16]. These result from interaction between open seawater and sea-floor sediment, and they are influenced by latitude, sea-floor temperature and bathymetric setting on the continental shelf.

Glauconitization results in a continuum of minerals from K-poor, disordered glauconitic smectite to K-rich, ordered glauconitic mica. Stages of development are defined by increasing potassium oxide content where 2 wt.%–4 wt.% K₂O is nascent stage, 4 wt.%–6 wt.% K₂O is slightly evolved (slightly mature), 6 wt.%–8 wt.% K₂O is evolved (mature), and greater than 8 wt.%



Figure 4. Stone City Bluff outcrop photos, the MGB is green and nearly vertical, A) looking west, upstream (the subject in this photograph has given written informed consent, as outlined in the PLOS consent form, to publication of their photograph), B) looking east, downstream.

doi:10.1371/journal.pone.0087656.g004

K_2O is highly evolved (highly mature) glauconitic minerals [16,21,25–29]. The level of maturity is a reflection of residence time on the sea floor in sediment-starved conditions. Potassium, at 0.4 parts per thousand (ppt), is one of six major dissolved constituents in normal seawater [30]. It is available for uptake during glauconitization. Evolution to the highly mature stage takes 10^3 to 10^6 years in recent material [16]. Optimal conditions for

glauconitization include a sea-floor temperature of 10–15°C, and unrestricted seawater circulation, allowing for winnowing accompanied by a slow sediment accumulation rate. Glauconitization commonly occurs in a substrate rich in fecal pellets and/or foraminiferal tests, which provide micro-reducing environments favorable for glauconitization. Oxidizing conditions may prevail in the surrounding substrate due to winnowing currents. Glauconitic

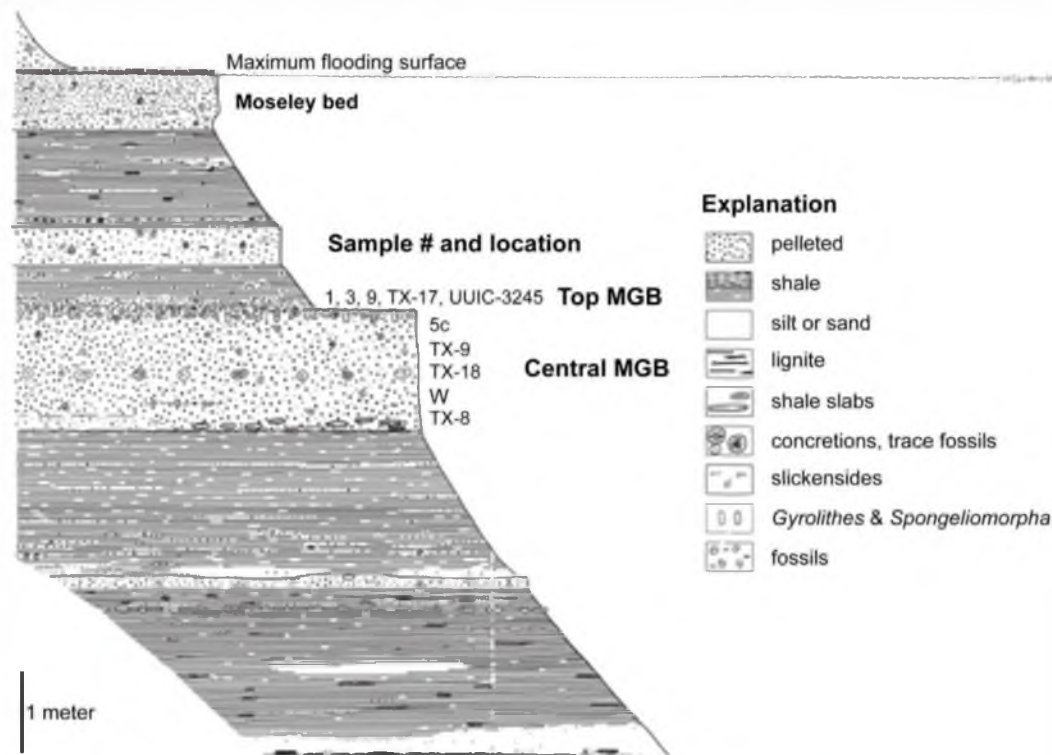


Figure 5. Upper units of the Stone City Member, sample number and location (modified after Stenzel [2]).
doi:10.1371/journal.pone.0087656.g005

minerals commonly are associated with body fossils and trace fossils indicating sufficient oxygen to support benthic life. The glauconitization process may be halted at any stage of the maturity continuum if the environment becomes unsuitable because of a change in sea level or burial depth. A high rate of detrital influx will inhibit or entirely prevent glauconitization. Once formed, glauconitic minerals are highly stable and resistant to dissolution in the marine environment, which suggests that they can be reworked or transported with little degradation in a changing environment [16,21,25–29].

Verdinzation, on the other hand, requires a shorter residence time on the sea floor [16]. Verdine facies minerals form rather quickly, probably in thousands of years, because of increased sea-floor temperature (~25°C). They tend to occur in shallower water under normal salinity and basic pH (7.5–8.5). Observed water depth where verdine minerals are forming today is between 15 and 60 m, and locally in 5 m depths, in common association with fecal pellets. Circulating currents are required in proximity to continental water input and abundant Si, Mg, and Fe in tropical to subtropical, warm water environments (Figure 7) [16,24,32]. Verdinzation progresses from light green to dark green clay minerals. Verdine facies clay minerals are comprised primarily of two clay mineral species characterized by 7.2 and 14.5Å x-ray diffraction peaks [16].

The predominant verdine mineral is odinite, which is an iron and magnesium 1:1, 7Å clay. It is classified by some authors in the kaolin-serpentine group and the dioctahedral kaolin sub-group of phyllosilicates [15] or by other authors in the serpentine group

[33]. Odinite was first described by Bailey [24] as serpentine-like, intermediate between dioctahedral and trioctahedral. It has total iron of about 75% Fe³⁺ and 25% Fe²⁺, and a nominal structural formula of [Fe³⁺,Mg,Al,Fe²⁺;Ti,Mn]₂(Si,Al)₄O₁₀(OH)₂ [15]. Odinite is commonly identified in modern environments and is considered a possible analog to the oolitic ironstone facies in ancient rocks [16,24,32]. Although few possible occurrences of odinite from the geologic record have been reported in the literature odinite, or its alteration products, may be more common than is generally recognized.

Verdinzation and glauconitization are processes that may be influenced by biogenic activity. Sediment-starved shelf environments often are characterized by high biological productivity. Biogenic activity, such as recycling of seafloor sediments by deposit-feeding and suspension-feeding organisms, can be prevalent in green marine clay environments at shelf depths. The effect of biological activity on clay mineral authigenesis, mineral growth and/or silicate weathering, is significant [23]. The MGB is a highly bioturbated, pelleted and fossiliferous unit. During deposition, biogenic activity on the seafloor was intense [2]. The existing mineralogy and geochemistry of the MGB may have been affected by animal-sediment interaction.

Diagenesis and weathering. Diagenesis refers to the physical and chemical reactions occurring in sediment after burial. Glauconitic minerals may be modified after burial, often showing an Al increase concomitant with Fe decrease. During weathering, glauconitic minerals may be altered in color and chemistry. In one study, Pestitschek et al. [34] described degradation over time

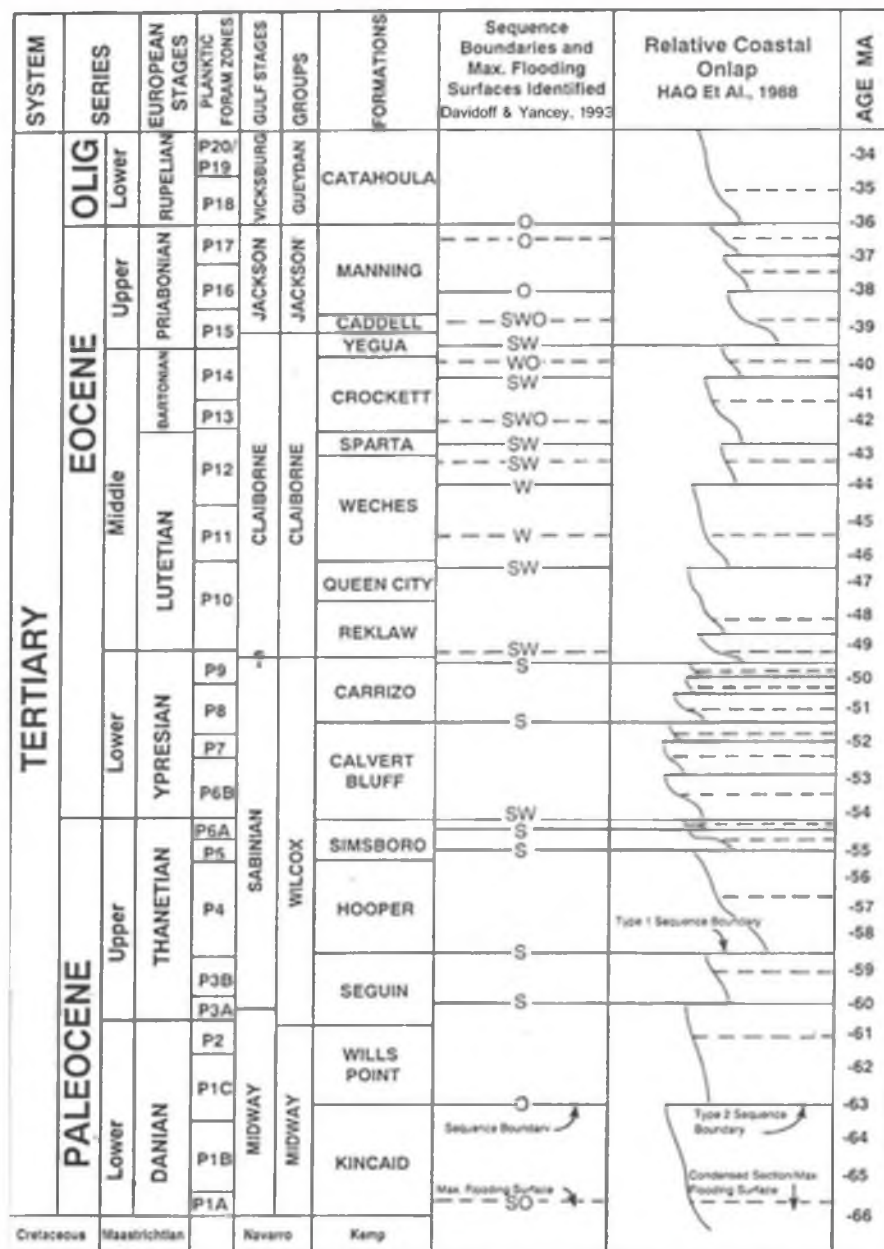


Figure 6. Stratigraphic chart and related lithostratigraphy of the Brazos River Valley, major sequence boundaries (solid lines) and maximum flooding surfaces (dashed lines), identified by S = seismic; W = well logs; O = outcrop (modified after Davidoff & Yancey [7]).

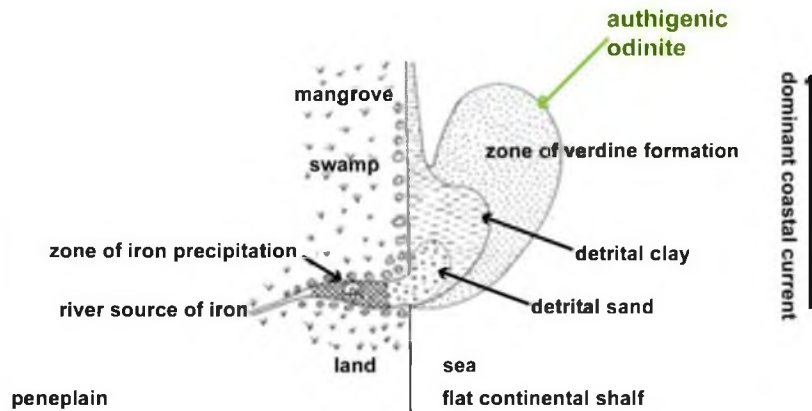
doi:10.1371/journal.pone.0087656.g006

between fresh and weathered glauconite. They compared chemical results of Upper Cretaceous glauconitic minerals on the surface with core samples in the subsurface and demonstrated a loss of both Fe and K during weathering. They suggested that weathering reverses the glauconitization process, as glauconitic minerals degrade to smectite. They found that fresh samples were

dark green, whereas the weathered samples were olive green to yellowish brownish green [34].

The MGB exhibits a variety of pellet colors, which may vary within a given pellet. This may be a function of different stages of diagenesis. Also, the possibility of weathering is suspected since the MGB is subaerially exposed. When mineralogical results of surface

Tropical Climate - Warm Sea Water Verdine Facies Model



(modified after Odin, 1988)

Figure 7. Diagrammatic verdine facies model depicting the idealized paleoenvironment at a tropical river mouth (modified after Odin [16]).

doi:10.1371/journal.pone.0087656.g007

and core samples from the MGB were compared, there was no evidence of degradation due to weathering. The MGB showed similar mineral composition in both core and in outcrop samples. Therefore, it may be reasonably assumed that weathering is not an important influence on the MGB pellets, and that the lack of glauconitic minerals in the MGB is not due to weathering. Glauconitic minerals are not known to alter to odinite [16].

The fate of odinite, a verdine facies mineral, during diagenesis and weathering is not well known. According to Ku and Walter [32], odinite forms very quickly and apparently is metastable, because most of the reported occurrences of odinite are less than 20,000 years old. When odinite is exposed to fully oxygenated seawater or atmospheric oxygen, it changes color from grayish green to yellowish red, and it has been known to oxidize to goethite. Several workers have suggested the verdine facies as a modern precursor for ancient oolitic ironstones and grain-coating chlorite [16,32]. Huggett et al. [11] suggest that serpentine-rich mixed-layer clays of the Claiborne Group may be diagenetically altered odinite, and that serpentine is intermediate between odinite and berthierine. Ryan and Hillier [35] suggest that odinite, or evolved verdine minerals, may be precursor to authigenic chlorite in the Jurassic Sundance Formation of Wyoming. Whether the MGB is comprised of authigenic verdine facies minerals or altered authigenic verdine minerals, the paleoenvironmental implications are essentially the same.

Methods

Sampling

The Stone City Bluff outcrop of the Crockett Formation is readily accessible for sampling. Concretionary burrows at top of the MGB can be removed easily due to the friable nature of the sediment. The upper section of Stone City Bluff, particularly the

MGB, was sampled for this study. Twenty-seven samples were collected at 60 cm intervals from two measured sections. Concretions, representative of filled burrows, were collected from the top of the MGB and from tumbled blocks. Eight samples were retrieved from a drill core (Stone #1 core at Texas A & M University). These represent unweathered samples of the Stone City Member. Additional samples, including concretionary burrows and pelleted sediment, were made available by JE Warne (Colorado School of Mines) [3]. Polished thin sections were prepared, and standard analytical procedures were used as described below.

The sections were measured and samples were collected via the public access site at the highway bridge over the Brazos River. No specific permissions were required. The field studies did not involve any endangered or protected species. The project did not involve any non-human primates or any other vertebrate animals.

Mineral Identification

Petrography of each thin section was described using a polarizing light microscope, and a variety of analytical techniques were employed to ascertain mineral composition and texture. X-ray diffraction (XRD) was carried out on oriented and unoriented samples to determine clay mineralogy. Electron microprobe (EMPA) analyses on selected pellets and matrix determined chemical composition and assisted with clay mineral identification. Mossbauer analyses were done on clay matrices and pellets to constrain mineralogy and determine iron oxidation state, which has bearing on EMPA data interpretation and significance for paleoenvironmental interpretation. QEMSCAN (Quantitative Evaluation of Minerals by Scanning Electron Microscopy) data were obtained to provide mineral maps and a textural view that complements, enhances, validates and quantifies the petrographic observations.

X-ray diffraction analysis. Clay minerals were examined from five central MGB samples (TX-8, W, TX-18, TX-9 & 5c) by X-ray diffraction (XRD) analyses. The 2 μm clay fraction was extracted by crushing, dispersion, and two-stage centrifuge. Oriented clay mounts were prepared and analyzed under conditions of air dried, ethylene glycolated, and heated to 375°C, then to 500°C for one hour. These were analyzed at 2° per minute from zero to 30° 2 θ , and examined in composite diffractograms. Randomly oriented powders were prepared by gently hand crushing bulk samples from TX-8 & TX-9 comprised of pellets and clay matrix from the central MGB. Pellets in samples 5c and TX-MGB were concentrated using a Frantz Magnetic Separator. TX-MGB is comprised of pellets from TX-8, W & TX-9. These were gently hand crushed and side loaded into an aluminum holder for analysis of unoriented powder. They were then analyzed at 2° per minute from zero to 66°. Eleven (11) peaks were indexed in the refinement, and quartz served as an internal standard. Selected samples were examined at high resolution, 0.5° per minute from 56° to 66° 2 θ .

Electron microprobe analysis. Thirty clay pellets from both the central MGB and the concretionary burrow fill at the top of the MGB, and 14 non-pellet, cement areas were analyzed with a Cameca SX-50 electron microprobe equipped with four wavelength-dispersive spectrometers. Clay pellets were selected for analysis based on color in thin section and false color in QEMSCAN images. In an attempt to locate a potassium X-ray signal, some spot analyses focused on QEMSCAN-identified glauconitic grains, although very sparse. The more numerous clay pellets showed a low potassium signal. One to four spots were analyzed on each pellet for a total of 44 clay analyses. Analytical conditions were 15 keV accelerating voltage, 20 nA beam current, and a defocused beam of 10–20 μm in diameter. A suite of natural minerals was employed as standards, and X-ray intensities were reduced using a phi-rho-z algorithm [36].

Mössbauer spectroscopy. Mössbauer analyses were used to constrain mineralogy and establish the iron oxidation state of pellets and matrix. The slightly magnetic pellets were separated from matrix in three central MGB samples (W, TX-9 & 5c) using a Frantz Magnetic Separator. Concentrated pellets and pellet free matrix were analyzed.

Sample mounts were prepared by gently mixing 30–40 mg of powdered sample with sugar to reduce preferred orientation. The mixtures were placed in a sample holder confined by Kapton tape. Mössbauer spectra were acquired at 295K using a source of ~40 mCi ⁵⁷Co in Rh on a WEB Research Co. model WT302 spectrometer. For each sample, the fraction of the baseline due to the Compton scattering of 122 keV gammas by electrons inside the detector was determined by measuring the count rate with and without a 14.4-keV stop filter (~2 mm of Al foil) in the gamma beam. Compton-corrected absorption was calculated for each individual spectrum using the formulation $A/(1-b)$, where b is the Compton fraction and A is the uncorrected absorption. Run times were 6–48 hours for each spectrum, and baseline counts were ~6–14 million after the Compton correction, as needed to obtain reasonable counting. Data were collected in 1024 channels and corrected for nonlinearity via interpolation to a linear velocity scale, which is defined by the spectrum of the 25 μm Fe foil used for calibration. Data then were folded before fitting.

Data were modeled using an in-house program from the University of Ghent, Belgium, called DIST_3E (an implementation of software described in Wivel and Morup [37]), which uses model-independent quadrupole splitting distributions for which the subspectra are constituted by Lorentzian shaped lines. This program does not presume any particular shape of the distribu-

tion, in contrast to other distribution programs (e.g., Recoil). All Mössbauer data are posted for public use at <http://www.mtholyoke.edu/courses/mdyar/database/>.

In all fits, isomer shift (IS) and quadrupole splitting (QS) of the doublets were allowed to vary, and widths of both peaks in each pair were coupled to vary in unison (i.e. one width for each doublet, but every doublet independent). In a few cases it was necessary to constrain peak widths to lie above a certain value to obtain reasonable parameters, but most spectra were fit with only the minimal constraints described above.

Error bars for Mössbauer measurements are discussed at length by Dyar [31] and Dyar et al. [38] for fits to well-resolved spectra studied here: ± 0.02 mm/s for IS and QS and $\pm 3\%$ absolute on areas.

QEMSCAN analysis. QEMSCAN is an automated mineralogy solution method capable of investigating fine details of samples of interest. Using both energy-dispersive X-ray (EDX) spectra and backscattered-electron imagery (BEI) obtained via an x-y raster scan pattern [39], QEMSCAN measures mineralogical variability across a sample's surface and can be used to quantify modal abundances of mineral species. Prior to each scan, instrument calibration is performed using the procedures outlined by Ayling [40].

Minerals are identified using a reference Species Identification Protocol (SIP), a hierarchical mineral database which determines what elements best fit a measured spectrum [41,42]. For this investigation, the Oil and Gas (O&G) v. 3.3 SIP is used, with an accelerating voltage of 20 Kev and specimen current of ~5 nA, and data are collected using iDiscover 5.2 beta software. A secondary SIP, Log5, also was used; however, it lacks detail in clay typing and therefore is less suitable for identification of verdine clays of interest.

Three representative polished and carbon-coated thin sections from the MGB (TX-18, TX-9 & TX-17) were analyzed using the O&G SIP. Total scan area was 3 by 3 mm, comprised of 9 blocks with sufficient overlap for easy stitching to produce a composite digital image. The resulting field images provide a 2-D view of the mineralogy of the sample illustrated in a color pattern from which quantitative modal mineral abundances can be extracted. Each analysis contains six false color digital images. The first image shows all the minerals detected, coded by various colors. The remaining five images characterize individual minerals textures and abundances. Pellets, grains and matrix are easily differentiated. Grain orientation, pellet size, shape, and abundance also are clearly apparent. QEMSCAN images were used to assist in selection of regions for analysis by electron microprobe.

Results

Petrography

Sediment. In a sedimentologic study of the central MGB, Zuschin and Stanton [9] recognized three microstratigraphic subunits: 1) homogeneous green minerals that they termed glauconitic siltstone, 2) bioturbated bioclastic, pelleted silty sandstone, 3) shell concentrations. Thin sections from the central MGB show bioclasts and pellets in a green clay matrix with quartz fragments. Area per cent, as determined by QEMSCAN, reveals sediment composed of clay pellets, as much as 50%, in a clay matrix. Quartz grains comprise up to 20%, and they are angular and poorly sorted. Shell fragments are a minor constituent, 2 to 4%. At top of the MGB, concretionary burrows contain varying amounts of clay pellets from 3 to 20%, with few quartz grains and shell fragments, less than 3%. Larger heterogeneous pellets (described below), are evident in the concretionary burrow fill.

Pellets. Two pellet types are recognized on the basis of size and composition: smaller clay pellets (cp) and larger heterogeneous pellets (hp). The clay pellets are green to black, tightly compacted ovoids that are easily observable with a hand lens. They are abundant in the central MGB (Figure 8). They also occur in varying amounts as burrow fill inside the concretions at top of the MGB (Figure 9). More obscure are the heterogeneous pellets that are found in both the central MGB and in burrows at the top of the MGB. In the concretionary burrow fill, the heterogeneous pellets were preferentially altered to apatite over siderite, which highlights their visibility, while the clay pellets remained unaltered. The two pellet types are displayed in photomicrographs of samples 3, UUIC-3245, and 9 top of the MGB with adjacent QEMSCAN false color images (Figure 9).

Abundance of clay pellets varies in the central MGB according to the three microstratigraphic subunits described above where they may comprise as much as 50 area %. At the top of the MGB within the concretionary burrows, clay pellets are scattered with some quartz and shell fragments in the matrix of siderite and apatite cement. The smallest clay pellets measure 0.2 mm length and 0.09 mm width, while the largest pellets average 1 mm length and 0.6 mm width. All are ovoid shape with some elongate ovoids. Clay pellets appear well indurated with sharp margins and smooth glossy surfaces. These pellets are thought to be of fecal origin based on their shape and the oxidation state of iron, which is chemically more reducing in the pellets compared to clay matrix. Very few pellets occur as internal filling of foraminifera tests. Angular quartz fragments occur primarily in the clay matrix and are not incorporated in the clay pellets. There is no evidence of internal canals within the clay pellets, as might be expected in decapod crustacean fecal pellets, such as *Palaxius* or *Favreina*. Although the most prominent burrows preserved in the MGB were excavated by decapod crustaceans, the fecal pellets in the sediment were produced by some other, presumably soft-bodied and unpreserved, animals.

The larger, heterogeneous pellets are not obvious in outcrop but are evident in thin section and in QEMSCAN images. Pellet shape in two-dimensional view is oval to circular, depending on thin section orientation. Pellets have sharp boundaries and consistent ovoid shape. Their size is consistently larger (average length 1 mm and width 0.6 mm) than the above-described green to black clay pellets. We see no evidence of diagenetic enlargement. These pellets are evident in the central bed and in the concretionary burrow fill at top of the MGB. In the central bed, microprobe and QEMSCAN analyses indicate that the heterogeneous pellet composition is dominated by clay minerals and tiny quartz fragments. At the top of the MGB, these pellets were altered to apatite and a lesser amount of siderite. Diagenetic processes did not alter or mask the original pellet shapes, and there is no evidence of internal canals. These larger, heterogeneous pellets indicate an alternate pellet producer. The pellet variety represents biological diversity in the MGB.

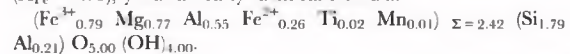
Color. The central MGB appears olive gray in outcrop. In thin section, the verdine clays appear green to brown. Stenzel [1] described the MGB as follows: "Olive-gray weathering to grayish-red, massive to poorly bedded, weathering to brownish-black, and grayish-red, sideritic calcareous concretions loosely spaced in the middle and crowded near the top to form a continuous clay ironstone layer, the bed forms a slight bench and a vertical face in the bluff." Upon close examination, the color of the smaller clay pellets varies from several hues of green to brown and black. Munsell colors of the pellets include light olive brown (5Y 5/6), moderate olive brown (5Y 4/4), olive gray (5Y 3/2), moderate brown (5YR 3/4), brownish black (5YR 2/1), and olive black (5Y

2/1) [43]. Clay pellets commonly appear homogeneous, while larger pellets are mottled. Rims are sometimes lighter in color than centers. Color often is linked with authigenic mineral maturity or weathering, because the color of clay changes during diagenesis [16,32,34,44].

Mineral Composition

Clay. XRD, EMPA and Mössbauer spectroscopy are common methods used to identify clay minerals of the verdine facies [16,24,32]. Each was employed in this study, and the results were compared with published data. Since a 7Å reflection characterizes a number of clay types including odinite, kaolinite, serpentine, vermiculite, berthierine, chlorite or mixtures of clays, resolution of which clay types are the most likely required detailed evaluations.

Odinite, the dominant verdine clay type, was indicated based on its characteristics as first described by Bailey [24]. It is a dioctahedral-trioctahedral Fe³⁺-rich 1:1 layer, 7.2Å clay mineral. It was published with the following structural formula which is based on sample #699: (Fe³⁺_{0.78} Mg_{0.77} Al_{0.56} Fe²⁺_{0.28} Ti_{0.02} Mn_{0.02})_{Σ=2.42} (Si_{1.79} Al_{0.21}) O_{5.00} (OH)_{4.00} [24]. This formula includes a correction for the amount of SiO₂ contamination (stated as ~3%, but actually 2.51%), ignores measured water (using stoichiometric water instead), ignores measured alkali elements (Na, Ca, K), assumes an Fe³⁺/Fe²⁺ ratio measured on a different sample, and is normalized to 14 positive charges in the octahedral+tetrahedral sites. Recalculating the 699 analysis using the same total measured iron but fixing the Fe³⁺/Fe²⁺ ratio at 3.0 (X_{Fe} = 0.75), yields a nearly identical formula.



X-ray diffraction analyses of both oriented and unoriented clay mounts consistently exhibited strong reflections at 7.2Å and 3.58Å. The oriented 2 μm clay, in a pellet-matrix mix from the central MGB, exhibited said reflections (Figure 10 and Figures S1 & S2). Another strong reflection occurs at 14Å in air-dried results. It is confirmed as smectite based on comparing diffraction patterns of air-dried and ethylene glycol treated samples where the 001 peak shifts to a very strong peak near 16.9Å. Illite is indicated by very weak 001, 002 and 003 reflections at 10.1, 5 & 3.34Å respectively. Kaolinite has reflections that coincide with odinite, but it was not confirmed here by other analyses. XRD patterns show no evidence for glauconitic minerals in the MGB. Peaks are not apparent at approximately 10.5 and 3.3, which would indicate glauconitic minerals.

Random oriented powders from MGB clay pellet separates yielded peaks at 7.249Å and 3.566Å (001 and 002) (Figure 11). The odinite-1M data base peaks are very similar at 7.150Å and 3.580Å [45]. Eleven peaks were indexed and compared with the odinite-1M data base in unit cell calculation (Table 1). This refinement process indicates that odinite is a reliable interpretation for the 7.2Å clay peaks that appear in all the x-ray diffractograms in this study.

X-ray diffraction analyses of randomly oriented powders, in a pellet-matrix mix, in the location of 060 were evaluated. In analyses of verdine facies minerals, Odin [16] found wide and asymmetric peaks between 1.56Å (59.23° 2θ) and 1.51Å (61.35° 2θ) in the vicinity of the 060 diffraction peak. This peak gradually decreases towards 1.50Å. Results for the three central MGB samples, comprised of pellets and clay matrix, show the 121- (*hkl*) peak of quartz at 1.54Å (59.970° 2θ) [46] which partially masks the reflections for verdine minerals. The broad peak, described by Odin [16] is subtle but present in MGB diffractograms which indicates the presence of verdine minerals (Figure S3). A 060 diffraction peak for kaolinite (62.31° 2θ) [33] is not present which

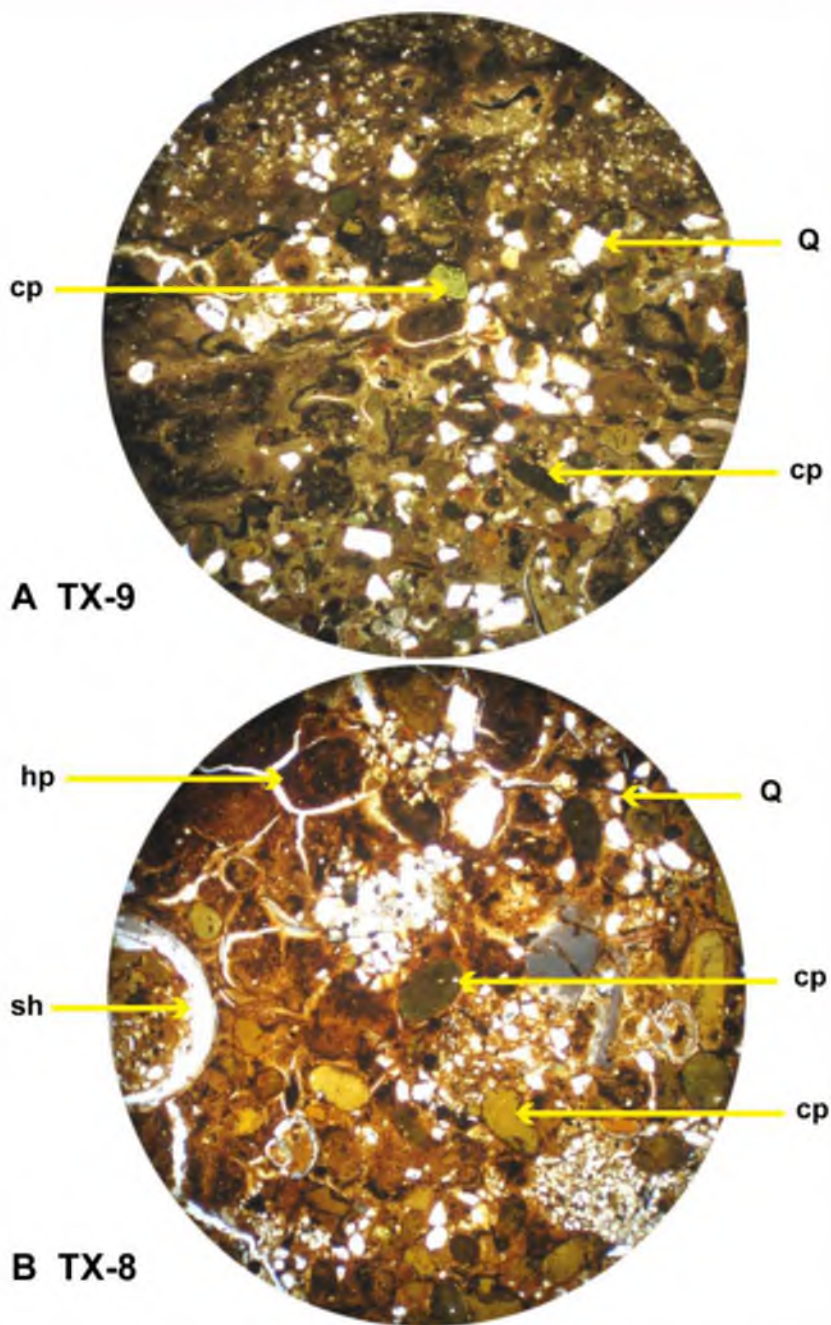
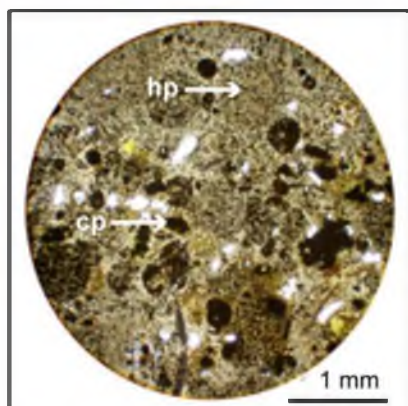


Figure 8. Photomicrographs from central MGB, A) TX-9, B) TX-8, cp = clay pellet, hp = heterogeneous pellet, sh = shell, Q = quartz.
 doi:10.1371/journal.pone.0087656.g008

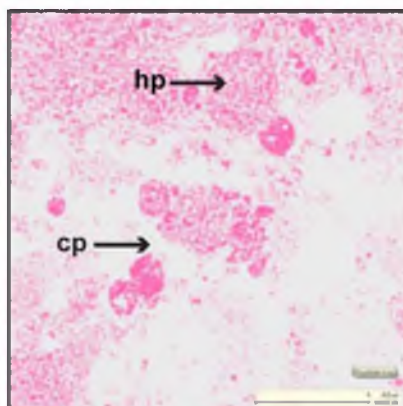
is consistent with EMPA and QEMSCAN results that show a lack of kaolinite in MGB samples.

The electron microprobe results of 31 EMPA spot analyses of MGB clay pellets show consistent composition among the important cations. Representative EMPA analyses are given in

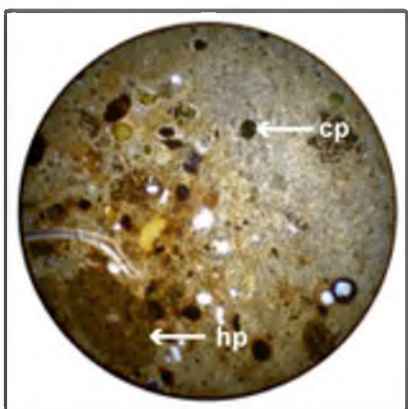
Table 2. The maximum, minimum and mean of the 31 analyses are compared with published results (Table 3). The data were converted to apfu (atoms per formula unit), and they are illustrated adjacent to samples #699 and #508 (odinite in the type locality) [16,24] and presented in Figure 12. The comparison shows fairly



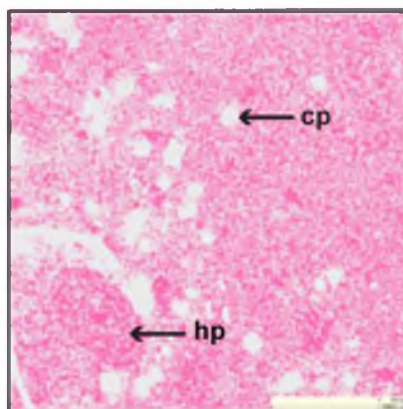
Sample 3



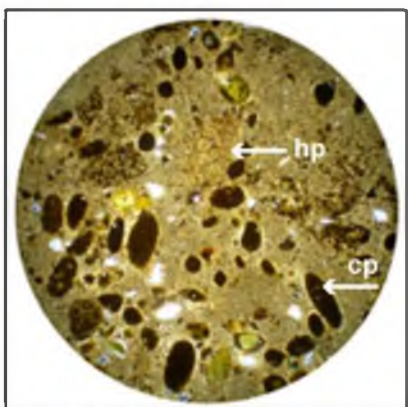
Apatite 18%



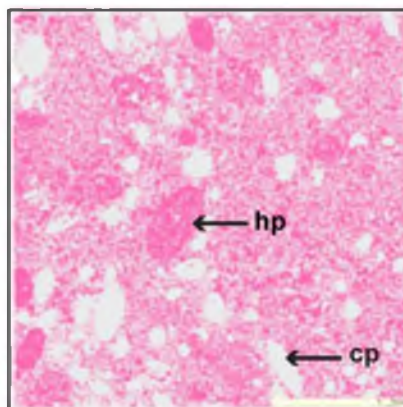
Sample UUIIC-3245



Apatite 46%



Sample 9



Apatite 46%

Figure 9. Top of MGB concretionary burrow fill, photomicrographs and QEMSCAN (false color) images, cp = clay pellets, hp = heterogeneous pellets, pink = apatite cement.
doi:10.1371/journal.pone.0087656.g009

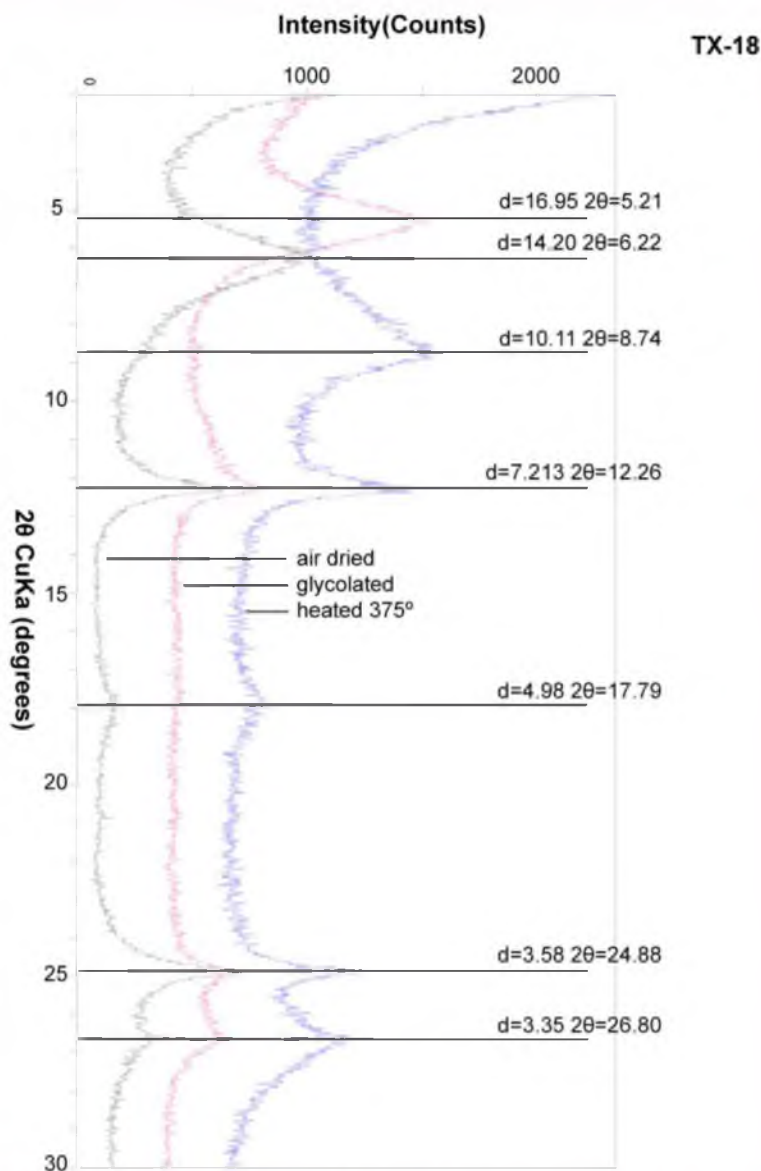


Figure 10. X-ray diffraction patterns of oriented, 2 μm clay fraction, from bulk sample TX-18, a mixture of 7 and 14Å clays (air dried, glycolated and heated to 375°).
doi:10.1371/journal.pone.0087656.g010

consistent apfu results for the important cations. The formula calculated herein follows Bailey's [24] procedure but fixes the atomic $\text{Fe}^{3+}/\text{Fe}^{2+}$ ratio at exactly 3.0. The following average structural formula calculated for MGB clay pellets is: $\text{Fe}^{3+}_{0.09}\text{Mg}_{0.45}\text{Al}_{0.67}\text{Fe}^{2+}_{0.30}\text{Ti}_{0.01}\text{Mn}_{0.01}\Sigma=2.33(\text{Si}_{1.77}\text{Al}_{0.23})\text{O}_{3.00}(\text{OH})_{4.00}$. Odin's formula for #699 is slightly more Mg rich, and Fe, Al poor. This identifies odinite as the dominant clay mineral in MGB clay pellets. Raw chemical data for odinite analyses in the MGB clay pellets are presented in Table S1.

Glaucouitic mineral grains, although small and very sparse, were the focus of some spot analyses in an attempt to locate a

potassium X-ray signal. The glaucouitic mineral analyses (>2 wt.% K_2O) were omitted from the above structural formula calculation for odinite. MGB clay pellets, for the most part, are low in K_2O , with an average of 1.5 wt. %. The few glaucouitic grains encountered were small and fractured. Three analyses showed $\text{K}_2\text{O} > 6$ wt. %, which qualifies as mature glaucouite. Thus, the Main Glaucouite Bed actually contains very little glaucouite (3% by QEMSCAN). Raw data for glaucouitic minerals and other clays are presented in Table S2.

Several clay types were characterized in a study of Claiborne Group iron-rich authigenic clays by Huggett et al. [11,21]. They

Table 1. Unit cell calculation from XRD data (odinite-1M (monoclinic)).

	Sample TX-MGB	SD	PDF# 00-048-1857	SD
a =	5.35	±0.01	5.38	±0.01
b =	9.38	±0.03	9.34	±0.02
c =	7.42	±0.03	7.39	±0.02
Beta =	104.79	±0.40	104.03	±0.25

Eleven peaks were indexed. MGB pellets compared with ICDD. All units are in angstroms (Å).
doi:10.1371/journal.pone.0087656.t001

used the general term serpentine for 7Å iron-rich mixed layer clays, including odinite. The average chemistry of clay pellets from the MGB is very similar to the average of 53 analyses for pellets from the upper 8 m of the Crockett Formation, which includes the MGB, from the same locality as this study [11]. All MGB clay pellet analyses from this study, including glauconitic grains, are displayed as total Fe₂O₃ plotted against Al₂O₃ together with the published results (Figure 13). The compositional variation of MGB clay pellets is evident, where they are seen to lie within the compositional field of authigenic iron-rich clays from other Claiborne Group clays [11]. Also shown are published analyses of other clays including nontronite, berthierine, Fe-smectite, vermiculite and kaolinite. These, along with the MGB clay pellets, tend to lie along a general trend between nontronite and kaolinite, and are distinctly lower in Al₂O₃ than berthierine (Figure 13) [11].

Mossbauer spectra were obtained on clay separates from the rock matrix and pellets (Figure S4), and Mossbauer parameters are provided in Table 4. Peak area ratios indicate a predominance of Fe³⁺ (63–81% of total Fe). Ferric/ferrous ratios in clays in fecal pellets are lower than in matrix clays from the same sample, indicating that the biogenic nature of the pellets provides micro-reducing environments on the seafloor favorable for the formation of verdine minerals. Figure 14 shows a plot of isomer shift vs. quadrupole splitting for the MGB clays together with representative published data for glauconite. For the MGB clays Fe³⁺ values of the isomer shift fall between 0.30 and 0.40. Of the eight samples, four had doublet pairs for Fe³⁺ resulting in a bimodal distribution in QS of 1.02–1.24 and 0.66–0.84. In the case of the other four samples in which there was a single doublet for Fe³⁺, the range in values for QS falls within the lower range, 0.70–0.83.

Collectively, these data suggest the presence of two slightly different octahedral sites for Fe³⁺, possibly suggesting some trioctahedral character in the clays. The difference in the average of the quadrupole splitting between the two sites, 0.41 mm/s, is similar to that reported for glauconite by Ali [47] but shifted to higher values by about 0.25 mm/s. Based on peak areas (Table 4), Fe³⁺ is more abundant in the site characterized by lower quadrupole splitting. The isomer shift for Fe²⁺ ranges from 1.13–1.25 mm/s, and the data fall into two clusters, especially defined by QS. There were no doublet pairs fit to the Fe²⁺ spectra. Nonetheless, the distinct bi-modal array of IS and QS values suggests again the presence of two octahedral sites for Fe²⁺. Because of its substantial Fe content, there is considerable literature on Mossbauer spectra of glauconite, and a number of workers have allocated Fe to *cis*-M2 and *trans*-M1 sites [47–51]. However, Rancourt and co-workers [52–54] have argued that these sites may not be positively delineated, and that the spectral data may be recording local distortion environments. Dyar [55]

suggested that hydrogen content may be responsible for variation around octahedral sites because of the difference in the location of hydroxyls around M1 and M2 sites. We do not have direct determination of H₂O contents of MGB clays, but they do have measureable F and Cl, and both vary in concentration. Substitution of F and Cl, and possibly O in OH sites could change the geometry of the adjacent *trans* and *cis* sites and be responsible for the bimodal behavior of MGB clays.

The Mossbauer Fe³⁺/Fe²⁺ ratio is diagnostic for identifying verdine clay minerals. The average Fe³⁺/Fe²⁺ ratio in MGB samples of matrix and pellets is 73:27%. A similar ratio of 73.6:26.4% was calculated for phyllite-V clay (later named odinite) in modern sea-floor clays [16]. The Fe³⁺/Fe²⁺ ratio of clay matrix is slightly higher than that of clay pellets: 78:23%, versus 68.5:31.5%, respectively. The biogenic nature of the pellets provides micro-reducing environments on the seafloor favorable for the formation of verdine minerals.

QEMSCAN reports chemical data according to the SIP mineral definition. The O&G SIP tests for clays in the following order: glauconite, illite, kaolinite, nontronite, smectite and chlorite. Odinite is not defined in the O&G SIP algorithm, but its composition strongly overlaps with chlorite, and odinite is known to alter to chlorite [24]. Therefore, the O&G SIP was adjusted to accommodate the MGB clay samples by changing the mineral name from chlorite to odinite for this study. During QEMSCAN analysis of MGB clays, some 50% ended up in chlorite groups by default and are regarded as odinite.

Odinite and small amounts of smectite, illite and glauconitic minerals (<3 area %) are displayed in various shades of green in digital false color on QEMSCAN textural maps (Figures 15, 16, 17). Textural and compositional variation in the central MGB (Figure 15) shows that clay matrix is predominantly odinite and illite, while clay pellets are predominantly odinite and smectite. Figure 16 demonstrates that odinite is dominant in both the matrix and clay pellets with minor amounts of illite, smectite and glauconitic minerals. Glauconitic minerals occur in fairly pure grains, although very few in number (about 3 area %). QEMSCAN analyses from the central MGB show that quartz grains average 18 area % and calcite averages about 3 area %, occurring as shell fragments.

Concretionary burrow fill at the top of the MGB is predominantly siderite and apatite cement, in various quantities. Sample UUIC 3245 had 46:43 area % apatite-siderite, while sample 9 had 46:39 apatite-siderite. Other concretionary burrows are dominated by siderite. Textural map, Figure 17, shows an 8:1 mixture siderite-apatite. False color pink represents the P₂O₅-rich mineral, apatite. Clay pellets remain unaltered even though they are incorporated in the concretionary burrow fill.

The identification of odinite, a key verdine mineral, is supported by all of the above analytical results. The unit cell calculation shows lattice parameters that are uniquely odinite. It is the dominant clay type in the MGB clay pellets. The structural formula calculated from EMPA data is consistent with that of odinite. X-ray diffraction results suggest an odinite, smectite, illite clay mixture. Verdine facies clays besides odinite include smectite and Fe³⁺ chlorite, sometimes referred to as swelling chlorite [16,24]. The MGB clay is moderately high in Fe, and Mossbauer spectroscopy found an approximate Fe³⁺/Fe²⁺ ratio of 3:1, which is consistent with odinite. QEMSCAN identified the dominant clay type of the MGB as chlorite-like, which has close similarity to odinite.

Siderite and apatite. Concretions at the top of the MGB are composed of a fine-grained apatite-silicate mixture. Analyses of siderite are presented in Table 5. Despite attempts with the

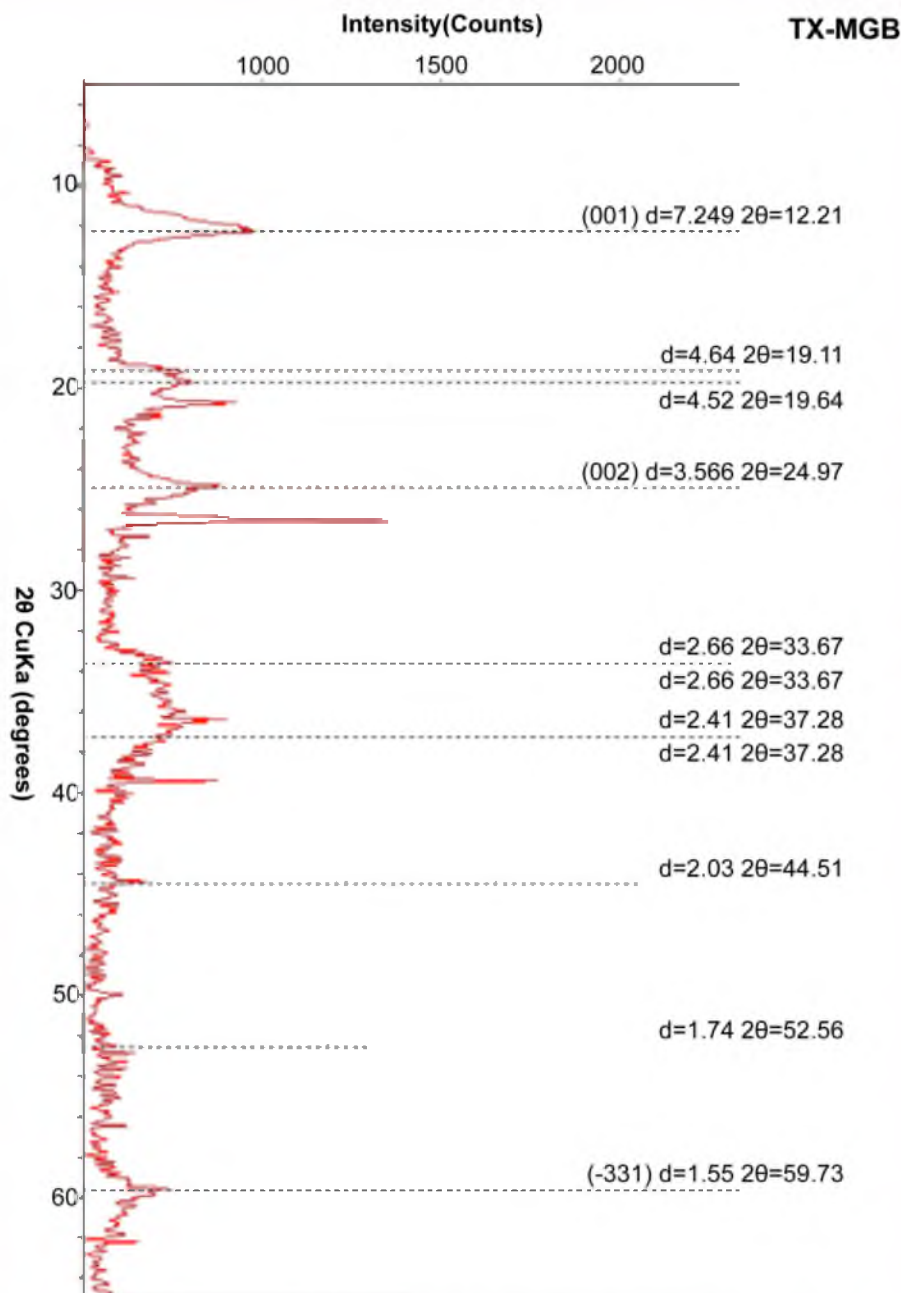


Figure 11. X-ray diffraction pattern of an unoriented powder mount of concentrated clay pellets, TX-MGB. Eleven labeled peaks were indexed in unit cell calculation for odinite-1M. Unlabeled peaks are quartz. Peak at $2\theta = 59.73$ is quartz overlapped by odinite. doi:10.1371/journal.pone.0087656.g011

electron microprobe to locate regions without a phosphorus X-ray signal, when measured, phosphorus was always detected, ranging in three samples from 0.8 to 4.0%, which corresponds to about 2–10% apatite. A small amount of Al_2O_3 was also recorded, and probably represents a minor amount of clay. Mole percent

carbonate end-members are calculated with $CaCO_3$ adjusted for the Ca-equivalent of apatite as determined from P_2O_5 concentrations when measured (Table 5). Mole fraction $FeCO_3$ ranges from 70–75%, consistent with the observation of Mozley [56] that marine siderite has <95 atom% Fe and that $Mg > Ca$. Huggett

Table 2. Representative analyses from MGB clay pellets, 11 each from the central MGB and concretionary burrow fill at the top of the MGB.

sample #	Central MGB -->				Top MGB -->				
	TX-8	TX-18	TX-18	Sc	9	9	W	TX-17	TX-17
n*	6	2	2	1	3	1	1	2	4
SiO ₂	33.9	33.2	35.5	33.9	33.7	34.4	34.8	35.7	32.8
Al ₂ O ₃	15.8	12.0	14.8	14.5	13.2	12.7	13.1	13.4	15.4
Fe ₂ O ₃ T	31.8	33.6	26.1	22.8	37.4	33.2	38.1	31.3	25.5
Fe ₂ O ₃	23.8	25.2	19.6	17.1	28.0	24.9	28.5	23.5	19.1
FeO	7.15	7.55	5.88	5.13	8.41	7.48	8.56	7.05	5.74
MgO	6.63	4.63	5.41	6.73	4.17	4.09	4.31	4.60	6.72
MnO	0.18	0.10	0.06	0.10	0.06	0.07	0.04	0.08	0.15
TiO ₂	0.30	0.24	0.24	0.22	0.16	0.20	0.07	0.23	0.21
CaO	1.03	1.12	1.37	0.42	0.84	0.85	0.36	0.87	0.55
Na ₂ O	0.08	0.05	0.06	0.10	0.10	0.09	0.14	0.06	0.09
K ₂ O	0.34	0.50	0.63	0.90	1.12	1.76	1.45	0.78	0.46
H ₂ O	11.9	11.1	11.4	10.9	11.6	11.3	11.9	11.6	11.1
F	0.03	0.52	0.19	0.36	0.02	0.16	0.00	0.41	0.23
Cl	0.06	0.02	0.07	0.14	0.30	0.00	0.18	0.01	0.19
Sum with FeO+Fe₂O₃	101.2	96.3	95.1	90.5	101.8	98.0	103.5	98.3	92.8

*Number of spot analyses in one pellet.
doi:10.1371/journal.pone.0087656.t002

et al. [11] report a slightly higher cation mole fraction of 0.79 for siderite from the MGB from a partial analysis.

Analyses of concretions consisting of a fine-grained mixture of apatite and one or more aluminosilicates are provided in Table 6. Assuming that all P is contained in apatite, and accounting for the equivalent CaO, the composition of the silicate component

(neglecting halogens) can be estimated. The calculated silicate component is similar in composition to MGB clays with respect to total Fe₂O₃ and Al₂O₃, although with slightly lower SiO₂, suggesting that the silicate in the phosphate-bearing cement is the same or very similar to the clay in the pellets and the matrix of the MGB.

Table 3. Maximum, minimum, mean and standard deviation of chemical analyses from MGB pellets and published odinite.

Oxide Wt %	MGB pellets				Oditite (samples 699 & 508)			
	Min	Max	Mean	SD	Min	Max	Mean	SD
			n = 31				n = 6	
SiO ₂	28.0	36.1	33.6	1.62	33.5	37.5	35.6	1.71
Al ₂ O ₃	11.5	16.5	14.4	1.41	11.0	12.2	11.8	0.67
Fe ₂ O ₃ T	22.8	38.2	30.1	4.57	25.1	26.4	26.2	0.51
Fe ₂ O ₃	17.1	28.6	22.6	3.43	17.9	19.5	20.4	3.01
FeO	5.13	8.59	6.76	1.03	6.10	6.50	6.25	0.15
MgO	3.95	7.90	5.71	1.16	9.70	11.0	9.78	0.68
MnO	0.04	0.31	0.14	0.07	0.00	0.33	0.22	0.17
TiO ₂	0.07	0.62	0.22	0.11	0.40	0.50	0.35	0.18
CaO	0.36	1.37	0.88	0.27	0.13	0.50	0.22	0.15
Na ₂ O	0.02	0.16	0.08	0.04	0.00	0.20	0.07	0.10
K ₂ O	0.26	1.76	0.71	0.40	0.35	1.30	0.63	0.44
H ₂ O	10.5	12.0	11.4	0.41	10.0	15.0	11.6	1.81
F	0.00	0.82	0.20	0.18				
Cl	0.00	0.60	0.09	0.12				
Sum*	76.9	115.3	96.7		89.1	104.6	96.8	

*Sum with FeO+Fe₂O₃.
doi:10.1371/journal.pone.0087656.t003

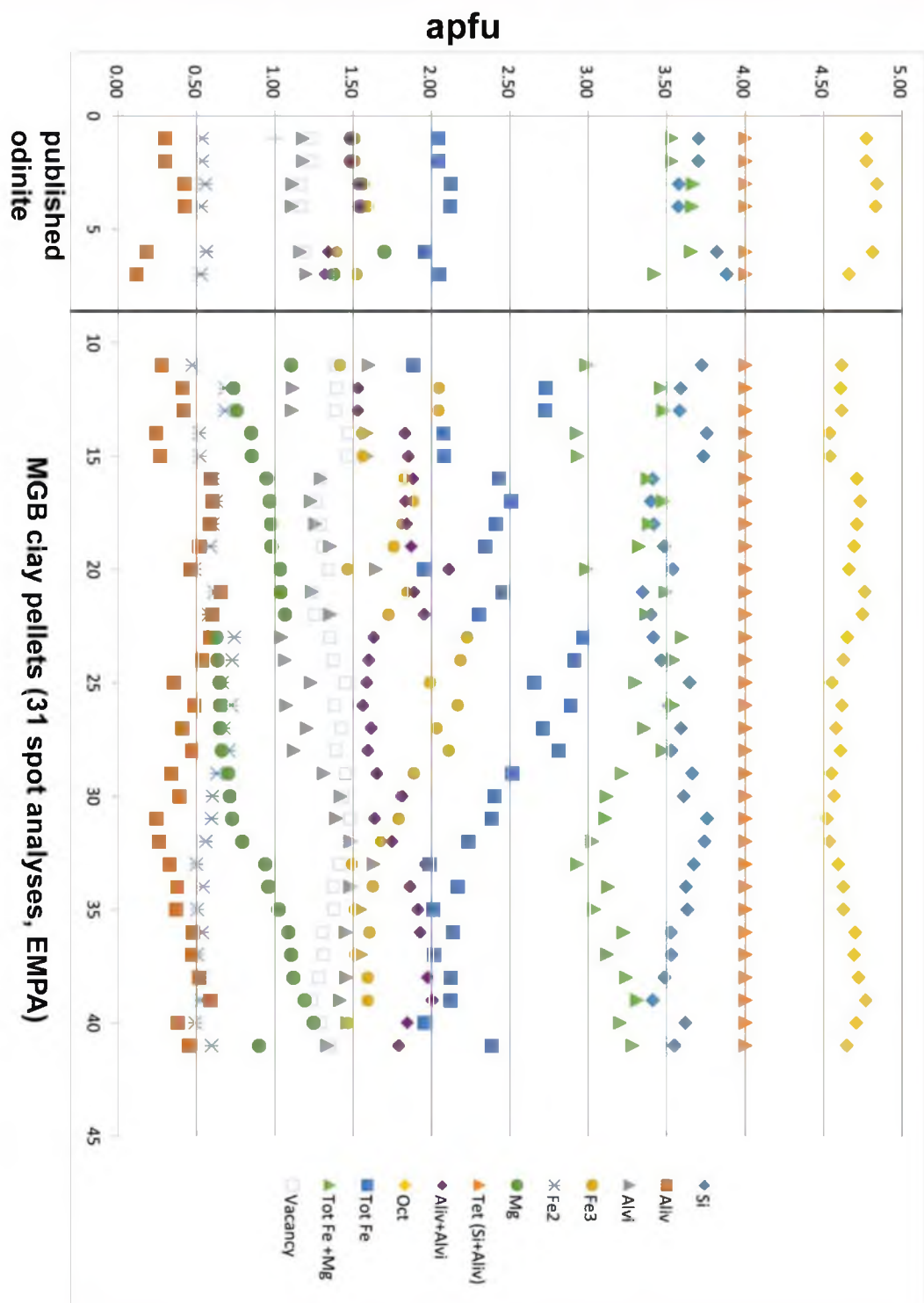


Figure 12. Chemical analyses (apfu), published [16,24] and MGB clay pellets, used to calculate mineral formula.
 doi:10.1371/journal.pone.0087656.g012

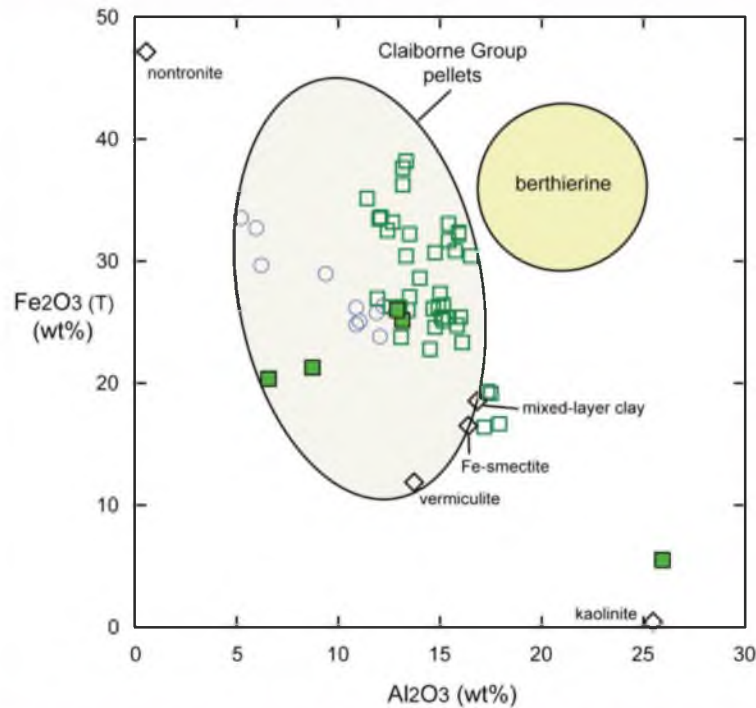


Figure 13. MGB clays plotted within the compositional field of iron-rich clays from the Claiborne Group. Open squares (green) are from the MGB and solid squares are glauconitic minerals from the MGB. Open circles are published analyses of odinite [16,24]. The range of compositions of clay in pellets from the Claiborne Group is indicated by the large oval [11,61]. The field of berthierine is from Brindley [61]. doi:10.1371/journal.pone.0087656.g013

Table 4. Mössbauer parameters of 7Å clay mixture.

Sample		5c		TX-9		TX-18	W	W	W
		matrix	pellets	matrix	pellets	pellets	matrix	m & p	pellets
ferric	IS	0.31	0.36	0.30	0.36	0.33	0.32	0.29	0.37
	QS	0.70	0.83	0.82	0.79	0.83	0.66	0.84	0.83
	Width	0.49	0.62	0.34	0.33	0.54	0.42	0.38	0.59
	Area %	81.3	66.4	46.3	30.2	77.1	65.8	39.0	68.3
ferric	IS			0.36	0.40		0.36	0.37	
	QS			1.20	1.07		1.23	1.24	
	Width			0.43	0.59		0.38	0.45	
	Area %			26.2	33.0		14.4	28.7	
ferrous	IS	1.21	1.13	1.25	1.12	1.21	1.25	1.22	1.14
	QS	2.31	2.61	2.33	2.60	2.25	2.31	2.28	2.59
	Width	0.40	0.22	0.26	0.32	0.30*	0.40*	0.30*	0.30*
	Area %	18.7	33.6	27.5	36.8	22.9	19.8	32.3	31.7
	% Fe ³⁺	81	66	72	63	77	80	68	68
	% Fe ²⁺	19	34	28	37	23	20	32	32

IS: Isomer shift (mm/s).

QS: Quadrupole splitting (mm/s).

Width: FWHM (mm/s).

Spectrum temperature 295 K.

*parameter fixed.

doi:10.1371/journal.pone.0087656.t004

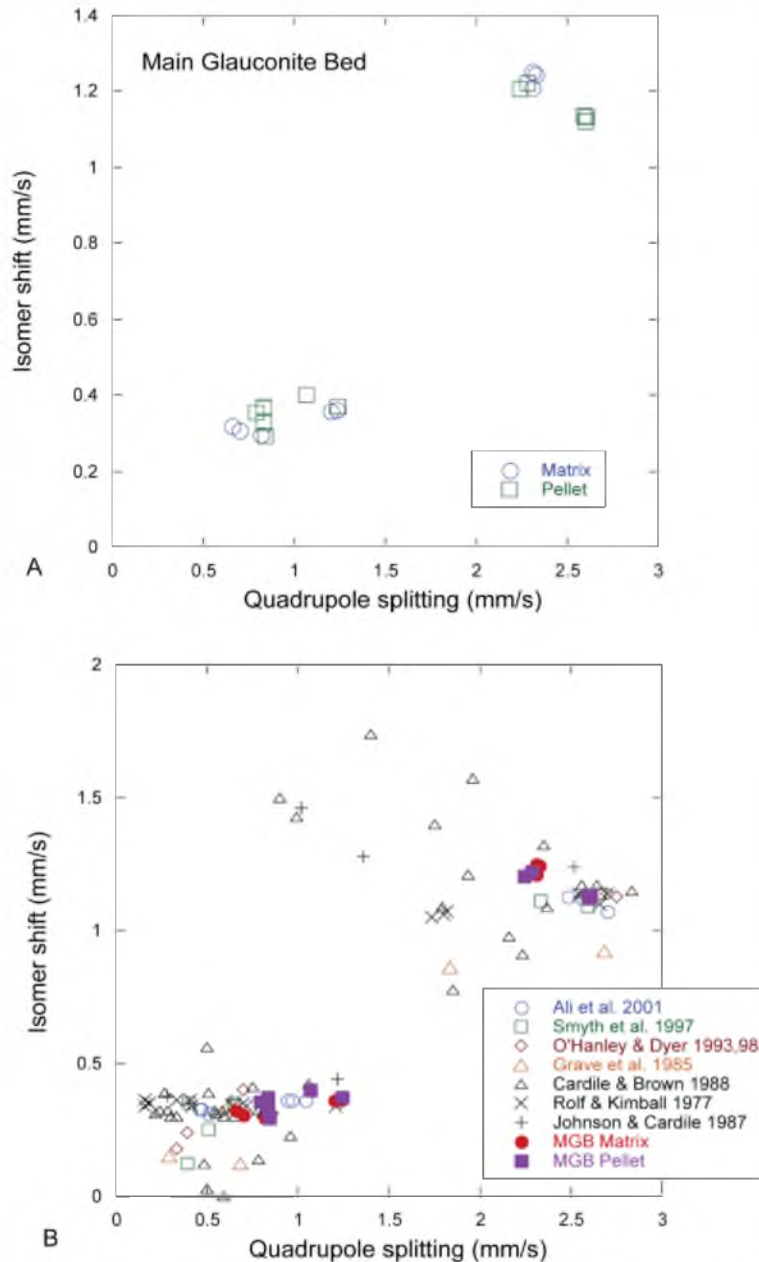


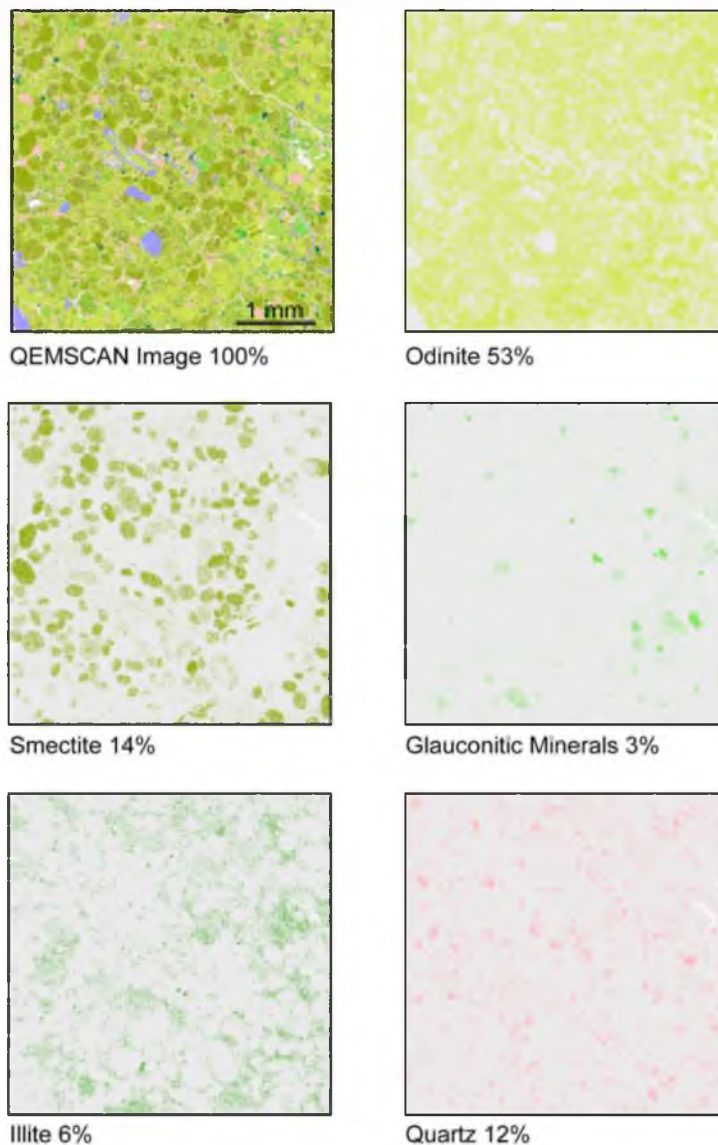
Figure 14. Plot of isomer shift vs. quadrupole splitting (in mm/s). A) Clays from the MGB (this study), B) MGB clays compared to published analyses of glauconite.

doi:10.1371/journal.pone.0087656.g014

Discussion

The detailed mineralogy and geochemistry of the MGB determined in this study relate to paleoecology, sedimentology and stratigraphic findings from previous studies. When integrated with the ichnology of the MGB, a coordinated approach to understanding the depositional environment in a sequence

stratigraphic context is possible. Verdine minerals, specifically odinite, were identified in the clay pellets. Thornton, in a 1994 master's thesis [10], also noted that the MGB clays had the characteristics of odinite. Whether the MGB is comprised of odinite or authigenic verdine minerals that were altered, the paleoenvironmental implications are the same. It is presumed that the present-day verdinization environment is key to understanding



TX-18

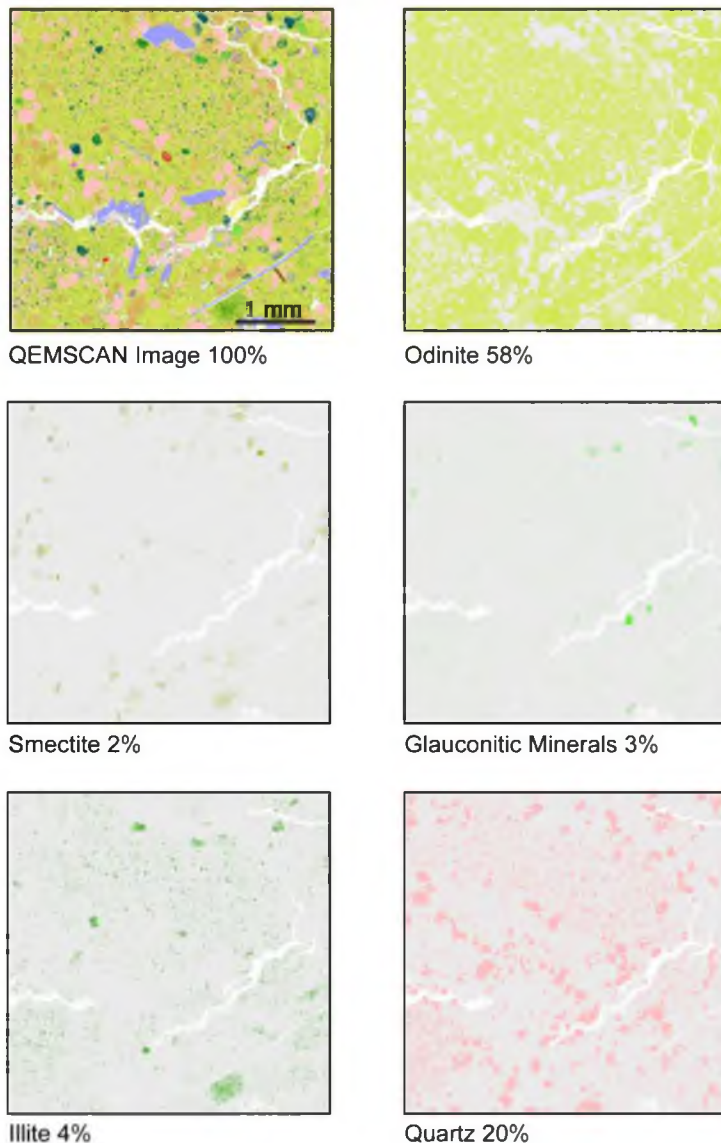
Figure 15. Central MGB QEMSCAN images with specific mineral area %, sample TX-18.
doi:10.1371/journal.pone.0087656.g015

the Middle Eocene continental shelf green marine clay environments.

Pelleted Component

The mineralogy of the clay pellets and their occurrence in the central MGB and in concretionary burrow fill at the top of the MGB has implications for understanding depositional processes. Odlinite-rich clay pellets are abundant in the central MGB. They are interpreted as fecal pellets based on their consistent shape, varied size, appearance and iron oxidation state. Their varied size

is attributed to multiple producers, which reflects a diverse faunal community. Fecal pellets originally must have contained organic matter, resulting in locally more reducing conditions than the surrounding environment [24]. The pellets provided a favorable site for verdinization, because verdine minerals tend to form within sheltered, reducing, granular microenvironments. Clay pellets of the MGB have a lower $\text{Fe}^{3+}/\text{Fe}^{2+}$ ratio than the clay matrix (Table 4), and consequently they reflect more reducing conditions, as would be expected for fecal material.

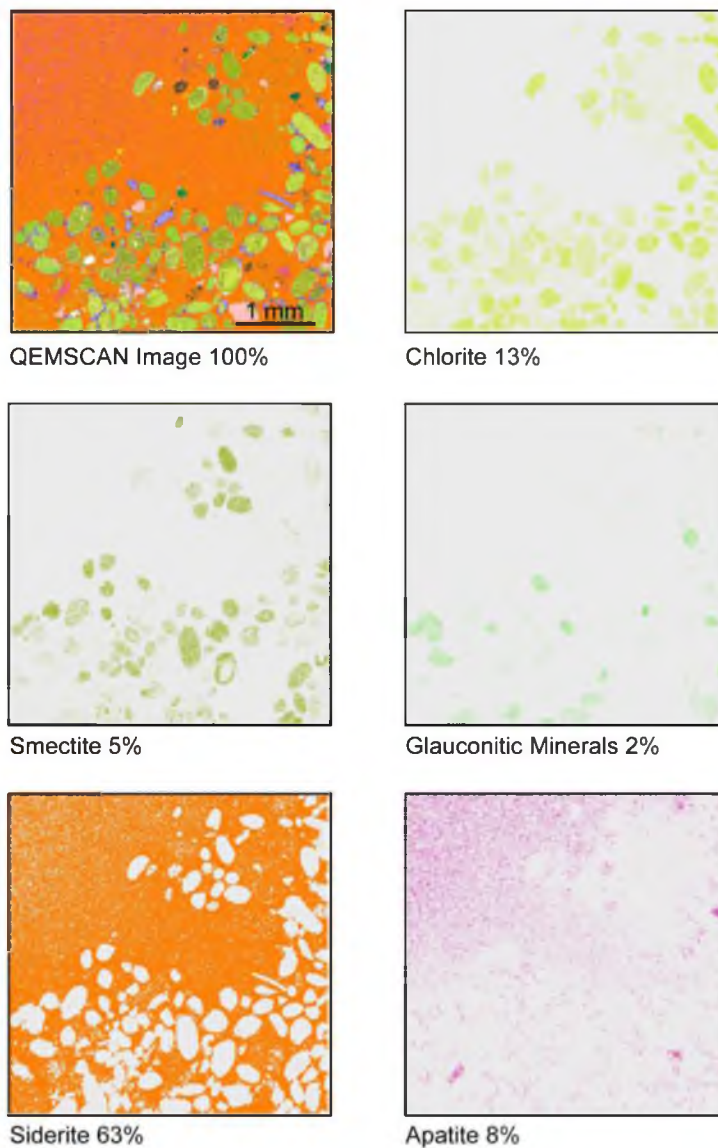


TX-9

Figure 16. Central MGB QEMSCAN images with specific mineral area %, sample TX-9.
doi:10.1371/journal.pone.0087656.g016

Clay pellets occur in both the central bed and in the concretionary burrow fill at top of the MGB. In the central bed, pellets are not evenly distributed throughout, suggesting that they may have been reworked by gentle winnowing and episodic storms. Clay pellets at the top of the MGB could have been introduced into the open burrows along with other detritus, possibly reworked from the central MGB, or they could have been left behind by occupants in the burrow fill. The clay pellets do not show characteristics of those produced by decapod crustacean burrowers.

The larger, heterogeneous pellets composed primarily of the apatite-cementing agent, can be seen in both the photomicrographs and the QEMSCAN mineral images of concretionary burrow fill. In comparison with the clay pellets, the apatite pellets are larger and more mineralogically heterogeneous (Figure 9). These pellets also occur in the central MGB as a loosely compacted unaltered mixture of clay and tiny clasts. At top of the MGB, these pellets were incorporated into the apatite and siderite-cementing agents of the concretionary burrow fill. Based on their affinity for phosphate minerals and their shape, they are



TX-17

Figure 17. Top of MGB QEMSCAN images with specific mineral area %, sample TX-17.
doi:10.1371/journal.pone.0087656.g017

interpreted as fecal in origin. Like the clay pellets, the apatite pellets could have been left behind by occupants in the burrow fill. They do not show the morphologic characteristics typical of pellets produced by decapod crustacean burrowers.

A very few fragmented glauconitic mineral grains (3 area %) occur in both the central and top of the MGB. Their existence is confirmed by electron microprobe on the basis of $K_2O > 2$ wt. % and by QEMSCAN analyses based on SIP definition. The fragmented nature of the grains lends support to the hypothesis that some winnowing and reworking of sediments may have

occurred, and that glauconitic minerals were transported from deeper environments where they originated. Glauconitic minerals, once formed, are very stable in the marine environment, and they may well survive transport of appreciable distance. The glauconitic grains may be more brittle than the non-glauconitic clay pellets, and so they tend to fracture more readily. Glauconitic grains found in the concretions were likely added with clastics in the burrow fill.

Table 5. Concretionary burrow fill, MGB top, siderite and mole percent carbonate end-members calculated with CaCO₃.

Sample	3	9	3245	1 plug 4	1 plug 8	Avg	SD
n°	1	3	1	1	1	7	
SiO ₂	2.30	2.50	1.90	1.16	2.42	2.05	0.55
TiO ₂	0.00	0.05	0.03	0.06	0.04	0.03	0.02
Al ₂ O ₃	1.60	0.90	1.00	0.50	1.14	1.01	0.40
FeO**	37.3	41.3	43.2	38.7	38.2	39.7	2.20
MnO	0.74	0.65	0.62	1.02	0.75	0.76	0.16
MgO	6.00	4.76	4.90	4.63	5.23	5.10	0.55
CaO	4.35	8.81	7.45	4.65	3.89	5.83	1.94
Na ₂ O	0.17	0.15	0.06	0.12	0.20	0.14	0.06
K ₂ O	0.21	0.08	0.06	0.05	0.19	0.12	0.08
P ₂ O ₅	0.76	4.04	2.66				
Total	53.4	63.3	61.9	50.9	52.0	54.7	5.3
% apatite	1.8	9.6	6.3				
Mol %							
CaCO ₃ ***	8.1	8.2	8.8	11.0	9.4	13.1	2.0
MgCO ₃	20.2	15.4	15.2	15.3	17.5	15.9	2.0
MnCO ₃	1.4	1.2	1.1	1.9	1.4	1.4	0.3
FeCO ₃	70.3	75.2	75.0	71.7	71.7	69.6	2.3

*Spot analyses in one grain.

**Total Fe as FeO.

***CaCO₃ corrected for apatite.

doi:10.1371/journal.pone.0087656.t005

Sequence Stratigraphy

In a sequence stratigraphic context, green minerals often are associated with condensed sections and transgressive-systems-tracts. A transgressive phase on a sediment-starved sea floor offers favorable conditions for the glauconitization or verdinization process. A regressive phase, on the other hand, may introduce a more energetic, oxidizing environment of higher sediment influx, which would inhibit clay authigenesis [25,29]. Green minerals of the verdine facies suggest the shallow inner shelf, more proximal zone of the transgressive surface and transgressive-systems-tract.

The MGB is part of a regionally mapped transgressive sequence during the Middle Eocene in the northwest Gulf of Mexico. The siliclastic depositional center was associated with the Houston Embayment (Figure 1) [57]. Deposition occurred during an interval of fluctuating sea level in sediment-starved conditions, interfingering with episodes of higher sedimentation rate. The basal contact of the MGB is sharp, irregular and burrowed. The central MGB has verdine facies clays that indicate shallow marine conditions with transgressive characteristics in proximity to river mouth influx (Figure 7). The upper contact of the MGB marks a boundary between two contrasting facies. It is irregular due to burrowing [2,13]. The burrows are interpreted as firmground trace fossils that often occur in temporarily dewatered and compacted sediment. The top of the MGB may highlight a coplanar transgressive surface–sequence boundary in a parasequence. It is possible that the top of the MGB could have been exposed in an intertidal environment. Then the open burrows were filled with detritus during renewed submergence. Subsequent apatite and siderite cementation of the firmground would have occurred in a subaqueous setting.

Table 6. Concretionary burrow fill, MGB top, a fine-grained mixture of apatite and one or more alumino-silicates.

Sample	3	3	9	3245	Avg	SD
n°	1	2	2	2	7	
SiO ₂	11.6	17.0	11.3	16.5	14.1	3.07
TiO ₂	0.20	0.19	0.15	0.17	0.18	0.02
Al ₂ O ₃	5.60	8.20	5.71	8.97	7.12	1.72
Fe ₂ O ₃ **	15.7	13.6	12.1	15.9	14.3	1.82
MnO	0.19	0.07	0.09	0.07	0.11	0.06
MgO	1.68	1.61	0.89	1.56	1.43	0.37
CaO	26.9	25.2	34.4	27.8	28.6	4.05
Na ₂ O	0.35	0.41	0.46	0.30	0.38	0.07
K ₂ O	0.34	0.45	0.31	0.47	0.39	0.08
P ₂ O ₅	19.8	18.6	23.9	19.4	20.4	2.36
F	1.96	1.90	0.01	0.02	0.97	1.10
Cl	0.03	0.03	2.36	2.00	1.11	1.25
sum	84.2	87.3	91.7	93.2	89.1	4.12
Less O = F,Cl	0.83	0.81	0.54	0.46	0.66	0.19
Total	83.4	86.5	91.2	92.7	88.5	4.29
% apatite	46.8	44.0	56.5	45.9	48.2	4.9

*Spot analyses in one grain.

**Total Fe as Fe₂O₃

doi:10.1371/journal.pone.0087656.t006

The Crockett Formation was deposited in a complex marginal marine environment with dynamic sea level fluctuation. It represents a shallow-water transition zone in an overall upward deepening sequence. While odinite formed *in situ* associated with the fecal pellets of the central MGB, the few glauconitic mineral grains in the MGB may be explained by detrital reworking. Grains can be transported widely in transgressive systems, and glauconite is stable geochemically in the marine environment.

Paleoenvironment

The paucity of glauconitic minerals indicates that seafloor conditions during deposition of the MGB were unsuitable for their formation, or that the glauconitization process was incomplete or arrested. This might mean a number of things. For example, perhaps sea-floor conditions were not consistently marine, too close to river mouth influx, too close to shore, or too shallow water depth. Sediment influx can inhibit the glauconitization process by not allowing enough time for glauconitic minerals to mature. The few, small glauconitic mineral grains in the MGB were often fractured, which indicates they may be of allochthonous origin, so it appears that the glauconitization process did not occur during deposition of the MGB.

On the other hand, verdinization apparently did occur. The presence of odinite, especially in the clay pellets, indicates a set of sea-floor environmental conditions pertaining to geochemistry, temperature, oxidation state, energy and latitude. The central MGB reflects depositional processes in a low energy, somewhat sheltered, shallow, warm, mostly marine environment. Sedimentation rate was sufficiently slow in proximity of continental input of iron and gentle winnowing currents to provide Eh and pH conditions suitable for verdine mineral authigenesis [16,24,32].

The change in mineralogy from the central bed to the top of bed indicates a change in the sea-floor environment. The central MGB was deposited in a near shore, subaqueous setting, while it is possible that the top of the MGB, with its concretionary burrow fill comprised of pellets and detritus, may have been in an intertidal environment. This interpretation is supported by characteristic burrowing patterns at top of the MGB. It represents an interval of non-deposition, dewatering, compaction and burrowing. Ultimately, the open burrows excavated by infaunal crustaceans were filled with sediment and bioclasts, indicating return to a subaqueous environment in moderate energy where precipitation of siderite and apatite cementing agents occurred.

A coordinated approach to understanding the paleoenvironment of the MGB incorporates verdine facie characteristics, ichnological signature, and findings from previous MGB studies. During a period of regional transgression, relatively high sea level, and some lateral continuity of facies, several coastal siliciclastic environments may apply. These include protected shoreface settings, large scale normal marine lagoons, inter-deltaic bays, sounds, or embayments. Tropical seagrass beds demonstrate high molluscan diversity, such as that observed in the MGB. Seagrasses were present in the Gulf and Caribbean during the warmer climatic conditions of Middle Eocene [58]. Seagrass environments are recognized only rarely in the geological record due to the low preservation potential of soft plants, but they probably were much more abundant than is normally realized. Benthic foraminiferal evidence would be instructive, however that was outside the scope of this study. In general, the setting of the MGB is characterized as shallow inner shelf, proximal to some terrestrial influence.

Conclusion

The MGB clays at Stone City Bluff of Middle Eocene, east-central Texas are characterized as verdine facies clay, largely comprised of the mineral odinite. Odinite is an iron and magnesium 1:1, 7Å clay. It is the main constituent of the clay fecal pellets and matrix of the central MGB. Few occurrences of odinite, other than modern odinite, are described in the literature. The MGB provides an informative example of odinite in the geologic record.

Odinite was established as the main constituent in clay pellets of the MGB through several analytical methods. X-ray diffraction found a 7.2Å clay mixture. Unit cell calculation indicated odinite-1M to be the most reliable interpretation. EMPA analysis of clay pellets, directed by QEMSCAN textural maps, identified the chemical composition. Mossbauer spectral analysis found the oxidation state at 3:1 Fe³⁺/Fe²⁺ ratio diagnostic of odinite. Thus, essential chemical data was obtained to calculate the average structural formula for clay pellets of the MGB as follows: Fe³⁺_{0.89} Mg_{0.45} Al_{0.67} Fe²⁺_{0.30} Ti_{0.01} Mn_{0.01} Σ = 2.33 (Si_{1.77} Al_{0.23}) O_{5.00} (OH)_{1.00}. Odin and Bailey [16,24] first described odinite in 1988, and they calculated a similar mineral formula that was slightly more Mg rich and Fe, Al poor.

Documentation of odinite and verdine facies clays in the MGB is an important finding of this report. The environmental conditions associated with modern verdine facies clay occurrences include tropical latitudes, nearby runoff with iron influx, and water depth between 15 and 60 m (locally in 5 m depth). The characteristic sea-floor conditions are normal to nearly normal salinity, positive Eh, elevated sea-floor temperature and common association with fecal pellets. Circulating, winnowing currents are required to stir the sediment slightly and provide oxygenation. It is

presumed that paleoenvironmental conditions were comparable during the Middle Eocene accumulation of authigenic verdine clays in the MGB.

The contrasting mineralogy between the central and the top of the MGB reflects a change in environmental conditions during its deposition. The central MGB has abundant pellets, comprised mostly of odinite, with lenses of shell concentrations and laminated sand. In contrast, the top of the MGB is a zone of concretions that are filled burrows comprised of pellets and detritus with siderite and apatite that formed as cementing agents. Glauconitic minerals are very sparse in both the central and top of the MGB and are probably allochthonous. A change in environmental conditions is reflected in a composite ichnofabric where deeper water biogenic activity in the central MGB is replaced by shallow water to intertidal burrowers in a firmground at the top of the MGB. The firmground was subsequently submerged and cemented.

The paleoenvironmental interpretation for the geologic section at Stone City Bluff has been the subject of numerous studies. This contribution of detailed mineralogy and geochemistry, although focused on the fecal pellets of the MGB, offers key information about processes during its deposition. With the identification of authigenic odinite or its alteration products, this study complements findings of previous studies. The MGB represents an ancient verdine facies paleoenvironment, which has implications for paleoecology, sedimentation rate, sequence stratigraphy and paleoclimate. It provides a coordinated approach to paleoenvironmental understanding of the dynamic depositional environment of the MGB at Stone City Bluff.

Supporting Information

Figure S1 X-ray diffraction pattern of oriented 2 μ clay from bulk sample TX-8, (air dried, glycolated, heated to 375° and heated to 500°C). (TIF)

Figure S2 X-ray diffraction pattern of oriented 2 μ clay from bulk sample TX-9, (air dried, glycolated, heated to 375° and heated to 500°C). (TIF)

Figure S3 X-ray diffraction patterns of randomly oriented powders TX-8, TX-18, and TX-9. Minerals of the verdine facies at the 060 diffraction peak are between 1.56Å (59.23° 2θ) and 1.51Å (61.35° 2θ). Quartz at the 121- (*hkl*) peak is 1.54Å (59.97° 2θ). (TIF)

Figure S4 Mossbauer Spectrum TX-9 & W, matrix & pellets. (TIF)

Table S1 EMPA analyses for all odinite raw data in oxides and apfu. (XLSX)

Table S2 EMPA analyses for all other clays, including glauconitic minerals in oxides. (XLSX)

Acknowledgments

The authors thank TE Yancey, JE Warme, CJ Flis, and JE Flis for access to critical samples and for comments about sedimentological and paleoecological implications. J Allen, NF Dahdah, MA Gorenc, PD Pahnke, WT Parry, WD Mace, and CG Jones provided valuable technical assistance. QEMSCAN Model EVO 50, SERIAL # E430 located at Energy and Geoscience Institute (EGI) was used for the QEMSCAN analyses, and the

microprobe and XRD analyses were accomplished in the Department of Geology and Geophysics at the University of Utah.

References

- Stenzel HB (1934) Decapod Crustaceans from the Middle Eocene of Texas. *Journal of Paleontology* 8: 38–56.
- Stenzel HB, Krause EK, Twining JT (1957) Pelecypoda from the type locality of the Stone City beds (middle Eocene) of Texas. Austin: Bureau of Economic Geology, University of Texas. 237 p., 222 p. of plates p.
- Stanton RJ, Jr., Warme JE (1971) Stop 1: Stone City Bluff: Trace fossils. A field guide to selected localities in Pennsylvanian, Permian, Cretaceous and Tertiary rocks of Texas and related papers. In: Perkins BF, editor. SEPM: School of Geoscience Louisiana State University Misc Pubs. 2–10.
- Stanton RJ, Jr. (1979) The Stone City Formation: in. Claiborne sediments of the Brazos Valley, southeast Texas: Field Trip Guidebook of the Houston Geological Society, Houston: 73–77.
- Yancey TE, Davidoff AJ (1994) Paleogene sequence stratigraphy of the Brazos River section, Texas. *Gulf Coast Association of Geological Societies Field Trip Guide*: 104.
- Yancey TE (1995) Depositional trends in siliciclastic deposits of the Stone City transgressive systems tract, middle Eocene, Texas. *Gulf Coast Association of Geological Societies Field Guide*: 581–586.
- Davidoff AJ, Yancey TE (1993) Eustatic cyclicity in the Paleocene and Eocene: data from the Brazos River Valley, Texas. *Tectonophysics* 222: 371–395.
- Davidoff AJ, Yancey TE (1993) Relating sequence stratigraphy to lithostratigraphy in siliciclastic-dominated shelf settings. Paleogene, central-east Texas. *Transactions of the Gulf Coast Association of Geological Societies* 43: 97–108.
- Zuschin M, Stanton RJ (2002) Paleocommunity reconstruction from shell beds: a case study from the Main Glauconite Bed, Eocene, Texas. *Palaios* 17: 602–614.
- Thornton CA (1994) Sediment diagenesis, fossil preservation, and depositional environment in the Stone City/Lower Cook Mountain transgression (Middle Eocene, Southeast Texas): A test of chemical taphofacies in the rock record [Master of Science]: Texas A&M University. 189 p.
- Huggett JM, Gale AS, McCarty D (2010) Petrology and palaeoenvironmental significance of authigenic iron-rich clays, carbonates and apatite in the Claiborne Group, Middle Eocene, NE Texas. *Sedimentary Geology* 228: 119–139.
- Davidoff AJ, Yancey TE (1993b) Eustatic cyclicity in the Paleocene and Eocene: data from the Brazos River Valley, Texas. *tectonophysics* 222: 371–395.
- Stanton RJ, Jr., Nelson PC (1980) Reconstruction of the trophic web in paleontology: community structure in the Stone City Formation (middle Eocene, Texas). *Journal of Paleontology* 54: 118–135.
- Berg RR (1979) Stratigraphy of the Claiborne Group. Lower Tertiary of the Brazos River Valley: Guidebook of the Houston Geological Society.
- Dyar MD, Gunter ME, Tasa D (2008) Mineralogy and optical mineralogy: Mineralogical Society of America Chantilly, VA.
- Odin GS (1988) Green Marine Clays: Oolitic Ironstone Facies, Verdine Facies, Glaucony Facies and Celadonite-Bearing Facies - A Comparative Study. Amsterdam: Elsevier. 445 p.
- Burst JF (1958) Mineral heterogeneity in glauconite pellets. *American mineralogist* 43: 481–497.
- Bhattacharyya DP (1983) Origin of Berthierine in Ironstones. *Clays and clay minerals* 31: 173–182.
- Triplehorn DM (1966) Morphology, internal structure, and origin of glauconite pellets. *Sedimentology* 6: 247–266.
- McCarty DK, Drits VA, Sakharov B, Zviagina BB, Ruffell A, et al. (2004) Heterogeneous mixed-layer clays from the Cretaceous Greensand, Isle of Wight, southern England. *Clays and clay minerals* 52: 552–575.
- Huggett JM, McCarty DK, Calvert CC, Gale AS, Kirk C (2006) Serpentine-nontronite-vermiculite mixed-layer clay from the Weches formation, Claiborne group, middle Eocene, northeast Texas. *Clays and clay minerals* 54: 101–115.
- Sánchez-Navas A, Martín-Algarra A, Eder V, Reddy BJ, Nieto F, et al. (2008) Color, Mineralogy and Composition of Upper Jurassic West Siberian Glauconite: Useful Indicators of Paleoenvironment. *The Canadian Mineralogist* 46: 1249–1268.
- Needham SJ, Worden RH, Mellroy D (2004) Animal-sediment interactions: the effect of ingestion and excretion by worms on mineralogy. *Biogeosciences* 1: 113–121.
- Bailey SW (1988) Odinite; a new dioctahedral-trioctahedral Fe (super 3+)-rich 1: 1 clay mineral. *Clay minerals* 23: 237–247.
- Amorosi A (1995) Glaucony and sequence stratigraphy: a conceptual framework of distribution in siliciclastic sequences. *Journal of Sedimentary Research, Section B: Stratigraphy and Global Studies* 65: 419–425.
- Huggett JM, Gale AS, Clauer N (2001) The nature and origin of non-marine 10 Å clay from the Late Eocene and Early Oligocene of the Isle of Wight (Hampshire Basin), UK. *Clay minerals* 36: 447–464.
- Hesselbo SP, Huggett JM (2001) Glaucony in ocean-margin sequence stratigraphy (Oligocene-Pliocene, offshore New Jersey, USA; ODP Leg 174A). *Journal of Sedimentary Research* 71: 599.
- Kronen J, Glenn CR (2000) Pristine to reworked verdine: keys to sequence stratigraphy in mixed carbonate-siliciclastic foreereef sediments (Great Barrier Reef). *Special Publication-SEPM* 66: 387–404.
- Stonewipther SA (1999) Genetic Characteristics of Glauconite and Siderite: Implications for the Origin of Ambiguous Isolated Marine Sandbodies. *Special Publication-SEPM* 64: 191–204.
- Thurman HV, Trujillo AP (1999) *Essentials of Oceanography*. Upper Saddle River New Jersey 07458: Prentice-Hall, Inc. 527 p.
- Dyar MD (1984) Precision and interlaboratory reproducibility of measurements of the Mossbauer effect in minerals. *American Mineralogist* 69: 1127–1144.
- Ku TCW, Walter LM (2003) Syndepositional formation of Fe-rich clays in tropical shelf sediments, San Blas Archipelago, Panama. *Chemical Geology* 197: 197–213.
- Moore DM, Reynolds RC, Jr. (1997) *X-Ray Diffraction and the Identification and Analysis of Clay Minerals*. book: 1–378.
- Pestitschek B, Gier S, Essa M, Kurzwil H (2012) Effects of Weathering on Glauconite: Evidence from the Abu Tartur Plateau, Egypt. *Clays and clay minerals* 60: 76–88.
- Ryan PC, Hillier S (2002) Berthierine/chamosite, corrensinite, and discrete chlorite from evolved verdine and evaporite-associated facies in the Jurassic Sundance Formation, Wyoming. *American Mineralogist* 87: 1607–1615.
- Pouchou JL, Pichoir F (1991) Quantitative analysis of homogeneous or stratified microvolumes applying the model "PAP": Electron probe quantitation. New York: Plenum Press.
- Wivel C, Mørup S (1981) Improved computational procedure for evaluation of overlapping hyperfine parameters distributions in Mössbauer spectra. *Journal of Physics E14*: 605–610.
- Dyar MD, Schaefer MW, Sklutte EC, Bishop JL (2008) Mossbauer spectroscopy of phyllosilicates: Effects of fitting models on recoil-free fractions and redox ratios. *Clay Minerals* 43: 3–33.
- Bradbury CD (2012) *Rapid Reconnaissance Methods of Investigation for Trace Components in Deep-Sea Sediments [Masters]: University of Utah*.
- Ayling B, Rose P, Petty S, Zemach E, Drakos P (2012) QEMSCAN (Quantitative evaluation of minerals by scanning electron microscopy): capability and application to fracture characterization in geothermal systems. *Proc. Thirty-Seventh Workshop on Geotherm Reserv Eng*. Stanford, California: Stanford University.
- Gottlieb P, Wilkie G, Sutherland D, Ho-Tun E, Suthers S, et al. (2000) Using quantitative electron microscopy for process mineralogy applications. *JOM Journal of the Minerals, Metals and Materials Society* 52: 24–25.
- Herberlah D, Williams MAJ, Halverson G, McTainsh GH, Hill SM, et al. (2010) Loess and floods: High-resolution multi-proxy data of Last Glacial Maximum (LGM) slackwater deposition in the Flinders Ranges, semi-arid South Australia. *Quaternary Science Reviews* 29: 2673–2693.
- Geological Society of America (2009) *Rock color chart with genuine Munsell color chips*.
- Amorosi A (1997) Detecting compositional, spatial, and temporal attributes of glaucony: a tool for provenance research. *Sedimentary Geology* 109: 135–153.
- JCPDS; JCoPDS (2005) *The International Center for Diffraction Data*. Newtown Square, PA. pp. over 500,000 entries.
- Zachariasen WH, Plettinger HA (1965) Extinction in quartz. *Acta Crystallographica* 18: 710–714.
- Ali AM, Hsia Y, Liu R, Zhang J, Duan W, et al. (2001) A Mossbauer study of evolution of glauconite from Chinese seas. *Spectroscopy letters* 34: 701–708.
- Johnston JH, Cardile CM (1987) Iron substitution in montmorillonite, illite and glauconite by 57 Fe Mossbauer spectroscopy. *Clays and Clay Mineralogy* 35: 170.
- Rolf RM, Kimball CW, Odum IE (1977) Mossbauer characteristics of Cambrian glauconite, central USA. *Clays and Clay Minerals* 25: 131–137.
- Drits V, Srodon J, Eberl D (1997) XRD measurement of mean crystallite thickness of illite and illite/smectite: Reappraisal of the Kubler index and the Scherrer equation. *Clays and clay minerals* 45: 461–475.
- Cardile CM, Brown IWM (1988) An 57 Fe Mossbauer Spectroscopic and x-ray diffraction study of New Zealand Glauconites. *Clay Minerals* 23: 13.
- Rancourt D (1994) Mossbauer spectroscopy of minerals. II. Problem of resolving cis and trans octahedral Fe2+ sites. *Physics and Chemistry of Minerals* 21: 250–257.
- Rancourt D, Ping J, Berman R (1994) Mossbauer spectroscopy of minerals. *Physics and Chemistry of Minerals* 21: 258–267.

Author Contributions

Conceived and designed the experiments: SCH AAE. Performed the experiments: SCH BPN EUP CDB MIDD. Analyzed the data: SCH BPN EUP CDB. Contributed reagents/materials/analysis tools: BPN EUP MIDD. Wrote the paper: SCH BPN EUP AAE CDB MIDD.

54. Rancourt D, Ping J, Boukili B, Robert J (1996) Octahedral-site Fe²⁺ quadrupole splitting distributions from Mossbauer spectroscopy along the (OH, F)-annite join. *Physics and Chemistry of Minerals* 23: 63–71.
55. Dyar MJ (2002) Optical and Mossbauer spectroscopy of iron in micas. *Reviews in mineralogy and geochemistry* 46: 313–349.
56. Mozley PS (1989) Relation between depositional environment and the elemental composition of early diagenetic siderite. *Geology* 17: 704–706.
57. Galloway WE, Ganey-Curry PE, Li X, Buller RT (2000) Cenozoic depositional history of the Gulf of Mexico basin. *AAPG bulletin* 84: 1743.
58. Eva AN (1980) Pre-Miocene Seagrass communities in the Caribbean. *Palaeontology* 23: 231–236.
59. Baker ET, Jr. (1995) Stratigraphic nomenclature and geologic sections of the Gulf Coastal Plain of Texas Austin, Texas: U.S. Department of the Interior, U.S. Geological Survey. 94–461.
60. Barnes VEPD (1995) *Geologic Atlas of Texas, Austin Sheet*. Francis Luther Whitney Memorial Edition ed. The University of Texas at Austin, Bureau of Economic Geology.
61. Brindley GW (1982) Chemical compositions of berthierines; a review. *Clays and clay minerals* 30: 153–155.

CHAPTER 5

TRACE FOSSILS AND ICHNOFABRICS ASSOCIATED WITH GLAUCONITIC MINERALS AT TWO CAMBRIAN SITES, WISCONSIN AND TEXAS

Upper Cambrian Reno Member, Lone Rock

Formation, Tunnel City Group,

Southwestern Wisconsin

Introduction

The Upper Cambrian Reno Member of the Lone Rock Formation, Tunnel City Group in southwestern Wisconsin has been described as “glaucopit wormstone” by previous workers because of its green color and prominent trace fossils (Berg, 1954; Schwartz, 1979). This unit provides an opportunity to examine the association of trace fossils and glaucopit minerals with sequence stratigraphic implications in a siliciclastic environment. Paleolatitude at this region of Wisconsin during Late Cambrian was approximately 10°S in the position of prevailing easterly winds. The climate was tropical. Sea level rose and fell, and shorelines transgressed and regressed in cycles over a shallow shelf. Benthic communities occupied the substrate and responded to the environmental fluctuations. The behavior of benthic organisms is reflected in ichnotaxa, ichnofabric, and ichnofacies of the cyclical sedimentary sequences. The associated

mineralogy and distribution of glauconitic minerals clarifies the nature of this Late Cambrian depositional environment.

The Reno Member is exposed at the intersection of U.S. Highway 61 and Wisconsin Highway 60 next to the Wisconsin River in Crawford County, north of Boscobel, Wisconsin (Figure 5.1). At this location trace fossils and glauconitic mineral grains occur throughout the exposed depositional sequence. The stratigraphy and sedimentology have been studied in detail by previous workers (Berg, 1954; Farkas, 1960; Michelson and Dott, 1973; Ostrom, 1970; Schwartz, 1979; Sutherland, 1986; Twenhofel, 1936), and evidence for eustatic sea level fluctuation has been described (Coe, 2005; Vail et al., 1977). The exposure at Boscobel displays numerous cyclical beds that are interpreted as storm deposits. The ichnofabric and sedimentary structures reflect episodes of low to moderate hydrodynamic energy in an environment where glauconitic minerals occur.

In this exposure of the Reno Member, the ichnofabric index ranges from *ii1* to *ii5* within beds. *Palaeophycus*, *Skolithos*, and *Diplocraterion* are the most common ichnogenera at the outcrop. Each is attributed to burrowing worms in softground marine environments belonging to the *Skolithos* ichnofacies. The associated sediment is fine grained quartz sand with glauconitic grains and some dolomite. Each bed shows an upward transition from primary sedimentary structures to biogenic sedimentary structures, reflecting a lam-scram (laminated to bioturbated) pattern. The upward increasing ichnofabric index (from *ii1* to *ii5*) is accompanied by upward decreasing glauconitic grain abundance. Each bed represents a progression from high energy to low energy and is interpreted as a storm event bed. *Palaeophycus* and *Skolithos* are

recognized in the upper part of most beds, while *Diplocraterion* is more concentrated in storm beds of the upper Boscobel section (Figure 5.2).

The glauconitic grains are incorporated into primary sedimentary structures, such as cross bedding, which suggests allochthonous or reworked origin. This observation suggests that the burrowing and the genesis of glauconitic minerals in the Reno Member did not occur at the same time. It appears that the shallow marginal marine processes reworked and redeposited the glauconitic grains in a substrate that was later occupied by burrowing organisms during quiescence. In other words, ichnotaxa that normally indicate shallow water are associated here with deeper marine glauconitic minerals. This finding has interesting sequence stratigraphic implications.

A relationship of ichnology and ichnofabric with glauconitic minerals is demonstrated in the Reno Member of the Tunnel City Group. A characterization of ichnotaxa, ichnofabric, and ichnofacies, along with a determination of distribution, maturity, and genesis of glauconitic minerals, is the objective of this study. The integration of these attributes contributes to understanding the Late Cambrian depositional environment and sequence stratigraphy of southwest Wisconsin. Additionally, it documents the behavioral response of burrowing organisms of a marine benthic community in the context of a tropical paleoclimate during a warm interval and fluctuating sea level.

Previous Work

Regional geology. Paleomagnetic reconstructions indicate a position of 10°S paleolatitude for this region of Wisconsin during the Late Cambrian in a position of

prevailing easterly winds. The shallow Franconian Sea (during Franconian time) transgressed gradually northward via several shoreline oscillations (Michelson and Dott, 1973; Ostrom, 1970). This regional interpretation is supported by paleocurrent direction data. The stratigraphy, petrology, isopach mapping, and a quartzite pebble train indicate a rapidly transgressing sea from the southwest (Hamblin, 1961; Michelson and Dott, 1973). Twenhofel (1936) proposed that Upper Cambrian greensands of Wisconsin reflected extremely shallow waters; in such a setting large violent waves could not form.

The Cambro-Ordovician stratigraphic sequence of Wisconsin is divided into five cycles of sedimentation, each a single transgressive-regressive (T-R) event. A single cycle consists of up to four lithofacies (Ostrom, 1970). The Late Cambrian is characterized by widespread, shallow siliciclastic continental margins of an epicratonic sea. It is associated with a first order global sea level highstand (Haq, 1995; Vail et al., 1977).

Early nomenclature for the Upper Cambrian of Wisconsin included the Franconia Formation (Berg, 1954; Farkas, 1960; Hamblin, 1961; Twenhofel, 1936). Later workers use Franconia Series designation in chronostratigraphic usage, where they developed lithostratigraphic units for southwestern Wisconsin. The Tunnel City Group contains the Lone Rock Formation to the southwest, which intertongues with the Mazomanie Formation sands to the north and east (Michelson and Dott, 1973; Ostrom, 1966, 1970). The Tunnel City Group, Reno Member consists of predominantly storm beds deposited below fair weather wave base in a lower shoreface environment. It represents the lower-energy shelf, and storm surges progressed to a more tidally dominated environment during shore line regression (Mortenson, 1981; Sutherland, 1986).

Local geology. The Reno Member formerly was included in the Upper Greensand of Wisconsin, and later it was termed the Bad Axe Sandstone Member of the Franconia Formation (Twenhofel, 1936). The depositional environment is interpreted as a slow sedimentation regime offshore, while the intertonguing Mazomanie Sandstone is interpreted as being deposited in the upper shoreface (Berg, 1954). Bedding in the Reno Member is cyclical with varied internal thicknesses, and the member can be divided into repeating units bounded by sharp erosional surfaces. The complete sequence consists of 1) a basal erosional surface overlain by a dark-green, flat-pebble conglomerate with a glauconite-rich matrix; 2) high-angle or horizontal planar or hummocky laminated sandstone; 3) quartz-glauconite sandstone with dolomite-filled burrows; and 4) completely bioturbated sediment with primary laminae preserved in patches. Whether the sequence is complete or incomplete, each has an erosional base and top (Sutherland, 1986). The repetitive bedding is indicative of alternating high and low-energy episodes. Symmetrical ripples, indicative of tidal oscillation, clay drapes, and bioturbation reflect the low-energy intervals, while basal erosional contacts, flat-pebble conglomerates, and low angle and horizontal planar laminations indicate high-energy episodes. The Reno Member accumulated below fair weather wave base in storm sequences with bioturbation occurring between storms (Sutherland, 1986). Thicker cross-bedded sandstone beds occur in the upper half of the Reno Member, and at the top of the member is a sandy dolomite, which formed during early diagenesis by alteration of calcite in the shallow water substrate (Berg, 1954).

Glauconitic minerals. Glauconitic minerals are common in Upper Cambrian sandstones of southwestern Wisconsin (Twenhofel, 1936). “Glauconitic wormstones”

dominate the Reno Member of the Tunnel City Group, while the intertonguing Mazomanie Formation lacks glauconite (Berg, 1954; Schwartz, 1979). Glauconitic grains in the Reno Member are concentrated in scour fill, appear in couplets alternating with quartz in cross stratified laminae, and gradually decrease upward in abundance within storm beds. This configuration suggests that quartz and glauconitic grains were hydrodynamically separated. The specific gravity of glauconitic minerals in the Reno Member was measured at 2.81 to 2.83 gm/cc and quartz grains at 2.65 with a difference between the two of about 0.17. Glauconitic grains are generally larger than the associated quartz (Sutherland, 1986), which is unlike most heavy mineral deposits. Most glauconitic grains were transported and rarely reflect their environment of origin (Berg, 1954; Sutherland, 1986). Within each bed, the abundance of quartz grains and dolomite increases upwards. Dolomite crystals fill many of the burrows in the Reno Member. Dolomite commonly occurs as a secondary mineral in association with trace fossils, although usually in carbonate rocks (Byers and Stasko, 1978).

Greensands in southwest Wisconsin were evaluated by early workers for the commercial value of potash. Thus the K_2O composition was carefully analyzed by concentrating green grains and analyzing them. Typical analyses of glauconitic minerals from Wisconsin showed K_2O content of concentrates from the Franconia Formation at 7.29% K_2O and the Upper Greensand at 6.10% K_2O , which indicates mature glauconitic minerals. The glauconitic mineral content varies greatly in the strata of the Franconia Formation. The same Boscobel exposure as in this study was examined by previous workers, and glauconitic mineral grains were reported as high as 20% of the matrix (Twenhofel, 1936). Most of the glauconitic grains occur in the basal, dark green part of

the cyclical beds. Glauconitic particles were described as rarely spherical and often ellipsoidal, and most appeared glossy or polished. Surfaces of glauconitic grains were curved, often impinged upon by associated quartz grains. Dimensions of glauconitic particles ranged from microscopic silt to ½ mm grains. Generally, the area was deemed to have insufficient potash quantity for surface mining (Twenhofel, 1936). Optimal conditions of glauconitization seem to exist at grain sizes between 200 and 500 microns (Odin, 1988), which is a common clay fecal pellet size. Smaller and larger sizes generally produce less mature glauconitic minerals, as if some specific distance is optimal from the outside of a glauconitized substrate.

Methods

Sampling. The sedimentary and biogenic structures in the Boscobel outcrop are readily visible. A section was measured, and samples were collected for later analysis. Photos were taken of each repeating unit to capture the basal and upper contacts, the progressive change in ichnofabric and color, and the individual trace fossils. Representative samples were obtained easily due to the friable nature of the rock. Samples include the basal flat-pebble conglomerate that has a glauconitic matrix to the completely bioturbated quartz and dolomite-rich top of bed. A representative group of samples are accessioned and stored in the ichnological collection at the University of Utah (UUIC).

Mineral identification. Oriented clay mounts were prepared for x-ray diffraction (XRD). Polished thin sections were prepared for microscopic petrography, electron microprobe (EMPA), and Quantitative Evaluation of Minerals by Scanning Electron

Microscopy (QEMSCAN). Plugs were prepared for particle mineral analyses using QEMSCAN. XRD was carried out on the 2- μm clay fraction to determine clay mineralogy. EMPA analyses of glauconitic grains determined chemical composition. QEMSCAN provided quantitative mineralogy and produced detailed mineral maps (in area %) in place of point counts and a textural view that enhanced petrographic observations. Combined results from the various analyses confirmed the mineral identification.

Thin section microscopy. Six thin sections were described using a polarizing transmitted light microscope. Percentage of quartz grains and glauconitic grains was estimated visually using comparison charts (Terry and Chilingar, 1955). Color of the glauconitic grains as seen in microscope is reported, according to standards (Munsell, 2009). Darker green suggests maturity, while lighter green suggests a nascent or immature stage of glauconitization. Other constituents are diagenetic dolomite, flattened clay pebbles, and feldspar grains.

Characteristics of grain texture including grain size, shape, and modal percentages were established. Relative grain size of quartz versus glauconitic grains provides information on density and settling rates of the two constituents in a dynamic environment. Grain shape, whether fractured or rounded, implies energy regime during depositional history. Glauconitic grain form has ichnological implications in that a very smooth ovoid and ellipsoid shape indicates clay fecal pellets as the original source (Boyer, 1977; Cloud, 1962). Grain contacts, whether line contacts, concavo-convex, or point to point reveal compaction information, especially where a glauconitic grain is concave around a quartz grain. Concentric bands that surround glauconitic grains

indicate diagenetic processes. Broken diagenetic rims provide temporal information. For instance, early diagenesis had to occur before grain reworking or transport. Petrographic characterization provides genetic information concerning autochthonous, allochthonous or reworked origin.

X-ray diffraction analysis. Oriented clay mounts were prepared for XRD by crushing, dispersion, and two-stage centrifuge to extract the 2 μm clay fraction. They were analyzed under air-dried, ethylene-glycolated, and heated (375° C) conditions for samples 2a, 3a, 5b, 6b, 7b, 8b, 4c, and 5c. These were analyzed at scan speed of 2° per minute from 2° to 30° 2 θ , with x-ray Cu (40kV/30mA). Jade software provided the diffraction peak position, intensity, shape, and breadth. The calculated diffraction pattern for pure glauconitic minerals, based on the NEWMOD computer program (Moore and Reynolds, 1997), is used for comparison. Also, the NEWMOD simulation of illite with varying Fe was employed in calculations to confirm the glauconitic minerals. Atoms of Fe between 0.5 and 1.0, and octahedral Fe³⁺ between 2.34 and 0.82 indicate glauconitic minerals (William T. Parry, oral communication, 2009).

Electron microprobe analysis. EMP analyses were obtained for green grains in the polished and carbon-coated thin section number R-WI-7B. This sample is from a glauconitic grain rich hummock at the base of a cyclical bed. Three grains were analyzed (two points per grain) for chemical composition using a Cameca SX-50 electron microprobe equipped with four wavelength-dispersive spectrometers. Analytical conditions were 15 keV accelerating voltage, 20 nA beam current, and a defocussed beam of 10–20 μm in diameter. A suite of natural minerals was employed as standards, and X-ray intensities were reduced using a phi-rho-z algorithm (Pouchou and Pichoir,

1991). Spot analyses focused on the pelleted green grains in an attempt to locate a potassium x-ray signal to identify glauconitic minerals and their degree of maturity.

QEMSCAN analysis. To support petrographic and EMPA data, QEMSCAN analyses were done. Thin section number R-WI-7B provided bulk mineral analysis (BMA), field scans, and mineral distribution maps. Two loose grain mounts provided particle mineral analyses (PMA). Since the QEMSCAN technique commonly is used in the mining industry, its use to investigate glauconitic sedimentary rocks is new. Two reference Species Identification Protocol (SIPs) were used. A SIP is a hierarchical mineral database to determine what minerals best fit a measured (EDAX) spectra (Gottlieb et al., 2000; Haberlah et al., 2010). Each SIP was adjusted slightly to enhance the ability to recognize the sedimentary minerals of interest.

The Barric 710 SIP was developed to identify minerals in crystalline rocks; therefore, it has quartz and micas in its data base. Quartz and glauconitic minerals are important constituents in the Reno Member samples, and glauconitic minerals were reasonably represented by the micas. Two polished, carbon-coated grain mounts were made for QEMSCAN analysis. Each was from a storm bed located in the middle of the exposed section. One was from the bottom of the storm bed, the other was from the top of the same bed. Samples were gently ground, sieved (particle size between 60 and 160 μm) and suspended with graphite in epoxy. These were analyzed using the Barric 710 SIP. Samples were measured for bulk chemistry (in area %). Time elapsed for the measurement was 01:20:00. Field size was 2000 by 2000 μm with seven fields analyzed for the bottom of the bed, and three fields were analyzed for the top of the bed. At 53 pixels per second, 5000 particles were evaluated.

A SIP designed for sedimentary rocks, named the “sedmin” SIP, was used to analyze thin section number R-WI-7B for a field scan of BMA. The sedmin SIP provided more detail for clay typing than a typical hard rock mining SIP. It was expected to be more suitable for identification of glauconitic sedimentary grains. The new SIP was developed by removing rare mining related minerals and entering standards from common sedimentary rocks (Richard Jarrard, oral communication, 2009). The sedmin SIP does not have glauconitic minerals in its database. Therefore, the SIP was adjusted to highlight the known glauconitic grains consistent with EMPA findings. Clays and micas were combined to reflect the pattern of glauconitic pellets of the Reno Member. Total scan area was 18 by 26 mm, which was scanned using a coarse point spacing of 10 μm . Field size was 2000 by 2000 μm , and field stitching with sufficient overlap produced a composite digital image.

Results

Combined results from the analytical methods determined the presence of mature glauconitic minerals in the Reno Member of the Lone Rock Formation at Boscobel. Results are supported by XRD, EMPA, and QEMSCAN analytical techniques. Characterization of occurrence is supported by sedimentary petrography and stratigraphic analysis. It confirms that at some time and place in the depositional history, conditions were favorable for the glauconitization process. The consistent size, shape, and glossy surface of glauconitic grains suggest that clay fecal pellets were the predominant original form prior to glauconitization. The concentric rings of mineralization around the pellets indicate early diagenetic processes before burial. The bent and broken nature of most

glaucconitic grains indicates that they were reworked in an environment of moderate to high energy and deposited in a compacted substrate. Incorporation of glauconitic grains into laminae of diagnostic sedimentary structures, such as hummocky cross stratification, suggests a specific, near shore depositional environment.

Characterization of glauconitic minerals. XRD results are displayed in diffraction patterns where the peak position and peak intensity ratio represent the mineralogy. Clay minerals generally are characterized by broad peaks and their identification often is imprecise. Glauconitic minerals and illite have profiles that are difficult to confuse with those of any other clay mineral; however, they have overlapping peak positions. Glauconitic minerals have a higher 001/003 intensity ratio than illite and a very weak or nonexistent 002 peak (Moore and Reynolds, 1997).

Results of the eight oriented clay mounts (air dried) are displayed in a composite diffractogram (Figure 5.3). The diffraction patterns show consistency of peak positions, variable peak intensity of 001 and 003, and weak 002 peaks among samples. Samples 2a, 5b, and 7b best reflect diffraction patterns expected for glauconitic minerals, with intense 001 and 003 peaks and weak 002 peaks. The remaining samples have diffraction patterns that suggest the presence of glauconitic minerals probably in a mix with glauconitic illite. One sample, 7b, is displayed in a composite diffractogram of air-dried, glycolated, and heated conditions (Figure 5.4). The profiles essentially are unaffected by ethylene glycol solvation and heating. Supporting 2-Theta and d-spacing data for all clay mounts are listed in Table 5.1 A. XRD results are clarified by using the NEWMOD simulation of illite with varying Fe (Table 5.1 B) (Moore and Reynolds, 1997). The number of trivalent iron atoms is listed in the two occupied octahedral sites, where values between

0.5 and 1.0 indicate glauconitic minerals. Results show that clay mounts 2a, 3a, 5b, 7b, and 5c represent glauconitic minerals, while 6b, 8b, and 4c show lower iron representative of glauconitic illite (William T. Parry, oral communication, 2009).

EMPA spot chemical analyses identified glauconitic minerals in the green pelleted grains of thin section R-WI-7B (Table 5.2 A). When compared with the published analyses on clays from the same area (Twenhofel, 1936), presumably done by wet chemistry, results were comparable (Table 5.2 B). Results for Fe_2O_3 average 22.4 wt. %, all reported as ferric iron, while published results show iron content slightly less, Fe_2O_3 (20–22 wt. %) FeO (3–4 wt. %). Interchangeable with Fe_2O_3 in the crystal lattice of glauconitic minerals is Al_2O_3 , which averages 7.6 wt. %, while Twenhofel (1936) found 9–11 wt. % Al_2O_3 . Al_2O_3 can vary because it is an indicator of weathering. K_2O averaged 8.4 wt. %, which defines highly mature glauconitic minerals in sample R-WI-7B. These analyses, though few in number, show consistent results and predominantly glauconitic minerals. A nominal formula for glauconitic minerals is $(\text{K}, \text{Na}, \text{Ca}) (\text{Fe}^{3+}, \text{Al}, \text{Fe}^{2+}, \text{Mg})_4 (\text{Si}, \text{Al})_8 \text{O}_{20} (\text{OH})_4$. The calculated formula from average EMPA results in this study is $([\text{Na}, \text{Ca}]_{0.44} \text{K}_{1.53}, \text{Ca}_{0.03})_{2.00} (\text{Mg}_{0.88} \text{Al}_{0.72} \text{Fe}^{3+}_{2.41})_{4.00} (\text{Al}_{0.56} \text{Si}_{7.44})_{8.00} \text{O}_{23.93} (\text{F}_{0.14} \text{OH}_{3.86})_{4.00}$.

A QEMSCAN field scan (BMA) was done on thin section R-WI-7B using the sedmin SIP. Results show 2-D digital images of the mineralogy in four false color field scans (Figures 5.5 A–D). Quantitative modal mineral abundances are specified in area %. The first image shows all the minerals detected. The remaining three images show abundance and texture of glauconitic minerals and clays, quartz, and K-feldspar, respectively. The image of glauconitic minerals and clays displays rounded ovoids and

ellipsoids of the pelleted fraction with matrix at 56%. Their size, shape, orientation, abundance, and distribution are apparent. The quartz (25% pink grains) and K-feldspar (6% purple grains) are displayed in textural distribution. Sample R-WI-7B represents the bottom of a bed, which is rich in glauconitic grains and mud rip-up clasts. Quartz and feldspar fragments are concentrated in the rip-up clasts and are easily differentiated from the glauconitic pellets and matrix. The field scans quantify observations made during thin section microscopy. The bimodal distribution of grain size relative to grain composition is displayed.

QEMSCAN (PMA) analysis of grain mounts using the Barric 710 SIP compared glauconitic grains from the bottom and top of a single storm bed. It provided a quantitative measure of the trend of upward decreasing micas, which represent glauconitic minerals, from 24% (bottom of bed) to 10% (top of bed). It also provides a quantitative measure of the upward increasing quartz, feldspar, and dolomite within a storm bed from 50–20–1 to 57–23–7%, respectively (Table 5.3 A).

Results of bulk chemistry for all the constituents in the field of view, as determined from the QEMSCAN SIP definition, are given in Table 5.3 B with calculated elemental mass percent and elemental oxide percent. These bulk chemical results are expected to be different from the EMPA spot analyses (Table 5.2 A) of a single grain. In fact, SiO₂ was much higher in the bulk sample than in the spot analysis. Fe₂O₃ and K₂O concentration, on the other hand, was much lower in the bulk sample than in the spot analyses of glauconitic pellets, which was expected. Bulk chemistry results (Table 5.3 B) also compare the bottom of a storm bed with the top. Both Fe₂O₃ and K₂O content show an upward decrease within the bed, which probably reflects the upward decrease in

abundance of glauconitic minerals rather than a change in the maturity of glauconitic minerals. These QEMSCAN chemical results support and expand upon the EMP analyses.

Sedimentology. The petrographic characteristics of abundance, sorting, grain shape, grain contacts, packing, and modal mineralogy indicate detrital processes in the depositional environment. A summary of petrographic results is provided in Table 5.4. Detailed petrographic analyses for each thin section are reported in the Appendix. For conformity, this study uses the previously introduced sedimentary rock descriptions for a typical bed: i.e., a basal flat-pebble conglomerate overlain by quartz-glauconitic feldspathic laminated sandstone, which grades upward into pale orange-tan, quartz-glauconitic feldspathic sandstone with dolomite-filled burrows that commonly are truncated by erosion (Sutherland, 1986).

Glauconitic grain abundance decreases upward within each storm bed. The three thin sections that represent basal storm beds, R-WI-2A, R-WI-7B, and R-WI-5C, showed higher glauconitic grain abundance, which is estimated at 10–20%, 40–50%, and 5–10%, respectively. Thin sections, R-WI-3A and R-WI-8A, represent the middle, laminated part of storm beds, with estimated glauconitic grain abundance at 3–5% and 5–20%, respectively. Here the glauconitic grains were incorporated into primary sedimentary structures, which commonly are accented by alternating green and white laminae. The mineral specific laminae indicate hydrodynamic separation probably due to different specific gravities and varied energy regime. Thin section R-WI-4C was from the upper trace fossiliferous part of a storm bed with estimated glauconitic grain abundance of 3–5%, in fine sand. Top of the exposure generally had more broken glauconitic grains, an

overall finer grain size, and unimodal distribution where glauconitic grains were about the same size as quartz grains. Glauconitic grains were least abundant in the upper bioturbated parts of beds, except where overlying storm scour introduced glauconitic grains into the spreiten of *Diplocraterion* burrows. These petrographic results reflect a decreasing energy regime within storm beds.

Arrows on the photomicrographs (Figures 5.6 A–G) indicate the grain characteristics described here in. Bent and broken glauconitic grains were observed in all six of the thin sections from bottom to top of the exposure at Boscobel. Concentric rings of glauconitic mineralization were evident around many of the glauconitic pellets (Figures 5.6 A, B, D, and E) termed diagenetic rims. The rims are composed of fairly uniform bands that were bent and broke with the glauconitic grain. The rims must have formed during early diagenesis, before detrital processes associated with storm bed deposition. This suggests that rims formed on the seafloor associated with the glauconitization environment.

Glauconitic grains commonly were larger than other detrital grains displaying bimodal distribution (Figures 5.6 A–G). Quartz and feldspar grains represent the smaller size fraction. Previous study of Reno Member glauconitic grains found they had slightly higher specific gravity (2.81 to 2.83 gm/cc) than the quartz grains at 2.65 (Sutherland, 1986). The glauconitic grains had higher mass per unit volume or higher density than the quartz grains, so it is logical to find the glauconitic grains concentrated in the flat pebble conglomerates of basal storm beds. Waning storm energy could winnow out the less dense quartz grains. The two grain types occur together in bimodal size distribution, whether in the bottom, middle, or upper storm bed. It is difficult to explain why the

larger more dense glauconitic grains occur with the smaller less dense quartz grains. An explanation based on grain provenance is fitting. The detrital quartz was terrestrial, while the glauconitic grains were marine offshore as in the glauconitization environment. Shallowing sea level would introduce the detrital quartz, while glauconitic grains would remain essentially unmoved from their site of origin. Ultimately, the two grain types were deposited together. Both were subjected to the storm activity and settling hydrodynamics of the epicratonic sea.

A variety of grain contacts were observed. There are sutured line contacts between some quartz grains (Figure 5.6 D), which indicate pressure solution during compaction. Concavo-convex contacts are numerous, where glauconitic grains curve around quartz grains, which confirms that they were softer when compacted (Figures 3.6 C, D, and G). The flattened clay pebbles were nonglauconitic rip-up clasts incorporated into the glauconitic matrix of basal storm beds (Figure 3.6 G).

In the upper parts of storm beds, burrowing and bioturbation were prevalent. The composition of individual burrows was fundamentally different from that of matrix as evident in color contrast. The tan burrows, usually *Skolithos*, probably were filled with fine sediment during quiescent intervals between storms. Rhombohedral dolomite crystals formed as a cementing agent in many of the burrows (Figures 5.6 E and F). Spreiten structure of *Diplocraterion* was accented by alternating laminae of glauconitic grains and quartz.

The petrographic characteristics certainly confirm that the glauconitic pellets and associated quartz grains were deposited in an environment with episodic energy. The glauconitic minerals are not in their environment of origin. Indeed, the sedimentology

indicates the allochthonous or reworked origin of glauconitic grains.

Stratigraphy. Each bed represents a storm event, bounded by a basal scour and topped by an erosional contact. Most beds include some parts of the typical storm bed, with average thickness of about 50 cm. The complete sequence in terms of sedimentary and biogenic structures consists of the following: 1) a basal erosional surface overlain by a dark-green, glauconitic matrix and flattened-clay pebbles with a hint of imbrication and preferred orientation of pellets (Figure 5.6 C); 2) hummocky-cross stratification (HCS) and/or wavy to planar lamination; 3) lamination interrupted by burrows, usually with dolomitized fill; and 4) thoroughly bioturbated sediment with primary laminae preserved in patches. Whether the sequence is complete or incomplete, each has an erosional base and top (Sutherland, 1986). Primary sedimentary and biogenic structures are sketched in Figure 5.2 and photographed in Figures 5.7–5.9.

Hummocky cross stratification (HCS) in the Reno Member is typically small scale, which is uncommon in the geologic record, but it might be expected in a setting where small waves were prevalent in the broad, epicratonic shallow shelf area of this Late Cambrian paleoenvironment (Twenhofel, 1936). HCS characteristically exhibits low angle cross stratification with widely varying directions of inclination. Swaley cross stratification (SCS) occurs as amalgamated HCS and generally indicates increased storm frequency. A discrete line of small-scale hummocks (20–30 cm across) marks the middle (part B) of the Boscobel section (Figure 5.10). Some scour surfaces occur within beds indicating intermittent erosional activity between larger storm events. The primary sedimentary structures described and illustrated here characterize a lower shoreface environment below fair weather wave base and within storm wave base. The biogenic

structures, which are intimately associated with the sedimentary structures, also indicate intermittent storm activity in a shoreface paleoenvironment.

Ichnology. The ichnology of the Reno Member was characterized on the basis of ichnotaxa (trace fossils), ichnofabric (degree and type of bioturbation), and ichnofacies (paleoenvironment). The predominant ichnogenera at Boscobel include *Palaeophycus*, *Skolithos*, and *Diplocraterion*, indicated by yellow arrows in Figures 5.11–5.13. Trace fossils occur only in the middle and upper parts of storm beds. The ichnofabric index ranges from *ii1* to *ii5* (i.e., from unbioturbated to intensely bioturbated), and this range was observed in a single storm bed (Figure 5.2). This trace fossil association typifies the *Skolithos* ichnofacies and also may occur in the *Cruziana* ichnofacies. Ichnodiversity is expected to be low in the *Skolithos* ichnofacies, as is the case in the Reno Member. Ichnotaxa were difficult to distinguish in the completely bioturbated zones at the top of some beds, especially in part A of the exposure (Figure 5.1 B) where ichnotaxa are dominated by *Palaeophycus*. Other beds were characterized by *Skolithos* and *Diplocraterion* at the top. Horizontal views of trace fossils were few, as there is little access to bedding planes in the Boscobel exposure. Vertical cross-sectional views of ichnotaxa and ichnofabric were numerous (Figures 5.11–5.13). Body fossils were not found in the Reno Member at Boscobel, although inarticulate brachiopods were described by earlier workers in the Franconia Formation of southwest Wisconsin (Twenhofel, 1936), which includes the Reno Member.

Palaeophycus. *Palaeophycus* is a simple, typically nonbranching burrow with a distinct burrow wall of clay, which distinguishes it from *Planolites*. It is oriented horizontal or oblique to bedding with fill that may be similar or slightly lighter in color.

It is a long-ranging (Precambrian to Recent) ichnotaxon (Miller, 2007). In the Reno Member, *Palaeophycus* was recognized in highly bioturbated zones (ii5) at the top of cyclical storm beds especially in the lower (part A) of the exposure at Boscobel. Burrows are oriented at various angles and filled with sediment usually lighter in color than the host sand (Figure 5.11).

Palaeophycus superficially resembles *Macaronichmus* in having a similar burrow diameter; smooth sides; nonbranching, sinuous trail; and occurrence in dense concentrations. *Palaeophycus* differs from *Macaronichmus* in possessing a distinct wall, which indicates occupation and stabilization of a permanent open burrow (Bromley, 1996). *Macaronichmus segregatis*, on the other hand, has sharply defined margins, and it is a feeding trace formed by selective ingestion of grains (Clifton and Thompson, 1978). *Macaronichmus* burrows have not been described in Cambrian rocks.

Palaeophycus can represent multiple behaviors including tunneling and dwelling of a suspension feeder or deposit feeder in an open burrow. It also has been suggested that in some cases it might be the burrow of a passive carnivore (Miller, 2007). If its behavioral significance was similar to that of *Macaronichmus*, then the burrower may have been a polychaete deposit feeder that thrived on organic matter on the surface of sand grains and lived in a dynamic environment (Clifton and Thompson, 1978). *Palaeophycus* is common in the *Skolithos* ichnofacies in a low to moderate energy, shallow marine setting.

Skolithos. *Skolithos* is a very common trace fossil at Boscobel (Figure 5.12 and 5.13). Some beds are monoichnospecific, but in other beds *Skolithos* occurs alongside *Diplocraterion*. *Skolithos* is common in Cambrian rocks worldwide, often in a high-

density ichnofabric termed “piperock” (Droser, 1991). *Skolithos* burrows in the Reno Member, although sometimes monospecific, are not closely crowded as in typical piperock. The vertical shafts are fairly straight and are not branched. They occur in fine grained sand in the upper part of storm beds. The burrow fill is structureless with no evidence of menisci. The *Skolithos* shafts are tan, which renders them readily visible against a darker green-gray matrix that includes some glauconitic grains. When examined in thin section, the burrow fill shows dolomite crystals, which may have formed penecontemporaneously from micrite burrow fill (Morrow, 1978) or secondarily if burrows served as conduits for dolomitizing fluids (Byers and Stasko, 1978). Burrow diameter is consistently about 0.2 to 1 cm, and the common ichnospecies is *S. linearis*.

Skolithos generally is regarded as a dwelling trace (Domichnion). During the Cambrian and Ordovician, the probable trace makers were worms (annelids or phoronids) behaving as suspension feeders (Bromley, 1996). The paleoenvironment consistently associated with *Skolithos* is moderate to high energy, shallow marine, softground, terrigenous in the *Skolithos* ichnofacies. This suggests a benthic community of suspension feeding opportunists as best suited to thrive in the warm, somewhat dynamic, shallow marine of Late Cambrian.

Diplocraterion. *Diplocraterion* is a vertical U-shaped burrow with a protrusive and/or retrusive spreite. The shafts are generally parallel and vertical to the bedding plane, sometimes with funnel-shaped shaft openings. *Diplocraterion* is common in Cambrian through recent rocks worldwide (Miller, 2007). In the Reno Member at Boscobel, *Diplocraterion* appears in increasing abundance in the uppermost storm beds (part C of the exposure, Figure 5.1). The U-shaped burrows clearly display a

characteristic spreite (mostly protrusive, but sometimes retrusive) between two nearly vertical shafts (Figure 5.13). Distance between shafts is 2–3 cm, depth of burrows 2 to 15 cm. The spreite is highlighted by alternating dark green glauconitic grains and lighter colored quartz and K-feldspar grains. Bottoms of the burrows are semicircular. The two shafts of the burrows are not always parallel; some diverge and others converge. The funnel-shaped openings were not observed at this exposure probably due to truncation of the burrow tops by storm erosion (Figure 5.13).

Diplocraterion represents a dwelling trace (domichnion). It is described as the burrow of a suspension feeder attempting to maintain a constant depth relationship between the base of the burrow and the sediment-water interface (Mason and Christie, 1986). Thus, the ethologic term *equilibrichnion* also applies (Bromley, 1996). The spreite is inferred to accommodate a paleoenvironment of repeating episodes of erosion and sedimentation due to low wave energy and intermittent storm wave energy.

Diplocraterion is a common constituent of the *Skolithos* Ichnofacies. This environment typically is developed in clean, well-sorted, loose, or shifting sand with moderate wave or current energy (Miller, 2007). *Diplocraterion* also may occur in the *Cruziana* ichnofacies (Ekdale et al., 1984). *Diplocraterion* reflects the interaction between marine benthic communities and substrate with fluctuating energy in a shallow marine setting. It is characteristic of a shallow subtidal and/or intertidal environment (Bromley, 1996; Cornish, 1986).

Diplocraterion and *Skolithos* commonly appear in the same formation, but they are segregated into separate beds. The reason for the separation, whether it is biotic interaction or depositional environment, is unknown (Cornish, 1986). This phenomenon

is apparent in the Reno Member where parts of some beds have *Skolithos* burrows alone, while other storm beds have both *Diplocraterion* and *Skolithos* burrows. *Diplocraterion* is more abundant in the upper part of the exposure, which represents the shallowing environment.

Ichnofabric. An upward increasing ichnofabric index (from *ii1* to *ii5*) characterizes the storm beds of the Reno Member of the Tunnel City Group. The cyclical beds reflect a lam-scam (laminated to bioturbated) pattern (Figure 5.2). Tops of beds are highly bioturbated (*ii4–ii5*), particularly in the lower section where *Palaeophycus* dominates with dispersed *Skolithos*. In the upper section, tops of beds are generally less bioturbated (*ii3–ii4*), where 10 to 40 percent of original bedding is disturbed.

Diplocraterion appears in the upper part of the exposure, and *Skolithos* persists. The tops of beds can best be described as a *Skolithos* ichnofabric, but not a true piperock ichnofabric. The ichnofabric at Boscobel reflects alternating cycles of erosion, deposition, and bioturbation as each cycle progresses from rapid to slow sedimentation. Trace makers, mostly suspension feeders, colonize during slow sedimentation, which contributes to upward increasing bioturbation. *Palaeophycus*, *Skolithos*, and *Diplocraterion* commonly are components of the ichnofabric in marine subtidal environments (Gérard and Bromley, 2008).

Ichnofacies. The Reno Member represents a shallow marine paleoenvironment, which is reflected by the *Skolithos* ichnofacies. The sediment indicates a clean, well sorted, soft substrate with rippled to cross bedded sand and a low ichnodiversity (Seilacher, 1967). The trace fossil assemblage (*Palaeophycus*, *Skolithos*, and *Diplocraterion*) at the top of beds in the Reno Member exhibits a predominantly vertical

orientation of burrows, which is common in the *Skolithos* ichnofacies. This would be an inhospitable environment to many life forms due to shifting sand, but it would be possible for adaptable vertical burrowers and predominant suspension feeding lifestyle (Bromley, 1996). The *Skolithos* ichnofacies in the Reno Member represents an opportunistic colonization of storm beds during periods of quiescence following a storm event. Ichnocoenoses of opportunistic ichnotaxa commonly reflect a low diversity and high density of organisms. Trace fossils characteristic of the *Cruziana* ichnofacies, which reflect deposit feeders and horizontal burrowers, were not prevalent in beds at Boscobel.

Discussion

The Boscobel section displays repeating cyclical storm beds common to the Reno Member of the Lone Rock Formation. The ichnotaxa, ichnofabric, ichnofacies, mineralogy, sedimentology, and primary sedimentary structures described and illustrated herein offer significant paleoenvironmental information. The trace fossil assemblage (*Palaeophycus*, *Skolithos*, and *Diplocraterion*) characterizes an environment of variable energy. The ichnofabric, which is reminiscent of lamscram storm beds, suggests intermittent high energy followed by periods of quiescence and occupation. The *Skolithos* ichnofacies indicates a siliciclastic marine environment proximal to the shoreline. The presence of glauconitic minerals indicates that change has occurred because this is not a glauconitization environment. All evidence points to a dynamic depositional history.

The repeating storm beds show a gradual change from bottom to top of the exposure at Boscobel, which suggests environmental change through time. The

ichnological change is most evident with the decreasing occurrence of *Palaeophycus*, the increasing numbers of *Skolithos*, and gradual appearance of *Diplocraterion* in the upper stratigraphic section. HCS, which is an indicator of the lower shoreface, also was less evident in the upper section. Petrographic analyses showed more fractured grains and unimodal grain size distribution in the upper section. All observations indicate that water shallowed from the bottom to top of the exposure and that higher energy intervals became more frequent. This suggests a transition from lower shoreface to middle and upper shoreface paleoenvironment in the Reno Member.

Ichnological implications. The ichnogenera at Boscobel (*Palaeophycus*, *Skolithos*, and *Diplocraterion*) are considered diagnostic of marine environment. *Diplocraterion* and *Skolithos* are present in many Cambrian Formations and establish the presence of a low-level, suspension feeding infaunal trophic group, interpreted to represent an intertidal environment (Cornish, 1986, Seilacher, 1967). In the Boscobel exposure they occur in storm beds below fair weather wave base. The Cambrian epicratonic seas, located near the Cambrian paleoequator, characteristically have numbers of suspension feeding traces (*Diplocraterion* and *Skolithos*), but few body fossils (Cornish, 1986) as was observed in the exposure at Boscobel.

Diplocraterion, with its long geologic range and fairly narrow environmental distribution, is a good indicator of depositional environment. *Diplocraterion* certainly indicates that the substrate was unstable. It is interpreted as a soft-bodied seafloor colonizer during transgressions (Cornish, 1986). It is associated with low biological diversity, which suggests an opportunistic benthic community. The presence of *Diplocraterion* indicates episodic events that occurred at unpredictable intervals, and in

this case, due to storms, which is reflected in the lam-scam ichnofabric in the exposure at Boscobel.

The Cambrian shallow marine tropical environment with broad epicratonic areas and warm seafloor would support a thriving community. Deposit feeding worms (of whatever affinity) and the suspension feeding fauna had ample opportunity for fecal pellet production. Fossilized feces now may be reflected in the abundant glauconitic pellets that are ubiquitous in Cambrian shallow marine detrital deposits, and they attest to a time rich in marine life. In fact, the Reno Member of the Lone Rock Formation contains an abundance of glauconitic grains. Morphology of the glauconitic grains suggests they had fecal pellet origin. Fecal pellets would have been produced by mud eaters, possibly trilobites or soft-bodied benthos, capable of pelletizing clay. The paleoenvironment favorable for fecal pellet production and preservation would be mud rich lagoon or quiet off shore, middle, and outer shelf, an ideal environment for glauconitic mineral authigenesis. The pellets provide the requisite chemically reducing sites for glauconitization.

Mineralogical implications. Analyses of green grains from the Reno Member confirm that the pelleted grains are glauconitic minerals. Assuming that glauconitization processes conform to uniformitarianism, glauconitic minerals would have formed on a fully marine sediment starved low energy shelf well below storm wave base (Carozzi, 1993; Odin, 1988). During the 10^5 to 10^6 years necessary for glauconitization, the fecal pellets underwent authigenesis. A substrate comprised of soft, malleable clay fecal pellets was exposed to the optimal water depth, Eh and pH that are favorable for the glauconitization process. Pellets became more brittle as they incorporated iron and

became glauconitized. Sea level would have been at a highstand in the sediment starved phase of transgression.

Sedimentological analyses of glauconitic grains in the Reno Member indicate that they do not occur in their environment of origin. They are concentrated in basal flat pebble conglomerates and HCS structures of storm beds. The glauconitized pellets, although physically resistant and chemically persistence in a marine environment, were bent and broken during reworking, deposition, burial, and compaction of the Reno Member. This is an energy regime different from the normal glauconitization environment. The glauconitic pellets clearly were subjected to detrital processes.

Many pelleted grains formed coatings of concentric rings, also comprised of glauconitic minerals. Petrographic evidence indicates that the diagenetic rims formed prior to detrital processes and prior to burial and compaction. The rims developed without evidence of impedance from surrounding grains. Glauconitic grains and rims were broken and bent as one unit. Sometimes the rims were missing, as if chipped off during detrital processes.

The puzzling bimodal grain size distribution, where larger and denser glauconitic grains occur with smaller and less dense quartz grains, can best be explained by grain provenance. Glauconitic grains were reworked in place, essentially at their site of origin, in a shallowing sea, while detrital quartz grains were introduced by sediment transport from a terrestrial source area. Ultimately, the two grain types occur together in storm bed deposits of the Reno Member.

Implications for paleoenvironment. The ichnology and mineralogy of the Reno Member reflect a multistage history. It was laid down during shallowing conditions of a

regression amidst the repeated transgressive-regressive sequences on a broad epicratonic shelf of Late Cambrian age in southwest Wisconsin. There are paleoenvironmental implications when hummocky and swaley cross-stratification incorporate glauconitic grains. Glauconitic pellets in the storm beds do not occur in their environment of origin. However, they may well occur near their approximate site of origin. During eustatic shallowing of sea level, the glauconitic bottom sediment was reworked in place by lower shoreface processes. Detrital quartz grains were introduced from a nearby terrigenous source. The mixture of glauconitic grains, some with rims intact, and quartz grains were sorted, fractured, and redeposited in primary sedimentary structures. Storm activity and burrowing organisms below fair weather wave base reworked the substrate without causing appreciable lateral transport of the sediment grains. The alternating green and buff laminae resulted from hydrodynamic separation of the minerals according to specific gravity.

The epicratonic shallow shelf represented by the Reno Member paleoenvironment displays glauconitic sediments that have been reworked and trace fossils that were not. It appears that the shallow marginal marine processes reworked and redeposited the glauconitic grains in a substrate that was later occupied by burrowing organisms during quiescence. In other words, shallow water ichnotaxa are associated with deeper marine glauconitic minerals.

Cambrian Lion Mountain Member, Upper

Riley Formation in Central Texas

Introduction

The Lion Mountain Member of the Upper Riley Formation is the second trace fossiliferous glauconitic occurrence of Cambrian age examined in this study. It is exposed at Hoover Point on Texas Farm Road 1431 in Burnet County central Texas. Cambro-Ordovician strata in this region accumulated during a transgressive-regressive shift in depositional environment (Chafetz, 1978). The Riley Formation is divided into three members: Hickory Sandstone, Cap Mountain Limestone, and Lion Mountain Sandstone (Figure 5.14).

The roadcut at the Hoover Point displays the Lion Mountain Member as a striking green sandstone with interspersed white lenticular nodules (Figure 5.15 A and B). The green rock is trace fossiliferous, glauconitic sandstone, and the white nodules consist of calcite cemented skeletal material, predominantly trilobite carapaces, that accumulated as lag in troughs of subaqueous megaripples (Chafetz, 1979; McBride, 1988). The glaucarenite is nearly devoid of trilobite fragments, while the nodules are full of trilobite fragments. McBride (1988) suggested depositional segregation of trilobite fragments from the host rock with concentration into the megaripples of the nodules with dissolution loss by formation waters a contributing factor to the lack of shells in the host rock.

The Upper Riley Formation has been well studied with a primary focus on the regional stratigraphy, paleontology, and petrology. The trace fossils in the Lion Mountain Sandstone, although readily visible, have not been the focus of previous

studies. This study of trace fossils, ichnofabric, and associated glauconitic minerals adds new perspective to the paleoenvironmental interpretation.

Previous Work

The Riley Formation comprises the basal Paleozoic strata of the Llano uplift. It rests nonconformably on the undulating pre-Paleozoic craton. It is a transgressive-regressive sequence, the uppermost member being Lion Mountain, which is a craton-wide regressive glauconitic sandstone that caps and completes the sequence. It is composed of trough cross-stratified, fossiliferous glaucarenites. Glaucarenites are sandstone in which glauconitic minerals make up more than 25% of the composition (Chafetz, 1978). These strata are overlain by a wide-spread unconformity, which makes the Riley Formation an unconformity bound unit (Bridge et al., 1947).

The display of trough cross-stratified, fossiliferous glaucarenites in the Lion Mountain Member indicates shallow subtidal to tidal-flat deposition (Chafetz, 1978). The white lenticular nodules that represent shell lag in troughs of subaqueous megaripples also are consistent with a high energy setting. The skeletal material is comprised of broken and nonbroken parts of trilobites, brachiopods, and echinoderms that became sites of extensive carbonate cementation as a result of high original porosity (Chafetz, 1979; McBride, 1988). The glauconitic grains were originally fecal pellets that were glauconitized and squashed together (Chafetz and Reid, 2000).

The glaucarenites of the Lion Mountain Sandstone and the Bliss Sandstone of southwestern New Mexico were studied together by Chafetz and Reid (2000). They are similar in age (Cambro-Ordovician) and similar in composition (glaucarenites).

Although the two are from two different formations approximately 1000 km apart, they both are trough cross-stratified deposits and are comprised of abundant glauconitic minerals. This unusual occurrence of glaucarenite in a high energy setting was the focus of detailed petrographic work by Chafetz and Reid (2000).

Some 300 thin sections were studied as part of a dissertation which provides invaluable petrographic data on the glaucarenites (Chafetz, 1978). Fibroradiated rims of authigenic glauconitic minerals were observed on glauconitic pellets, quartz grains and skeletal grains. The glauconitic pellets probably formed in a seafloor glauconitization environment, while the rims formed by precipitation of glauconitic minerals in the free spaces surrounding the pellets. Presence of the fibroradiated rims on glauconitic grains was considered important supporting evidence for the conclusion that glauconitic minerals of the Cambro-Ordovician from the southwestern US formed in place (autochthonous), in a shallow-water, high-energy environment under conditions that are different from today (Chafetz and Reid, 2000).

The glauconitization zone in modern oceans is at water depths greater than 50 m on the seafloor of middle to outer shelf and deeper. This is confirmed by numerous studies (Logvinenko, 1982; Odin, 1988; Rao et al., 1993). Chafetz and Reid (2000) suggested that glauconitic minerals formed at a much more rapid rate in the Early Paleozoic than in modern oceans. The warm sea water temperature, the possibility of significant seafloor hydrothermal fluxes, and the abundance of elements and compounds (e.g., S, Fe, Mn, CH_4) suggest that the chemistry of Cambrian seas may have been different from today. These conclusions are interesting and will be taken into account in the discussion of the Lion Mountain Cambro-Ordovician paleoenvironment.

Methods

Sampling. At the Hoover Point outcrop of the Lion Mountain Sandstone, primary and biogenic sedimentary structures are visible in the vertical section. Also, fallen blocks are readily available for inspection of bedding plane surfaces and three dimensional ichnofabric. Samples were collected and photos were taken from the trace fossiliferous strata. Individual trace fossils and bioturbation were visible by color contrast. Representative samples were obtained easily due to the friable nature of the rock. A representative group of samples are accessioned and stored in the ichnological collection at the University of Utah (UUIC).

Mineral identification. Oriented clay mounts, polished thin sections, and a polished rock chip were prepared for analyses. Detailed microscopic petrography was carried out on thin sections. XRD was carried out on the 2- μ m clay fraction to determine clay mineralogy. EMPA analyses of glauconitic grains determined chemical composition. QEMSCAN provided quantitative mineralogy and produced detailed mineral maps (in area %) in place of point counts and a textural view that enhanced petrographic observations. Combined results from the analyses confirmed the mineral identification.

Thin section microscopy. Petrography of five thin sections was described using a polarizing transmitted light microscope on samples numbered LM-TX-18, 19, 24, 26, and 27. Percentage of quartz grains and glauconitic grains was estimated visually using comparison charts (Terry and Chilingar, 1955). Color of the glauconitic grains was reported according to standards (Munsell, 2009). Darker green suggests maturity, while lighter green suggests a nascent or immature stage of glauconitization. The other

constituents described were fossil carapace segments (probably from trilobites) and echinoderm fragments.

Characteristics of grain texture including grain size, shape, and modal percentages were established. Size of quartz grains was measured and bimodal occurrence noted. Grain shape, whether large and rounded or small and angular, reflects the energy regime during depositional history. The predominant glauconitic grain form was originally pelleted, although shape was deformed by pressure, amalgamation, and squeezing between the quartz grains. Grain contacts, whether line contacts, concavo-convex, or point to point, reveal compaction information. Rims that surround glauconitic grains indicate diagenetic processes. The rims, whether broken or impinged, reveal information about the timing of glauconitization. Ultimately, petrographic characterization provided genetic information concerning autochthonous, para-autochthonous (reworked), or allochthonous origin.

X-ray diffraction analysis. Oriented clay mounts were prepared for XRD by crushing, dispersion, and two-stage centrifuge to extract the 2- μm clay fraction. They were analyzed under air-dried, ethylene glycolated, and heated (250° C) conditions for samples numbers LM-TX-18, 19, 24, and 26. These were analyzed at a scan speed of 2° per minute from 2° to 30° 2 θ , with x-ray Cu (40kV/30mA). Jade software provided the diffraction peak position, intensity, shape, and breadth. The calculated diffraction pattern for pure glauconitic minerals, based on the NEWMOD computer program (Moore and Reynolds, 1997), was used for comparison.

Electron microprobe analysis. EMP analyses were obtained on green grains in the polished and carbon-coated thin section numbered LM-TX-24. This sample is from a

highly glauconitic part of the Lion Mountain Member. Two grains and five points were analyzed for chemical composition using a Cameca SX-50 electron microprobe equipped with four wavelength-dispersive spectrometers. Analytical conditions were 15 keV accelerating voltage, 20 nA beam current, and a defocused beam of 10–20 μm in diameter. A suite of natural minerals was employed as standards, and X-ray intensities were reduced using a phi-rho-z algorithm (Pouchou and Pichoir, 1991). Spot analyses focused on the pelleted green grains in an attempt to locate a potassium x-ray signal to identify glauconitic minerals and their degree of maturity.

QEMSCAN analysis. The QEMSCAN technique was effective in illuminating the sediment texture and distribution maps of quartz versus glauconitic minerals. Two reference Species Identification Protocol (SIPs) were adjusted and employed to provide robust data sets. A SIP is a hierarchical mineral database to determine what minerals best fit a measured (EDAX) spectrum (Gottlieb et al., 2000; Haberlah et al., 2010). The Barric 710 SIP was used on the polished rock chip, which was well suited for bulk mineral field scan analysis. In the SIP data base, mica represents glauconitic minerals. The sample was run at high and low resolution with 38 fields at 20- μm pixel size and three fields at high resolution of 5- μm pixel size. Field size was 2000 by 2000 μm . Samples were measured for bulk mineralogy and bulk chemistry (in area %) using assumed standard mineral chemical formulas.

The “sedmin” SIP was used to analyze thin section number LM-TX-24, also well suited for a field scan. The sedmin SIP does not include glauconitic minerals in its database, so the SIP was adjusted to highlight the known glauconitic grains consistent with XRD and EMPA results. Clays and micas were combined to reflect the pattern of

glaucconitic pellets in the Lion Mountain Member. Total scan area was 18 by 26 mm, which was scanned at medium resolution, 10 μm point spacing. Field size was 2000 by 2000 μm .

Results

Combined results from the analytical methods determined the presence of mature glauconitic minerals in the Lion Mountain Member of the Riley Formation at Hoover Point. Results were supported by XRD, EMPA, and QEMSCAN analytical techniques. Characterization of the glauconitic minerals was supported by sedimentary petrography, while stratigraphic analysis determined their occurrence in the depositional system. Results confirm that at some time early in the depositional history, conditions were favorable for the glauconitization process. The grain overgrowths comprised of glauconitic minerals indicate early diagenetic processes, possibly before burial. Incorporation of glauconitic grains into laminae of cross trough stratification, suggests a near shore depositional environment. The amalgamated and squeezed glauconitic grains indicate a soft grain consistency during compaction history.

Characterization of glauconitic minerals. XRD results of four oriented clay mounts (air dried) are displayed in a composite diffractogram (Figure 5.16). Diffraction patterns are consistent among the four samples in peak position and intensity. Each pattern has a high 001/003 intensity ratio and very weak 002 peak, which is diagnostic of glauconitic minerals (Moore and Reynolds, 1997). Although glauconitic minerals and illite have overlapping peak positions, the two clay minerals are differentiated by the 002 peak intensity, which is very weak for glauconitic minerals and recognizable for illite.

XRD results from the Lion Mountain Member samples show an insignificant 002 peak consistent with glauconitic minerals. The profiles were unchanged by ethylene glycol solvation and heating.

EMPA spot chemical analyses focused on the green grains of thin section LM-TX-24. Results from 5 spot analyses are Fe_2O_3 average 27 (in wt. %), all reported as ferric iron, and Al_2O_3 average 4.1% (Table 5.5 A). Examples of published analyses show comparable results in Table 5.5 B. In comparison, the Cambrian Reno Member samples from Wisconsin have lower iron and higher aluminum oxide (22.4 % Fe_2O_3 and 7.6 % Al_2O_3). The higher aluminum oxide often reflects subaerial weathering (Ku and Walter, 2003). K_2O averaged 8.6%, which defines highly mature glauconitic minerals in sample LM-TX-24. These analyses, though few in number, show consistent results and indicate glauconitic minerals. A nominal formula for glauconitic minerals is $(\text{K}, \text{Na}, \text{Ca}) (\text{Fe}^{3+}, \text{Al}, \text{Fe}^{2+}, \text{Mg})_4 (\text{Si}, \text{Al})_8 \text{O}_{20} (\text{OH})_4$. The calculated formula from average EMPA results in this study is $([\text{Na}, \text{Ca}]_{0.44} \text{K}_{1.53}, \text{Ca}_{0.03})_{2.00} (\text{Mg}_{0.88} \text{Al}_{0.72} \text{Fe}^{3+}_{2.41})_{4.00} (\text{Al}_{0.56} \text{Si}_{7.44})_{8.00} \text{O}_{23.93} (\text{F}_{0.14} \text{OH}_{3.86})_{4.00}$ (Erich U. Petersen, 2014, written communication). EMPA spot chemical analyses are consistent with XRD results from clay mounts, which clearly identify the glauconitic mineral composition.

QEMSCAN results from the polished rock chip using the 710 Barric SIP display a mineral map in low resolution (Figure 5.17 A) and another in high resolution (Figure 3.17 B). The glauconitic grain contacts are highlighted by weathering or alteration products at the grain margins. Their remnant pelleted morphology is visible, although the glauconitic grains were squeezed and deformed during deposition, burial and compaction. The high resolution results show quartz grains of 48 area %, while glauconitic minerals,

represented as micas, are 39% (Table 5.6 A and Figure 5.17 B).

Results of bulk chemistry for all the constituents in the field of view (Figure 5.17 B) are given in Table 5.6 B with elemental mass % and elemental oxide % as calculated from the QEMSCAN SIP definition. These bulk chemical results are expected to be different from the EMPA spot chemical analyses (Table 5.5 A) of a single grain. In fact, SiO₂ was much higher in the bulk sample than in the spot analysis. Fe₂O₃ and K₂O concentration, on the other hand, was much lower in the bulk sample than in the spot analyses of glauconitic pellets, which was expected.

QEMSCAN images from thin section LM-TX-24 using the sedmin SIP are reported in Figures 5.18 A–D. When results were compared between samples (thin section and rock chip) and between SIP definitions (the sedmin SIP versus the 710 Barric SIP) variability was evident. Quartz content is 62% in the thin section (Figure 5.18 C), while it is 48% in the rock chip (Figure 5.17 B). Variability in quartz content is expected in this dynamic environment.

Further, glauconitic minerals, grouped under “other” constituents, represented in gray, is 31%, using the sedmin SIP (Figure 5.18 B). Glauconitic minerals, grouped under “mica,” in false color green, are 39%, using the 710 Barric SIP (Figure 5.17 B). Variability is expected between samples and between different SIP definitions. Although this was an experiment that tested different SIP definition in the identification of glauconitic minerals, it was illustrative and the results are comparable. Mineral maps from both SIP definitions reveal the bimodal size of quartz grains and the squeezed and deformed morphology of glauconitic minerals between quartz grains. The <1% apatite content, which represents body fossil fragments, probably trilobites, is readily apparent.

Sedimentology. The Lion Mountain glauconitic unit commonly was termed a glaucarenite by Chafetz (1979). It also can be classified as a glauconitic quartz arenite (Carozzi, 1993). It is a sandstone with over 25% glauconitic grains. A summary of petrographic results is provided in Table 5.7. Five thin sections (LM-TX-18, 19, 24, 26, and 27) were described, and photomicrographs were annotated (Figures 5.19 A–E). The characteristics described herein are indicated by black arrows.

The glauconitic component was estimated at 20 to 40% from thin sections, which is comparable to the QEMSCAN results. Glauconitic minerals appeared dark green corresponding to highly mature glauconitic minerals. Glauconitic material occurs in clumps of amalgamated pellet-shaped grains (Figures 5.19 A, B, and C). Remnant pellet margins remain readily visible highlighted by diagenetic rims or surficial weathering (Figures 5.19 A–E). Rims of various thickness commonly remained intact even though the grain had been squeezed and contorted. Glauconitic grains were squeezed against and between quartz grains (Figures 5.19 A–D) suggesting that they were softer than the quartz and affected by burial compaction and overburden pressure. The rims, composed of glauconitic minerals, were generally un-impinged by surrounding grains, which indicates that they probably were formed during early diagenesis on the seafloor within the glauconitization environment. This suggests formation prior to reworking, deposition, squeezing, and compaction. Broken glauconitic grains were not apparent. Previous workers (Chafetz and Reid, 2000) identified fibroradiated rims on the glauconitic pellets and drew an alternate conclusion, which was that glauconitization of pellet rims formed later within the near shore depositional environment.

Quartz occurs in two grain sizes: coarse and medium-to-fine. The two size

fractions occur together in bimodal size distribution (Figures 5.19 A–E). Coarse grains, which comprise 10 to 20% of the quartz grains, were well rounded and spherical and displayed cracks (Figures 5.19 A–E). The medium to fine size quartz, which comprise the remaining 40 to 50% of the quartz grains, often were subrounded and lacked sphericity, as if they were fragments of the larger quartz grains (Figures 5.19 A–E). Thus, the medium to fine size fraction would have been subjected to less time in the depositional system for rounding and sphericity. Body fossils, which display a long, slender, tapered morphology, comprise less than 1% (Figures 5.19 A, B, D, and E). They represent Cambrian arthropods and probably are segments of trilobite carapaces. They commonly were preserved intact, except where crushed between quartz grains.

The larger than normal pore size, comprised of glauconitic material, was observed in all thin sections (Figures 5.19 A–E). It was caused by clumps of glauconitic pellets that were deposited with the detrital quartz. The clumps were squeezed and forced into surrounding pore space during compaction. This resulted in concavo-convex and amalgamated grain contacts. Also, quartz-to-quartz grain contacts showed concavo-convex alignment (Figures 5.19 D and E) and sutured line contacts, which indicates pressure and solution pressure during compaction. The petrographic characteristics, compositional abundance, and texture indicate detrital processes during its deposition.

Stratigraphy. The sediments in the Lion Mountain Member were incorporated into primary sedimentary structures (Figure 5.20 A and B). The laminae are accented by alternating green glauconitic grains and white quartz laminae. There are paleoenvironmental implications when glauconitic grains are incorporated into trough cross stratification, planar lamination, and mega ripples. It means that deeper marine

sediments were incorporated into shallow marine structures. The megaripples are accented by cemented shell/carapace lag that accumulated in the troughs (Figure 5.20 A). The sedimentary structures described and illustrated here characterize upper shoreface within fair weather wave base. This signifies a high energy, near shore paleoenvironment.

Grain provenance for the quartz clasts was terrestrial, while grain provenance for glauconitic grains was the marine seafloor within the glauconitization environment. Shallowing sea level and continental proximity would introduce detrital quartz, while glauconitic grains would remain in the proximity of their site of origin. Ultimately, the glauconitized pellets and coarse grained quartz were mixed together in a high energy, near shore environment of the Cambrian epicratonic sea. Some of the brittle and cracked coarse quartz grains must have fractured in the process. All grain types (glauconitic pellets, coarse quartz, and medium to fine quartz) were reworked, moderately sorted, and redeposited. This represents a high energy environment, and so the glauconitic grains are not in their environment of origin. It reflects a transgressive-regressive stratigraphic sequence.

Ichnology. The trace fossil assemblage of the Hickory Sandstone Member of the Lower Riley Formation was examined by Cornish (1986). The Hickory Member is the basal sandstone unit on the craton margin, and it exhibits high energy marine settings. Trace fossils, commonly vertical shafts, established the presence of a low-level suspension feeding infaunal trophic group. This information was not available from the body fossil record (Cornish, 1986). The Lion Mountain Member of the Upper Riley Formation, which is the upper regressive unit in the system, also represents a high energy

marine setting. The predominant ichnogenera of the Lion Mountain are *Skolithos* (vertical shafts) (Figure 5.21 A and B) and *Planolites* (horizontal tunnels) (Figure 5.22 A and B). The implications of the trace fossil assemblage exposed at Hoover Point have not been examined until now.

At the Hoover Point exposure, both horizontal and vertical views of trace fossils and ichnofabric are readily available. Individual burrows were evident because of contrasting color and grain size. Burrow fill commonly was darker green with *Planolites* and gray and finer grained with *Skolithos*. Some of the roadside boulders exhibited intense bioturbation, where individual ichnotaxa were difficult to distinguish. On the whole, trace fossils in the Lion Mountain Member exhibited low ichnodiversity, which is a typical characteristic of the *Skolithos* ichnofacies. The ichnofabric index ranged from *ii1* to *ii5*, and the bedding plane bioturbation index (*bpb*) ranged from 1 to 5 (i.e., from unbioturbated to intensely bioturbated).

The pellets that were glauconitized and the trilobite fragments occur together in the Lion Mountain glaucarenite matrix. This suggests a similar provenance. Glauconitic films were not apparent on the trilobite fragments in this study; however, glauconitic rims were observed on some echinoderm fragments (Chafetz and Reid, 2000). The glauconitization environment and the seafloor habitat for open-water trilobites and other fauna must have been the same at some time during fluctuating sea level of the transgression and regression.

Skolithos. *Skolithos* is common in Cambrian rocks worldwide and appears in low density in cross bedded sandstones at Hoover Point (Figure 5.21 A and B). The vertical shafts are fairly straight and are not branched. The burrow fill is structureless with no

evidence of menisci. In the Lion Mountain Sandstone, *Skolithos* was found in a matrix of fewer glauconitic grains and steeper cross beds than *Planolites*.

Skolithos generally is regarded as a dwelling trace (domichnion). During the Cambrian and Ordovician, the probable trace makers were worms (annelids or phoronids) behaving as suspension feeders (Bromley, 1996). The paleoenvironment consistently associated with *Skolithos* is moderate to high energy, shallow marine, softground, terrigenous in the *Skolithos* ichnofacies. This suggests a benthic community of suspension feeding opportunists that were well suited to thrive in the warm, tropical, dynamic, shallow marine of Late Cambrian ocean.

Planolites. The geologic range of *Planolites* is from Precambrian to the present in a variety of settings from low energy to intertidal dynamic energy (Miller, 2007). Its paleoenvironment commonly is associated with a marine softground, and it may represent a mixed *Skolithos-Cruziana* ichnofacies association. In Lion Mountain strata at Hoover Point, *Planolites* is conspicuous and prevalent (Figure 5.22). It appears as mottled ichnofabric (*ii3*) in vertical view at the outcrop and in positive relief on beds with moderate bedding plane bioturbation (*bpb3*). As is characteristic of *Planolites*, the burrows are unlined, unbranched, nonmeniscate, and horizontal and occur in dense patches with numerous cross-overs. They appear like random scribbles on the bedding plane. Tunnel diameter is about 5 mm.

Planolites exhibits horizontal mobility and represents deposit feeding and/or grazing behavior (i.e., domichnia, repichnia, or fodinichnia). It commonly characterizes the *Cruziana* ichnofacies, but it is not exclusively in that ichnofacies. At Hoover Point, *Planolites* may represent an opportunistic response to shifting substrate and water

agitation of a shoreface environment of mixed *Skolithos-Cruziana* ichnofacies.

Planolites in the Lion Mountain Member represents later shallow water occupation of reworked deeper glauconitic substrate.

Discussion

The Lion Mountain Member ichnotaxa, ichnofabric, ichnofacies, mineralogy, sedimentology, and primary sedimentary structures offer essential paleoenvironmental information that must be evaluated in unison. The trace fossil assemblage indicates a shallow marine, terrigenous, *Skolithos* ichnofacies and possibly a mixed *Skolithos-Cruziana* ichnofacies. The ichnofabric, which ranges from 1 to 5, indicates ethologic challenges during occupation of shifting substrate. The sedimentology and stratigraphy are consistent with a high energy, upper shoreface depositional environment. On the other hand, the presence of glauconitic minerals indicates that the environment once was low energy off shore with slow sediment accumulation and stable substrate, which is typical of the glauconitization environment. The evidence indicates that a change occurred during the depositional history, which is consistent with sea level fluctuation, where the transgressive Cap Mountain Limestone is overlain by the regressive Lion Mountain Sandstone. The shallowing sea brought glauconitic sediment in contact with waves and currents of the upper shoreface environment. Terrigenous quartz clasts were introduced and shallow water opportunistic trace fossils then occupied the substrate.

Compare and Contrast the Two Cambrian Sites

Every geological environment is unique in its own way. However, comparing and contrasting depositional environments, whether it is present compared with past, or northern location compared with southern location, has merit in providing clues to understanding. The two Cambrian sites in this study are separated geographically, but have many similarities as well as interesting differences. The sedimentary units are not precisely age dated, but are described as representing Upper Cambrian (Reno Member Wisconsin) and Cambro-Ordovician (Lion Mountain Member, Texas) (Chafetz, 1978; Sutherland, 1986). Each site is characterized by trace fossiliferous, glauconitic mineral-rich deposits. Each represents a marine terrigenous shoreface setting. Both sites reflect fluctuating sea level, transgression and regression, on the margin of the broad Cambrian craton. Both were laid down during shallowing conditions of a shoreline regression. The Reno Member of Wisconsin represents a lower shoreface depositional environment, while the Lion Mountain Member of Texas represents the upper shoreface.

An important realization that supports why glauconitic minerals are common in the geologic record, in a variety of depositional environments, is that once formed they are chemically and stable in the marine environment. Thus, glauconitic grains persist through changing conditions and sediment transport. As a result, allochthonous or para-autochthonous origin is common. The source substrate before glauconitization commonly is fecal pellet-rich, although other offshore marine substrates, such as foraminiferal-rich sediment, support glauconitization as well. The two Cambrian sites examined here had a para-autochthonous origin; that is, they were reworked in place with very little transport, and the source substrate included abundant fecal pellets.

Ichnological Comparison

Trace fossils at each Cambrian site reflect a thriving benthic community in a dynamic paleoenvironment. Deposit feeding worms and suspension feeding burrowers were prolific in the shallow broad epicratonic areas, warm seawater, and tropical environment. They occupied the seafloor substrate and left burrows and tunnels. The trace fossils illustrate their behavioral response to the dynamic paleoenvironment.

In summary, the ichnogenera in the Reno Member at Boscobel, Wisconsin, include *Palaeophycus*, *Skolithos*, and *Diplocraterion*, while the ichnogenera in the Lion Mountain Member at Hoover Point, Texas, include *Skolithos* and *Planolites*. Each site represents the marine terrigenous *Skolithos* ichnofacies, while the Lion Mountain ichnotaxa also could characterize a mixed *Skolithos-Cruziana* ichnofacies. The *Skolithos* ichnofacies reflects an opportunistic benthic colonization of low biological diversity. The *Skolithos-Cruziana* ichnofacies, also exhibiting a low ichnodiversity, reflects a gradual grade and gradual seaward transition to the offshore with varied local energy levels (Howard and Frey, 1984). The signature of burrowing organisms represents substrate perturbation during and after final deposition and before burial and preservation. It was dominated by vertically burrowing organisms and horizontal tunneling infauna of worms, which is common in many Cambrian paleoenvironments (Seilacher, 1967). The fecal pellets, which have been preserved by glauconitization, represent an earlier, seafloor environment that was located off shore.

There is an observed abundance of glauconitic sediment in rocks of Cambrian age. In contrast, there is a lack of glauconitic sediment in rocks older than late Precambrian (Bentor and Kastner, 1965). Both the Lion Mountain Member and the Reno

Member contain abundant glauconitized pellets. The glauconitic grains formed off shore and were persistent enough to survive high energy processes associated with a shallowing sea, specifically, the episodic storms during deposition of the Reno Member and the intertidal processes during deposition of the Lion Mountain Member. Ultimately, the glauconitized fecal pellets were deposited with detrital quartz in a shoreface paleoenvironment.

Mineralogical Comparison

Analyses of the green pelleted grains confirmed mature glauconitic minerals at each Cambrian site. EMPA results show slightly higher K₂O from the Lion Mountain samples than from the Reno Member (8.6–8.4 wt. %, respectively), which is a reflection of time on the seafloor. The Reno Member glauconitic minerals were slightly more aluminum rich and Lion Mountain Member more ferric iron rich. Al-Fe substitution is evident in glauconitic minerals (Figure 5.23) (Barbara P. Nash, 2009, written communication). Higher aluminum relative to iron oxide is an indicator of subaerial weathering (Ku and Walter, 2003), which suggests that the Reno Member sediments were exposed and subjected to more extensive weathering than the Lion Mountain Member.

Composition of the sediment at each site primarily was quartz clastics and glauconitic grains. Quartz is finer grained in the Reno Member lower shoreface storm beds than in the Lion Mountain intertidal (fine compared to coarse grained). Glauconitic grains are soft with a hardness of 2, compared to quartz with a hardness of 7. This relative difference is reflected in the deformation of glauconitic pellets, which commonly were bent, squeezed and amalgamated during reworking, burial, and compaction. When

associated with quartz, it is logical that the glauconitic grains would show more plastic deformation than the quartz grains. A few broken glauconitic grains were noted in the Reno Member, but most were bent, while amalgamated glauconitic grains were prevalent in the Lion Mountain Sandstone. The quartz and glauconitic grains occurred together in moderately sorted deposits, often displayed in alternating green and white laminae of primary sedimentary structures.

Petrographic analyses of samples from each site showed bimodal grain size. The best explanation for this phenomenon is dual provenance, where the quartz clastics were introduced by sediment transport from a terrestrial source area and the glauconitic grains were reworked at their site of origin on the seafloor. Shallowing of sea level during shoreline regression introduced the terrestrial detrital quartz to the glauconitic grain-rich substrate, which was originally associated with the deeper glauconitization environment.

Glauconitic grains reflect the original size of the fecal pellet (from 250 to 500 μm in length), which was fairly consistent. The Reno Member bimodal distribution showed glauconitic pellets relatively larger than the quartz grains. The Lion Mountain bimodal distribution showed some quartz grains relatively larger than the glauconitic pellets. The medium to fine grained fractured quartz and elongate carapace fragments were also in the mix in Lion Mountain sediments.

The bimodal texture and relative sizes based on mineral composition provide significant paleoenvironmental information. In the Reno Member, fine grained quartz reflects lower shoreface. It is mixed with glauconitic pellets that were relatively larger. The Lion Mountain Member, coarse to fine grained quartz, reflects upper shore face intertidal deposition. It is also mixed with glauconitic pellets that are sometimes in

clumps equivalent to the coarse grained quartz. In each case, the glauconitic grains persist in a fecal pellet size range. All observations support dual provenance for the sediment composition. All sedimentologic and mineralogic evidence supports the interpretation of a regressive event in the Late Cambrian system.

Thin section microscopy and QEMSCAN results revealed diagenetic rims on glauconitic grains at both sites. The rims are composed of glauconitic minerals and often appear without evidence of impedance from surrounding grains. Glauconitic grains and rims were deformed as one unit. The Reno Member displayed concentric layered rims of glauconitic minerals, and the Lion Mountain Member reportedly had fibroradiated rims (Chafetz and Reid, 2000), although they are not visible in samples examined here. The question arises whether the rims formed in the glauconitization environment off shore or later as open space fill in the pore spaces of trough-cross stratified deposits. The interpretation here is that rims on glauconitic grains formed prior to detrital processes and prior to burial and compaction. It is unlikely that pellets or pellet rims were glauconitized in the high energy upper shoreface environment in which they are found today.

Implications for Paleoenvironment

It is reasonable to assume that the glauconitization process during the Cambrian was similar to the glauconitization process today. The glauconitic minerals formed in fully marine sediment on a starved, low-energy shelf at water depth greater than 50 m, with specific Eh and pH and temperature (Carozzi, 1993; Odin, 1988). Sea level would have been at a highstand during the sediment-starved phase of the transgressive episode. Fecal pellets would provide microenvironments of reduction and become glauconitized

on the seafloor. The process may have taken 10^5 to 10^6 years, or less. In warm tropical Cambrian seas, the chemical reaction may have been accelerated. This interpretation is consistent with each of the Cambrian sites examined here.

The possibility that the chemistry of seawater during the Cambrian was different from that today cannot be ruled out. The suggestion that significant seafloor hydrothermal fluxes may have resulted in abundance of S, Fe, Mn, and CH_4 and changed the redox of the oceans was proposed as a factor in glauconitization of Lion Mountain sediments (Chafetz and Reid, 2000). An increase in available iron would be favorable for glauconitization. Also, an increase in global temperature, such as during the Cambrian and Cretaceous, is linked to an increase in glauconitic mineral formation. The question remains whether the increase in glauconitization was due to more favorable seawater chemistry or to a climatic shift and rise in global sea level, or both.

It is probable that fecal pellets and glauconitization shared the same off shore environment. However, the zone of prevalent fecal pellets on the seafloor is 0 to 30 m depth, while the zone of glauconitization is 50 to 300 m; thus the shoreline must shift and water must deepen to glauconitize the fecal pellets (Figure 1.6) (Odin, 1988). Mature glauconitic grains signify that extensive transgression occurred because conditions must persist for 10^4 to 10^6 years for development of mature glauconitic minerals, which indicates extensive transgression.

Then the shallowing sea caused the reworking and redeposition of the glauconitic bottom sediment in a mix with terrigenous quartz. Waves, currents, and storms of the shoreface environment prevailed at both Cambrian sites during shoreline regression. Trace fossils characteristic of near shore high energy environment were emplaced in the

substrate. As a result, shallow water ichnotaxa became associated with deeper marine glauconitic pellets.

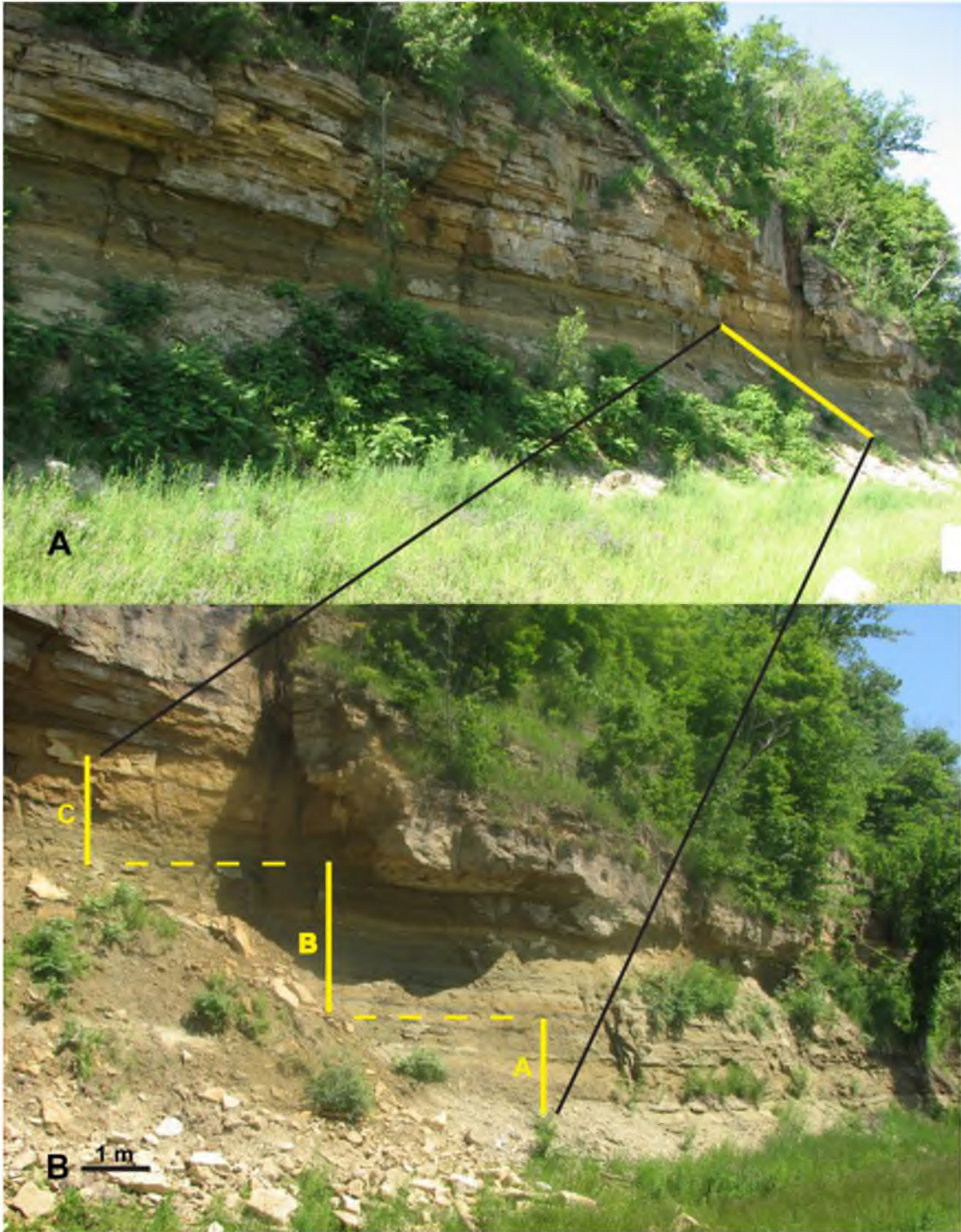


Figure 5.1 Exposure of the Upper Cambrian Reno Member of the Lone Rock Formation north of Boscobel, Wisconsin. A) View of the outcrop showing location of the measured section; B) close up view of the section measured in three parts, lower, middle, and upper (A, B, and C).

R-WI – Reno Member, Wisconsin

2A – 5C – sample #s for thin sections

2a – 5c – sample #s for clay mounts

tsm – thin section microscopy

XRD – X-Ray Diffraction

EMPA – Electron Microprobe Analysis

QEM – QEMSCAN field scan

lam-scam – laminated to scrambled

SCS – Swaley-Cross-Stratification

HCS – Hummocky-Cross-Stratification

WL – Wavy Lamination

PL – Planar Lamination

FPC – Flat-Pebble-Conglomerate

ii – ichnofabric index, bioturbation

Pph – *Palaeophycus* trace fossils

Sk – *Skolithos* trace fossils

Dp – *Diplocraterion* trace fossil

Legend

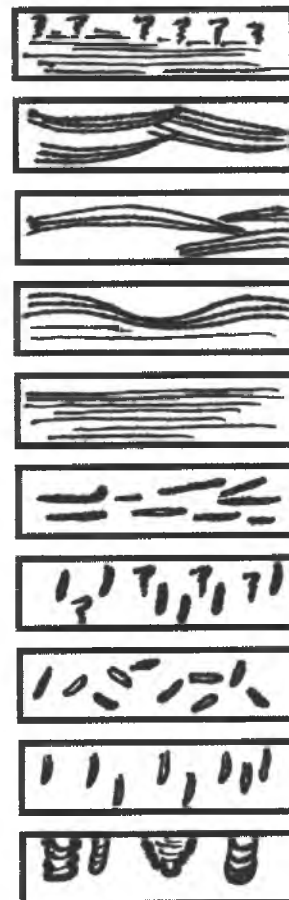


Figure 5.2 Measured section of the Reno Member at Boscobel, Wisconsin.

feet/bed #	stratigraphic section	bed thickness	sample #	analyses	sedimentary & biogenic structures	glauconitic minerals	ichnofabric	trace fossils
10		0.55			HCS	lo	ii4 ii1	
9		1.40			lam-scrum HCS FPC	lo in lams hi	ii5 ii4 ii3 ii1	Dp Sk
8		1.40	top of bed 7b bottom of bed	QEM XRD QEM	lam-scrum PL FPC	lo hi	ii4 ii3 ii2 ii1	Sk
7		0.98	R-WI-8B 6b	tsm XRD	lam-scrum PL		ii3 ii2 ii1	Sk
6		0.75	R-WI-7B 5b	tsm XRD EMPA QEM	HCS PL	in HCS	ii1 ii1	
5		0.30			FPC	hi	ii1	Sk Pph
4		2.40			bioturbation lam-scrum	lo	ii5 ii4	
3		0.60	R-WI-2A R-WI-3A 3a	tsm tsm XRD	WL PL	hi	ii3	
2		0.90	2a	XRD	biogenic structures	med	ii5 ii4	Sk
1		0.53			HCS		ii1	Sk

Figure 5.2 Continued

feet/bed #	stratigraphic section	bed thickness	sample #	analyses	sedimentary structures	glauconitic minerals	ichnofabric	trace fossils
18		0.4			WL		//2	Sk
17		1.24			lam-scrum WL PL		//3 //2 //1	Dp Sk
16		1.9			lam-scrum PL FPC	hi	//3 //1	Dp Sk
15		0.83	R-WI-5C 5c R-WI-4C 4c	tsm XRD EMPA OEM tsm XRD EMPA OEM	lam-scrum WL FPC	hi	//3 //1	Dp Sk
14		0.7			PL	lo	//1	
13		1.4			HCS		//1	
12		2.25	8b	XRD	lam-scrum PL lam-scrum SCS	lo	//2-4 //4 //2 //4 //2 //1	Dp Sk
11		1.05			SCS HCS FPC	lo hi	//2 //2 //1	Sk

Figure 5.2 Continued

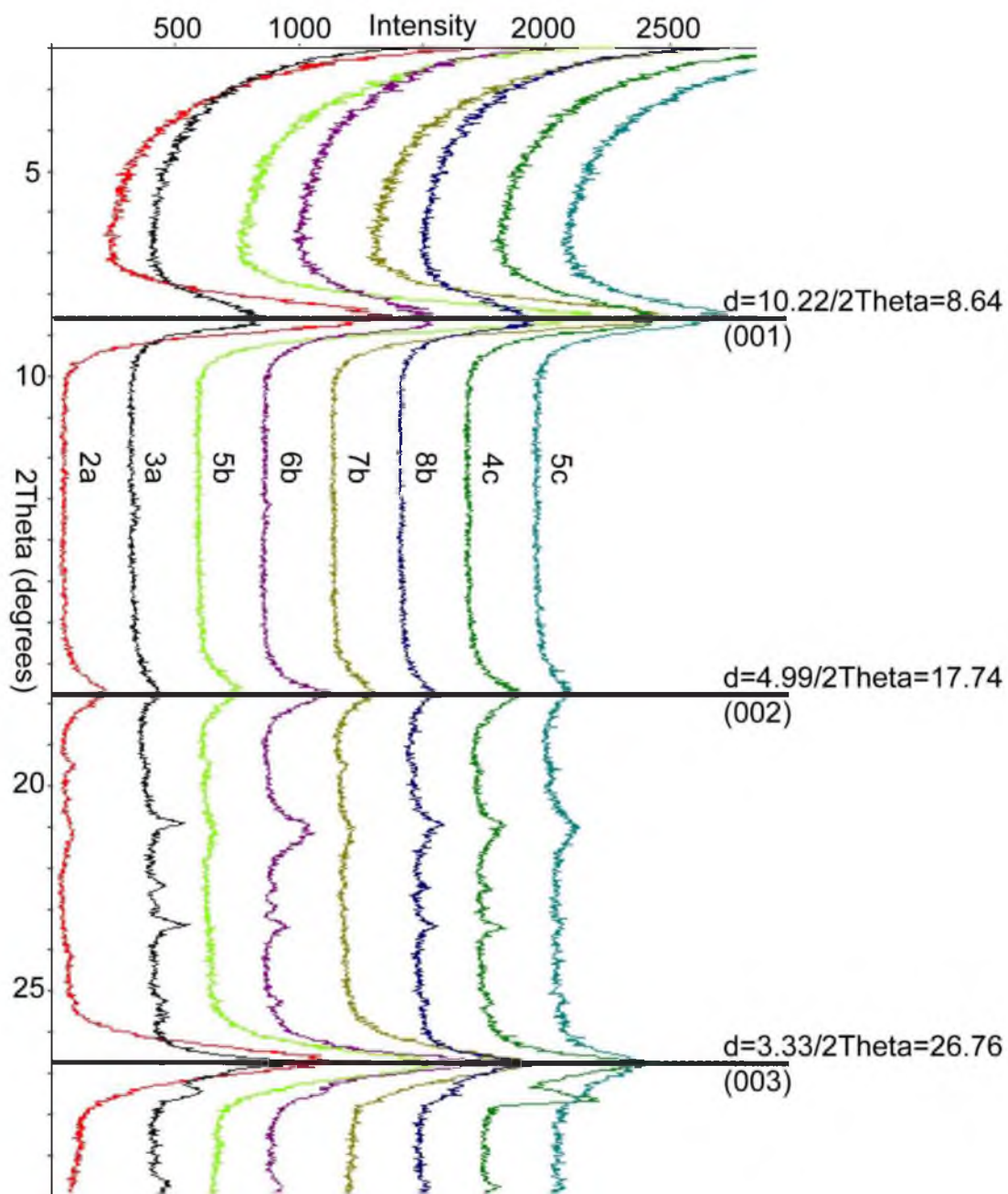


Figure 5.3 Composite X-ray diffractogram of eight oriented clay mounts under air dried conditions from the Reno Member.

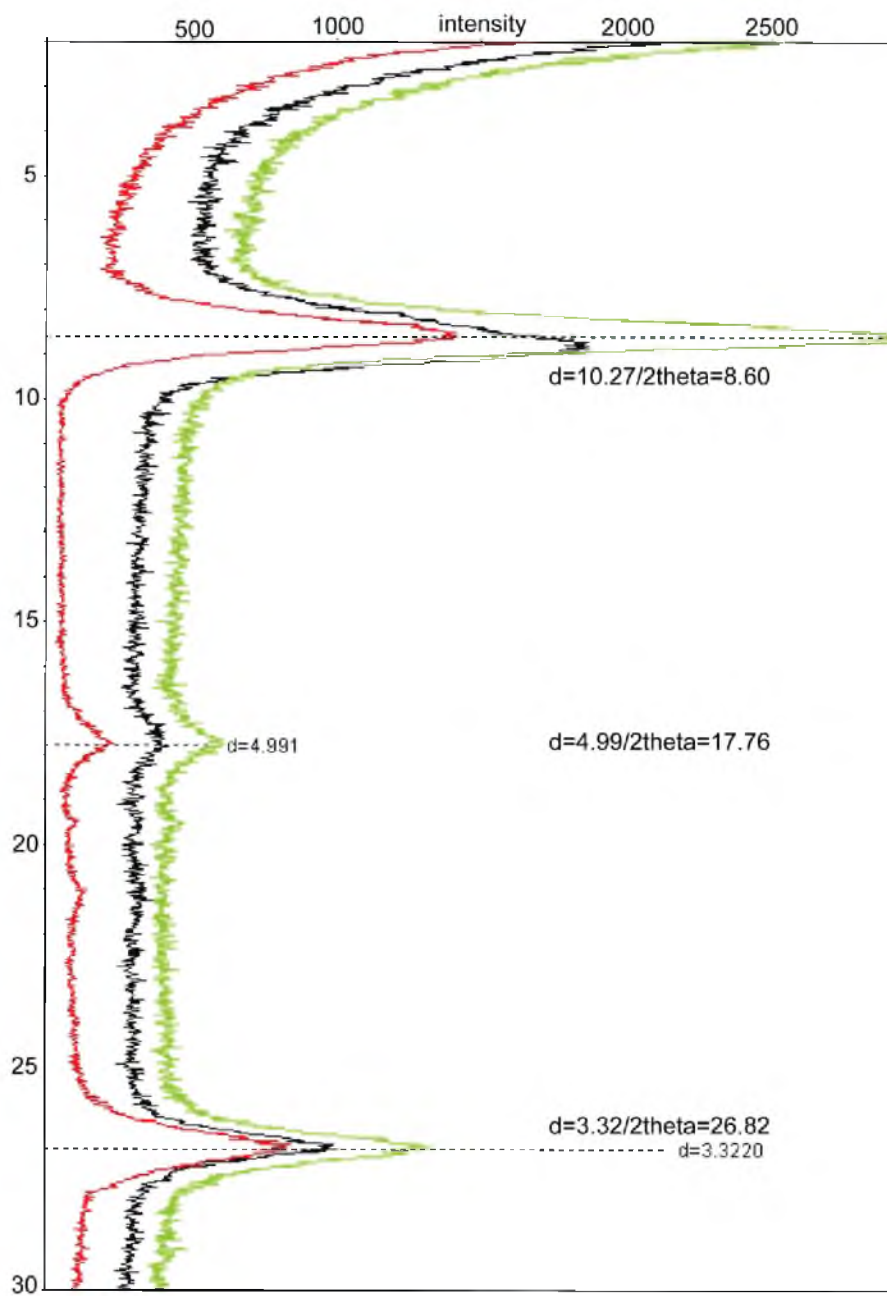


Figure 5.4 Composite X-ray diffractogram of clay mount 7b under air-dried, glycolated, and heated conditions.

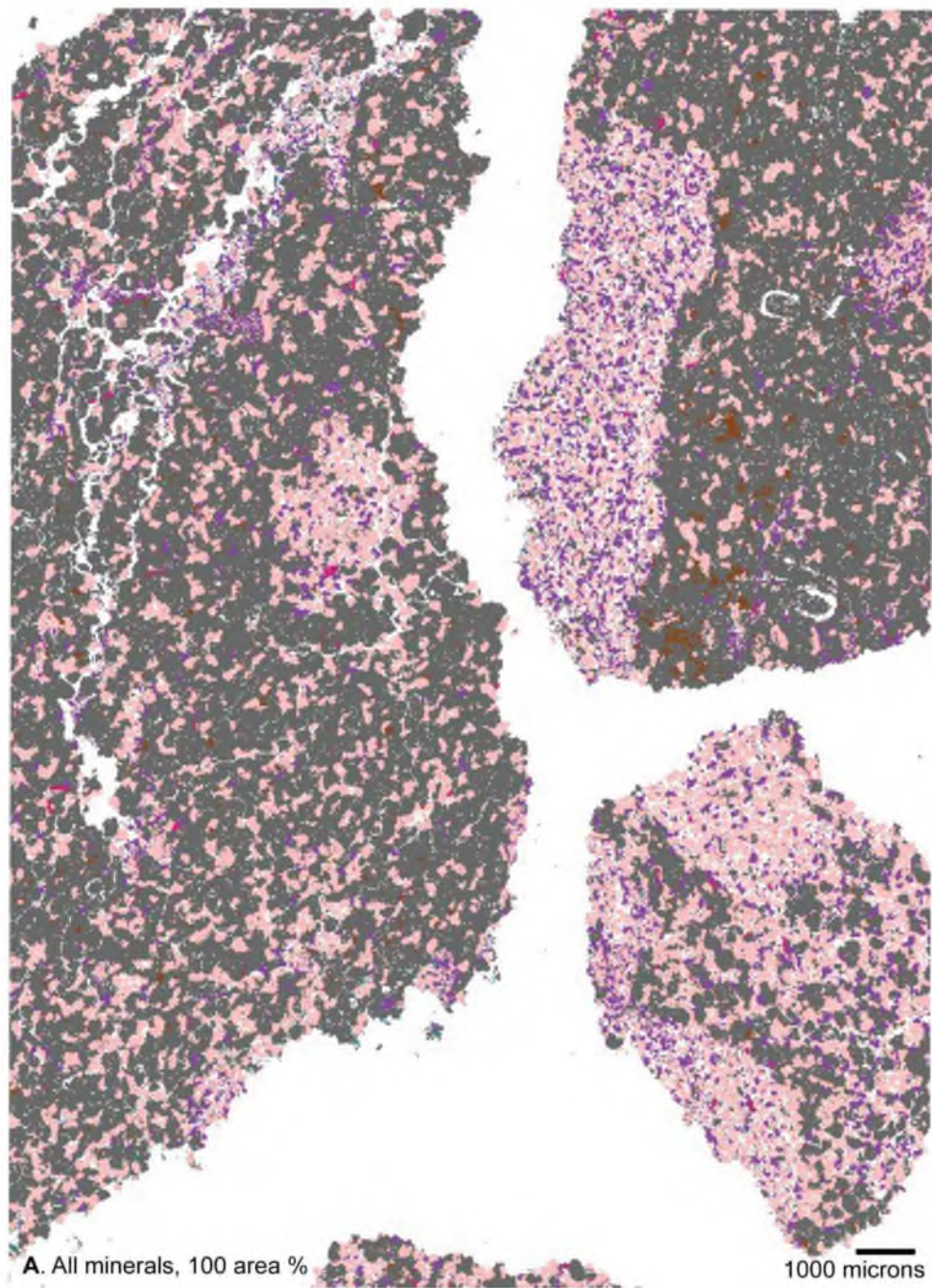


Figure 5.5 QEMSCAN (BMA) images from thin section R-WI-7B. A) field scan representing all minerals, 100 area %; B) field scan representing glauconitic minerals and clays, 56 area %; C) field scan representing quartz, 25 area %; D) field scan representing K-feldspar, 6 area %.

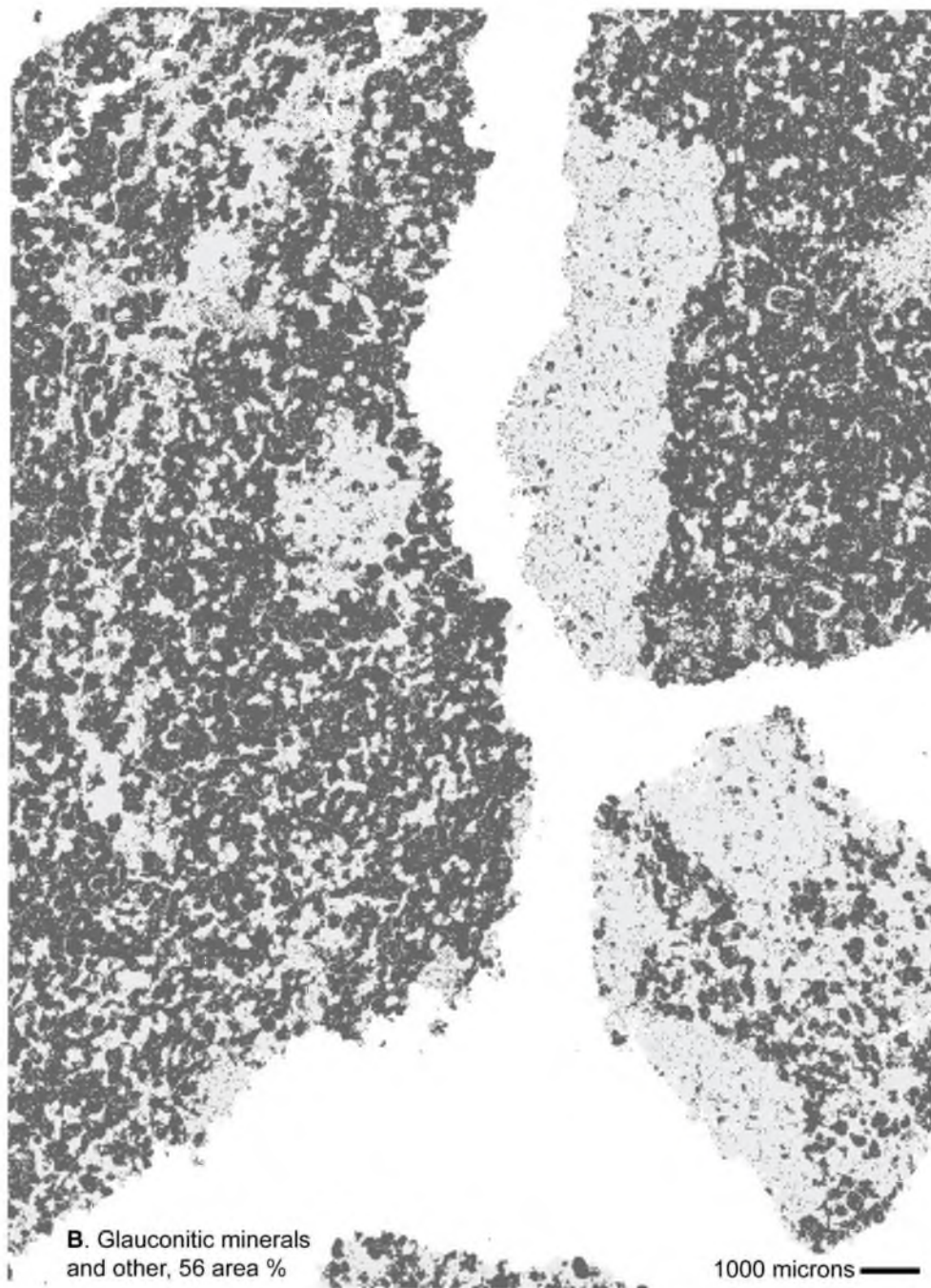


Figure 5.5 Continued

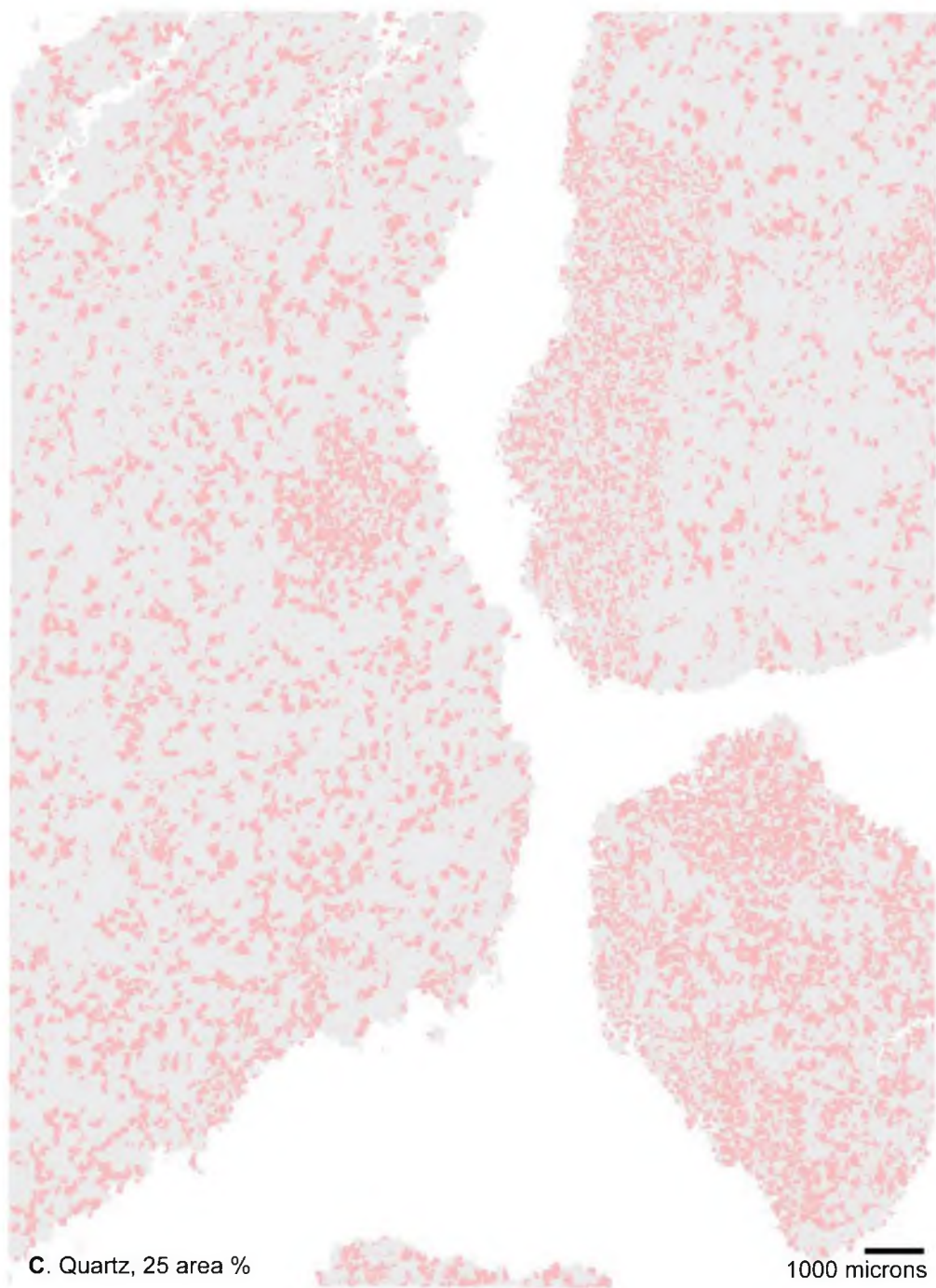


Figure 5.5 Continued

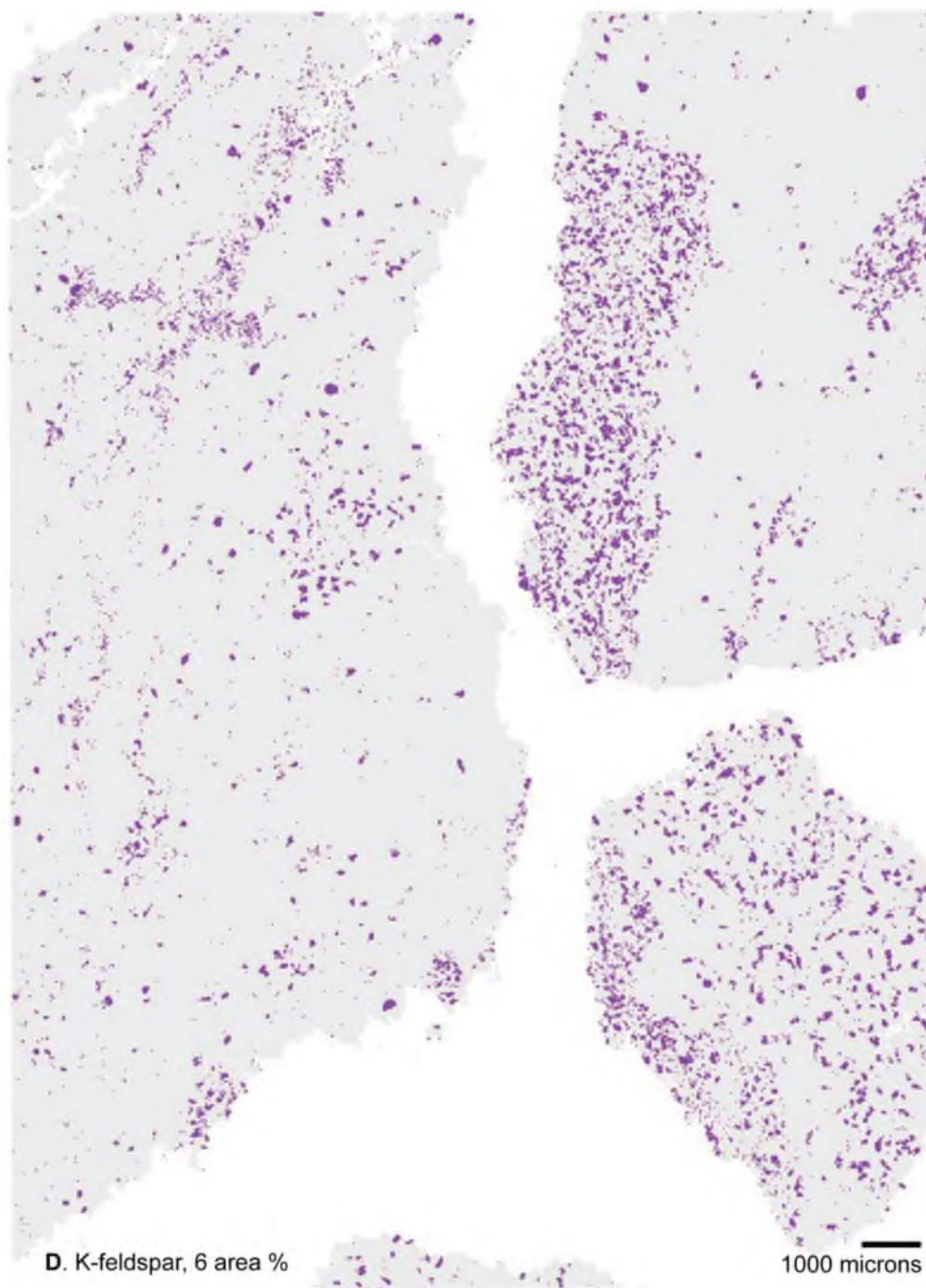


Figure 5.5 Continued

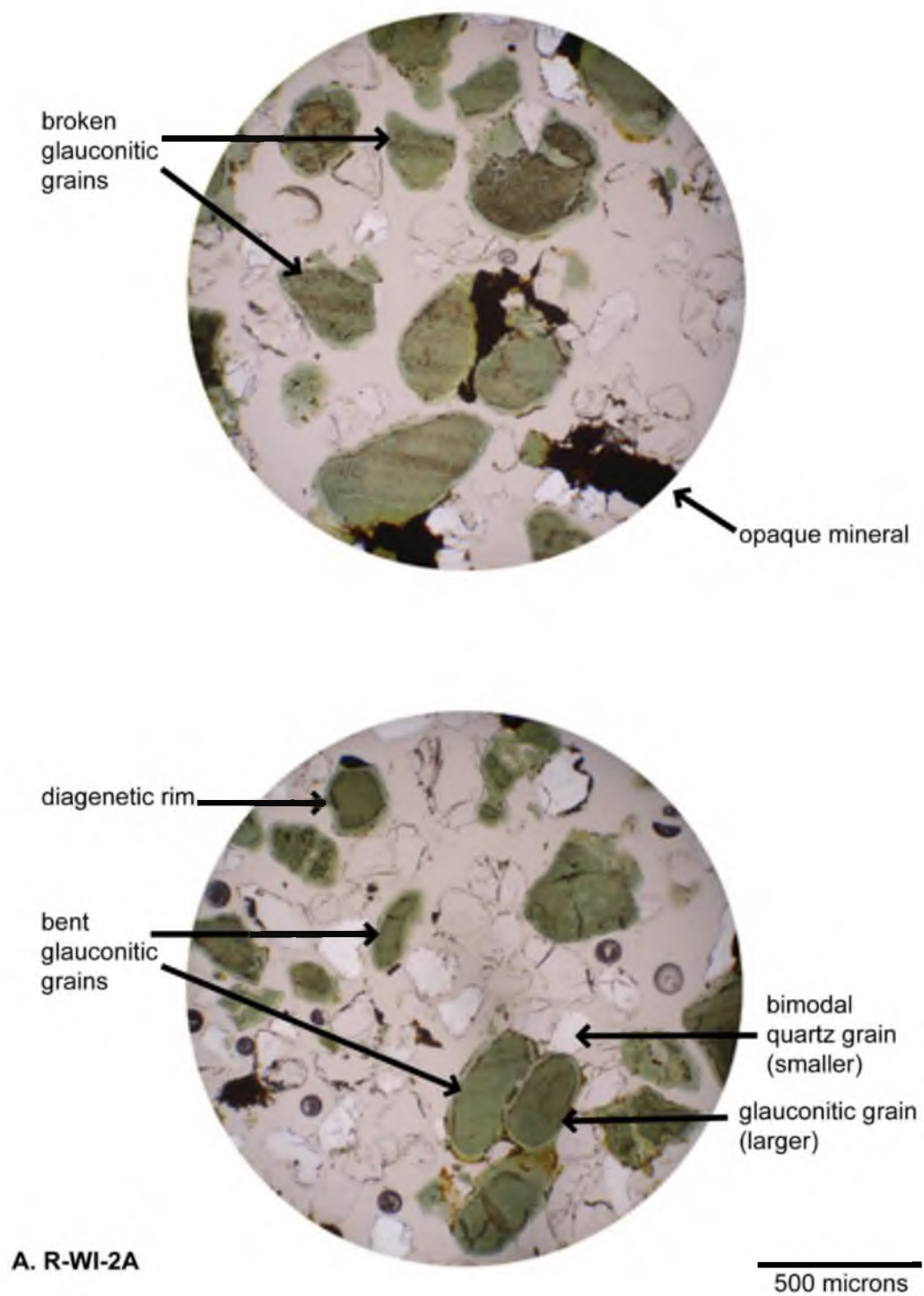
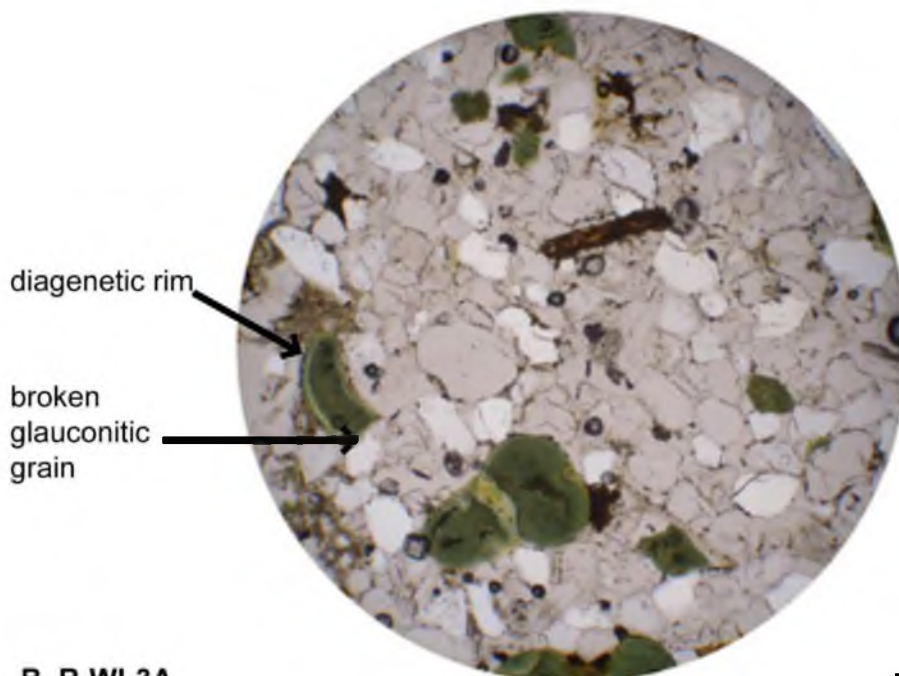
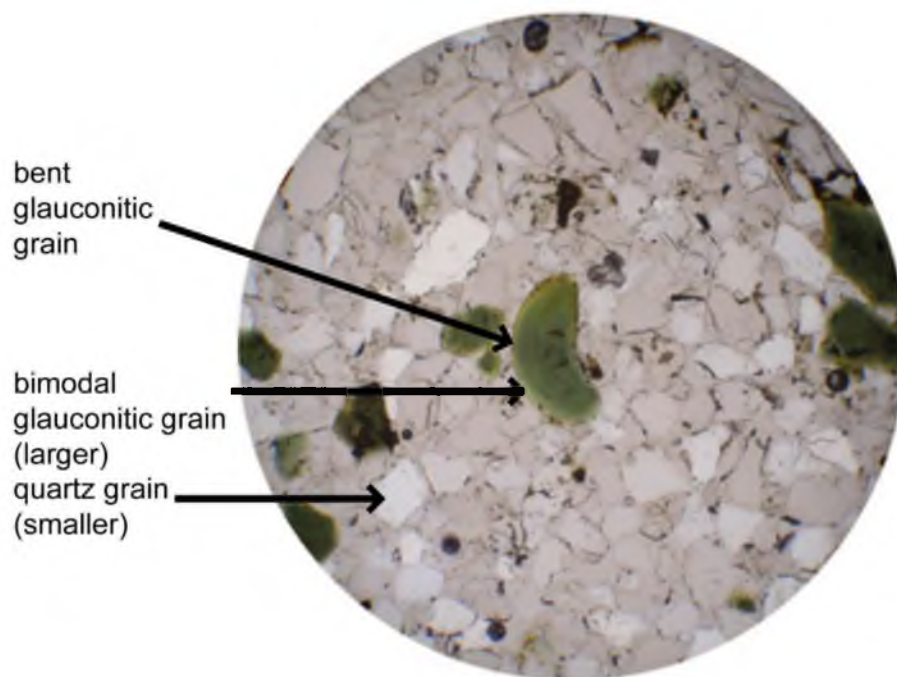


Figure 5.6 Photomicrographs of thin sections in stratigraphic order. A) sample R-WI-3A; B) sample R-WI-2A; C) sample R-WI-7B; D) sample R-WI-8B; E) sample R-WI-4C; F) sample R-WI-5C.



B. R-WI-3A

500 microns

Figure 5.6 Continued

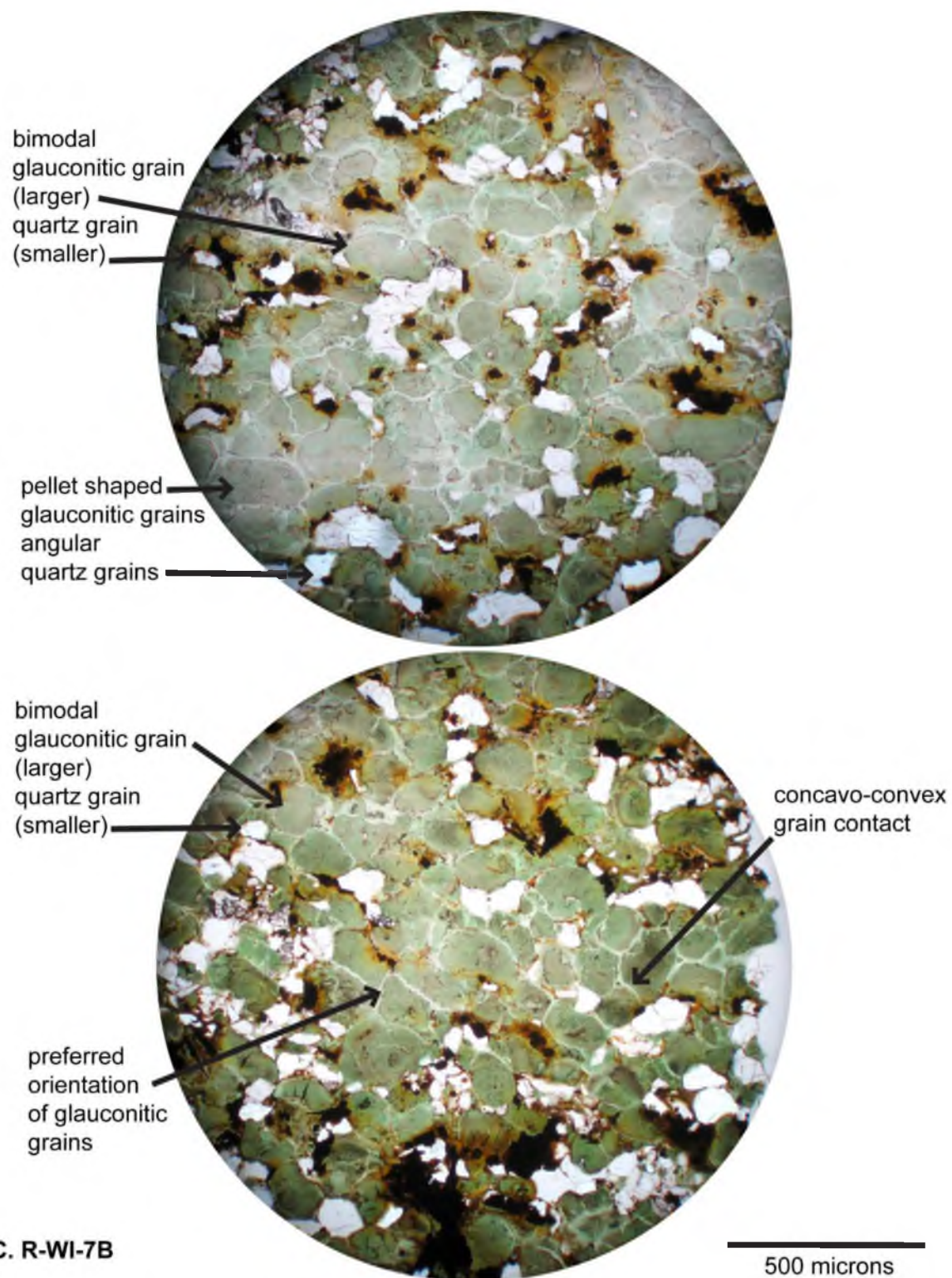


Figure 5.6 Continued

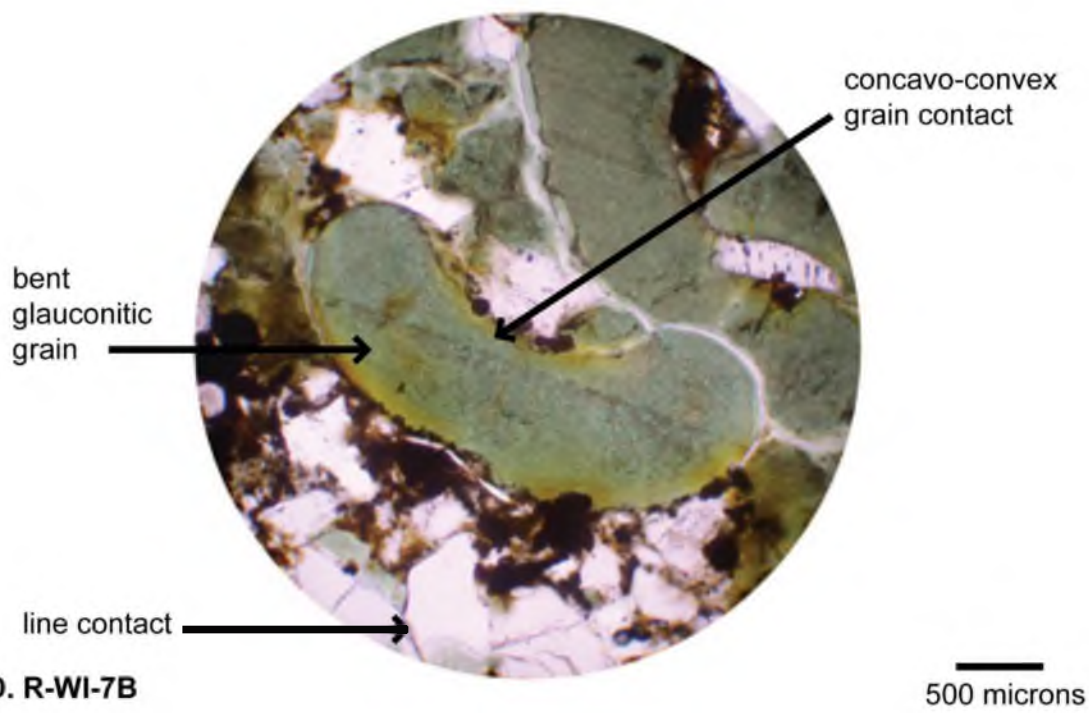
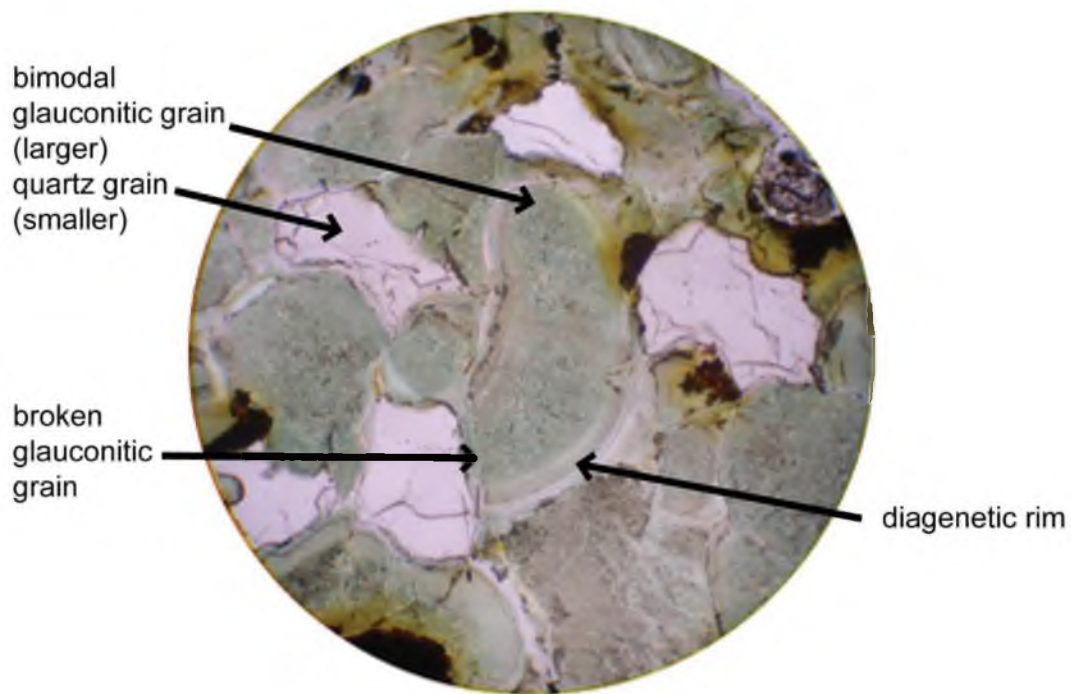
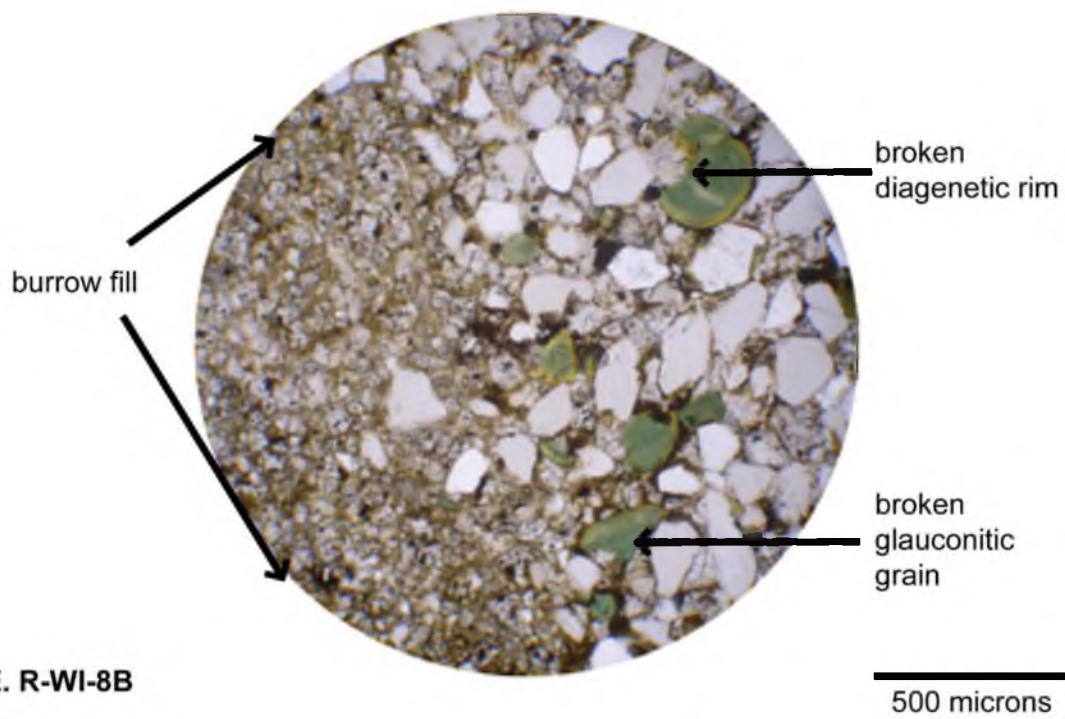
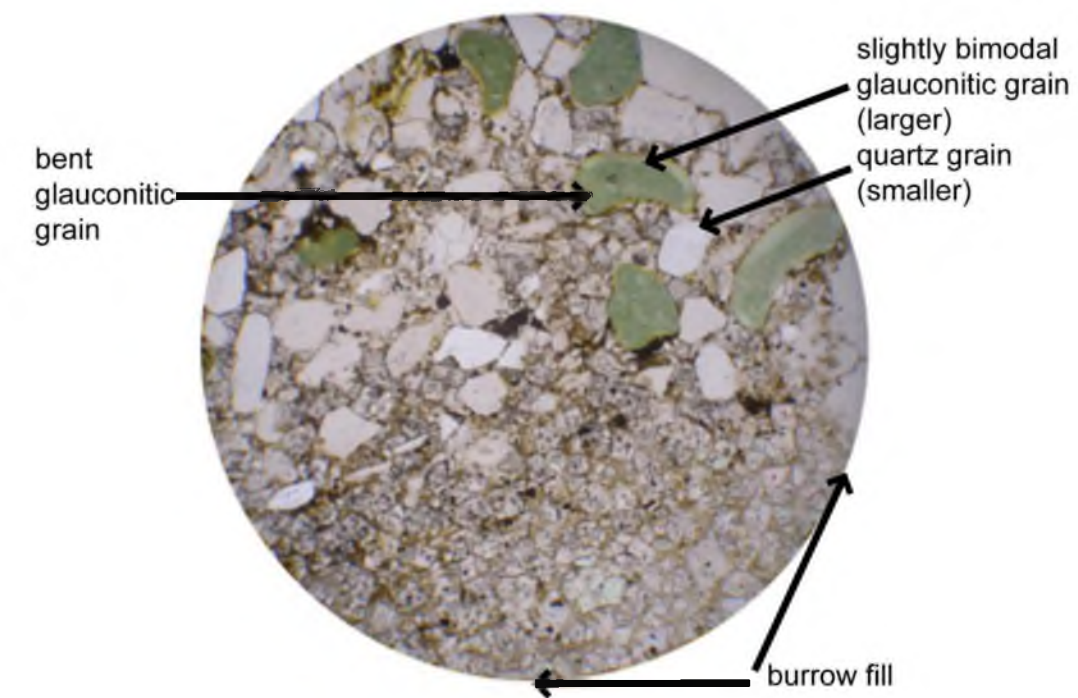
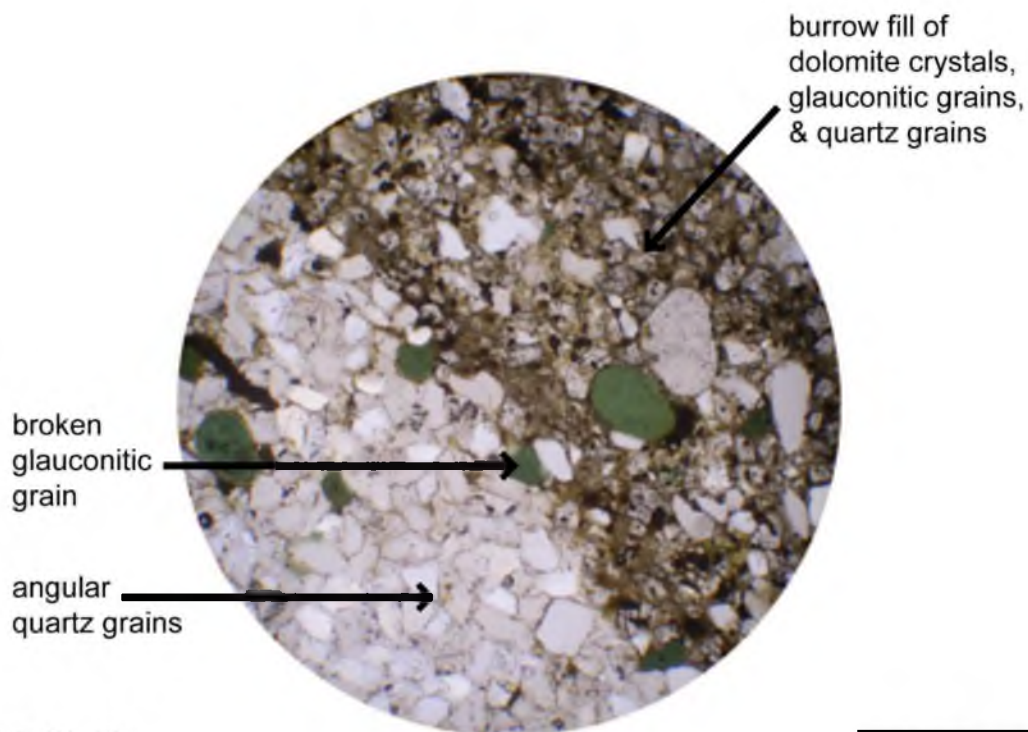
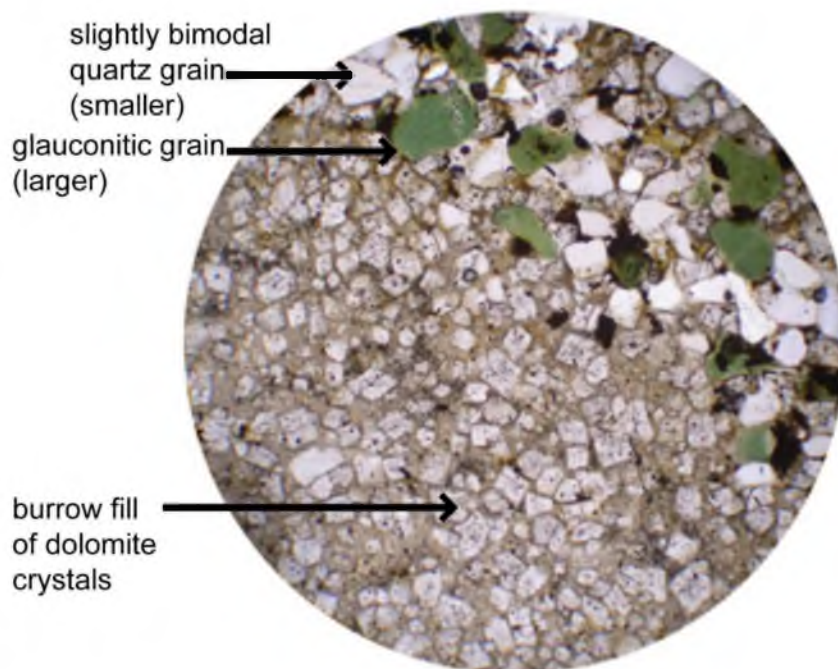


Figure 5.6 Continued



E. R-WI-8B

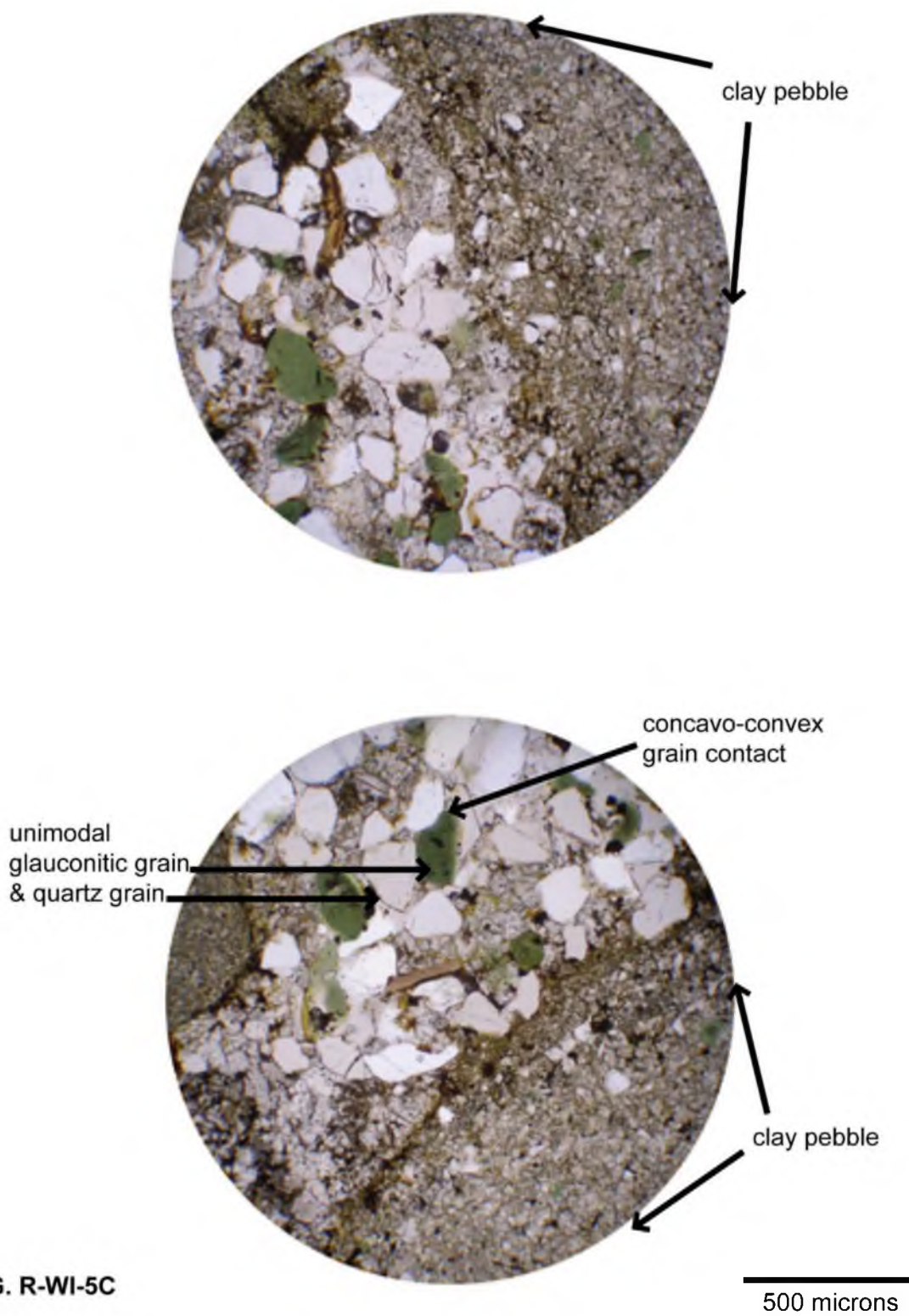
Figure 5.6 Continued



F. R-WI-4C

500 microns

Figure 5.6 Continued



G. R-WI-5C

Figure 5.6 Continued

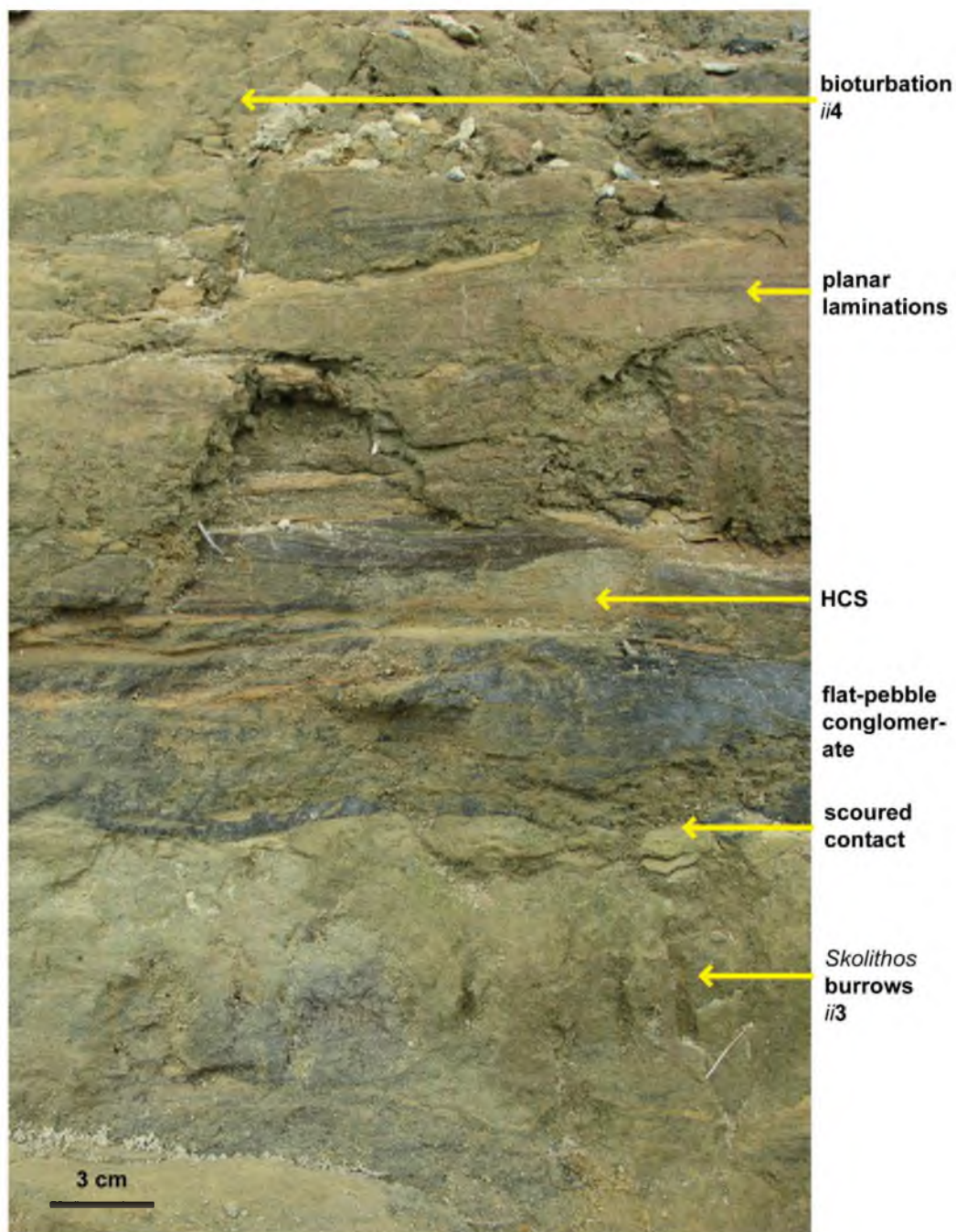


Figure 5.7 Parts of two storm beds, showing typical primary biogenic and sedimentary structures (from part B (middle) of the Boscobel, Reno Member exposure).

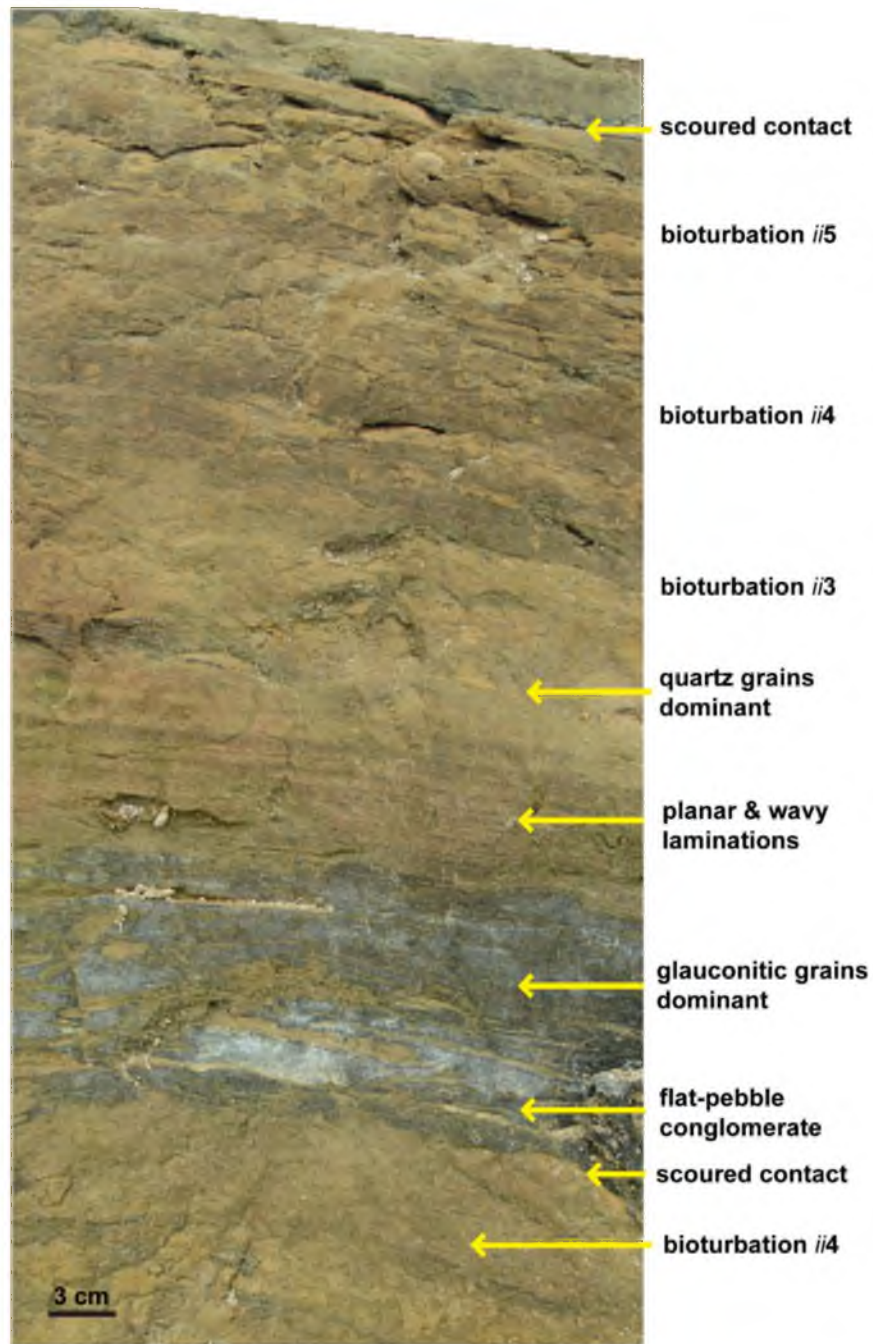


Figure 5.8 Typical storm bed showing basal scour atop bioturbated sediment, representative sedimentary structures, and scoured top (from part B (middle) of the Boscobel, Reno Member exposure).

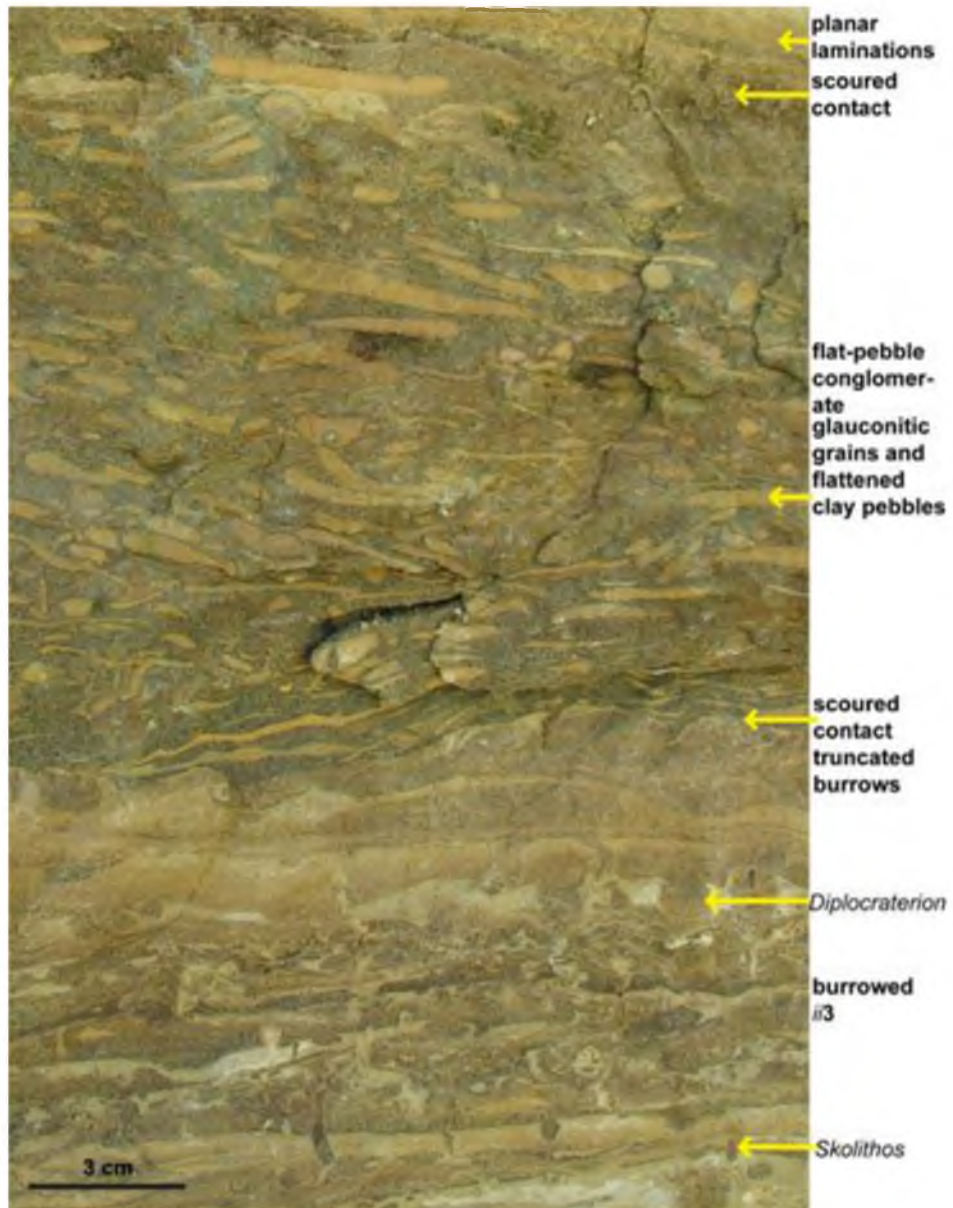


Figure 5.9 Burrows excavated in laminated sediment topped by an erosional scour surface that truncated *Diplocraterion* trace fossils and is overlain by thick (15–20 cm) flat-pebble conglomerate (from part C (upper) of the Boscobel, Reno Member exposure).

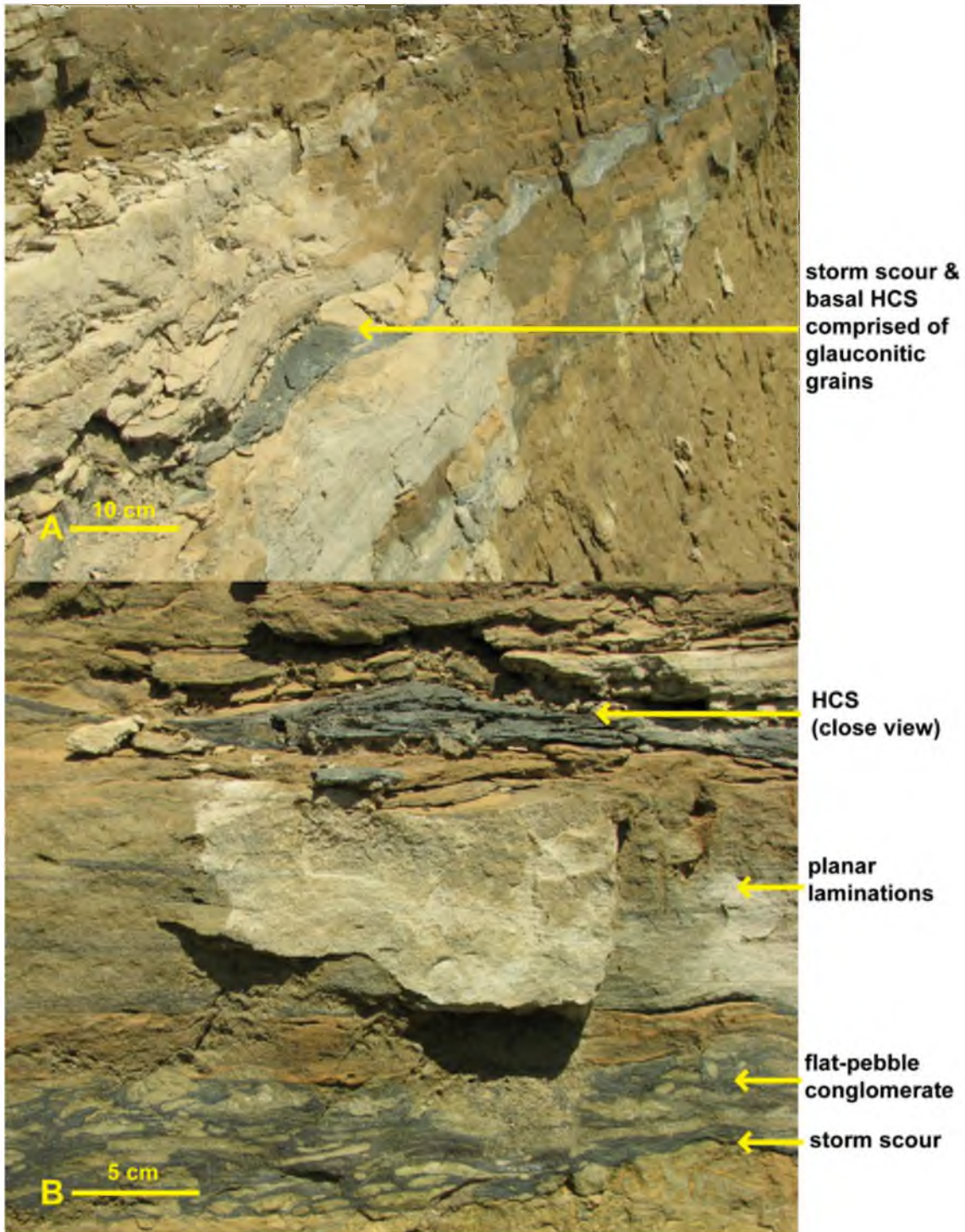


Figure 5.10 Hummocky-cross stratification (HCS) in the Boscobel exposure. A) discrete line of small-scale hummocks composed of glauconitic grains; B) close up view of a hummock showing thinning laminae at edges.

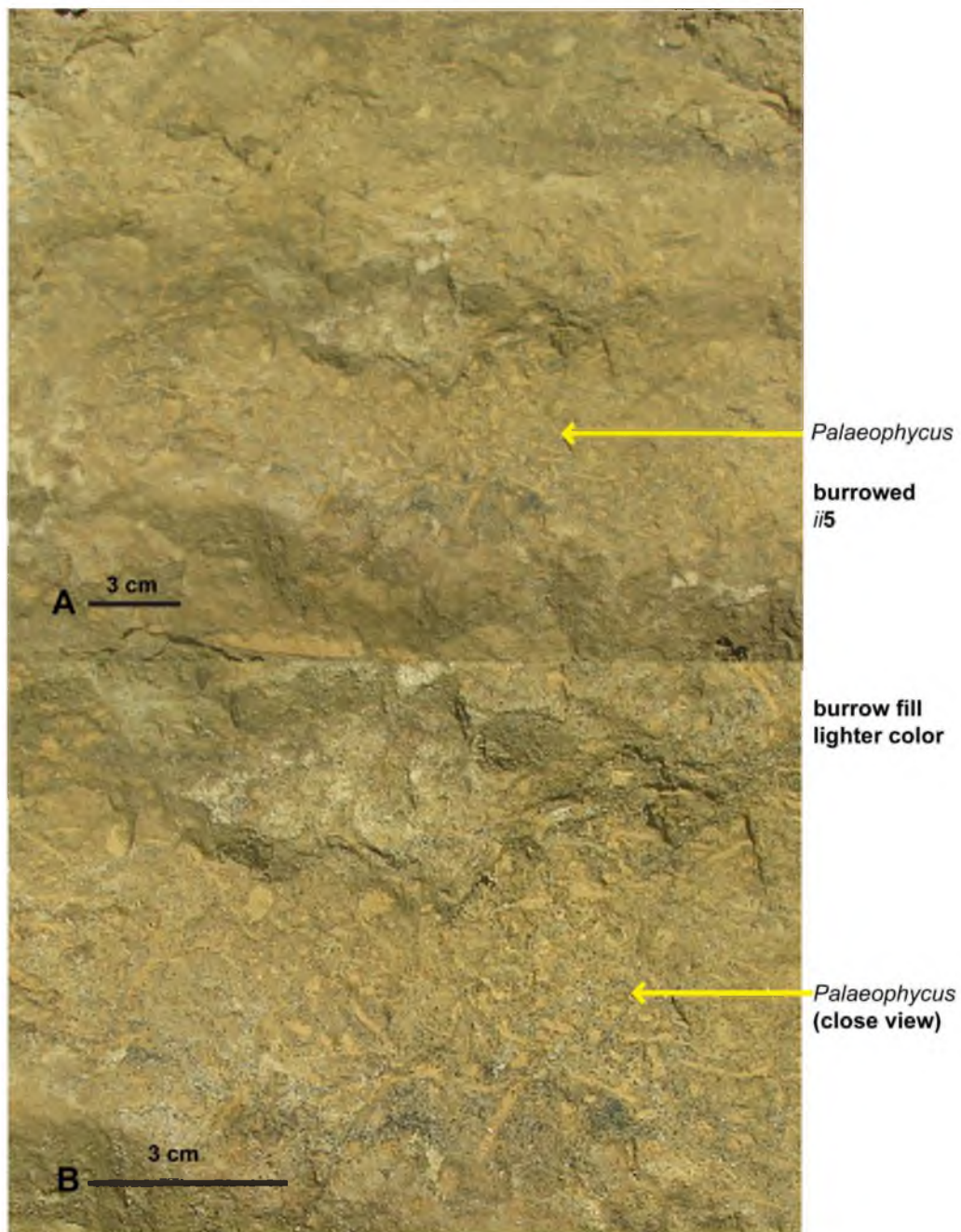


Figure 5.11 *Palaeophycus* trace fossils in part A (lower) Boscobel, Reno Member exposure. A) Individual burrows filled with tan clay/dolomite; B) Close up view of *Palaeophycus* trace fossils.

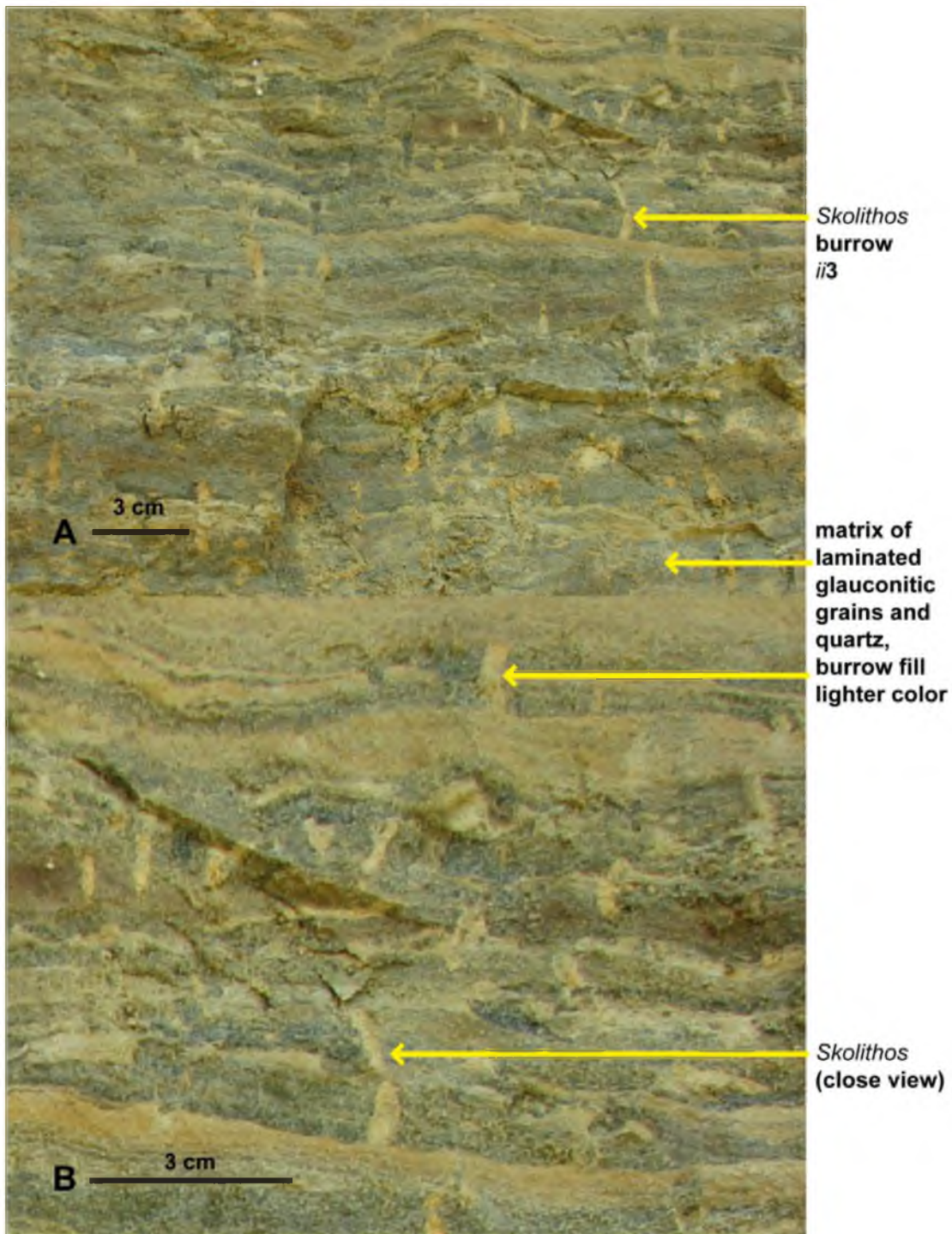


Figure 5.12 *Skolithos* trace fossils, accentuated by dolomite and excavated in laminated sediment rich in glauconitic grains (from part C of exposure). A) Broad view; B) close up view of *Skolithos*.

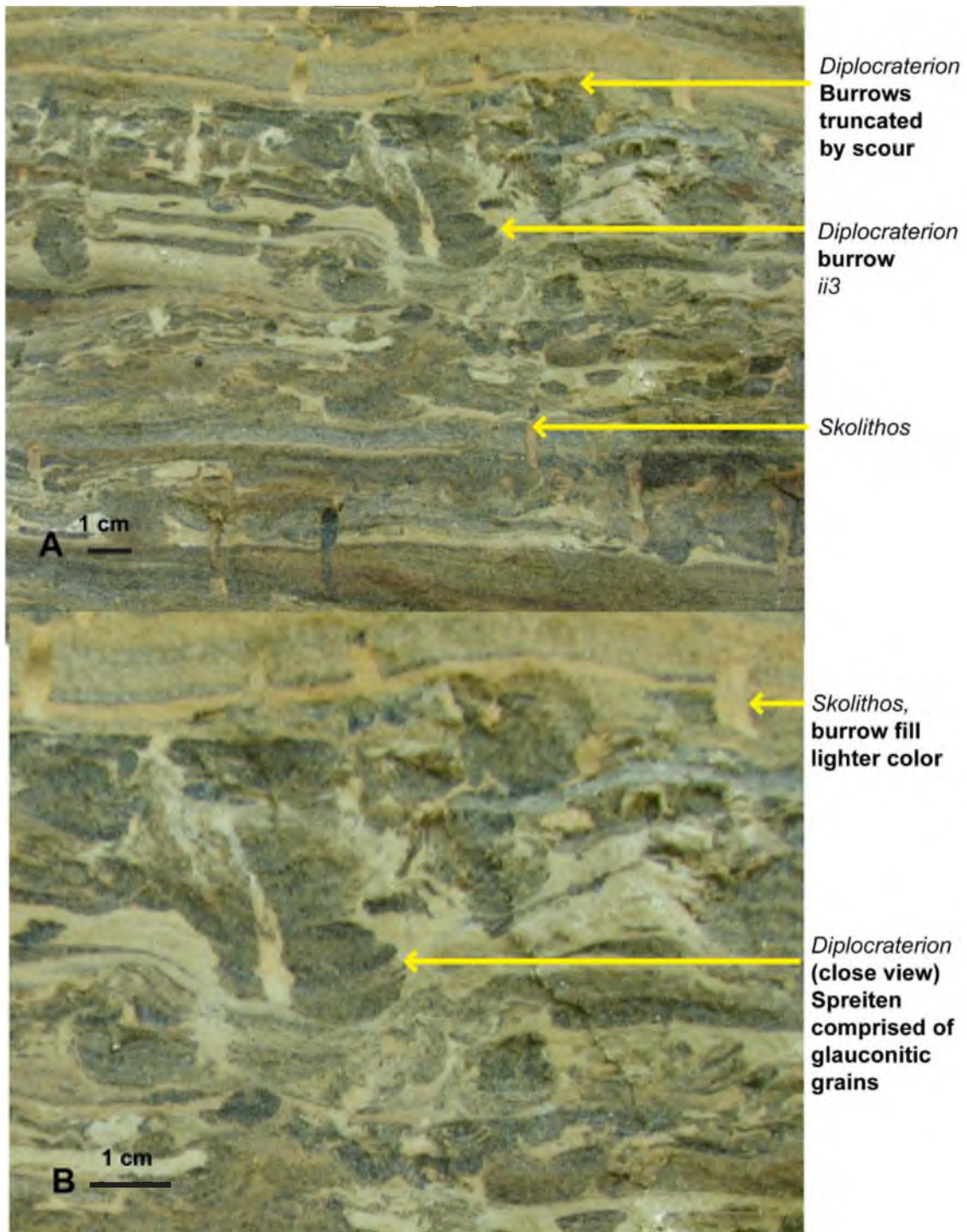


Figure 5.13 *Diplocraterion* trace fossils with spreiten highlighted by laminae containing dark green glauconitic grains (from part C, upper exposure). A) Broad view; B) close up view.

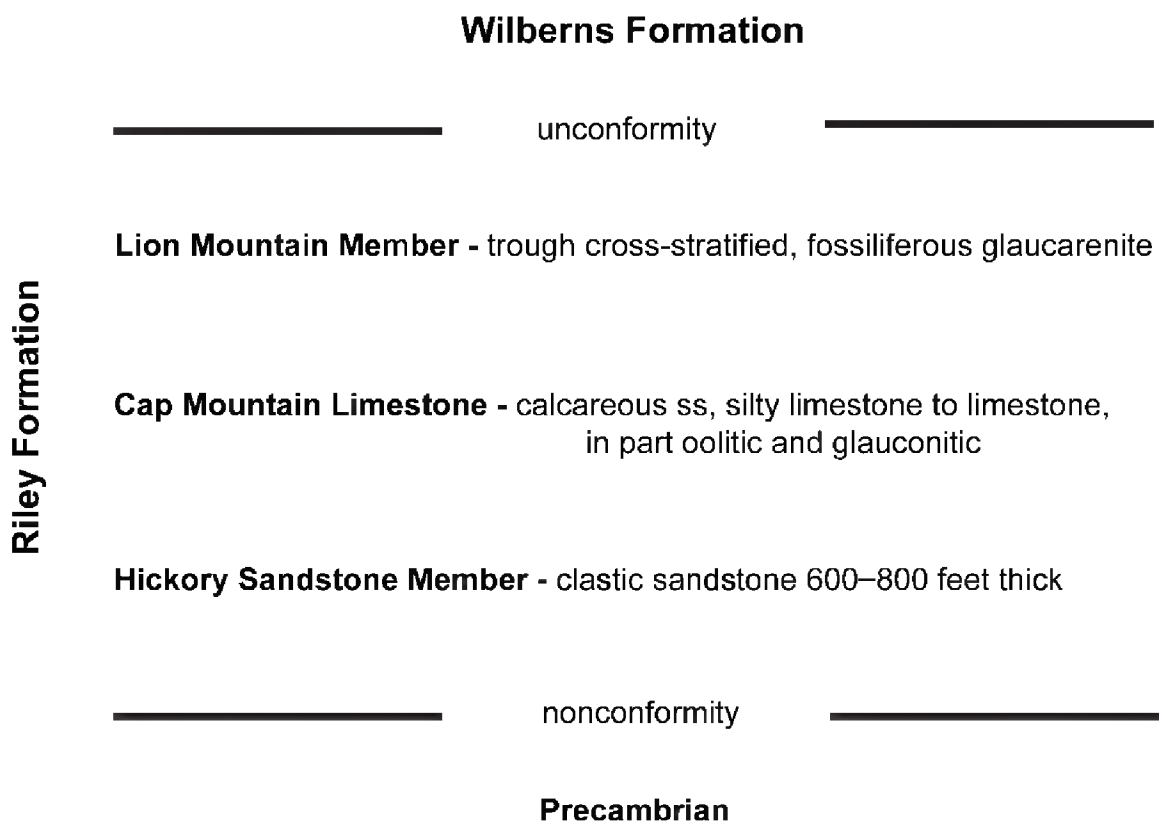


Figure 5.14 Stratigraphic section showing the three members of the Cambrian Riley Formation of Texas. The Upper Riley Formation includes the Lion Mountain Member.

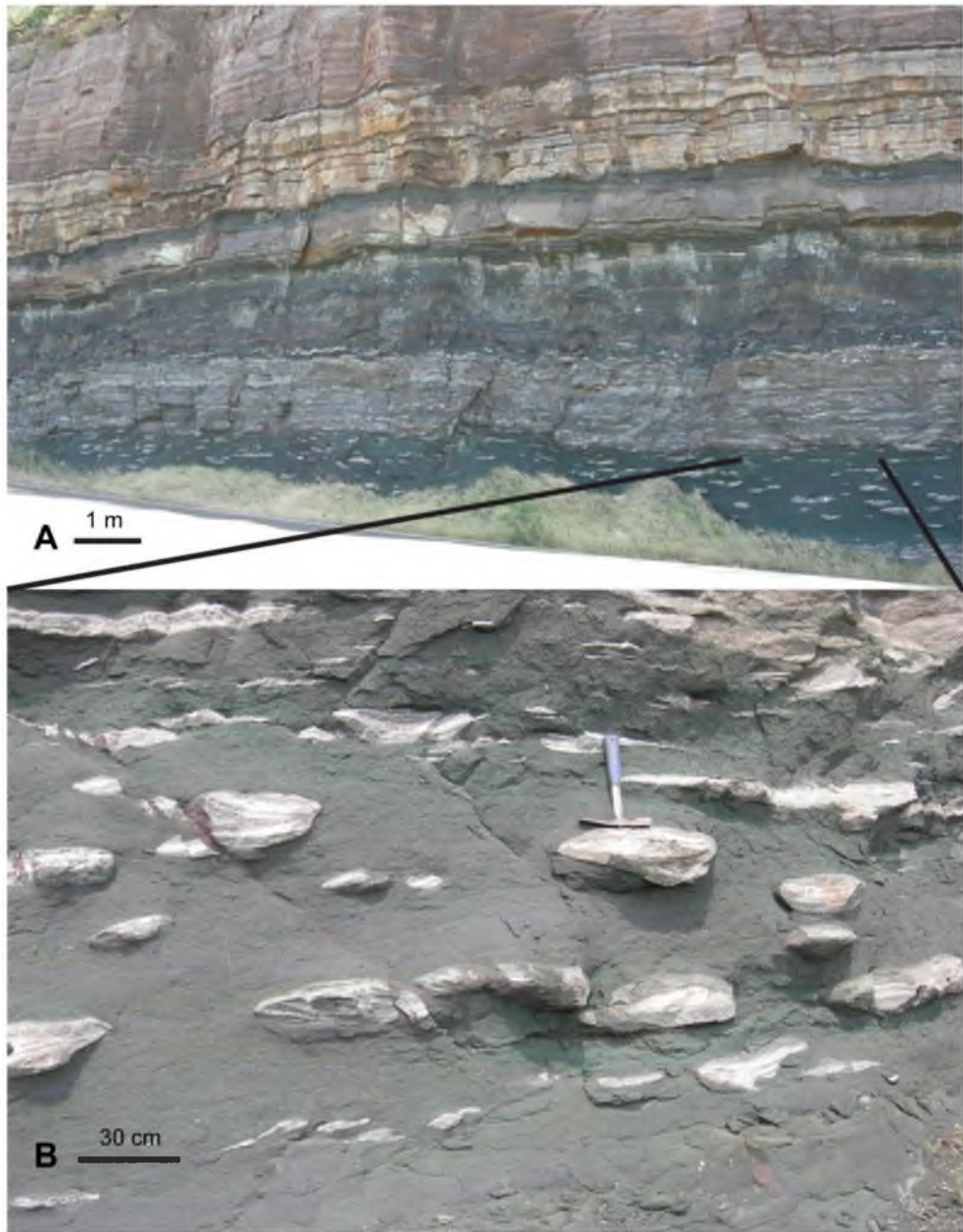


Figure 5.15 Exposure of the Cambrian Upper Riley Formation, the Lion Mountain Member, at Hoover Point, central Texas. A) View of the road cut; B) close up view of the Lion Mountain Member showing dark green glauconitic minerals and white nodules.

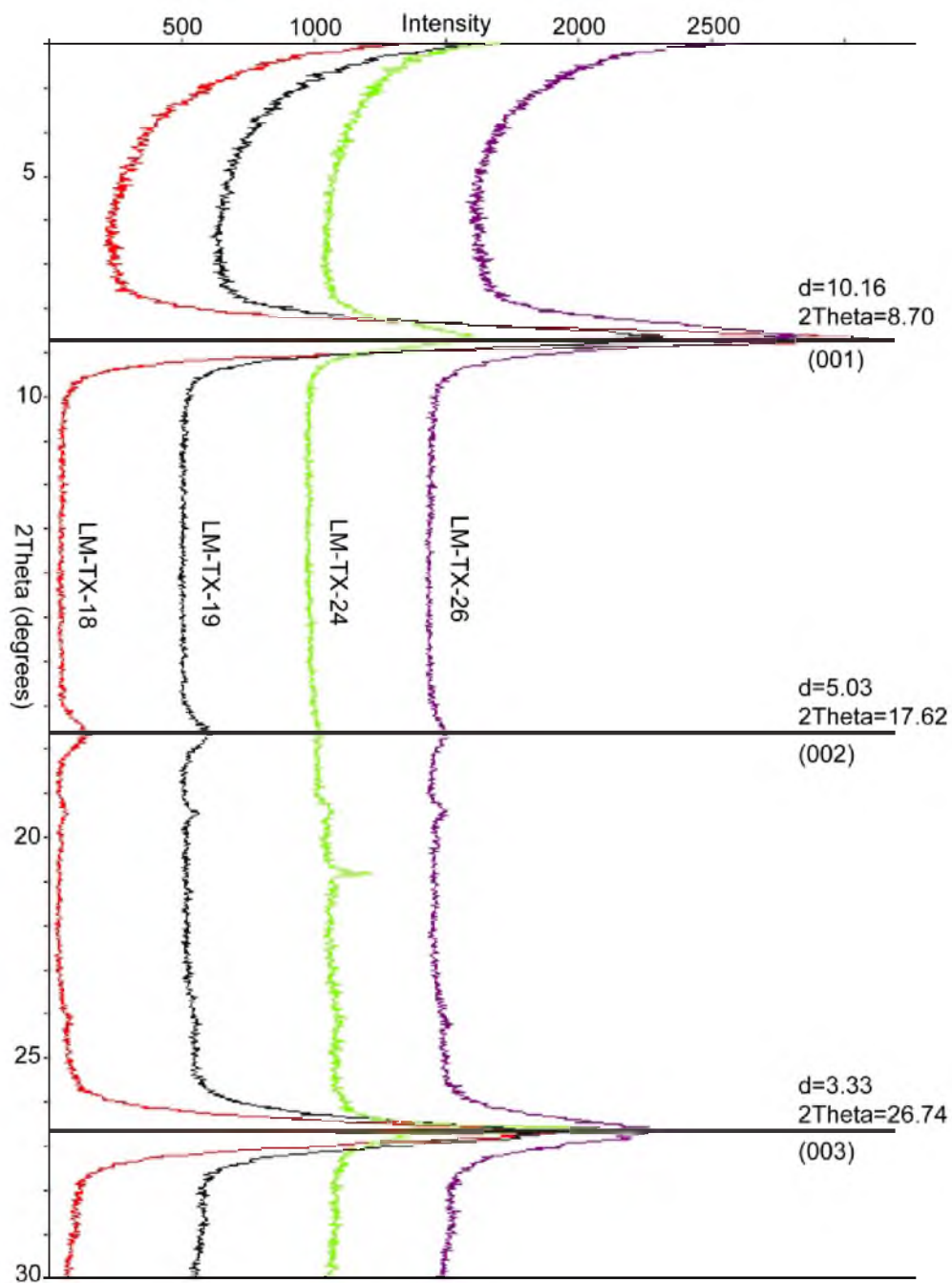
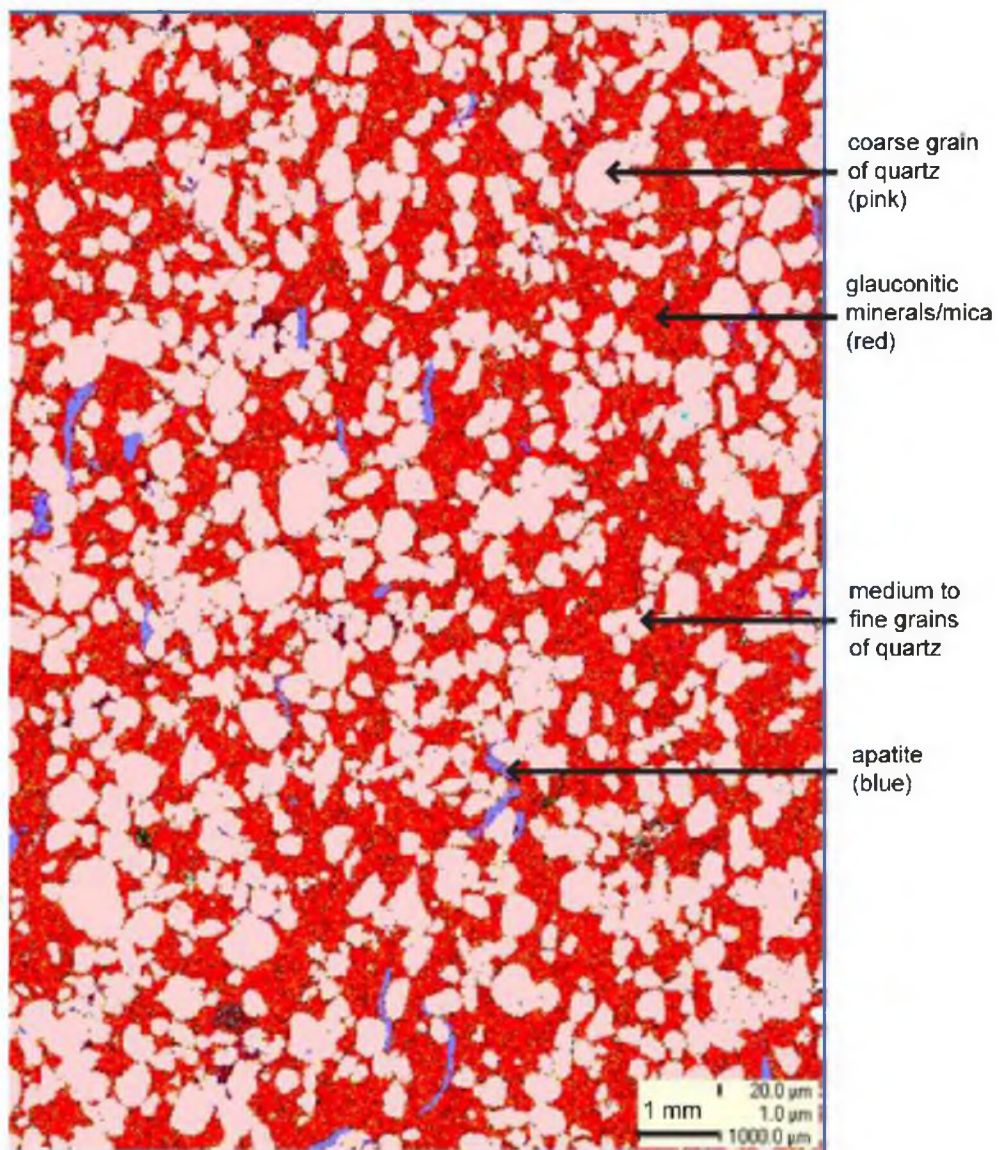


Figure 5.16 Composite X-ray diffractogram of four oriented clay mounts under air-dried conditions from the Lion Mountain Member.



A

Figure 5.17 QEMSCAN Barric 710 SIP mineral maps from a polished rock chip. A) 20 µm scale, glauconitic minerals in red; B) 5 µm scale glauconitic minerals in green.

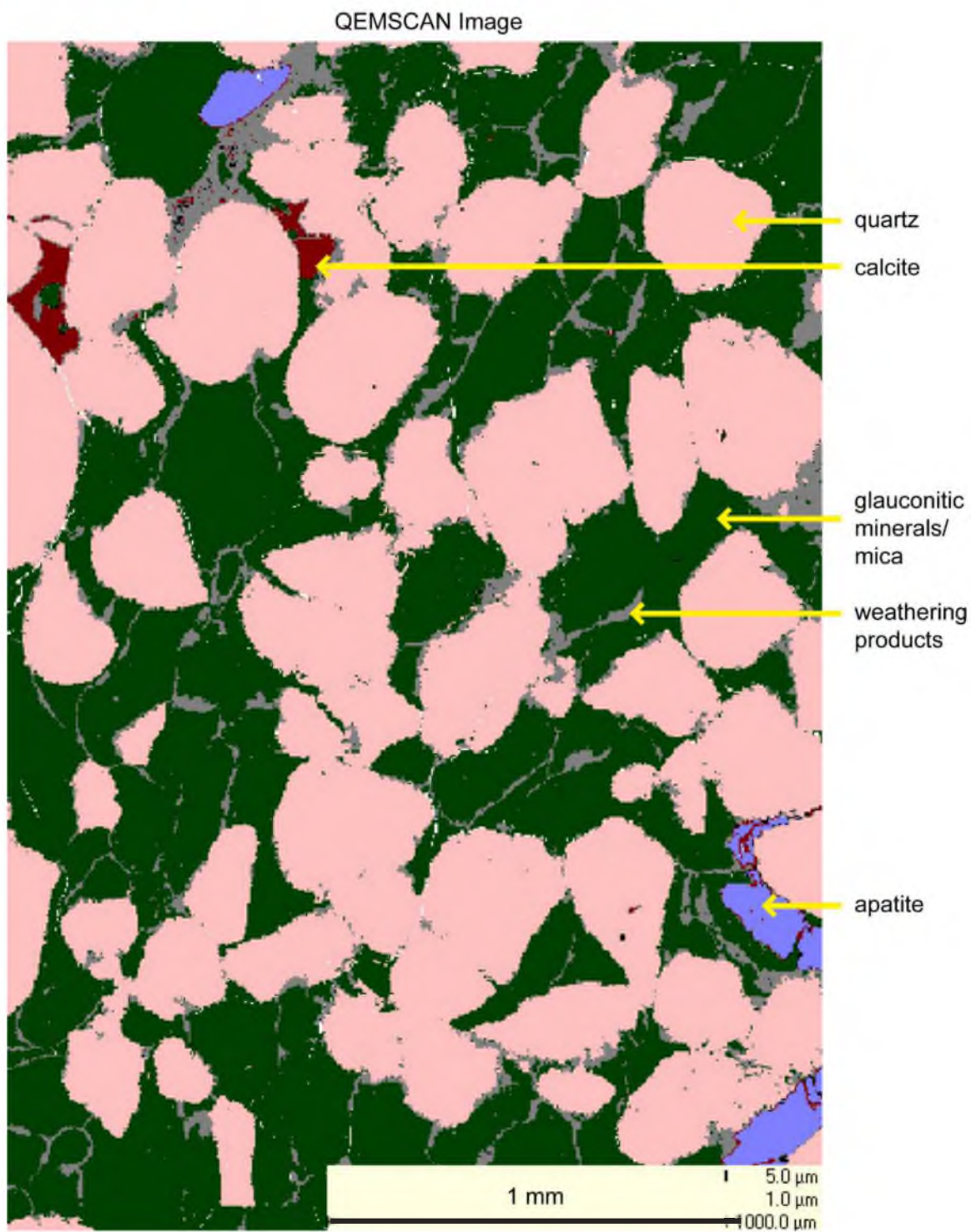
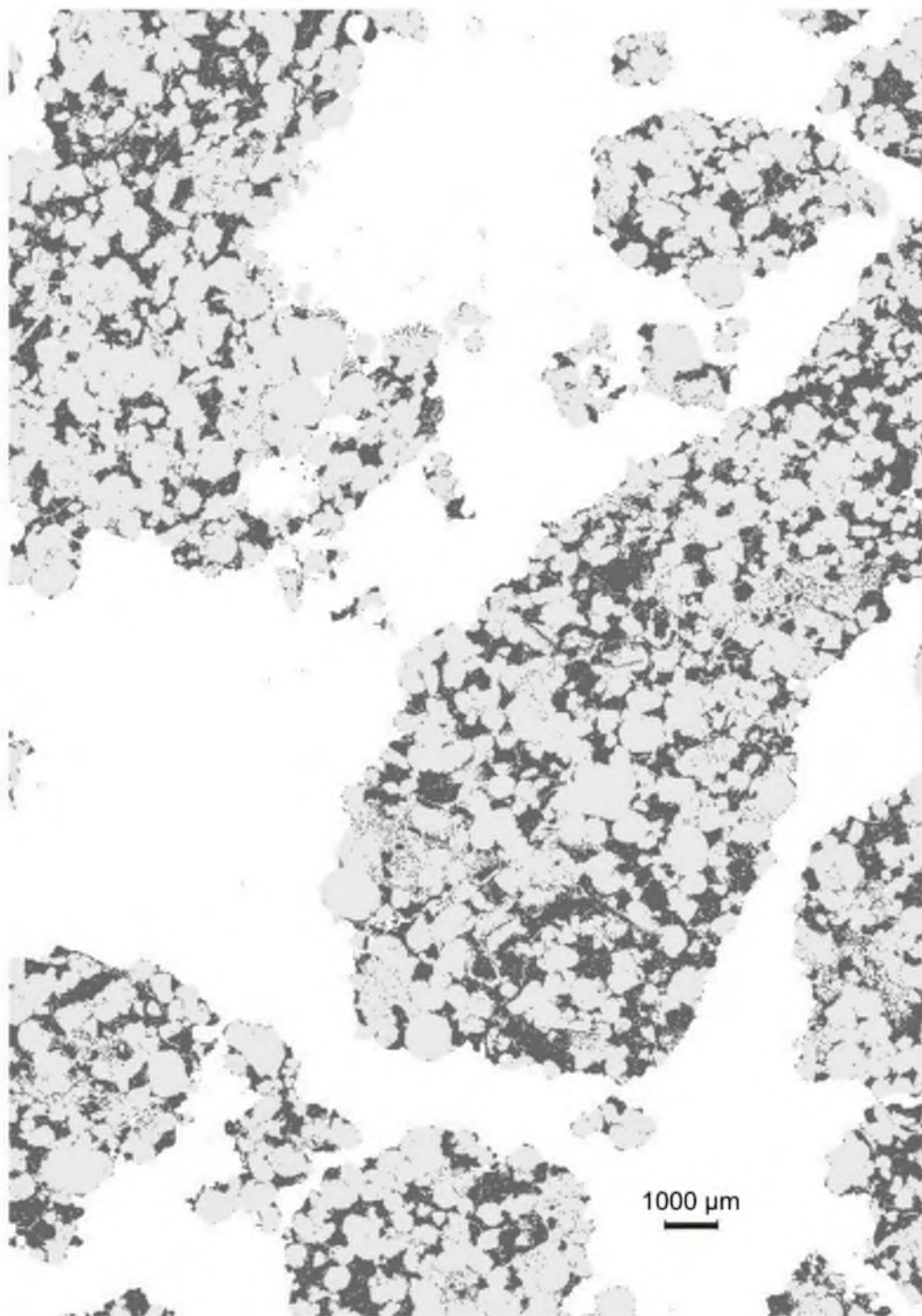
**B**

Figure 5.17 Continued



A. All minerals, 100 area %, apatite is pink.

Figure 5.18 QEMSCAN sedmin SIP mineral maps from thin section LM-TX-24. A) All minerals, 100 area %, apatite is bright pink; B) glauconitic minerals and other; C) quartz grains; D) Dolomite.



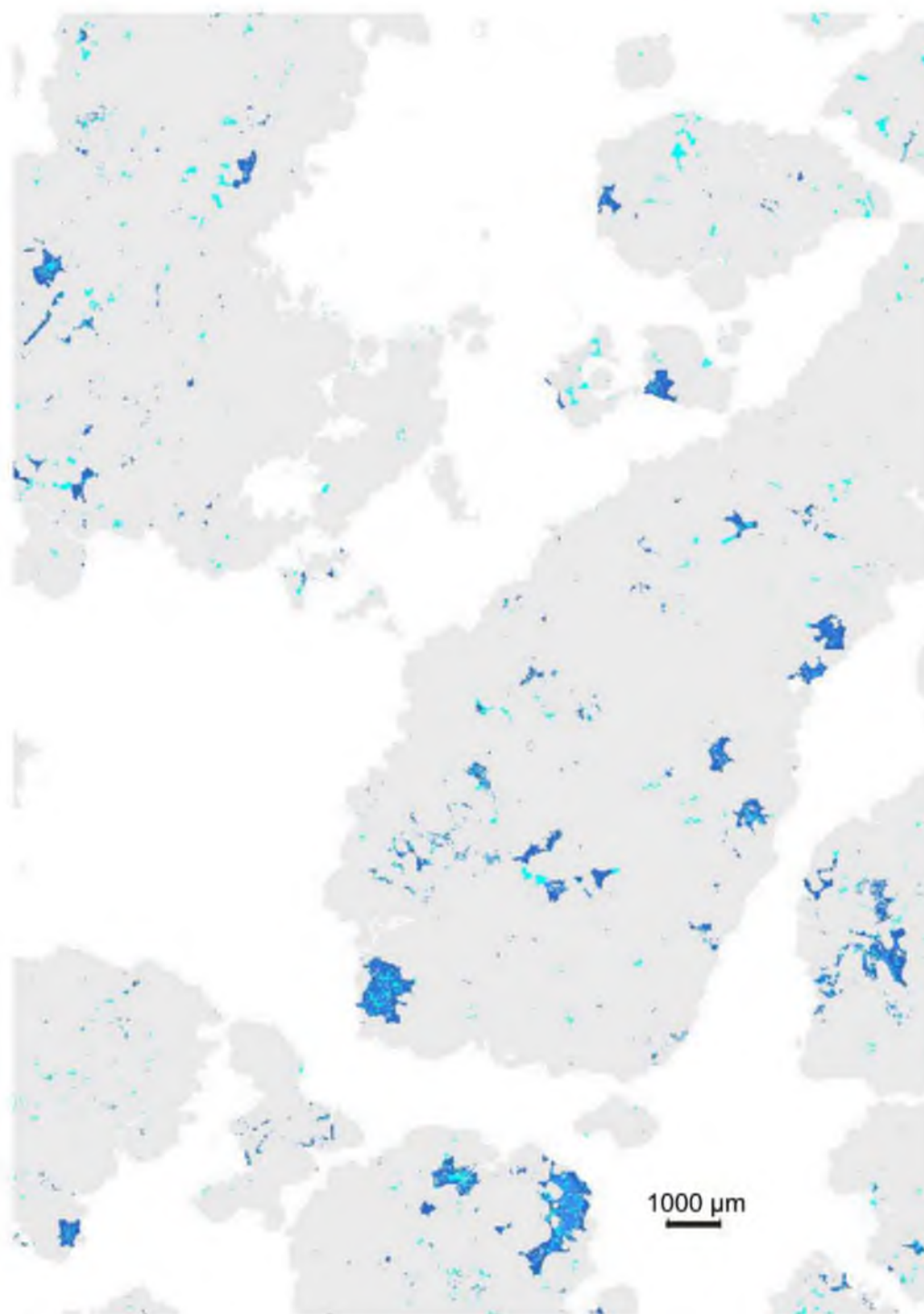
B. Glauconitic minerals and other, 31 area %

Figure 5.18 Continued



C. Quartz, 62 area %

Figure 5.18 Continued



D. Dolomite, 2 area %

Figure 5.18 Continued

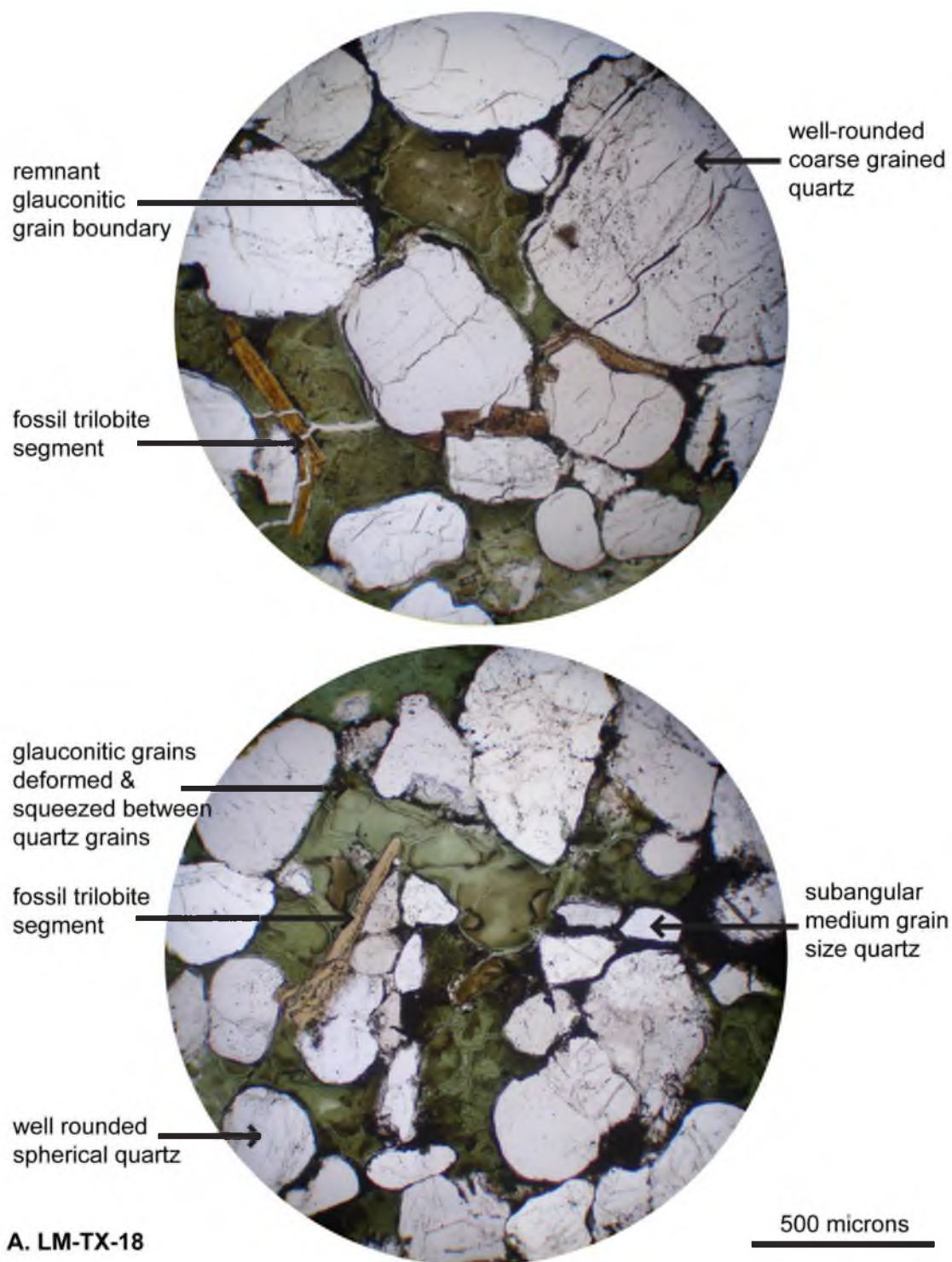


Figure 5.19 Annotated photomicrographs, two views from each thin section. A) LM-TX-18; B) LM-TX-19; C) LM-TX-24; D) LM-TX-26; E) LM-TX-27.

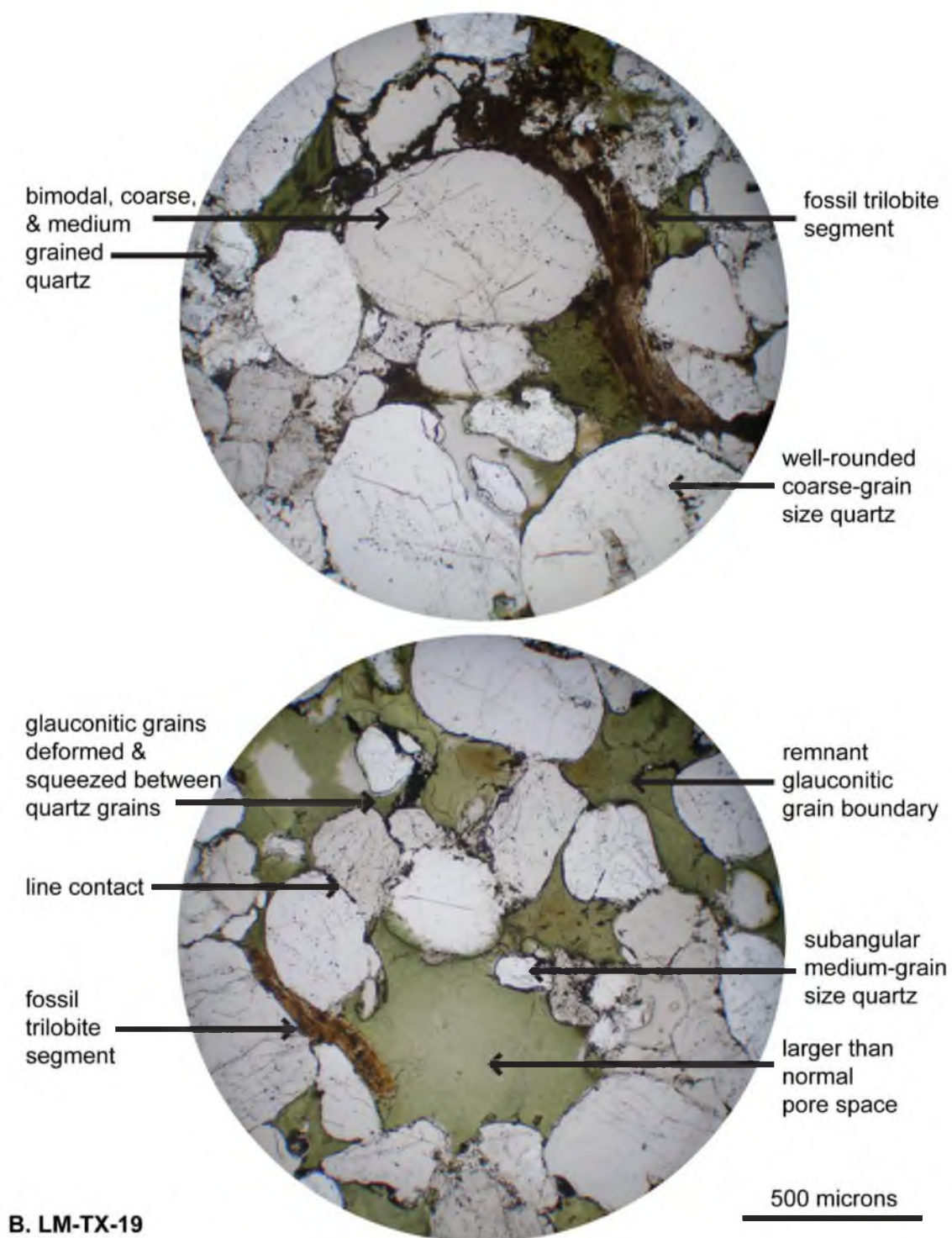


Figure 5.19 Continued

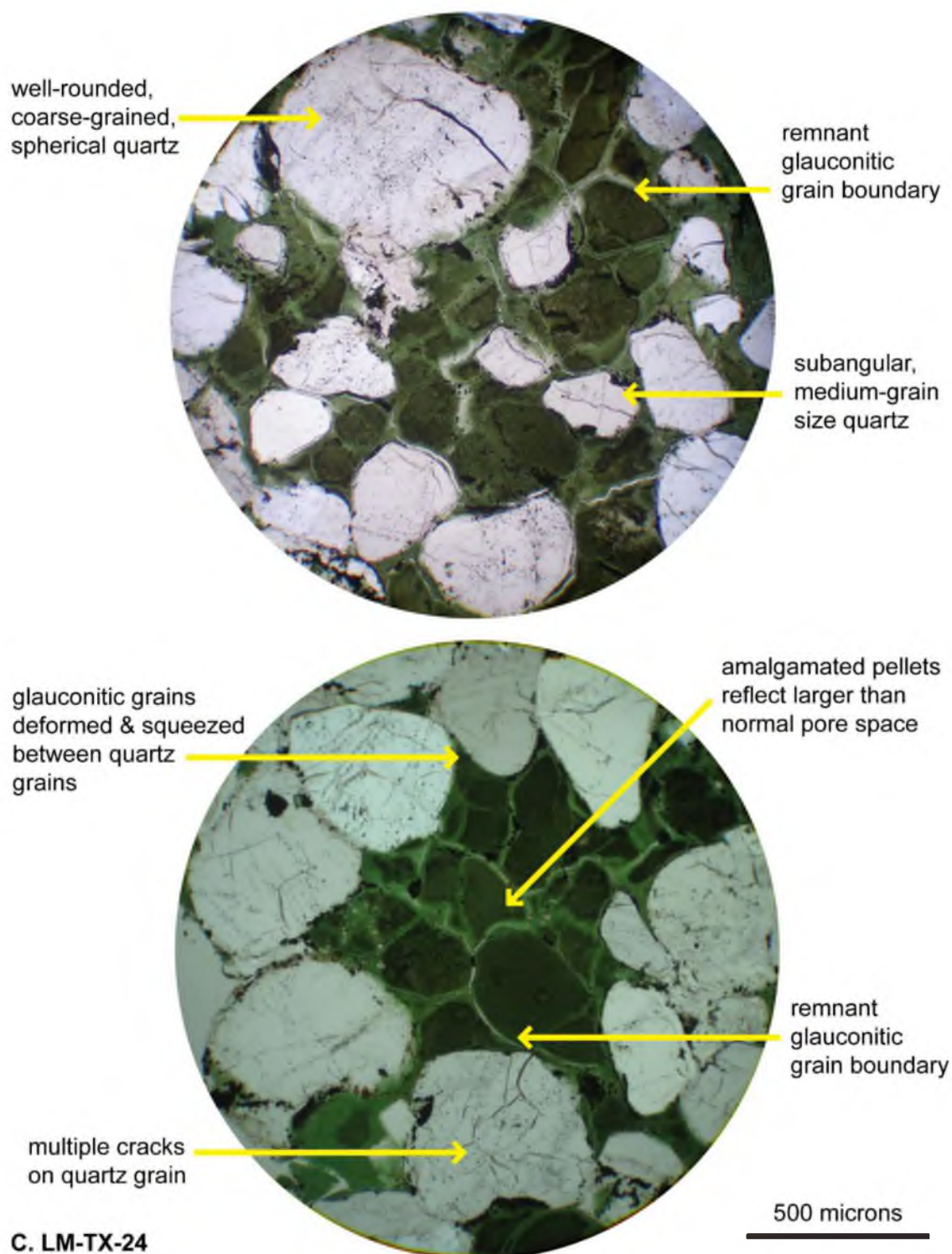


Figure 5.19 Continued

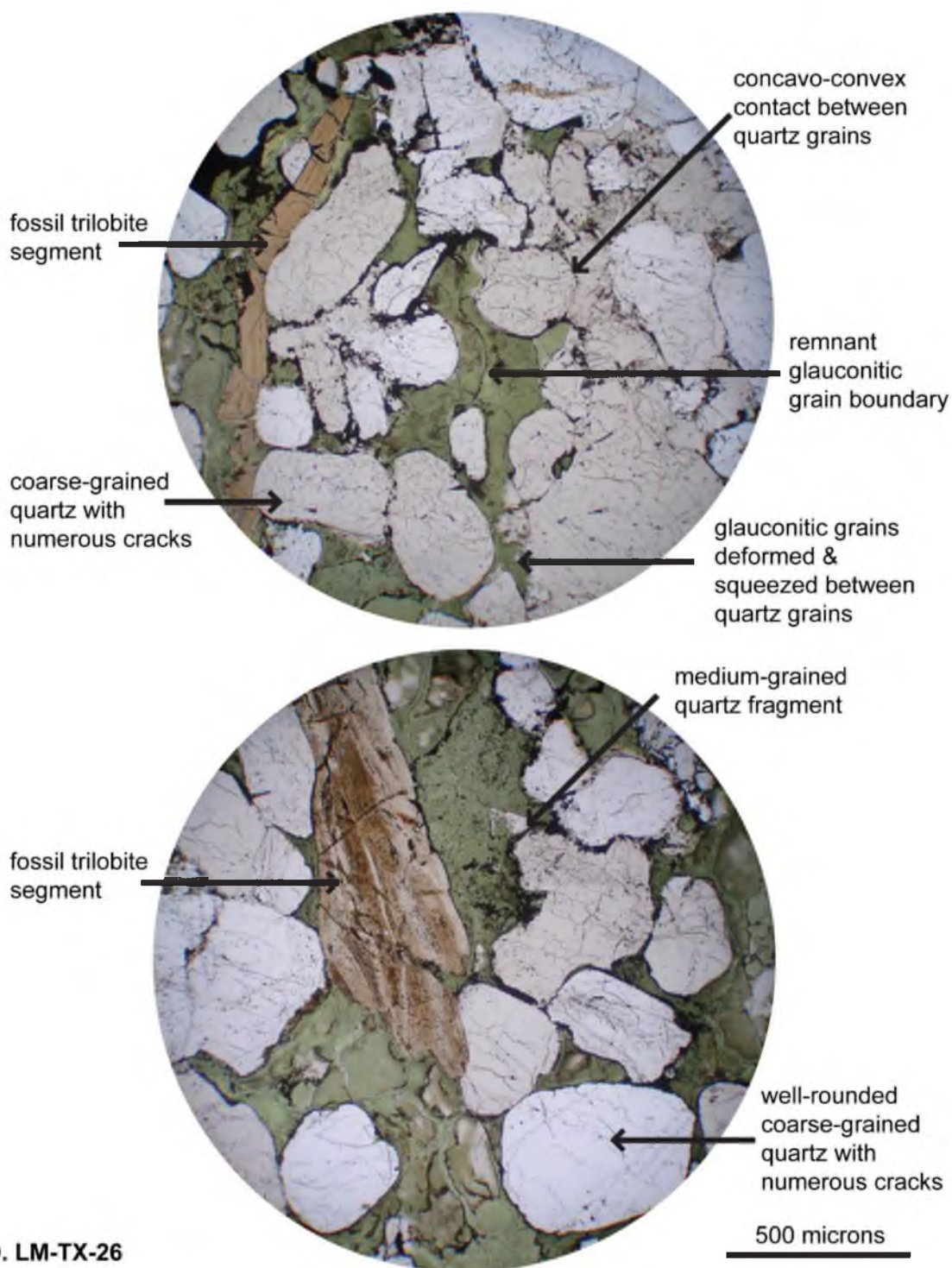


Figure 5.19 Continued

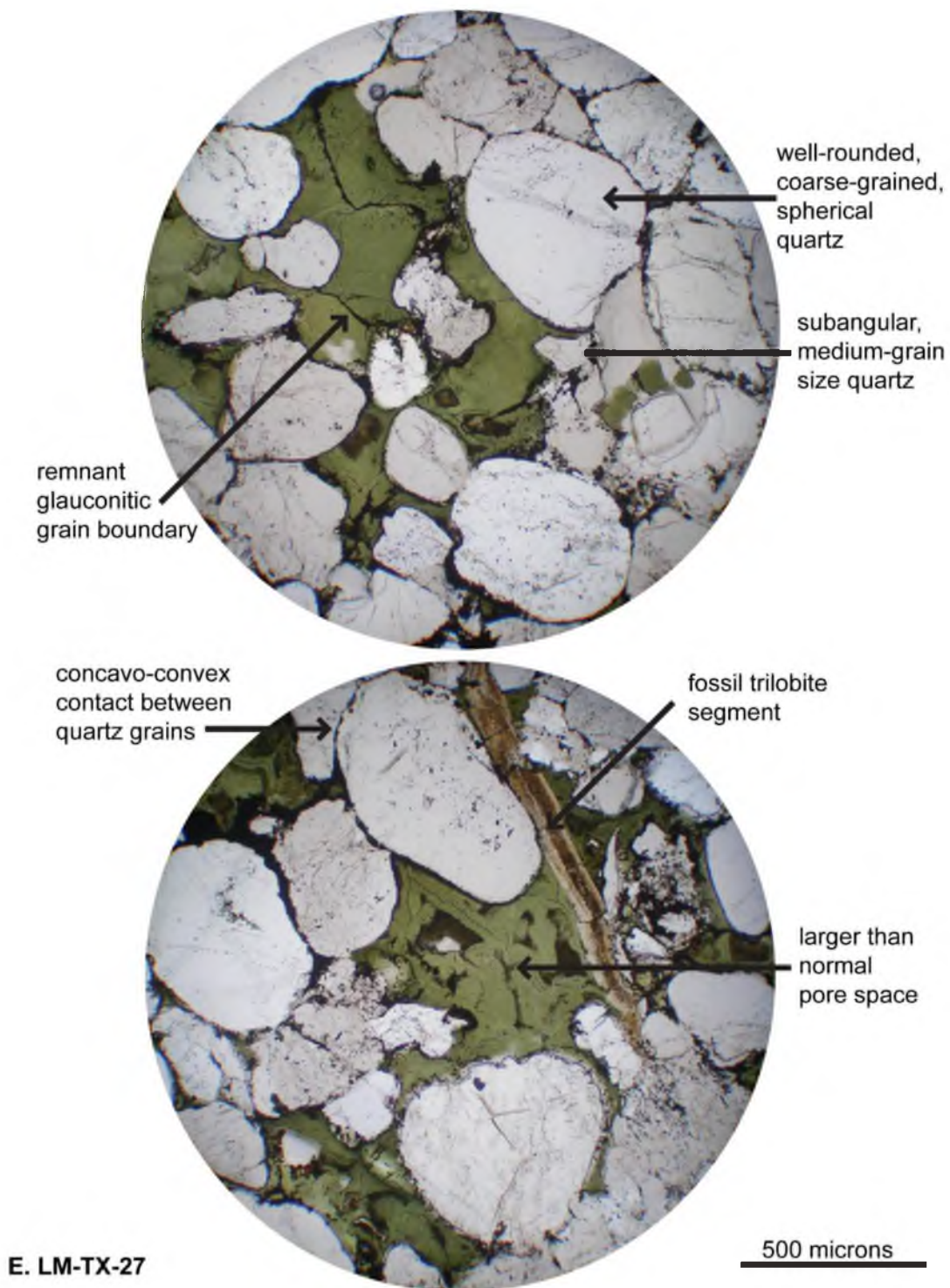


Figure 5.19 Continued

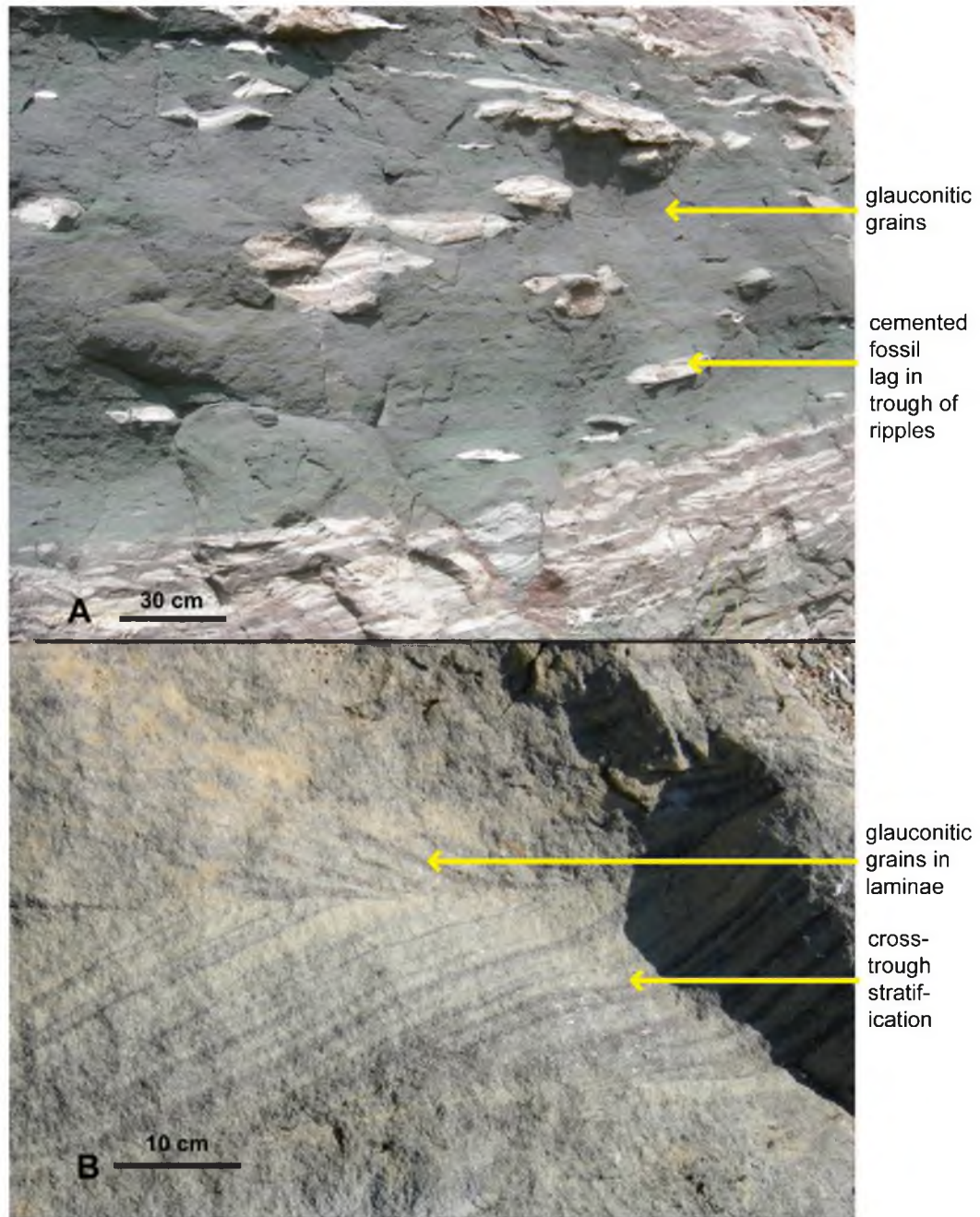


Figure 5.20 Sedimentary structures in the Lion Mountain Member at Hoover Point. A) Broad view showing white nodules that are cemented shell lag in troughs of mega ripples; B) close up view showing trough cross stratification with laminae of glauconitic minerals.

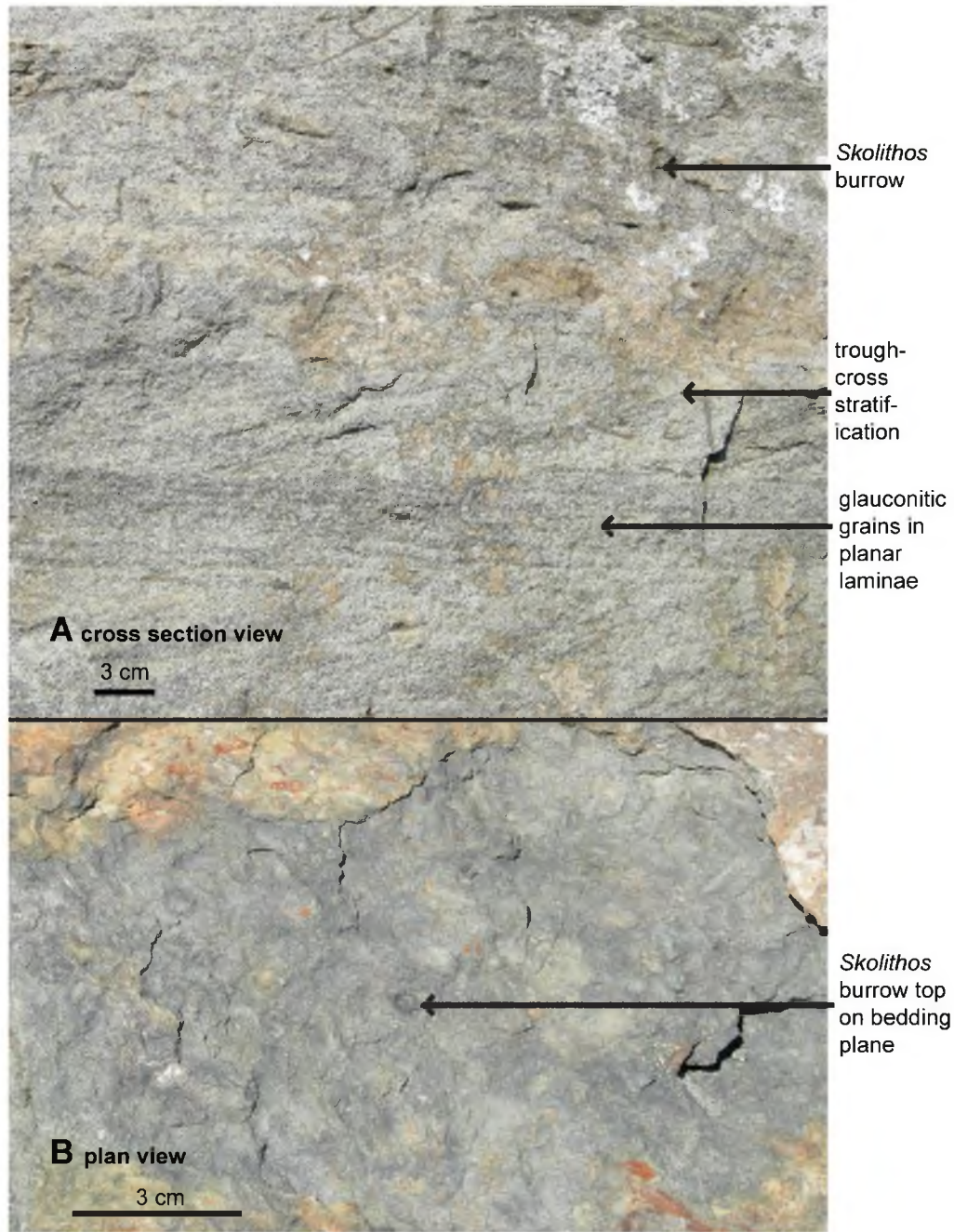


Figure 5.21 *Skolithos* trace fossils in the Lion Mountain Member at Hoover Point. A) Cross section view showing *Skolithos* shafts with parallel and cross laminated glauconitic sediment; B) plan view of *Skolithos*.

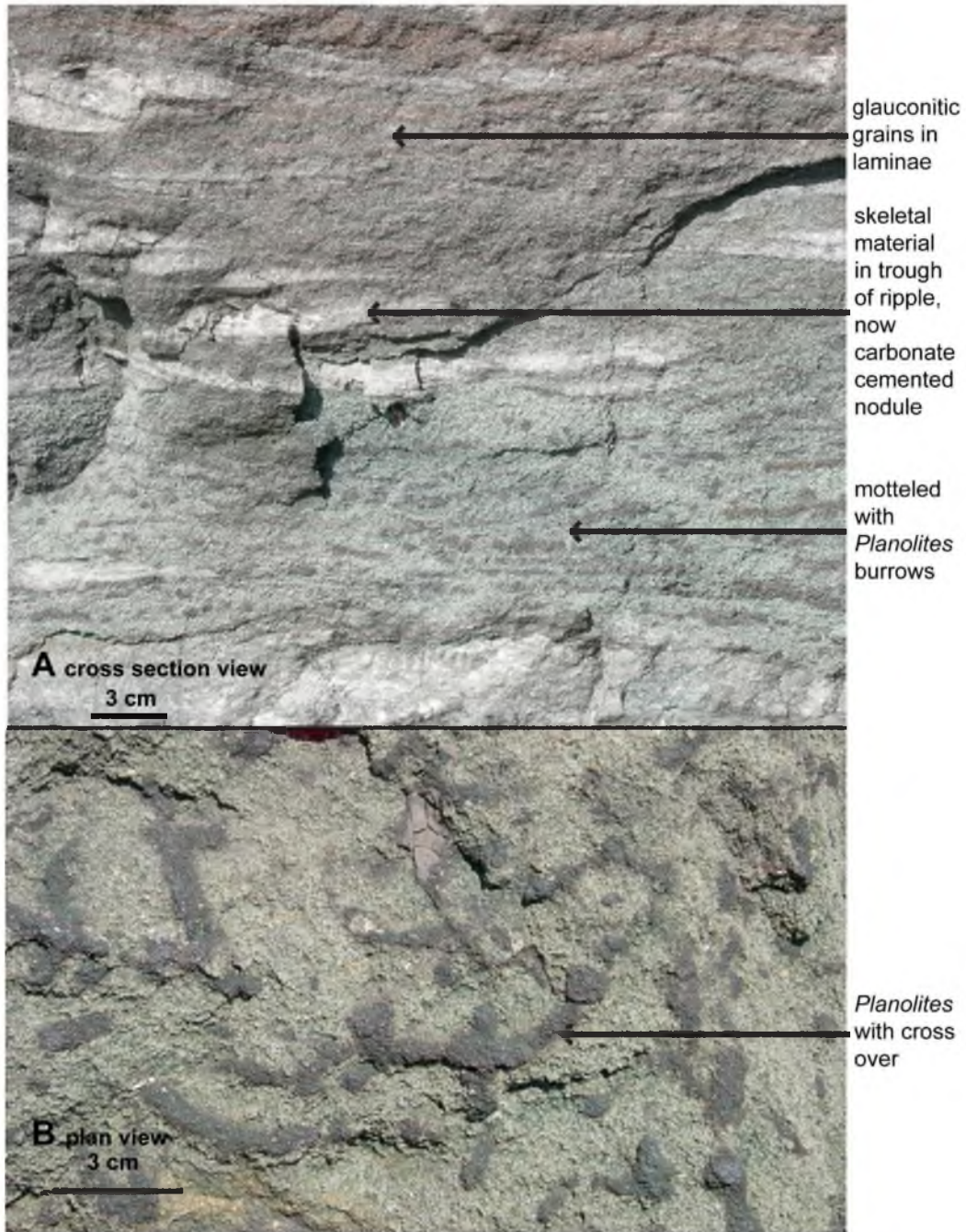


Figure 5.22 *Planolites* trace fossils in the Lion Mountain Member at Hoover Point. A) Cross section view showing mottling from *Planolites* burrows and parallel laminae with calcite cemented nodules; B) plan view of *Planolites* tunnels.

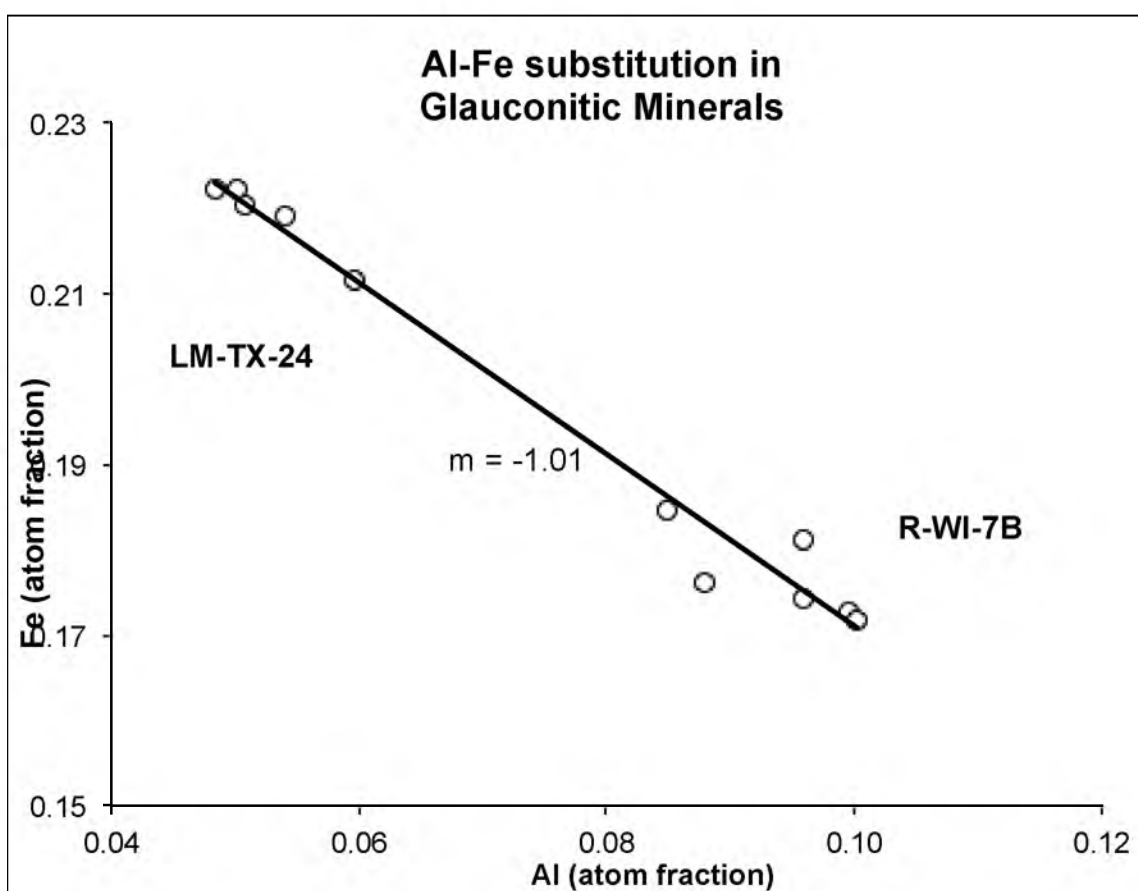


Figure 5.23 EMPA results showing Al-Fe substitution in glauconitic minerals from two samples. LM-TX-24 is from the Lion Mountain Member, Cambrian of Texas and R-WI-7B is from the Reno Member, Cambrian of Wisconsin (Barbara P. Nash, 2009, written communication). Higher aluminum is a reflection of subaerial weathering (Ku, Odin, 1988).

Table 5.1 SRD results from eight caly mounts. A) 2-Theta and d-spacing for the 001, 002, and 003 diffraction peaks with average and standard deviation; B) calculated atoms of iron based on peak arc and the NEWMOD simulation model for illite (ad is air dried).

A

Sample # clay mounts	(001) 2-Theta	d- spacing	(002) 2-Theta	d- spacing	(003) 2-Theta	d- spacing
R-WI-						
5c ad	8.66	10.2030	17.64	5.0232	26.80	3.3238
4c ad	8.64	10.2252	17.84	4.9689	26.80	3.3239
8b ad	8.70	10.1560	17.86	4.9626	26.78	3.3262
7b ad	8.58	10.2972	17.76	4.9907	26.76	3.3286
6b ad	8.76	10.0863	17.76	4.9899	26.78	3.3262
5b ad	8.60	10.2735	17.74	4.9956	26.78	3.3263
3a ad	8.64	10.2275	17.64	5.0237	26.78	3.3263
2a ad	8.58	10.2981	17.70	5.0072	26.70	3.3361
AVG	8.65	10.2209	17.74	4.9952	26.77	3.3272
STDEV	0.06	0.0730	0.08	0.0225	0.03	0.0039

B

Sample # clay mounts	area 001	area 002	002/001	log 002/001	atoms of Fe*	clay mineral
R-WI-						
5c ad	29565	3351	0.11334	-0.9456	0.50	glauconitic
4c ad	36696	6447	0.17569	-0.7553	0.33	glauconitic illite
8b ad	24601	3743	0.15215	-0.8177	0.39	glauconitic illite
7b ad	57634	5649	0.09802	-1.0087	0.56	glauconitic
6b ad	34332	7786	0.22679	-0.6444	0.24	glauconitic illite
5b ad	70610	5827	0.08252	-1.0834	0.63	glauconitic
3a ad	24301	2484	0.10222	-0.9905	0.54	glauconitic
2a ad	60544	5757	0.09509	-1.0219	0.57	glauconitic

* The number of trivalent iron atoms in the two occupied octahedral sites per the four tetrahedral sites.

Table 5.2 Chemical results. A) EMPA results of spot chemical analyses from sample R-WI-7B Boscobel (gr is a pelleted grain); B) published chemical analyses (Twenhofel, 1936).

A

EMPA spot chemical analyses (R-WI-7B) Boscobel								
	gr.1-1	gr.1-2	gr.1-3	gr.3-1	gr.2-1	gr.2-2	AVG	STDEV
SiO₂	52.4	51.9	50.9	52.1	52.8	52.6	52.1	0.67
Al₂O₃	8.12	7.73	7.65	6.85	7.13	8.15	7.6	0.52
Fe₂O₃	22.1	22.0	22.7	23.4	22.4	21.9	22.4	0.55
MgO	4.11	4.06	4.01	4.12	4.28	4.09	4.1	0.09
CaO	0.19	0.18	0.18	0.18	0.17	0.18	0.2	0.01
K₂O	8.46	8.59	8.34	8.50	8.32	8.33	8.4	0.11
F	0.49	0.23	0.29	0.13	0.27	0.49	0.3	0.15
sum	96.0	94.8	94.2	95.3	95.4	95.8	95.3	0.67
Less O	0.21	0.11	0.13	0.06	0.12	0.22	0.1	0.06
Total	95.8	94.7	94.1	95.3	95.3	95.6	95.1	0.64

?

?

B

	Sample 1 Franconia	Sample 2 Upper Greensand
SiO₂	45.91	48.5
Al₂O₃	11.47	9
Fe₂O₃	21.9	20
FeO	3.97	3.1
MgO	3.07	3.7
CaO	0.81	0.4
Na₂O	trace	1.5
K₂O	7.29	6.1
Total	99.6	99.6

?

Table 5.3 QEMSCAN analyses of two grain mounts (bottom of bed & top of bed) as determined from the Barric 710 SIP definition. A) Mineralogy with color legend in area %; B) Bulk chemistry calculated for all constituents in the field of view.

A

color	Mineral	bottom of bed	top of bed
	Quartz	49.68	56.69
	Micas*	24.20	10.33
	Feldspar	19.70	22.69
	Others	1.47	0.78
	Chlorite	1.36	0.67
	Fe Silicate	1.22	0.45
	Dolomite	0.87	6.60
	Nontronite	0.72	0.20
	Amphibole	0.62	1.29
	Calcite	0.12	0.18
	Plagioclase	0.04	0.14
	Background	0.02	0.04

*Micas represent glauconitic minerals.

B

Sample- PMA top of bed	Si	Al	Fe	Mg	Ca	K	C	F	H	O
elemental mass %	35.72	2.96	1.41	2.60	1.81	4.06	0.95	0.12	0.06	50.03
elemental oxide %	76.42	5.60	2.01	4.31	2.54	4.89	3.48	0.12	0.53	-
bottom of bed										
elemental mass %	34.75	3.60	2.48	4.05	0.40	4.96	0.14	0.28	0.13	48.75
elemental oxide %	74.34	6.80	3.55	6.72	0.56	5.97	0.50	0.28	1.16	-

Table 5.4 Summary of petrographic results in the Cambrian section at Boscobel, Wisconsin, based on thin section microscopy. Results are listed in the order of stratigraphic occurrence with oldest at the bottom.

Sample number R-WI-	% glauconitic grains and size	% quartz grains and size	Modal distribution, size versus composition	Sample location within storm bed	Glauconitic grain character	Glauconitic grain genesis
5C	5–10%, fine sand	20–30%, fine sand	unimodal, very few larger glauconitic grains	bottom of bed, flat-pebble conglomerate	pelleted, bent, and broken	allochthonous or reworked in place
4C	3–5%, fine sand	20–30%, fine sand	bimodal, glauconitic grains are slightly larger	upper bed, laminations and burrows	pelleted, bent, and broken	allochthonous or reworked in place
8B	5–20%, fine to medium sand	30–40%, fine sand	bimodal, glauconitic grains are slightly larger	middle bed, hummocky laminations	pelleted, bent, and broken	allochthonous or reworked in place
7B	40–50%, fine to medium sand	10–20%, fine sand	bimodal, glauconitic grains are larger	bottom of bed, distinct band of hummocks	pelleted, bent, and broken	allochthonous or reworked in place
2A	10–20%, medium sand	10–20%, fine sand	bimodal, glauconitic grains are larger	bottom of bed, glauconitic band	pelleted, bent, and broken	allochthonous or reworked in place
3A	3–5%, fine to medium sand	40–50%, fine sand	bimodal, glauconitic grains are larger	middle bed, laminated, burrowed, rip-up clasts	pelleted, bent, and broken	allochthonous or reworked in place

Table 5.5 Chemical results. A) EMPA results of spot chemical analyses from sample LM-TX-24 Hoover Point, Texas (gr is a green grain); B) published chemical analyses (Odin, 1988).

A

EMPA spot chemical analyses (LM-TX-24) Hoover Point, Texas							
	gr.1-1	gr.1-2	gr.2-1	gr.2-2	gr.2-3	AVG	STDEV
SiO₂	49.8	49.5	50.4	50.3	49.9	50.0	0.38
Al₂O₃	3.79	4.64	4.02	3.97	4.26	4.1	0.33
Fe₂O₃*	27.3	25.7	27.4	27.5	27.1	27.0	0.72
MgO	4.26	4.03	4.10	4.07	4.08	4.1	0.09
CaO	0.19	0.20	0.14	0.15	0.13	0.2	0.03
K₂O	8.43	8.45	8.64	8.62	8.75	8.6	0.14
F	0.23	0.05	0.00	0.11	0.09	0.1	0.09
others	0.11	0.06	0.19	0.11	0.22	0.1	0.07
sum	94.1	92.6	94.9	94.8	94.5	94.2	0.92
Less O	0.11	0.03	0.01	0.06	0.04	0.0	0.04
Total	94.0	92.6	94.8	94.8	94.5	94.1	0.92

* Total iron reported as Fe₂O₃

B

Various published analyses			
	*	**	***
SiO₂	46.7	53.5	43.5
Al₂O₃	7.2	3.58	8.22
Fe₂O₃	22.7	24.3	28.8
FeO	1.1	3.37	0.96
MgO	3.4	3.78	2.92
CaO	1.4	-	0.14
K₂O	4.3	6.62	6.42
H₂O-			4.25
H₂O+			6.07
Total	98.8	95.2	102.4

* Average of analyses from modern glaucony, Gulf of Guinea (in wt. %) (Odin, 1988).

** Percent oxide in glauconite (MinDat on line)

*** Glauconite pellets Lower Cretaceous (in wt. %) (Bentor et al., 1965)

Table 5.6 QEMSCAN data from Lion Mountain (LM) polished rock chip, determined from the Barric 710 SIP definition. A) Mineralogy in area % and color legend for Figure 5.17 B, micas represent glauconitic minerals (dark green); B) chemistry calculated for all constituents in the field of view in area % (Figure 5.17 B) based on standard mineral chemical formulas.

A

Mineral Name

	Quartz	47.955
	Micas	39.059
	Weathering Products	11.337
	Apatite	0.784
	Calcite	0.534
	Others	0.330

B

Sample LM								
rock chip	Al	Fe	Mg	Ca	K	C	F	H
elemental mass %	2.44	9.24	6.6	0.56	3.51	0.06	0.44	0.19
elemental oxide %	4.61	13.21	10.94	0.79	4.22	0.23	0.44	1.74

Table 5.7 Summary of petrographic results from five thin sections, Lion Mountain Member, Cambrian of Texas.

Sample Number LM-TX-	% glauconitic grains	% quartz grains	Modal quartz grain size coarse/medium	Glauconitic grain character	Fossil content
18	30–40% glauconitic grains	50–60% quartz grains bimodal size	10% coarse well-rounded spheres, 40% medium size	amalgamated pelletoids in coarse size clumps	trilobite segment parts ~1%
19	20–30% glauconitic grains	60–70% total quartz grains bimodal size	10% coarse well-rounded spheres, 50% medium size	amalgamated pelletoids in coarse size clumps	trilobite segment parts ~1%
24	30–40% glauconitic grains	50–60% total quartz grains bimodal size	10% coarse well-rounded spheres, 50% medium size	amalgamated pelletoids in coarse size clumps	no trilobite parts
26	30–40% glauconitic grains	50–60% total quartz grains bimodal size	10% coarse well-rounded spheres, 50% medium/fine	amalgamated pelletoids in coarse size clumps	trilobite segment parts ~1%
27	20–30% glauconitic grains	60–70% total quartz grains bimodal size	10–20% coarse well- rounded spheres, 50% medium	amalgamated pelletoids in coarse size clumps	trilobite segment parts ~1%

References

- Bentor, Y.K., and Kastner, M., 1965, Notes on the mineralogy and origin of glauconite: *Journal of Sedimentary Petrology*, v. 35, no. 1, p. 155–166.
- Berg, R.R., 1954, Franconia formation of Minnesota and Wisconsin: *Geological Society of America Bulletin*, v. 65, no. 9, p. 857–882.
- Boyer, P.S., Guinness, E.A., Lynch-Blosse, M.A., and Stolzman, R.A., 1977, Greensand fecal pellets from New Jersey: *Journal of Sedimentary Petrology*, v. 47, no. 1 March, p. 267–280.
- Bridge, J., Barnes, V.E., and Cloud, P.E., 1947, Stratigraphy of the upper Cambrian, Llano uplift, Texas: *Geological Society of America Bulletin*, v. 58, no. 1, p. 109–124.
- Bromley, R.G., 1996, *Trace Fossils: Biology, Taphonomy and Applications*: New York, Taylor & Francis, 361 p.
- Byers, C.W., and Stasko, L.E., 1978, Trace fossils and sedimentologic interpretation: McGregor Member of Platteville Formation (Ordovician) of Wisconsin: *Journal of Sedimentary Research*, v. 48, no. 4, p. 1303–1310.
- Carozzi, A.V., 1993, *Sedimentary Petrography: Sedimentary Geology Series*: Englewood Cliffs, NJ, PTR Prentice Hall, 263 p.
- Chafetz, H.S., 1978, A trough cross-stratified glauconite: a Cambrian tidal inlet accumulation: *Sedimentology*, v. 25, no. 4, p. 545–559.
- Chafetz, H.S., 1979, Petrology of carbonate nodules from a Cambrian tidal inlet accumulation, central Texas: *Journal of Sedimentary Research*, v. 49, no. 1, p. 215–222.
- Chafetz, H.S., and Reid, A., 2000, Syndepositional shallow-water precipitation of glauconitic minerals: *Sedimentary Geology*, v. 136, no. 1, p. 29–42.
- Clifton, H.E., and Thompson, J.K., 1978, *Macaronichnus segregatis*: a feeding structure of shallow marine polychaetes: *Journal of Sedimentary Research*, v. 48, no. 4, p. 1293–1302.
- Cloud, P.E., 1962, Environment of calcium carbonate deposition west of Andros Island, Bahamas: *United States Geological Survey Professional Paper 350*, 138 p.
- Coe, A.L., 2003, *The Sedimentary Record of Sea-level Change*: New York, Cambridge University Press, 288 p.
- Cornish, F.G., 1986, The trace-fossil *Diplocraterion*: Evidence of animal-sediment interactions in Cambrian tidal deposits: *Palaios*, v. 1, p. 478–491.

- Droser, M.L., 1991, Ichnofabric of the Paleozoic Skolithos ichnofacies and the nature and distribution of Skolithos piperock: *Palaios*, v. 6, p. 316–325.
- Ekdale, A.A., Bromley, R.G., and Pemberton, S.G., 1984, *Ichnology: Trace fossils in sedimentology and stratigraphy*: Tulsa, Oklahoma, Society of Economic Paleontologists and Mineralogists, SEPM short course, no. 15, 317 p.
- Farkas, S.E., 1960, Cross-lamination analysis in the Upper Cambrian Franconia formation of Wisconsin: *Journal of Sedimentary Research*, v. 30, no. 3, p. 447–458.
- Gérard, J.R.F., and Bromley, R.G., 2014, *Ichnofabrics in Clastic: Sediments Applications to Sedimentological Core Studies, A Practical Guide*: Tulsa, Oklahoma, American Association of Petroleum Geologists, 97 p.
- Gottlieb, P., Wilkie, G., Sutherland, D., Ho-Tun, E., Suthers, S., Perera, K., Jenkins, B., Spencer, S., Butcher, A., and Rayner, J., 2000, Using quantitative electron microscopy for process mineralogy applications: *Journal of the Minerals, Metals and Materials Society*, v. 52, no. 4, p. 24–25.
- Haberlah, D., Williams, M.A.J., Halverson, G., McTainsh, G.H., Hill, S.M., Hrstka, T., Jaime, P., Butcher, A.R., and Glasby, P., 2010, Loess and floods: High-resolution multi-proxy data of Last Glacial Maximum (LGM) slackwater deposition in the Flinders Ranges, semi-arid South Australia: *Quaternary Science Reviews*, v. 29, no. 19, p. 2673–2693.
- Hamblin, W.K., 1961, Paleogeographic evolution of the Lake Superior region from Late Keweenawan to Late Cambrian time: *Geological Society of America Bulletin*, v. 72, p. 1–18.
- Haq, B.U., 1995, *Sequence stratigraphy and depositional response to eustatic, tectonic, and climate forcing*, Dordrecht: Boston, Kluwer Academic Publishers, Coastal systems and continental margins, v. 1, 381 p.
- Howard, J.D., and Frey, R.W., 1984, Characteristic trace fossils in nearshore to offshore sequences, Upper Cretaceous of east-central Utah: *Canadian Journal of Earth Sciences*, v. 21, no. 2, p. 200–219.
- Ku, T.C.W., and Walter, L.M., 2003, Syndepositional formation of Fe-rich clays in tropical shelf sediments, San Blas Archipelago, Panama: *Chemical Geology*, v. 197, no. 1–4, p. 197–213.
- Logvinenko, N., 1982, Origin of glauconite in the recent bottom sediments of the ocean: *Sedimentary Geology*, v. 31, no. 1, p. 43–48.
- Mason, T.R., and Christie, A.D.M., 1986, Palaeoenvironmental significance of ichnogenus *Diplocraterion torell* from the Permian vryheid formation of the Karoo Supergroup, South Africa: *Palaeogeography, Palaeoclimatology, Palaeoecology*, v. 52, no. 3, p. 249–265.

- McBride, E.F., 1988, Contrasting diagenetic histories of concretions and host rock Lion Mountain Sandstone (Cambrian), Texas: Geological Society of America Bulletin, v. 100, p. 1803–1810.
- Michelson, P.C., and Dott, R.H., Jr., 1973, Orientation analysis of trough cross stratification in upper Cambrian sandstones of western Wisconsin: Journal of Sedimentary Petrology, v. 43, no. 3, p. 784–794.
- Miller, W.C., 2007, Trace fossils: Concepts, Problems, Prospects: Amsterdam, Netherlands, 611 p.
- Moore, D.M., and Reynolds, R.C., Jr., 1997, X-Ray Diffraction and the Identification and Analysis of Clay Minerals: New York, Oxford University Press, 378 p.
- Morrow, D.W., 1978, Dolomitization of lower Paleozoic burrow-fillings: Journal of Sedimentary Research, v. 48, no. 1, p. 295–305.
- Mortenson, J.J., 1981, Stratigraphy and Sedimentology of the Mazomanie Formation (Upper Cambrian) in Southwestern Wisconsin [MS thesis]: Madison, University of Wisconsin, 139 p.
- Munsell, 2009, Rock Color Chart with Genuine Munsell Color Chips: Grand Rapids, Michigan, Geological Society of America, 8 p.
- Odin, G.S., 1988, Green Marine Clays: Oolitic Ironstone Facies, Verdine Facies, Glaucony Facies and Celadonite-Bearing Facies—A Comparative Study, Amsterdam, Elsevier, Developments in Sedimentology, 445 p.
- Ostrom, M.E., 1966, Cambrian stratigraphy of western Wisconsin, UWG & NHS, Information Circular, IC-7, 79 p.
- Ostrom, M.E., 1970, Sedimentation Cycles in Lower Paleozoic Rocks of Western Wisconsin, *in* Field Trip Guide Book for Cambrian-Ordovician Geology of Western Wisconsin: Wisconsin Geological and Natural History Survey Information Circular 11, p. 10–34.
- Pouchou, J.L., and Pichoir, F., 1991, Quantitative Analysis of Homogeneous or Stratified Microvolumes Applying the Model “PAP” Electron Probe Quantitation, New York, Plenum Press, 400 p.
- Rao, V.P., Lamboy, M., and Dupeuble, P., 1993, Verdine and other associated authigenic (glaucony, phosphate) facies from the surficial sediments of the southwestern continental margin of India: Marine Geology, v. 111, no. 1, p. 133–158.
- Schwartz, K.A., 1979, Core Stratigraphy and Petrography of the Reno Member of the Lone Rock Formation, at a Dam Site, Vernon County, Western Wisconsin [MS thesis]: Madison, University of Wisconsin, 80 p.

- Seilacher, A., 1967, Bathymetry of trace fossils: *Marine Geology*, v. 5, no. 5-6, p. 413–428.
- Sutherland, J.L., 1986, *Stratigraphy and Sedimentology of the Upper Cambrian Lone Rock Formation, Western Wisconsin—Focus on the Reno Member* [MS thesis]: Madison, University of Wisconsin, 81 p.
- Terry, R.D., and Chilingar, G.V., 1955, Summary of "Concerning some additional aids in studying sedimentary formations" by M.S. Shvetsov: *Journal of Sedimentary Petrology*, v. 25, no. 3, p. 229–234.
- Twenhofel, W.H., 1936, The greensands of Wisconsin: *Economic Geology*, v. 31, no. 5, p. 472–487.
- Vail, P.R., Mitchum, R.M.J., and Thompson, S., 1977, *Seismic Stratigraphy and Global Changes of Sea Level, Part 4: Global Cycles of Relative Changes of Sea Level: Seismic Stratigraphy—Applications to Hydrocarbon Exploration: The American Association of Petroleum Geologists, Memoir no. 26, p. 83–97.*

CHAPTER 6

TRACE FOSSILS AND ICHNOFABRICS ASSOCIATED WITH GLAUCONITIC MINERALS IN TWO MESOZOIC SEAWAYS, UTAH AND WYOMING

Cretaceous Shannon Sandstone

Introduction

The Shannon Sandstone (Campanian) in Wyoming reflects major marine transgressions of the Cretaceous Interior Seaway during warm climate. The Shannon Sandstone, which occurs within the Cody Shale, was deposited in a transgressive-regressive sequence during the Late Cretaceous (Ranganathan and Tye, 1986; Tillman and Martinsen, 1984; Walker and Bergman, 1993). Ichnologic observations, particularly *Macaronichmus segregatis*, indicate sandy shoreface depositional environment (Clifton and Thompson, 1978; Droser and Bottjer, 1989; Quiroz et al., 2010; Seike, 2007).

Glaucconitic minerals were identified in the Shannon Sandstone, often in the form of pellets incorporated into primary sedimentary structures and biogenic structures. The Shannon Sandstone provides an ideal opportunity to study the association of trace fossils and glauconitic minerals. This perspective provides supportive insight to the latest interpretation of these enigmatic isolated marine sandbodies (Bergman, 1994).

Previous Work

The lower Campanian Shannon Sandstone in the Powder River Basin is in the Cody Shale of the Montana Group. It is up to 50 m thick and consists of sand bodies within marine mudstone. The sand bodies are aligned roughly parallel to the regional paleo-shoreline, and each contain coarsening upward stratigraphic successions. The Shannon has been extensively studied in the subsurface and in outcrop because numerous oil fields produce from the elongate northwest-southeast trending sand bodies (Amorosi, 2011; Gaynor and Swift, 1988; Ranganathan and Tye, 1986; Stonecipher, 1999). Various interpretations and sequence stratigraphic models have been proposed to explain the depositional setting from offshore, shelf sand-ridge (Tillman and Martinsen, 1984) to incised shoreface sand bodies (Bergman, 1994; Walker and Bergman, 1993). The geologic setting includes overlying bioturbated muddy sediments that indicate marine transgression in association with high frequency transgressive-regressive sequences during the Late Cretaceous. Biogenic structures and glauconitic minerals are described in several facies, including mudstones, bioturbated sandstones, and glauconitic cross-bedded sandstones (Amorosi, 2011; Tillman and Martinsen, 1984; Walker and Bergman, 1993).

Trace fossils in the Shannon Sandstone are diverse and locally abundant throughout the unit. The ichnogenera *Chondrites*, *Macaronichmus*, *Ophiomorpha*, *Rosselia*, *Schaubcylindrichmus*, *Skolithos*, *Teichichmus*, *Terebellina*, and *Thalassinoides* have been reported by previous workers in various transitional to shallow-marine facies within the formation (Tillman and Martinsen, 1984; Walker and Bergman, 1993). The key trace fossil, *Macaronichmus segregatis*, is associated with midforeshore to shallow

shoreface zones (Seike, 2007). The animals producing these burrows today are annelid worms that are restricted to mid latitudes, of approximately 35 to 45 degrees N (Clifton and Thompson, 1978; Droser and Bottjer, 1989; Quiroz et al., 2010; Seike, 2007).

Methods

A section in the upper part of a Shannon sand body was measured on the west flank of the Salt Creek Anticline in northern Wyoming (Figure 6.1 A and B). This section included a prominent trace fossiliferous zone containing abundant *Macaronichmus segregatis*. Several samples were collected, and biogenic and primarily sedimentary structures were photographed in place. Three samples were analyzed using thin section microscopy, and one sample (shWY-2) was analyzed using QEMSCAN (Quantitative Evaluation of Minerals by Scanning Electron Microscopy) and electron microprobe. The QEMSCAN technique used the Oil and Gas version3 (20 KV) SIP (Species Identification Protocol) as the reference database. Minerals were identified and textural variability of grains and matrix were differentiated using a 20- μ m probe spacing. Selected green pellets were analyzed by EMPA (electron microprobe analysis) to confirm geochemical composition.

Results

Trace fossil associations observed in the measured section represent the *Skolithos* Ichnofacies. Biogenic structures, primarily intense bioturbation by *Macaronichmus segregatis* (Figure 6.2), dominated part of the measured section. Trough-cross stratification and planar laminae were prevalent in the upper section. Ichnofabric indices

(Bottjer et al., 1987) ranged from *ii1* in unburrowed, trough cross-bedded sandstones to *ii5* in *Macaronichmus*-dominated foreshore and shallow shoreface sandstones. The ichnological observations made at this exposure support the interpretation by previous workers of lower intertidal to shallow offshore-marine depositional setting (Bergman, 1994; Walker and Bergman, 1993).

QEMSCAN results for the green clay minerals in sample # shWY-2 show 1.3% glauconitic minerals, 7.7% Fe-K smectite, and less than 1% chlorite and kaolinite (in area %). The QEMSCAN mineral map (Figure 6.3 A) displays the predominant clays in false color green, which reflect a pellet morphology (Figure 6.3 B). Clays were differentiated based on Fe-Al-K composition, where the glauconitic clays must have Fe, but Al is not required, and the Fe-K smectite has higher Al and lower Fe than the glauconitic clay. Both green clay types have K. Other clastics include fine quartz sand, 50%, and feldspars, 14%. Grains were moderately sorted, rounded to subangular, spherical to elongate, grain supported, with 21% void space and a lack of cement (Figure 6.3 A and B). These characteristics attest to the favorability of the Shannon Sandstone as a hydrocarbon reservoir and explain why it has been so well studied. QEMSCAN values were normalized to account for the 21% void space.

A glauconitic pellet (circled in Figure 6.3 A and B, sample # shWY-2) was analyzed by EMPA and found to have 6% K₂O and 16% Fe₂O₃ (in wt. %), which confirmed mature glauconitic minerals in the pellet. The calculated mineral formula for the glauconitic minerals in the Shannon Sandstone is (K_{0.52} Na_{0.01} Ca_{0.02}) (Fe⁺³_{0.84} Mg_{0.35} Ti_{0.01} Al_{0.62})_{2.00} (Al_{0.39} Si_{3.61})_{4.00} O_{11.83} (F_{0.10} (OH_{1.93}))_{2.00}. EMPA geochemical results for Fe-K smectite are 5% K₂O, 16% Al₂O₃, and 6% Fe₂O₃. Results for glauconitic minerals

and Fe-K smectite are compared in Figure 6.4. The calculated mineral formula for the Fe-K smectite from average EMPA results is $(K_{0.66} Na_{0.03} Ca_{0.01}) (Fe^{+2}_{0.18} Mg_{0.13} Ti_{0.02} Al_{1.67})_{2.00} (Al_{0.19} Si_{3.81})_{4.00} O_{10.12} (OH)_{2.00}$. It is probably a weathering product of the glauconitic minerals. Although stable in the marine environment, glauconitic minerals are susceptible to alteration to aluminum-rich clay with subaerial exposure. Thus, the original glauconitic material in the Shannon Sandstone, before weathering, was probably about 10%, which is the sum of glauconitic and Fe-K smectite minerals according to QEMSCAN results. Some pellets were deformed as if reworked or affected by burial compaction.

Discussion

Glauconitic pellets occur in the Shannon Sandstone associated with the *Macaronichmus* ichnofabric. Both characteristics have implications for paleoenvironment. *Macaronichmus* is a burrow type found today in the midforeshore to shallow shoreface zones of modern coastal environments. It is produced by opheliid polychaete worms (e.g., *Ophelia* and *Euzonus*), which exhaustively churn the sediment, usually well-sorted sand, by feeding on buried organic material while filling their burrow with clean sand and pushing heavy minerals, such as glauconitic grains, aside to the burrow margins (Clifton and Thompson, 1978; Seike, 2007). The presence of abundant *Macaronichmus* in the Shannon Sandstone indicates midforeshore to shallow shoreface zones (Seike, 2007).

Presumably the glauconitic minerals formed on a quiet shelf in a typical glauconitization environment before shallowing of the water and reworking of the

sediment. The grains were incorporated into primary sedimentary structures and biogenic structures, such as ripplemarks, crossbeds, and burrows of the Shannon Sandstone. Since glauconitic grains are highly stable in the marine environment, they persisted during reworking and/or transport. It is inferred that they were originally associated with the adjacent Cody Shale. During lowering of sea level (shoreline regression), glauconitic pellets were probably incorporated into the incised shoreface sand bodies of the Shannon Sandstone, as interpreted by Walker and Bergman (1993).

The findings have paleoclimatic implications for the Late Cretaceous (Campanian) epicontinental seaway. *Macaronichmus segregatis* burrows today are restricted to midlatitudes (approximately 35 to 45 degrees N) in a subtropical-temperate climatic zone or are attributed to upwelling of cold bottom water (Quiroz et al., 2010). Glauconitization occurs at seafloor temperatures of 10 to 15°C and is common at middle latitudes. This suggests that the Shannon Sandstone of the Cody Shale had similar paleoclimatic conditions at the time of deposition.

Jurassic Stump Formation

Introduction

The Jurassic Stump Formation in northern Utah reflects a major marine transgressive sequence. It unconformably overlies the eolian sands of the Entrada Formation and is overlain by shallow marine tidal and eolian strata of the basal Morrison Formation (Eschner and Kocurek, 1986; Wilcox, 2007). It was deposited in response to sea level rise in the Late Jurassic epicontinental seaway (Caputo and Pryor, 1991; Hallam, 1988), which transgressed southward leaving a signature of glauconitic sands

and ichnofabrics. Trace fossils and glauconitic minerals were investigated for clues to understanding the paleoenvironment and sequence stratigraphy.

Previous Work

The Upper Jurassic Curtis and Redwater Members of the Stump Formation outcrop in the Uinta Mountains region of northeastern Utah. Detailed mapping for a master's thesis by Wilcox (2007) found that the Curtis Member is about 10–50 m thick and consists primarily of tan to gray, coarse to very fine grained sandstone with thin interbeds of green to gray siltstone and mudstone. The Redwater Member is about 20–35 m thick and consists primarily of gray mudstone with thin interbeds of medium to very fine grained sandstone and sandy fossiliferous oolitic grainstone. During the final stage of the Jurassic Western Interior seaway, the Curtis and Redwater Members were deposited as a basal marine sandstone and an overlying mudstone as the epicontinental sea transgressed across the Entrada eolian erg (Eschner and Kocurek, 1986; Kocurek and Dott, 1983). The units represent a single transgressive-regressive sequence (Wilcox, 2007). The Curtis is interpreted as a shallow marine bar and interbar complex based on sedimentary structures, such as sigmoidal tidal bundles (Caputo and Pryor, 1991; Kreisa and Moila, 1986). The Redwater Member represents deepening water from shoreface to fully marine shelf deposits (Wilcox, 2007).

Trace fossils, as described by Wilcox (2007), commonly occur in the basal Redwater Member, which disconformably overlies the Curtis Member. This sandstone/mudstone unit is an intensely bioturbated transgressive lag deposit. It contains glauconitic sandstones interbedded with dark gray mudstones. Although individual

burrows usually are unrecognizable along this intensely bioturbated transgressive surface, integrated interpretation suggests a transgressive surface overlain by a condensed section where green clay minerals occur. Biostratigraphic data indicate that the Stump Formation and basal Morrison deposition occurred during early to late Oxfordian time (Wilcox, 2007). The paleoclimate was hot and arid at a tropical paleolatitude during a warm climate (Kocurek and Dott, 1983).

Methods

Several exposures of the Redwater Member in northeastern Utah were examined and sampled (Figure 6.5). Few trace fossils were found, except from the top of Redwater/basal Morrison, where *Thalassinoides* and tiny horizontal burrows marked rippled sandstone. The samples collected from Orchid Draw were from silty laminae of the basal Redwater Member of the Stump Formation. Sample # V UT-11 was analyzed using thin section microscopy, QEMSCAN, and electron microprobe. QEMSCAN mineral maps displayed mineralogical and textural variability of the grains and matrix. Using the Oil and Gas version3 SIP (20 KV) SIP, scans were done across the thin section on a 20 μm spacing. A 4 by 4 mm area was analyzed. Glauconitic minerals are included in the reference data base of this SIP, and they were identified based on the mineral formula for true glauconite. Selected grains were then analyzed by EMPA to confirm geochemical composition.

Results

The QEMSCAN mineral map shows pelleted clays displayed in false color green (Figure 6.6 A). Pellet composition is 10% glauconitic and 4% Fe-K smectite (in area %). The pellet shape is ovoid and ellipsoid with sharp margins (Figure 6.6 B), which suggests origin as fecal pellets. Some pellets are deformed, bent, or fractured, indicating stress, probably due to reworking and/or burial compaction. Other minerals include 40% interstitial calcite/micrite cement with some dolomite, 34% quartz grains, and 2.7% feldspar. Quartz grains are angular to rounded, spherical, to elongate. Preferred orientation is not apparent in the pellets or quartz grains; however, the calcite cement shows preferred orientation, possibly due to stress related to folding of the Split Mountain Anticline.

EMP analyses of a glauconitic pellet (circled in Figure 6.6 A and B, V UT-11) yields 7.5% K₂O and 19% Fe₂O₃ (in wt. %), which defines mature glauconitic minerals. The Fe-K smectite, which also has a green hue under transmitted light microscope, is 13% Fe₂O₃, 14 % Al₂O₃, and 5.8 % K₂O. The calculated mineral formula for the glauconitic minerals is $(K_{0.67} Na_{0.02} Ca_{0.03}) (Fe^{+3}_{1.00} Mg_{0.37} Ti_{0.01} Al_{0.62})_{2.00} (Al_{0.42} Si_{3.58})_{4.00} O_{11.93} (F_{0.05} (OH)_{1.95})_{2.00}$. The Fe-K smectite is associated with the glauconitic pellets, sometimes as grain rims, which suggest it is a weathering product. The Fe-K smectite shows more Al₂O₃ and less Fe₂O₃ than the glauconitic minerals (Figure 6.7). The calculated mineral formula from average EMPA results for the Fe-K smectite is $(K_{0.49} Na_{0.01} Ca_{0.04}) (Fe^{+3}_{0.44} Mg_{0.30} Fe^{+2}_{0.23} Ti_{0.0} Al_{1.01})_{2.00} (Al_{0.07} Si_{3.93})_{4.00} O_{11.95} (F_{0.05} (OH)_{1.95})_{2.00}$. Other clay minerals comprise less than 1% of the total analyzed area according to QEMSCAN. Trace fossils are reported in the basal Redwater Member

(Wilcox, 2007), but few were found in the northeastern Utah outcrops examined for this study.

Discussion

Analytical results reveal that glauconitic minerals are present (10 area %), which means that glauconitization did occur within proximity of the Redwater Member site of deposition. Whether the samples represent the heart of the condensed section described by Wilcox (2007) is unclear. The quartz clastics are very fine grained, which indicates low energy possibly associated with condensed section deposition. The glauconitic pellets show some deformation, which suggests some reworking or transport. Primary sedimentary structures are lacking in the mudstone of the Redwater Member. Thin section microscopy shows that the sparse glauconitic pellets were spread throughout the sample without obvious grain orientation. Whether this accumulation is autochthonous, reworked, or allochthonous is unclear. Further investigation to establish the trace fossil signature would clarify origin of glauconitic minerals.

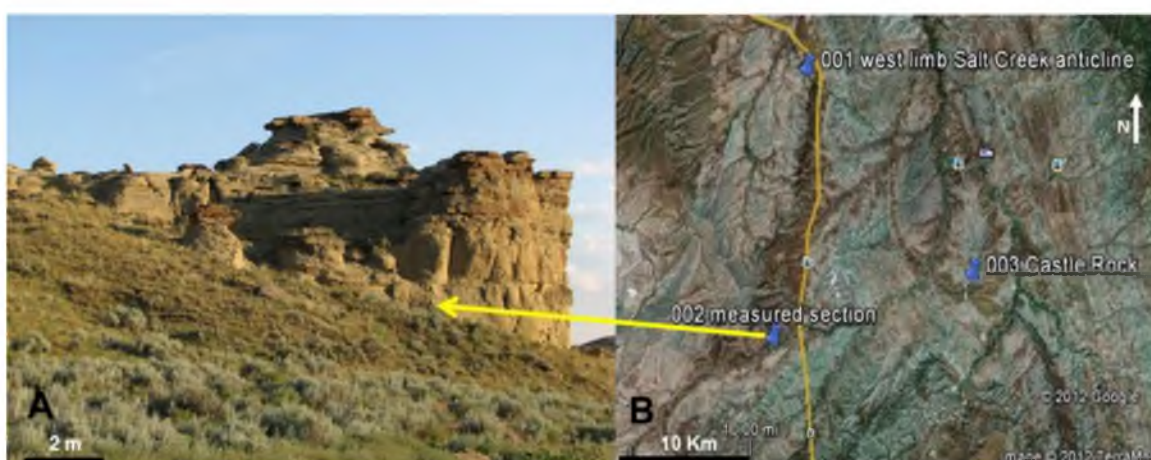


Figure 6.1 Exposure of Upper Cretaceous (Campanian) Shannon Sandstone in the Cody Shale of the Montana Group on the west flank of the Salt Creek Anticline, north of Casper, Wyoming. A) Aerial photo, push pins indicate sample locations in the Castle Rock region (modified after Google Earth image); B) blow up view showing location of the measured section where sample shWY-2 was collected for analyses.



Figure 6.2 *Macaronichnus segregatis* in plan view showing intense bioturbation and *Macaronichnus* ichnofabric in sandstone with burrow fill of clean sand.

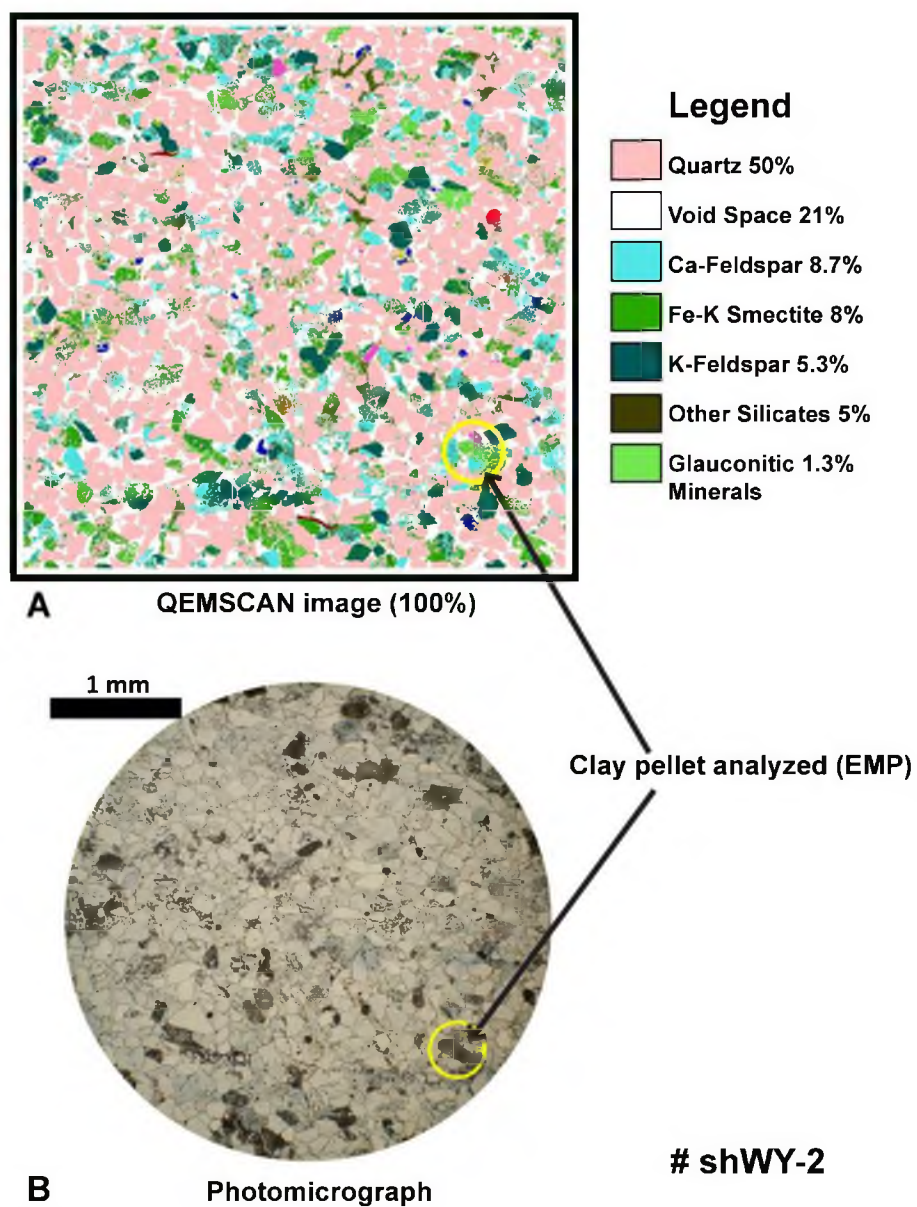


Figure 6.3 QEMSCAN mineral map from sample # shWY-2 (Oil and Gas version3 SIP). Circled pellet was analyzed with EMPA. A) All minerals, 100 area %, with legend; B) photomicrograph of the scanned area in natural light.

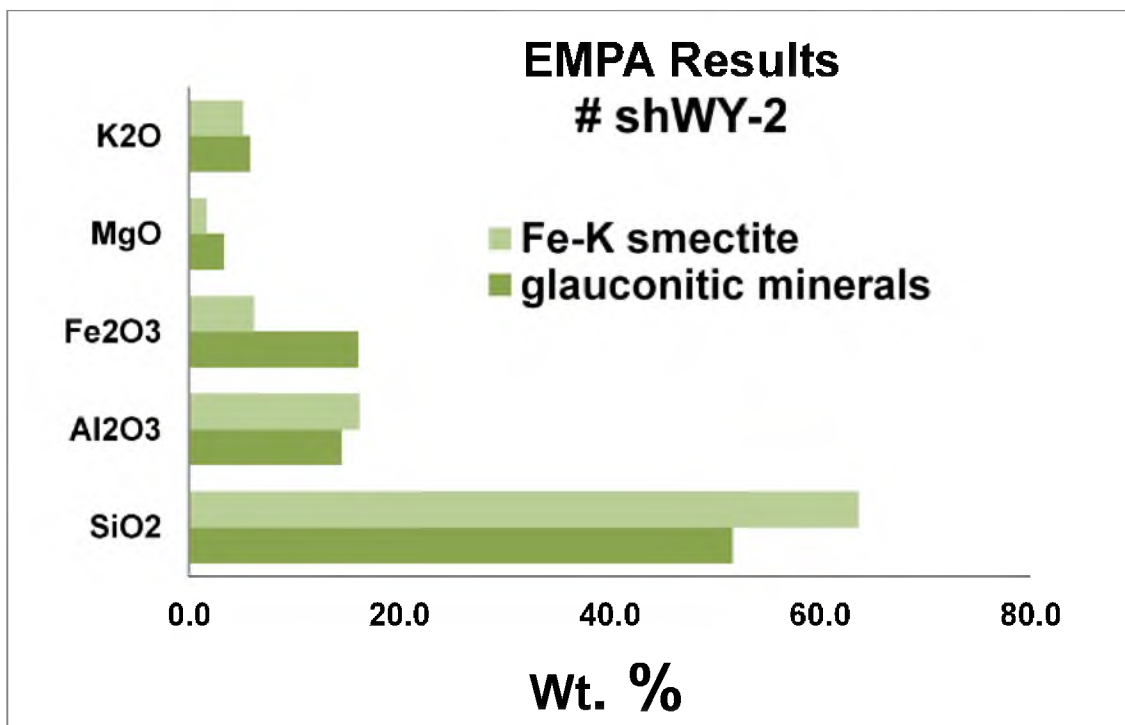


Figure 6.4 EMPA results from the pellet circled in Figure 6.3 (shWY-2). Dominant oxides are compared. Glauconitic minerals have higher Fe₂O₃ and lower Al₂O₃ than Fe-K smectite.

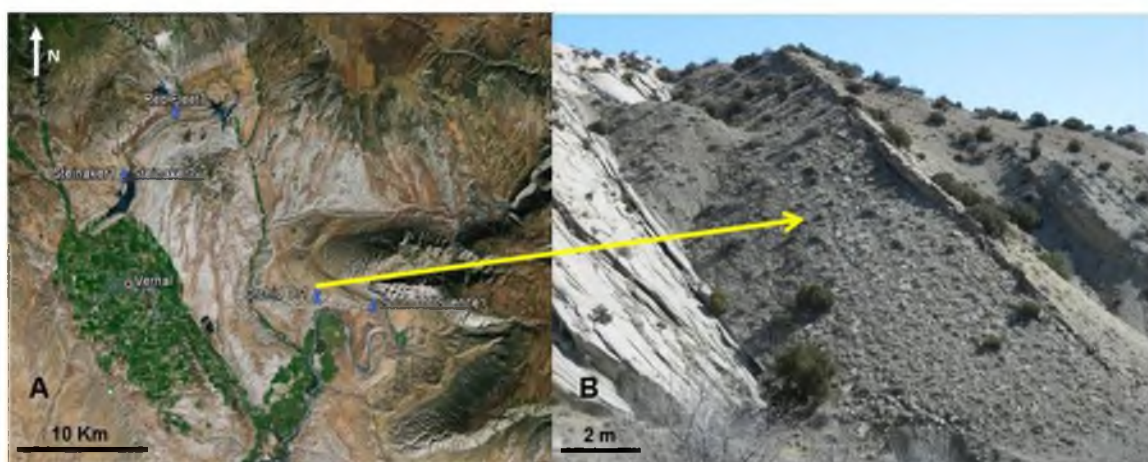


Figure 6.5 Exposures of the Upper Jurassic Curtis and Redwater Members of the Stump Formation in the Uinta Mountain region, northeastern Utah. A) Aerial photo, push pins indicate sample locations in the Vernal Utah area (modified after Google Earth image); B) blow up view of the “Orchid Dr1” sample location in Orchid Draw where V UT-11 was collected for analyses.

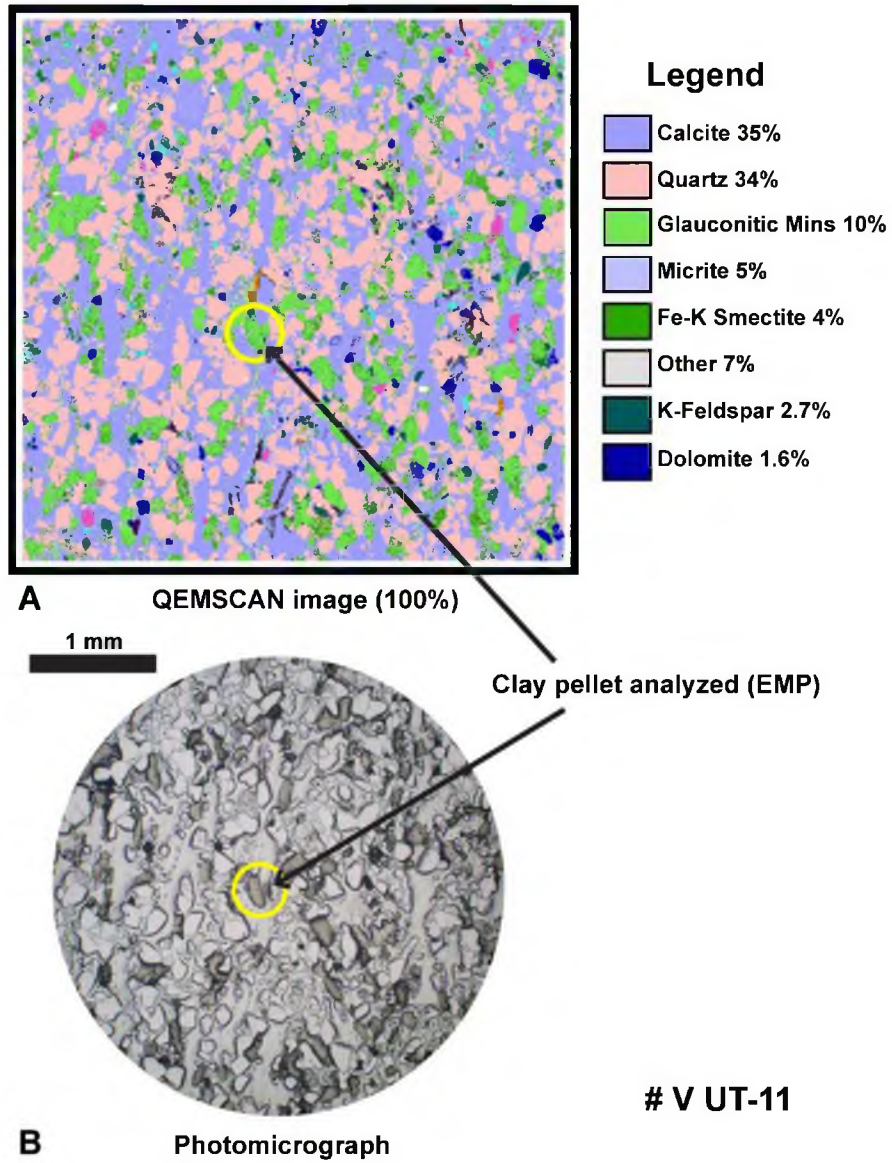


Figure 6.6 QEMSCAN mineral maps from sample # V UT-11 (Oil and Gas version3 SIP). Circled pellet was analyzed with EMPA. A) All minerals, 100 area %, with legend; B) photomicrograph of the scanned area in natural light.

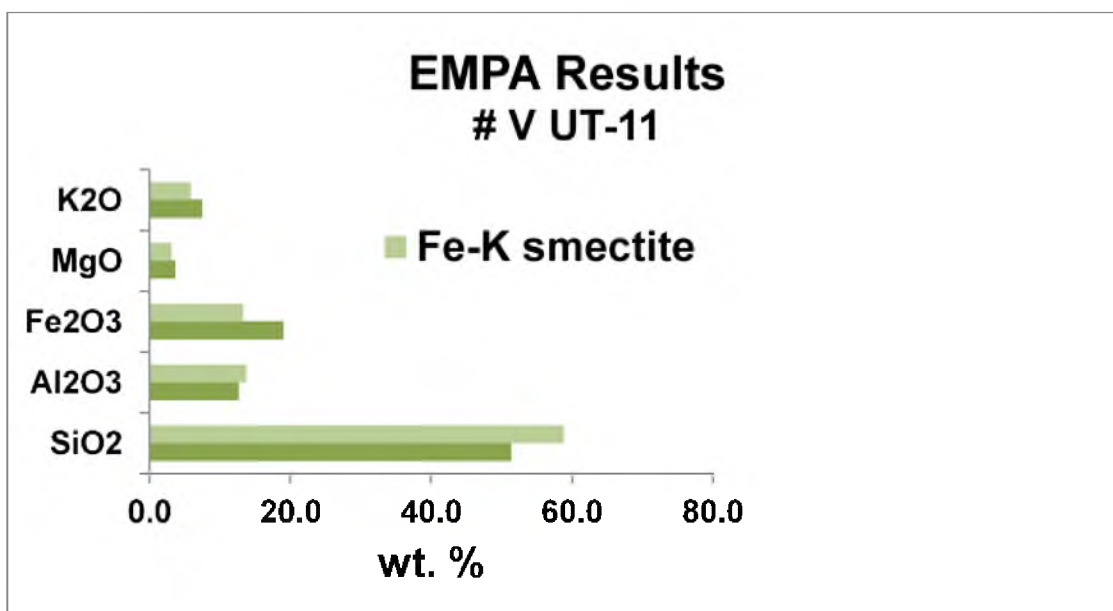


Figure 6.7 EMPA results from the pellet circled in Figure 6.6 (V UT-11). Dominant oxides are compared. Glauconitic minerals have higher Fe₂O₃ and lower Al₂O₃ than Fe-K smectite.

References

- Amorosi, A., 2011, The problem of glaucony from the Shannon Sandstone (Campanian, Wyoming): *Terra Nova*, v. 23, no. 2, p. 100–107.
- Bergman, K.M., 1994, Shannon Sandstone in Hartzog Draw-Heldt Draw fields (Cretaceous, Wyoming, USA) reinterpreted as lowstand shoreface deposits: *Journal of Sedimentary Research*, v. 64, no. 2, p. 184–201.
- Bottjer, D.J., Droser, M.L., and Savrda, C.E., 1987, New concepts in the use of biogenic sedimentary structures for paleoenvironmental interpretation: *Society of Economic Paleontologists and Mineralogists, Pacific Section, Volume and Guidebook*, Los Angeles, California, 65 p.
- Caputo, M.V., and Pryor, W.A., 1991, Middle Jurassic tide-and wave-influenced coastal facies and paleogeography, upper San Rafael Group, east-central Utah: *Geology of East-Central Utah: Utah Geological Association Publication*, v. 19, p. 9–27.
- Clifton, H.E., and Thompson, J.K., 1978, *Macaronichnus segregatis*: a feeding structure of shallow marine polychaetes: *Journal of Sedimentary Research*, v. 48, no. 4, p. 1293–1302, *in* Wilgus, C.K. et al, *Sea Level Changes—an integrated approach: Society of Economic Paleontologists and Mineralogists, Special Publication no. 42*, p. 261–273.
- Kocurek, G., and Dott Jr., R.H., 1983, Jurassic paleogeography and paleoclimate of the central and southern Rocky Mountains region, *in* *Proceedings, Mesozoic Paleogeography of the West-Central United States: Society of Economic Paleontologists and Mineralogists, Rocky Mountain Section*, v. 2, p. 101–116.
- Kreisa, R.D., and Moila, R.J., 1986, Sigmoidal tidal bundles and other tide-generated sedimentary structures of the Curtis Formation, Utah: *Bulletin of the Geological Society of America*, v. 97, no. 4, p. 381–387.
- Quiroz, L.I., Buatois, L.A., Mángano, M.G., Jaramillo, C.A., and Santiago, N., 2010, Is the trace fossil *Macaronichnus* an indicator of temperate to cold waters?: Exploring the paradox of its occurrence in tropical coasts: *Geology*, v. 38, no. 7, p. 651–654.
- Ranganathan, V., and Tye, R.S., 1986, Petrography, diagenesis, and facies controls on porosity in Shannon Sandstone, Hartzog Draw Field, Wyoming: *American Association of Petroleum Geologists, Bulletin*, v. 70, no. 1, p. 56.
- Seike, K., 2007, Palaeoenvironmental and palaeogeographical implications of modern *Macaronichnus segregatis*-like traces in foreshore sediments on the Pacific coast of central Japan: *Palaeogeography, Palaeoclimatology, Palaeoecology*, v. 252, no. 3, p. 497–502.

- Stonecipher, S.A., 1999, Genetic characteristics of glauconite and siderite: Implications for the origin of ambiguous isolated marine sandbodies: Society of Economic Paleontologists and Mineralogists, Special Publication, v. 64, p. 191–204.
- Tillman, R., and Martinsen, R., 1984, The Shannon shelf-ridge sandstone complex, Salt Creek anticline area, Powder River basin, Wyoming: Siliciclastic shelf sediments: Society of Economic Paleontologists and Mineralogists, Special Publication, v. 34, p. 85–142.
- Walker, R.G., and Bergman, K.M., 1993, Shannon Sandstone in Wyoming: a shelf-ridge complex reinterpreted as lowstand shoreface deposits: *Journal of Sedimentary Research*, v. 63, no. 5, p. 839–851.
- Wilcox, W.T., 2007, Sequence Stratigraphy of the Curtis, Summerville and Stump Formations, Utah and Northwest Colorado [MS thesis]: Miami University, Ohio, 216 p.

CHAPTER 7

CONCLUSION

Summary

The Middle Eocene, Main Glauconite Bed (MGB) in Texas reflects an interval of shallowing during a regionally documented marine transgression on the Gulf of Mexico coastal plain. The types and preservation modes of the firmground trace fossils at the top of the MGB suggest an intertidal environment. The concomitant mineralogical finding that clay fecal pellets are comprised of odinite supports the shallow, upper shoreface interpretation. The integrated approach of using ichnological signature and vertebrate mineral characteristics, coordinated with findings from previous studies, is key to understanding the depositional environment of the MGB.

Findings with respect to the Cambrian sites in Texas and Wisconsin reflect deposits at tropical paleolatitude in epicratonic seas. Each of these two sites shows an influx of terrigenous quartz clastics that mixed with glauconitic minerals in a shoreface environment. Abundant fecal pellets were glauconitized during marine transgression, and then during subsequent regression they were reworked by waves, currents, and storms. Quartz clastics were incorporated with the glauconitic pellets, which establishes dual provenance for the deposit. They were redeposited, resulting in moderately to poorly sorted texture. At that time, burrowing organisms that are characteristic of a near shore,

high energy environment occupied the substrate. As a result, shallow water ichnotaxa became associated with deeper marine glauconitic pellets.

Based on modern occurrences of glauconitic minerals, their occurrence in the ancient strata described here indicate a particular depositional setting and environmental conditions. They formed in open seawater near the seawater-substrate interface, with little or no detrital input. Sea floor temperature was 10–15° C, depths 50 m to 300 m, pH around 8 with unrestricted sea water circulation, and a microreducing environment, such as in fecal pellets, at the oxidation-reduction boundary (Carozzi, 1993; Odin, 1988). In a sequence stratigraphic context, authigenic glauconitic minerals are associated with condensed sections on a sediment starved seafloor, associated with gradual sea level rise and transgressive-systems tracts. The environment where odinite occurs is less well documented. Modern occurrences are found in the tropics at water depths of 5 to 50 m with a nearby river mouth influx of iron (Bailey, 1988; Odin, 1988).

Discussion

Study sites for this dissertation were selected on the basis of a known occurrence of green marine sediments in the geologic record (Figure 1.1). Most sites also had a prevalent trace fossil signature. The exception was the Jurassic Curtis Formation of Utah, where trace fossils were not found in the Vernal, Utah, exposures. Although mineralogical results at most sites confirmed the presence of glauconitic minerals, the Middle Eocene Stone City Bluff in Texas also was shown to have the rare green mineral, odinite. All remaining sites contained trace fossiliferous glauconitic minerals. Although each site represented a unique paleoenvironment, the common thread among them is the

evidence for significant change during the depositional history. Commonly, the ichnotaxa represented shallow water, near shore paleoenvironment, while the glauconitic sediment represented deeper water. Careful investigation and integrated interpretation of the mineralogy, sedimentology, and ichnology revealed the pattern of sea-level fluctuation at each site. In fact, transgression followed by regression, probably on a parasequence level, is the common interpretation.

Each of the seven study sites has a different trace fossil assemblage. Each assemblage represented foreshore and shoreface environments where low diversity, opportunistic ichnotaxa were prevalent. The marine softground, high energy, and episodic conditions defined by the *Skolithos* Ichnofacies was most common. A composite ichnofabric is evident in the Middle Eocene Main Glauconite Bed (MGB) of Texas, which represents a marine firmground in the intertidal zone, as defined by the *Glossifungites* Ichnofacies. A transitional ichnofacies (*Cruziana-Skolithos*) was described in the Cambro-Ordovician site of central Texas. Characterization of ichnofabrics and ichnofacies at each site aided in deciphering the paleoenvironments and the sequence stratigraphic implications.

Most notably, the change from *Cruziana* Ichnofacies to *Glossifungites* Ichnofacies, as reflected in the Main Glauconite Bed (MGB) of central Texas, defines a parasequence in a complex transition zone. An intensely bioturbated condensed section representing a subaqueous depositional environment was topped by an interval of nondeposition, dewatering, compaction, and burrowing. This omission surface (hiatus) is defined by firmground intertidal trace fossils. Eventually, the firmground burrows were filled with detrital sediment with a return to subaqueous environment. The vertical

change in ichnofabric and ichnofacies in the MGB represents transgression-regression on a parasequence level. The ichnological findings, supported by the mineralogical findings, define a parasequence level shallowing event. It falls within the upward deepening transition sequence at Stone City Bluff, which is topped by a maximum flooding surface.

Pellet morphology indicates that fecal pellets comprised the original substrate at all seven sites before precipitation or crystallization of the green minerals. This observation supports those of other workers that pellets are the most common habit of glauconitic minerals. Pelleted substrate in modern oceans is most prevalent from the shoreline to about 30 m depth, while glauconitization in modern oceans occurs at > 50 m to 300 m or more (Odin, 1988). Thus, the glauconitization zone probably shifted shoreward over the pelleted seafloor to produce the abundant glauconitic pellets. Consequently, mature glauconitized pellets suggest a significant marine transgression that was long in duration, perhaps over an interval of 10^4 to 10^6 years (Figure 1.5).

The pelletization of clay by suspension feeding and deposit feeding fauna is a common behavior by marine benthic organisms. Abundant pellets in the substrate reflect a thriving benthic community. In modern oceans, some of the highest biological productivity occurs at continental margins with favorable nutrient supply within the euphotic zone at depths ranging from 0 to 100 m (Thurman and Trujillo, 1999). Therefore, abundant pellets, represented as glauconitic pellets in the geologic record, indicate zones and times of high biological productivity in the paleo-ocean. Previous studies have investigated the link between glauconitic minerals, nutrient-enriched waters and paleo upwelling or paleo phytoplankton blooms (Brasier, 1992; Parrish et al., 2001; Parrish and Gautier, 1988). Certainly, abundant glauconitized pellets have

paleoenvironmental implications.

Paleoclimatic Implications

Each of the seven sites examined during this study correlate with a Phanerozoic climatic warm interval (Figure 1.2). The observed link between the occurrence of green minerals and climatic warm modes suggests that the association may be significant in paleoclimatic research. As paleoclimate models become more refined, glauconitization could play an important role in interpretation. Modifications to the Phanerozoic climate model termed GEOCARBSULF, which addresses O₂ and CO₂ in the ocean-atmosphere system, are ongoing (Berner, 2006, 2009). During modifications, implications of glauconitization should be considered.

There is biological participation in the glauconitization process regardless of pellet habit. There are a variety of sea floor substrates that can be glauconitized, which include bioclasts and rock grains (Triplehorn, 1966). In any case, sea-floor substrate rich in glauconitic minerals reflects high biological productivity, which would be supported by high nutrient supply (Parrish et al., 2001; Parrish and Gautier, 1988). Terrestrial runoff, even before the appearance of land plants, could be an important source of nutrients. Also, there is an important observed link between transgressive seas and glauconitization. Times of higher relative sea level tend to coincide with climatic warm modes in the Phanerozoic. Thus, glauconitic minerals offer information about paleoclimate.

The two Cambrian sites investigated here have abundant glauconitic minerals. Each was deposited at an equatorial latitude in a tropical climate while shallow seas

transgressed on and off of the craton. The Cambrian strata are rich in shallow marine fossils mostly represented by trace fossils. Evidence suggests a thriving benthic fauna, which would be driven by thriving primary producers in nutrient-rich water. Prior to the late Precambrian, glauconitic minerals were absent from the geologic record (Benton and Harper, 2009). Findings at the two Cambrian sites support the association of abundant glauconitic minerals, fossiliferous levels, and warm paleoclimate.

The stable isotopes of carbon (^{13}C : ^{12}C) offer an important quantitative measure in paleoclimatic studies. Carbon fixation by organisms preferentially incorporates ^{12}C and leaves ^{13}C behind in the ocean-atmosphere system. Episodes of high primary productivity, or high phytoplankton production, take CO_2 out of the system and add O_2 to the system. Plankton abundance means increased food for mud eaters and suspension feeders. Some of the fixed carbon is passed into the sediment by the benthic fauna in the form of fecal pellets. Eventually, a large amount of organic carbon (^{12}C) could be tied up in the sea floor sediments as buried organisms and fecal pellets. Thus, during episodes of high primary productivity, ^{12}C is taken out of the system and stored in sediments. Correspondingly, this duration would be represented by a high ^{13}C signature, and a positive $\delta^{13}\text{C}$ anomaly could be recorded in the geologic record (O'Leary, 1988). An episode of high primary productivity can be reflected in abundant authigenic glauconitic minerals in the sediment (Parrish et al., 2001; Parrish and Gautier, 1988). Primary productivity has been linked to climatic change in the Phanerozoic (O'Leary, 1988) (Patricia Garcia, 2013, written communication). The possible link between glauconitization of sea floor organics and paleoclimate has not been explored. Regarding the ^{12}C that was fixed during pelletization, the question remains, was ^{12}C buried in sea

floor sediments or was it released to the ocean-atmosphere during authigenesis of the glauconitic minerals?

Verdinization processes, which result in the formation of odinite, also have paleoclimatic implications. The climatic warm interval known as the Middle Eocene Climatic Optimum (MECO) coincides with deposition of the MGB in Texas, which is comprised of fecal pellets that have been altered to odinite. The MECO warming event at ~40.6–40.0 Ma (Bohaty and Zachos, 2003) was one of the most severe, short-term global climate perturbations of the Cenozoic. It is characterized by a gradual 4 to 6°C temperature increase that affected ocean surface waters and deep water (Galazzo et al., 2013). The increase in temperature, if associated with elevated moisture, would have increased discharge of nutrient-rich terrestrial runoff, thus highly increasing the primary productivity. The MGB exhibits unusually prolific biological productivity (Stanton and Nelson, 1980).

Verdine minerals, such as odinite, are found exclusively in tropical latitudes in modern oceans, so they can provide climatic information when identified in the geologic record. Odinite in the MGB suggests an expansion of the tropics during the MECO. The trace fossils and body fossils in the MGB provide an excellent opportunity to document a benthic community response to the MECO. The MGB provides the first reported evidence of response to the MECO climatic perturbation in North America. It exhibits infaunal animal behavior as reflected in the trace fossils, community diversity as reflected in the body fossils, and tropical climate as indicated by the verdine mineralogy. It represents dynamic seafloor conditions and high biological productivity in a nearshore benthic environment. For comparison, the well-studied extreme warming event known as

the Paleo-Eocene Thermal Maxima (PETM) deeply affected marine biota on the continental shelves (Galazzo et al., 2013) (Scott Wing, 2014, oral communication). Thus, characterization of the faunal response to the MECO as seen in the MGB is a significant endeavor. Such information could provide a reliable ancient analogue for warming today.

Conclusions

- 1) Green marine deposits commonly contain glauconitic minerals and, to a lesser degree, verdine minerals. Their identification and maturity is critical for paleoenvironmental interpretation. If the grains are glauconitic, then glauconitization occurred in its history. If they contain odinite, there are alternative paleoenvironmental implications, for instance, tropical climate and near-by terrestrial run off.
- 2) Both glauconitization and verdinization processes commonly occur in fecal pellets. Important in the process is a fully marine shelf substrate, microreducing conditions associated with the substrate that influenced the mineral authigenesis, and marine transgression.
- 3) Mature glauconitic grains signify that extensive transgression occurred. For instance, the zone of prevalent fecal pellets on the sea floor is 0 to 30 m, while the zone of glauconitization is 50 to 300 m, so the shoreline must shift and water must deepen in order to promote glauconitization of the fecal pellets. These conditions must persist for 10^4 to 10^6 years in order for development of mature glauconitic minerals, which would indicate extensive transgression.

- 4) Regression follows the transgression and is accompanied by shallowing sea level. This is the logical interpretation for the many reworked glauconitic mineral deposits. During regression, quartz grains from terrestrial runoff often were combined and reworked with the glauconitic grains that remained essentially in place.
- 5) Glauconitic minerals are chemically stable in the marine environment. Although glauconitic grains are soft and may be deformed during reworking and transportation, they persist and are found to be physically stable as well as chemically stable. On the other hand, verdine minerals, which are dominated by odinite, are not as stable and may readily alter to chlorite if left exposed.
- 6) Because of the stability of glauconitic minerals, reworked or allochthonous deposits are common. Incorporation of glauconitic grains into primary sedimentary structures with a mix of quartz grains indicates a reworked, or allochthonous, deposit. Textural characteristics, such as sorting and compositionally controlled bimodal grain size, are diagnostic. Dual provenance, marine origin for the glauconitic grains and terrestrial source for the quartz grains, is the logical interpretation when resolving the depositional history.
- 7) The trace fossils, ichnofabric, and ichnofacies that are associated with the glauconitic mineral-rich deposits characterize the final depositional process in the history of the glauconitic deposits. In such a case, the ichnotaxa are not linked to the actual pellet producers or to the original glauconitization environment. The glauconitic sediments were reworked and redeposited in place, and then the burrowing organisms subsequently occupied the substrate, as reflected in the trace

- fossils. In other words, shallow marine trace fossils occupied what used to be a deeper water (glaucconitic) marine substrate.
- 8) Odinite is not common in the geologic record, but it was identified with confidence in the pellets of the MGB. Burial and preservation must have ensued for the odinite to have remained unchanged. Modern deposits of odinite are found exclusively within tropical latitudes near a river mouth source of iron. The MGB is assumed to have had a similar depositional environment. Because the paleolatitude of the MGB site is outside the range of the tropics today, the tropics in the Eocene had to be expanded during deposition of the MGB. Occurrence of odinite suggests autochthonous accumulation because odinite cannot tolerate extensive reworking.
 - 9) Timing of MGB accumulation correlates with the MECO climatic warm episode. This supports the conclusion that the MGB represents a warm (tropical) climate. Verdine mineral authigenesis, the prolific and diverse shallow marine life, and the warm paleoclimate occurred together and define the MGB. This finding offers tremendous opportunity to record behavioral response of a diverse benthic community to extreme climate warming.
 - 10) Glaucconitic minerals, although common throughout the Phanerozoic, were not formed at a constant rate. They were associated with intervals of high sea level and/or periods of high biological productivity, and they tend to correlate with warm climate. Such phenomena could provide a fossil based proxy for paleoclimatic studies in a qualitative sense.
 - 11) As paleoclimatologists refine quantitative measures of carbon in the geologic

record, they should consider the effects of glauconitization. The effects may be minor, but at present are poorly understood. The pertinent question arises whether glauconitic minerals represent fixation of ^{12}C , or if they signify the opposite, that is, ^{12}C release over the years of glauconitization.

Future

Several hypotheses and questions are suggested for further study. The prospect of a link between glauconitic mineral authigenesis and paleoclimate could be a valuable biotic or abiotic paleoclimate proxy. There is a well-documented link between autochthonous glauconitic mineral deposits and marine transgressions. Biological participation in glauconitization has been widely accepted. Delineation of where a paleo oxygen minimum layer impinged upon the sea floor or where paleo upwelling zones have occurred have been examined only briefly (Parrish et al., 2001; Parrish and Gautier, 1988). Further establishment of such links could provide significant aid to detailed paleoenvironmental interpretations.

Confirmation of other ancient verdine mineral (odinite) deposits will be extremely important. Establishment of odinite as the dominant mineral in MGB pellets in this study was unprecedented. It is the first documented occurrence of odinite preserved in the geologic record. Additional findings will support the MGB results. When identified, odinite has important paleoenvironmental and paleolatitudinal implications.

Deposition of the MGB coincides with the MECO, which represents an interval of major climatic warming. Paleocology of the MGB, especially in terms of the unusually high molluscan diversity, has been thoroughly studied (Stanton and Nelson, 1980;

Zuschin and Stanton, 2002). Documentation of behavioral response, as recorded in the trace fossils, to such climatic perturbations is the essence of this study. No other sites have been described in North America that represent the MECO time frame (Galazzo et al., 2013). There are several enigmatic “glauconitic shell beds” around the Gulf Coastal Plain and the Atlantic Coastal Plain that represent Middle Eocene (Warren D. Allmon, 2009, written communication). The Gosport Sand and Lisbon Formation of Alabama and the Doby’s Bluff Tongue unit of Mississippi, to name a few, are glauconitic shell beds that should be examined with a new climate perspective.

Other related issues that deserve further exploration include the following. Evidence shows crustacean diversity to be greatest during climatic warm episodes (A.A. Ekdale, 2013, oral communication). Crustacean burrows are especially prominent in the MGB, which suggests a direct link to a warm climate. Further evidence should support the hypothesis of expanded tropics during the MECO. The glauconitic shell beds mentioned above contain molluscan populations that are described as having unusually large shells and/or unusually diminutive shells (Warren D. Allmon, 2009, written communication). It will be significant to determine if this observation of shell sizes may be related to higher sea-floor temperature and/or changed ocean chemistry. The benthic fauna would be affected directly by a major climate change, so a change in shell size may reflect such a climate change. All such paleoecological aspects should be examined with the new warm climatic perspective.

References

- Bailey, S.W., 1988, Odinite; a new dioctahedral-trioctahedral Fe (super 3+)-rich 1:1 clay mineral: *Clay Minerals*, v. 23, no. 3, p. 237–247.
- Benton, M.J., and Harper, D.A.T., 2009, *Introduction to Paleobiology and the Fossil Record*: Chichester, UK, Wiley-Blackwell, xii, 592 p.
- Berner, R.A., 2006, GEOCARBSULF: A combined model for Phanerozoic atmospheric O₂ and CO₂: *Geochimica et Cosmochimica Acta*, v. 70, no. 23, p. 5653–5664.
- Berner, R.A., 2009, Phanerozoic atmospheric oxygen: New results using the GEOCARBSULF model: *American Journal of Science*, v. 309, no. 7, p. 603–606.
- Bohaty, S.M., and Zachos, J.C., 2003, Significant Southern Ocean warming event in the late middle Eocene: *Geology*, v. 31, no. 11, p. 1017–1020.
- Brasier, M.D., 1992, Nutrient-enriched waters and the early skeletal fossil record: *Journal of the Geological Society*, v. 149, no. 4, p. 621–629.
- Carozzi, A.V., 1993, *Sedimentary Petrography: Sedimentary Geology Series*: Englewood Cliffs, NJ, PTR Prentice Hall, 263 p.
- Dyar, M.D., 1984, Precision and interlaboratory reproducibility of measurements of the Mössbauer effect in minerals: *American Mineralogist*, v. 69, p. 1127–1144.
- Galazzo, F.B., Giusberti, L., Luciani, V., and Thomas, E., 2013, Paleoenvironmental changes during the Middle Eocene Climatic Optimum (MECO) and its aftermath: The benthic foraminiferal record from the Alano section (NE Italy): *Palaeogeography, Palaeoclimatology, Palaeoecology*, v. 378, p. 22–35.
- O'Leary, M.H., 1988, Carbon isotopes in photosynthesis: *Bioscience*, v. 38, no. 5, p. 328–336.
- Odin, G.S., 1988, *Green Marine Clays: Oolitic Ironstone Facies, Verdine Facies, Glaucony Facies and Celadonite-Bearing Facies—A Comparative Study*, Amsterdam, Elsevier, *Developments in Sedimentology*, 445 p.
- Parrish, J.T., Droser, M.L., and Bottjer, D.J., 2001, A Triassic upwelling zone: The Shublik Formation, Arctic Alaska, USA: *Journal of Sedimentary Research*, v. 71, no. 2, p. 272–285.
- Parrish, J.T., and Gautier, D.L., 1988, Upwelling in Cretaceous Western Interior Seaway: Sharon Springs Member, Pierre Shale: *American Association of Petroleum Geologists, Bulletin*, v. 72, no. 2, p. 232–233.

- Stanton, R.J., and Nelson, P.C., 1980, Reconstruction of the trophic web in paleontology: community structure in the Stone City Formation (Middle Eocene, Texas): *Journal of Paleontology*, v. 54, no. 1, p. 118–135.
- Thurman, H.V., and Trujillo, A.P., 1999, *Essentials of Oceanography: Upper Saddle River, New Jersey*, Prentice-Hall, Inc., 527 p.
- Triplehorn, D.M., 1966, Morphology, internal structure, and origin of glauconite pellets: *Sedimentology*, v. 6, no. 4, p. 247–266.
- Zuschin, M., and Stanton, R.J., 2002, Paleocommunity reconstruction from shell beds: a case study from the Main Glauconite Bed, Eocene, Texas: *Palaios*, v. 17, no. 6, p. 602–614.

APPENDIX

CAMBRIAN OF WISCONSIN DETAILED

PETROGRAPHY

Thin section microscopy was performed on six samples under transmitted light with polarizing light microscope. Composition was estimated visually using comparison charts (Terry and Chilingar, 1955). Color was estimated using the Rock Color Chart with genuine Munsell color chips (Munsell, 2009).

R-WI-3A

Sample Description

This sample was taken from the middle of a thin (0.8 ft thick) storm bed with sharp contacts at the base and top. Chunks of dolomitic burrow fill are displayed in the thin section. The hand sample displays undisturbed *Skolithos* burrows in laminated sand (*ii2*), as well as rip-up clasts of dolomitic chunks and possible clay pebbles. Glauconitic grains decrease upward and *Skolithos* burrows increase upward.

Composition

Quartz grains are smaller and more abundant than glauconitic grains. Glauconitic grains are incorporated into laminations. Approximate modal percentage is 3 to 5% of

the larger pelleted glauconitic grains and 40 to 50% of the smaller quartz grains with some feldspar grains. The rest is chunks of dolomite crystals that may be remnant fragments of burrow fill that became rip-up clasts. A few opaque, metallic minerals are present.

Color

Glauconitic grains are grayish green (10GY 5/2) to dark yellowish green (10GY 4/4) with rims of dark greenish yellow (10Y 6/6). Cement in the clasts of dolomite crystals is brown.

Texture

Grain size. There is bimodal grain size. Glauconitic grains are larger than quartz grains. Quartz grains are equidimensional to elongate with an average 180 μm length and 120 μm width, which is fine sand. Glauconitic grains have ovoid shape with average 310 μm length and 190 μm width, which is fine to medium sand.

Rounding and sphericity. Quartz grains are sub angular to rounded with low to high sphericity. Glauconitic grains are well rounded, especially where diagenetic rims occur. Grain shape is spherical to ovoid to ellipsoid and resembles fecal pellets. Pellets commonly are broken and those edges are irregular or scalloped.

Packing. Some grains show line contacts between quartz and glauconitic grains. Other glauconitic grains are concave around quartz grains with a smooth convex edge where not impinged upon by quartz grains. Glauconitic grains often are bent, which probably is a function of compaction. Within the burrows, dolomite rhombohedral

crystals are matrix supported.

R-WI-2A

Sample Description

This sample was collected from a glauconite-rich stringer at the base of a thick (3.2 ft.) storm bed.

Composition

Approximate modal percentage is 10 to 20% of the larger pelleted glauconitic grains, and 10 to 20% of the smaller quartz and feldspar grains. A few opaque, metallic minerals are present.

Color

Glauconitic grains are grayish green (10GY 5/2) to gark yellowish green (10GY 4/4) with rims of dark greenish yellow (10Y 6/6).

Texture

Grain size. There is bimodal grain size. Glauconitic grains are larger than quartz grains. Quartz grains average 230 μm length and 150 μm width, which is fine sand. Glauconitic grains average 380 μm length and 270 μm width, which is medium sand. One glauconitic grain has a long axis of 600 microns. The standard deviation of pellet width is distinctly lower than that of pellet length.

Rounding and sphericity. Quartz grains are subangular to rounded and range

from low to high sphericity. Glauconitic grains are well rounded, often with rims of concentric rings. Many glauconitic grains have an irregular shape due to fracturing. Shape is spherical to ovoid to ellipsoid and resembles fecal pellets.

Packing. Glauconitic grain contacts often are concavo-convex as they are bent around another grain, which probably occurred during compaction. Diagenetic rims of concentric bands surround many of the glauconitic grains. Some rims are clearly truncated due to fracturing. This indicates that concentric bands formed before glauconitic grain reworking or transport. This suggests allochthonous or reworked origin of glauconitic minerals.

Diagenetic Minerals

Concentric rings of glauconitic minerals occur as rims around the glauconitic pellets. Diagenetic opaque metallic minerals are a minor constituent. Little to no dolomite is evident.

R-WI-7B

Sample Description

This sample was taken from glauconitic-grain-rich symmetrical ripples. The ripple layer is a distinct band (0.2 ft thick) that extends laterally in the outcrop for some 20 feet. The ripple layer is underlain by a sharp contact and overlain by planar laminations. This sample represents the bottom of a thin bed about 0.4 ft thick. Top of the bed is a less distinct scour. EMPA and QEMSCAN analyses were conducted on this sample.

Composition

The pelleted glauconitic grains comprise 40 to 50% of the matrix, while quartz and feldspar grains comprise 10 to 20%. Clasts comprised entirely of quartz and feldspar are incorporated into the glauconitic matrix. Little dolomite is detected in the matrix or the clasts (0.06 area %), as determined by QEMSCAN analysis. Opaque metallic minerals, some appearing in cubic form, act as cement and comprise about 5%. They are identified as magnetite and hematite according to QEMSCAN analysis.

Color

Glauconitic grains are grayish green (10GY 5/2) to dark yellowish green (10GY 4/4) with rims of dark greenish yellow (10Y 6/6). Opaque metallic minerals show an iron stain halo.

Texture

Grain size. There is bimodal grain size. Glauconitic grains are slightly larger than quartz grains. Quartz grains are equidimensional to elongate with an average 230 μm length and 160 μm width, which is fine grained sand. Very few of the glauconitic grains retain the ovoid to ellipsoid pelleted shape because of damage, but where they are intact, the average length is 360 μm and width is 240 μm , which represents fine grained to medium sand. The standard deviation of pellet width is consistently lower than that of pellet length, which supports fecal pellet origin.

Rounding and sphericity. Quartz grains are subangular to subrounded with many internal cracks, and sphericity is equidimensional to elongate. Glauconitic grains

are well rounded with some rims of concentric rings. Some edges are angular where broken or flattened from compaction effects. Glauconitic grains are spherical to ovoid to ellipsoid and resemble fecal pellets where intact.

Packing. Some grain contacts are straight, which indicates packing and cementation by pressure solution. Others are concavo-convex, which indicates compaction of malleable glauconitic grains. This sample is well compacted. Glauconitic grains are amalgamated with some interpenetration of quartz grains. A slight preferred grain orientation is evident.

Diagenetic Minerals

Concentric rings of glauconitic minerals occur as rims around the glauconitic pellets. Opaque metallic minerals occur between grains as a cementing agent. Dolomite rhombohedra are not present in this sample.

R-WI-8B

Sample Description

This sample was taken from laminated sediment at the base of a typical lam-scam bed, immediately above a contact. Glauconitic grains are more abundant in some laminations. Chunks of cemented dolomite crystals occur chaotically and may represent rip-up clasts of diagenetic burrow fill.

Composition

Quartz grains comprise 30 to 40% and glauconitic grains comprise 5% to 20% of the matrix. The higher percentage of glauconitic grains occurs in the green laminations. Dolomite occurs as a cementing agent in the burrow fill and makes up nearly 100% of the composition. Possibly two kinds of rip-up clasts occur in this sample, dolomite cemented burrow fill and clay-rich flat pebbles. Opaque metallic minerals comprise about 5%.

Color

Glauconitic grains are grayish green (10GY 5/2) to dark yellowish green (10GY 4/4) with rims of dark greenish yellow (10Y 6/6).

Texture

Grain size. There is bimodal grain size. Glauconitic grains appear slightly larger than quartz grains. Quartz grains are equidimensional to elongate where average length is 240 μm and average width is 150 μm , which represents fine grained sand. Glauconitic grains have ovoid to ellipsoid pelleted shape with an average length of 310 μm and width of 180 μm , which is fine grained to medium sand. The standard deviation of pellet width is distinctly lower than that of pellet length, which supports fecal pellet origin.

Rounding and sphericity. Quartz grains are subangular to subrounded and spherical to elongate. Glauconitic grains are well rounded, and the diagenetic rims follow the rounded shape. Glauconitic grains are angular where broken and scalloped edges occur. They are spherical to ovoid to ellipsoid and resemble fecal pellets where intact.

Packing. Quartz grains have line contacts, which indicate pressure solution during compaction. A few glauconitic grains are concavo-convex shape, which is a function of compaction. Many are fractured. Where dolomite rhombohedra occur, they are dispersed in the cement. Some crystal contacts are point to point, which indicates that they are matrix supported.

Diagenetic Minerals

Concentric rings of glauconitic minerals occur as rims around some glauconitic pellets. Dolomite rhombohedra are a significant constituent of the burrow fill in this sample. Opaque minerals occur between grains as diagenetic cement in both the burrow fill and the matrix.

R-WI-4C

Sample Description

This sample was taken from the upper part of a bed where both *Diplocraterion* and *Skolithos* burrows occur. The bed is typical lam-scam, 0.9 ft thick, with a sharp basal contact marked by flat pebble conglomerate and upper contact where the tops of *Diplocraterion* burrows are truncated by erosion. Some scours occur within the bed.

Composition

Quartz grains comprise 20 to 30% of the matrix and glauconitic grains, about 3 to 5%. Rhombohedral dolomite crystals occur as burrow fill and as a cementing agent. The burrow fill is monomineralic dolomite, where it comprises nearly 100%. Few quartz and

glaucanitic grains are incorporated into the burrow fill. Unidentified biogenic material, probably body fossils, in the form of long stick-like pieces are present. Opaque minerals comprise less than 5%.

Color

Glaucanitic grains are grayish green (10GY 5/2) to dark yellowish green (10GY 4/4) with rims of dark greenish yellow (10Y 6/6). Cement in the burrow fill is brown.

Texture

Grain size. There is bimodal grain size. Glaucanitic grains are larger than quartz grains; however, many glaucanitic grains are broken; therefore, their size is similar to that of quartz grains. Quartz grains are equidimensional to elongate where average length is 190 μm and average width is 130 μm , which is fine grained sand. Glaucanitic grains have ovoid to ellipsoid pelleted shape with average length of 210 μm and average width of 150 μm , which is fine grained sand. There is no significant difference between the standard deviation of pellet width and pellet length.

Rounding and sphericity. Quartz grains are subangular to well rounded and spherical to elongate. Glaucanitic grains are well rounded, but they may have scalloped edges where fractured or flat edges where influenced by grain contacts. They are spherical to ovoid to ellipsoid where intact and resemble fecal pellets. Diagenetic rims are thin to nonexistent.

Packing. The nonburrowed matrix is well compacted. Line contacts occur between many quartz grains. Where diagenetic dolomite occurs between grains, crystal

contacts are point to point. Some glauconitic grains show concavo-convex contacts, which is a function of compaction. Glauconitic grains have smooth edges except where fractured.

Diagenetic Minerals

Concentric rings of glauconitic minerals occur as rims around the glauconitic pellets. Dolomite rhombohedra are a significant constituent of this sample. Some opaque minerals occur between grains as diagenetic cement.

R-WI-5C

Sample Description

This sample was taken from the bottom of a bed just above a sharp contact. The matrix is mostly quartz grains with some glauconitic grains. Flattened clay rip-up clasts are prevalent in the flat pebble conglomerate. The clasts have very few quartz and glauconitic grains.

Composition

Quartz grains comprise 20 to 30% of the matrix, some feldspar grains are included. Glauconitic grains comprise 5 to 10%. The rip-up clasts are predominantly clay with a few quartz and glauconitic grains included. Rhombohedral dolomite crystals and clay occur as cement. Unidentified biogenic material, probably body fossils, in the form of long stick-like pieces are present. Opaque minerals comprise less than 5%.

Color

Glaucinitic grains are grayish green (10GY 5/2) to dark yellowish green (10GY 4/4) with rims of dark greenish yellow (10Y 6/6).

Texture

Grain size. There is unimodal grain size. There are very few larger glauconitic grains. Quartz grains are equidimensional to elongate where average length is 220 μm and average width is 150 μm , which is fine grained sand. Glaucinitic grains are few and often fractured. They have ovoid pelleted shape with an average length of 200 μm and width of 120 μm , which is fine grained sand. Grain size of the matrix is fairly well sorted. There is no real contrast in size between quartz grains and glauconitic grains. Most glauconitic grains are fractured. There is no significant difference between the standard deviation of glauconitic grain width and length.

Rounding and sphericity. Quartz grains are subangular to subrounded and spherical to elongate. Glaucinitic grains are well rounded, but many have scalloped edges where fractured or flat edges where influenced by grain contacts. They are spherical to ovoid to ellipsoid where intact, and they resemble fecal pellets. Diagenetic rims are thin to nonexistent.

Packing. The matrix is well compacted. Line contacts occur between many quartz grains. Where diagenetic dolomite occurs between grains, crystal contacts are point to point. Some glauconitic grains show concavo-convex contacts, which is a function of compaction.

Diagenetic Minerals

A few concentric rings of glauconitic minerals occur as thin rims around the glauconitic pellets. Dolomite rhombohedra are a significant cementing agent in this sample. Some opaque minerals occur between grains.

References

- Munsell, 2009, Rock Color Chart with Genuine Munsell Color Chips: Grand Rapids, Michigan, Geological Society of America, 8 p.
- Terry, R.D., and Chilingar, G.V., 1955, Summary of "Concerning some additional aids in studying sedimentary formations" by M.S. Shvetsov: *Journal of Sedimentary Petrology*, v. 25, no. 3, p. 229–234.